Identification of compatibility factors in the maize – *Colletotrichum graminicola* interaction

Identifizierung von Kompatibilitätsfaktoren in der Interaktion von Mais mit *Colletotrichum graminicola*

Der Naturwissenschaftlichen Fakultät
der Friedrich-Alexander-Universität Erlangen-Nürnberg
zur
Erlangung des Doktorgrades Dr. rer. nat.

vorgelegt von
Anna Maria Voitsik
(geb. Koszucka)

aus Bydgoszcz, Polen

Als Dissertation genehmigt von der Naturwissenschaftlichen
Fakultät der Friedrich-Alexander-Universität
Erlangen-Nürnberg

Tag der mündlichen Prüfung:	07. Aug 2017
Vorsitzender des Promotionsorgans:	Prof. Dr. Georg Kreimer
Gutachter:	PD Dr. Lars Voll
Gutachter:	Prof. Dr. Andreas Burkovski

to my Family

dla mojej Rodziny

Part of this work is included in the following publications:

Voitsik AM, Münch S, Deising HB, Voll LM (2013) Two recently duplicated maize NAC transcription factor paralogs are induced in response to *Colletotrichum graminicola* infection. BMC Plant Biology **13:** 85

Voll LM, Horst RJ, Voitsik AM, Zajic D, Samans B, Pons-Kühnemann J, Doehlemann G, Münch S, Wahl R, Molitor A, Hofmann J, Schmiedl A, Waller F, Deising H B, Kahmann R, Kämper J, Kogel KH, Sonnewald U (2011) Common motifs in the response of cereal primary metabolism to fungal pathogens are not based on similar transcriptional reprogramming. Frontiers in Plant Physiology **2**: 39. doi: 10.3389/fpls.2011.00039

Münch S, Ludwig N, Floß DS, Sugui JA, Koszucka AM, Voll LM, Sonnewald U, Deising HB (2011) Identification of virulence genes in the corn pathogen *Colletotrichum graminicola* by *Agrobacterium tumefaciens*-mediated transformation. Molecular Plant Pathology **12**: 43

TABLE OF CONTENTS

LIST OF ABBREVIATIONS

ACC	1-aminocyclopropane-1-carboxylic-acid
AOX	alternative oxidase
AS	anti-sense line
ATMT	*Agrobacterium tumefaciens*-mediated transformation
BSA	bovine serum albumin
CCR	carbon catabolite repression
CET	central experiment
Cg	*Colletotrichum graminicola*
CgM2	*C. graminicola* (Ces.) Wils. [teleomorph *Glomerella graminicola* (Politis)] wild type strain CgM2
Col-0	*Arabidopsis thaliana cv*. Col-0
dpi	days post infection
DTT	diothiothreitol
E2	ubiquitin-conjugating enzyme (E2 ligase)
ETR	electron transport rate
F	forward
F16BP	fructose-1,6-bisphosphate
FBPase	fructose-1,6-bisphosphatase
flg22	flg22 peptide
FW	fresh weight
GAPDH	glyceraldehyde-3-phosphate dehydrogenase
Glc	glucose
G1P	glucose-1-phosphate
G6PDH	glucose-6-phosphate dehydrogenase
GOX	glycolate oxidase
Hex	hexose
Hex6P	hexose-6-phosphate
hpi	hours post infection
INA	2,6-dichloroisonicotinic acid
JA	jasmonic acid
KO	knock-out
KPHMT	ketopantoate hydroxymethyltransferase
LDH	lactate dehydrogenase
LB	left border
LF	left flank
nPG	*n*-propyl gallate
NPQ	non-photochemical quenching
NRQ	relative transcript level
OMA	oatmeal agar
ORF	open reading frame
OX	overexpressing line

PAL	phenylalanine ammonia-lyase
PAMP	pathogen-associated molecular pattern
PDA	potato dextrose agar
PEP	phosphoenolpyruvic acid
PEPCK	phosphoenolpyruvate carboxykinase
PFD	photon flux density
3-PGA	3-phosphoglyceric acid
PGI	phosphoglucose isomease
PGK	phosphoglycerate kinase
PGM	phosphoglucomutase
PPi	pyrophosphate
PR	pathogenesis-related
PSII	photosystem II
	reverse
RB	right border
RF	right flank
ROS	reactive oxygen species
SA	salicylic acid
SHAM	salicylhydroxamic acid
S6P	sucrose-6-phosphate
Suc	sucrose
TCA	tricarboxylic acid
Ubc8	ubiquitin-conjugating enzyme 8
UDP-Gl	UDP-glucose
UGPase	UDP-Glucose-Pyrophosphorylase
WT	wild type
Y(II)	photosystem II quantum yield

SUMMARY

Colletotrichum graminicola is a phytopathogenic fungus causing anthracnose disease of maize. It exhibits a hemibiotrophic lifestyle, combining bio- and necrotrophy. The fungus spreads from plant to plant by rain-swept conidia. Once conidia get in contact with plant surface, they germinate and form appressoria, specialised structures to penetrate into the host tissue, in which biotrophic primary hyphae are developed. Approximately 3 days post inoculation, fungus switches to the necrotrophic phase and starts to produce invasive secondary hyphae that destroy the host tissue, which leads to development of lesions and rapid disease progress.

Anthracnose leads to severe yield losses in various predominantly tropical and subtropical crop plants and thus, understanding the mechanisms underlying the development of this disease has economical impact. One major research target is to identify compatibility factors in host and the pathogen that play a crucial role for the specific interaction.

In the frame of this thesis, compatibility factors in the maize - *C. graminicola* interaction were identified by combined maize transcriptome-metabolome analysis and analysis of *C. graminicola* mutants exhibiting reduced virulence. Maize microarray hybridisation revealed that transcripts of two NAC transcription factors, *ZmNAC41* and *ZmNAC100*, accumulated in leaves infected with *C. graminicola*, compared to mock-treated leaves. Further experiments with wild type CgM2 and mutant strains of *C. graminicola* showed that the expression of both *NACs* positively correlated with the pathogenicity of the fungus and that induction of *ZmNAC41*occured already at pre-penetrations stage, while *ZmNAC100* was induced solely upon successful penetration. Moreover, both genes were responsive to jasmonic acid treatment and transcripts of both genes accumulated also in senescing leaves. It can be assumed that ZmNAC41 and ZmNAC100 are new defence-associated maize NACs, that may possibly also play a role during leaf senescence and thus, might link defence and senescence signaling pathways. A phylogenetic classification, including identification of conserved protein motifs and promoter elements, of all maize NAC transcription factors present in the first complete assembly of the maize genome revealed that ZmNAC41 and ZmNAC100 are most related to NACs that are associated with defence responses.

The initial microarray experiment also showed that two *alternative oxidases* (*AOX2* and *AOX3*) are induced in *C. graminicola*-infected maize leaves. *AOX3* transcript accumulated already during pre-penetration phase but the induction of *AOX3* was much

higher upon penetration. Infection experiments with *C. graminicola* pathogenicity mutants showed a positive correlation of *AOX3* transcript amount with pathogenicity of the fungal strain. *AOX3* responded to treatment with jasmonic acid and salicylic acid analogues, mimicking hormones regulating the plant defence response. Treatment with inhibitors of AOX restricted *C. graminicola* growth *on planta*, but as mutant maize plant lacking AOX could not be generated, it was not possible to assess the effect of *AOX* deletion on infection. Further research focused on the effect of *AOX* genes on the *Arabidopsis thaliana* - *Colletotrichum higginsianum* interaction which revealed that susceptibility of Arabidopsis could not be linked to expression level of *Aox1a*, which is a main leaf isoform. Based on the presented data, it cannot be resolved if alternative oxidase is induced as a part of host defence or if *C. graminicola* actively up-regulates AOX to attenuate reactive oxygen species (ROS) production and subsequent ROS-mediated defence responses in the host.

In a second part of this thesis, a re-screening of a *C. graminicola* T-DNA insertion mutant collection for weak phenotypes led to identification of five novel *C. graminicola* mutants affected in pathogenicity. One insertion mutant allowed the identification of the novel compatibility factor, ubiquitin-conjugating enzyme 8 (CgUbc8). *CgUbc8* knock-out strains exhibited reduced virulence due to diminished appressoria melanisation and penetration rate. The accumulation of glycogen in conidia of insertion mutant and *CgUbc8* knock-out strains was decreased. Subsequent analysis of glycolytic and gluconeogenetic enzyme activities in *C. graminicola* revealed that glucose degradation via glycolysis might be up-regulated in conidia of insertion mutant and *CgUbc8* knock-out strains compared to wild type CgM2. Moreover, lower activity of malate dehydrogenase, a target of carbon catabolite repression (CCR) in strains lacking CgUbc8 suggested that CgUbc8 might be involved in regulation of CCR in *C. graminicola*. The experimental evidence however, still needs to be provided.

ZUSAMMENFASSUNG

Colletotrichum graminicola ist ein phytopathogener Pilz, der Anthraknose auf Mais verursacht. Der Pilz weist einen hemibiotrophen Lebensstil auf, der aus einer initialen biotrophen und einer darauf folgenden nekrotrophen Phase besteht. Konidien von *C. graminicola* werden durch Regentropfen verbreitet, keimen nach dem Kontakt mit der Pflanzenoberfläche aus und bilden Appressorien, spezialisierte Penetrationsorgane, die in das Wirtsgewebe eindringen und biotrophe primäre Hyphen in den infizierten Zellen ausbilden. Etwa drei Tage nach Inokulation wechselt der Pilz zur nekrotrophen Phase und beginnt invasive sekundäre Hyphen zu bilden, die das Wirtsgewebe zerstören, was zur rapiden Entstehung von Läsionen als Anthraknosesymptomen führt.

Da die Anthraknose starke Ertragsverluste an vor allem tropischen Nutzpflanzen verursacht, ist es aus ökonomischen Gründen wichtig, die Mechanismen zu verstehen, die zur Krankheitsentwicklung führen. Eine zentrale Strategie in der Untersuchung von Pflanzen-Pathogen-Interaktionen ist Identifizierung von Kompatibilitätsfaktoren in Pathogen und Wirt, die entscheidende Rollen für den Ausgang der Interaktion spielen.

Im Rahmen dieser Arbeit wurden Kompatibilitätsfaktoren in der Interaktion von Mais und *C. graminicola* identifiziert, zum einen mithilfe von kombinierter Transkriptom - Metabolom Analyse, zum anderen durch die Untersuchung von *C. graminicola*-Pathogenitätsmutanten. Hybridisierungsexperimente mit Mais-Microarrays zeigten, dass Transkripte von zwei NAC Transkriptionsfaktoren, *ZmNAC 41* and *ZmNAC100*, in *C.graminicola*-infizierten Blättern im Vergleich zur Kontrollblättern akkumulierten. Durch Infektionsexperimente mit Wildtyp CgM2 und *C. graminicola*-Pathogenitätsmutanten stellte sich heraus, dass das Expressionsniveau beider *NACs* positiv mit der Pathogenität des verwendeten Pilzstammes korrelierte und dass die Induktion von *ZmNAC41* bereits während der Prä-Penetrationsphase, die Induktion von *ZmNAC100* ausschließlich nach erfolgreicher Penetration stattfand. Außerdem akkumulierten Transkripte von beiden Genen in seneszenten Blättern und nach Behandlung mit Jasmonat. Es kann daher angenommen werden, dass mit ZmNAC41 und ZmNAC100 neue Abwehr-assoziierte NACs aus Mais identifiziert werden konnten, die vermutlich auch in Seneszenz involviert sind und somit als Bindeglied zwischen der Abwehr- und Seneszenz-Signalwegen verstanden werden können. Die im Rahmen dieser Arbeit geleistete phylogenetische Klassifizierung aller Mais-NAC-Transkriptionsfaktoren auf Basis der aktuellen Annotation des Maisgenoms konnte zeigen, dass ZmNAC41 und

ZmNAC100 die stärkste Verwandtschaft zu solchen NAC-Transkriptionsfaktoren aufweist, die beschriebenermassen eine Rolle in der pflanzlichen Abwehr spielen.

Das zu Beginn der Arbeit durchgeführte Microarray-Experiment zeigte ferner, dass zwei *Alternative Oxidasen* (*AOX2* und *AOX3*) in *C. graminicola*-infizierten Blättern induziert werden. Transkripte von *AOX3* akkumulierten bereits während der Prä-Penetrationsphase, die transkriptionelle Induktion von *AOX3* stieg jedoch nach der Penetration noch deutlich weiter an. Infektionsexperimente mit *C. graminicola* Wildtyp CgM2 und Pathogenitätsmutanten zeigten eine positive Korrelation der *AOX3*-Transkriptmenge mit der Pathogenität des Pilzes. Das *AOX3*-Gen wurde außerdem durch die Behandlung mit Jasmon- und Salicylsäure-Analoga induziert, die pflanzliche Abwehr regulieren. Behandlung mit Inhibitoren der Alternativen Oxidase hemmte das Wachstum von *C. graminicola in planta*. Allerdings war es nicht möglich, der Einfluss einer *AOX*-Deletion auf den Infektionsverlauf zu evaluieren, da Mais-Mutanten mit fehlender AOX nicht verfügbar waren. Weitere Untersuchungen fokussierten sich daher auf den Einfluss von AOX auf die Interaktion von *Arabidopsis thaliana* mit dem verwandten Pathogen *Colletotrichum higginsianum*, da hier beide Interaktionspartner genetisch zugänglich sind. Die Experimente zeigten jedoch dass die Expression des *Aox1a*-Genes, der wichtigsten AOX-Isoform in Blättern, nicht mit der Suszeptibilität von Arabidopsis korrelierte. Auf Basis der durchgeführten Experimente kann nicht abschließend bewertet werden, ob die Alternative Oxidase ein Bestandteil der Wirtsabwehr ist, oder ob *C. graminicola* die *AOX*-Expression aktiv hochreguliert, um die Produktion von reaktiven Sauerstoffspezies (RSS) und die darauffolgende RSS-abhängige Abwehr abzuschwächen.

Im zweiten Teil der vorliegenden Arbeit konnten fünf neue Mutanten mit nur schwach beeinträchtigter Pathogenität aus einer Kollektion von *C. graminicola*-T-DNA-Insertionsmutanten isoliert werden. Anhand von Untersuchungen an einer dieser *C. graminicola*-Pathogenitätsmutanten konnte ein weiterer Kompatibilitätsfaktor identifiziert werden, das *Ubiquitin-konjugierende* Enzym 8 (Ubc8). Die Insertionsmutante und die darauffolgend hergestellte *CgUbc8*-Deletionsmutante zeigten verminderte Virulenz aufgrund einer verringerten Melanisations- und Penetrationsrate. Der Glykogeninhalt in Konidien von CgUbc8-Deletions- und Insertionsmutanten war verringert. Die Analyse von glykolytischen und glukoneogenetischen Enzymaktivitäten in *C. graminicola*-Konidien zeigte dass der glykolytische Glukoseabbau in Insertion- und *CgUbc8* Deletionsmutanten hochreguliert sein könnte. Ferner wurde in *C. graminicola*-Stämmen mit fehlender Ubc8 eine niedrigere Aktivität der Malatdehydrogenase beobachtet. Dies kann darauf hindeuten dass CgUbc8 in

der Steuerung der Katabolitrepression von *C. graminicola* (eng. Carbon Catabolite Repression = CCR) beteiligt ist, da Malatdehydrogense durch CCR reguliert ist. Die Vermutung bedarf noch der experimentellen Überprüfung.

1 INTRODUCTION

1.1 Infection strategies of phytopathogens

Plant pathogens utilise three main infection strategies i.e. biotrophy, hemibiotrophy or necrotrophy. Biotrophs e.g. rust fungi, depend completely on nutrient provision by their hosts and rely on living host tissue to complete their life cycle. To obtain the nutrients without injuring host cells, the pathogens have developed specialised structures called haustoria, which are well separated from the plant plasma membrane by an interfacial layer (Mendgen and Hahn, 2002). In contrary, necrotrophs e.g. *Alternaria brassicicola* or *Botrytis cinerea*, derive nutrients from and proliferate within the dead host tissue (Oliver and Ipcho, 2004). Such pathogens secrete lytic enzymes and toxins to cause a collapse of the infected cells and finally to get access to the nutrients (Alfano and Colmer, 1996; Walton, 1996). However, some pathogens have combined the two life styles and take the advantages from both of them. The hemibiotrophic infection strategy can be observed in *Colletotrichum* (see below) and *Magnaporthe* species (Perfect and Green, 2001; Koeck et al., 2011).

1.1.1 The life cycle of *Colletotrichum graminicola*

Colletotrichum graminicola (Cesati) Wilson [teleomorph *Glomerella graminicola* (Politis)] is the causal agent of anthracnose leaf blight and stalk rot on maize (*Zea mays*), which can lead to substantial yield loss. Fungus growing saprophytically on the overwintered plant debris on the fields serves as a source of primary inoculum. Young seedlings are infected in spring by fungal spores splashed with rain drops from acervuli, specialised structures that mitotically produce conidia, formed on maize residues (Bergstrom and Nicholson 1999). The fungal development *in planta* can be divided into discrete phases i.e. germination, penetration, proliferation and sporulation (Divon and Fluhr, 2007). When conidia get in the contact with plant surface, they start to produce germination tubes and appressoria at their tips, specialised structures essential for the penetration into the host tissue. By the melanisation step and accumulation of osmotically active compounds, an extraordinarily high turgor pressure within the appressorium is generated. This process, along with various cell wall degrading enzymes secreted by the fungus, facilitates the mechanical piercing of the cell wall by the penetration peg that emerges from the appressorium. The penetration event is followed by biotrophic growth within the host tissue, when the fungus

establishes large primary hyphae in penetrated cells. However this phase is quite short and approximately three days after the initial penetration, a switch to the necrotrophic growth phase occurs and the fungus starts to produce long and narrow secondary hyphae. They spread rapidly through the infected tissue, however it is not clear how host cells are killed. In *C. graminicola* genome, non-ribosomal peptide synthetase and polyketide synthase genes were identified (O'Conell et al., 2012), that in fungi code for enzymes producing secondary metabolites toxic to the host. At the necrotrophic stage, macroscopic symptoms of anthracnose i.e. chlorotic spots and subsequently formed dark-coloured necrotic lesions can be observed on the infected leaves. Finally, the fungus forms acervuli on the leaf surface and conidia distributed from them by the rain drops serve as secondary inoculum for the upper leaves and stems of the same plant or other plants (Bergstrom and Nicholson, 1999; Perfect and Green, 2001; Mendgen and Hahn, 2002).

1.2 Virulence factors of phytopathogenic fungi

Virulence factors are pathogen-derived molecules that counteract host defence responses (Briggs and Johal, 1994; see also chapter 1.3). The mechanisms of their activity are diverse. Pathogens may deploy them to directly kill the host cells like it was observed for low-molecular weight toxic secondary metabolites e.g. host-selective toxins from the fungal genera *Alternaria* and *Cochliobolus* (Toyoda et al., 2002). Another group of virulence factors enabling the interaction with the host plants (i.e. compatible interaction) consist of effector proteins that can counteract induced defence responses. For instance, these are enzymes detoxifying host-derived antimicrobial compounds e.g. tomatinase from *Colletotrichum coccodes* (Sandrock and Vanetten, 2001) or suppressors of plant defence like CgDN3 form *Colletotrichum gloeosporioides*, which dampen localised host response similar to hypersensitive response (Stephenson et al., 2000). Furthermore, it was reported that some fungal transcription factors are required for pathogenicity e.g. STE12-like transcription factor from *Colletotrichum lindemuthianum* that induces the expression of genes coding for pectinolytic enzymes (Hoi et al., 2007). Likewise, the hydrolytic enzymes themselves, which are involved in host cell wall degradation, are conferring virulence, as it was shown for *pelB*-encoded pectate lyase of *Colletotrichum gleosporioides* (Yakoby et al., 2001) or *Bcpg1* gene from *Botrytis cinerea* encoding a polygalacturonase (ten Have et al, 1998).

Numerous gene products that are crucial for the fungal development *in planta*, are conferring virulence of phytopathogenic fungi. Two genes of *Magnaporthe grisea*, *MPG1*

coding for hydrophobin and *PTH11* encoding a novel transmembrane protein, were shown to be essential for appressoria formation and thus for full pathogenicity (Beckerman and Ebbole, 1996; DeZwaan et al., 1999). Furthermore, targeted disruption of *CAP20* gene from *Colletotrichum gleosporioides*, which is uniquely expressed in the appressorial cell wall, resulted in complete loss of pathogenicity (Hwang et al., 1995, Hwang and Kolattukudy, 1995). Melanisation of appressoria is a crucial step during fungal development, allowing for successful penetration of the host epidermis. Thus, as expected, *Colletotrichum lagenarium* knock-out mutant of melanin biosynthetic gene *THR1*, encoding a 1,3,8-trihydrosynaphtalene reductase, is not able to establish a compatible interaction with the host plant (Perpetua et al., 1996). Likewise, a *Sfp-type 4'-phosphopantetheinyl transferase 1* mutant of *C. graminicola* is impaired in synthesis of polyketides (PK) and PK-derived melanin. It rarely forms non-melanised appressoria, which are unable to pierce intact leaf surface (Horbach et al., 2009). Disruption of chitin synthesis has also negative effect on development of appressoria. In *C. graminicola chitin synthase V* (*CgChsV)* mutant appressorial cell walls disintegrate after maturation, appressoria are also less melanised compared to the wild type strain (Werner et al., 2007). This mutant is still able to invade host cells, when stabilised osmotically, but infection hyphae formed inside the host cells are swollen and significantly impaired in their development. No anthracnose symptoms are observed on *CgChsV* mutant-colonised leaves. Development of a *Colletotrichum lindemuthianum* mutant, deficient in the *CLTA1* gene encoding a GAL4-like transcription activator, is unaffected until the biotrophic stage; however, the mutant fails to produce secondary hyphae (Dufresne et al., 2000). The same arrest in biotrophic development was reported for the *Colletotrichum graminicola cpr1* mutant which is lacking the gene coding for a putative signal peptidase, which possibly leads to a disruption in the secretion of proteins essential for the development of necrotrophic hyphae (Thon et al., 2002).

1.2.1 Fungal metabolic genes as virulence factors

A significant number of virulence factors comprises of metabolic genes involved in nutrient acquisition during fungal development *in planta*. The successful colonisation of host cells depends on the adjustment of the fungal metabolism towards utilisation of available nutrients.

During the germination phase, phytopathogenic fungi are completely dependent on internal nutrients stores as they do not have an access to the host-derived nutrients. Glycogen,

trehalose, mannitol and lipids are common storage compounds in spores (Thevelein, 1984; Thines et al., 2000; Both et al., 2005; Voegele et al., 2005). Thus, enzymes involved in catabolism of these compounds are induced during germination (Both et al., 2005). The expression of a gene coding for isocitrate lyase (ICL), a glyoxysomal enzyme enabling the remobilisation of fatty acids , is enhanced in *Tapesia yallundae* during the pre-penetration stage of the infection (Bowyer et al., 2000) and mutants disrupted in this gene exhibit reduced virulence (Idnurm A & Howlett, 2002; Wang et al., 2003). The same influence on virulence was reported for the knock-out mutant of malate synthase, another enzyme of glyoxylate cycle (Solomon et al., 2004). In addition to energy and carbon supply, lipid remobilisation plays a key role in appressoria turgor generation through glycerol accumulation, as reported for the *Magnaporthe grisea icl* mutant exhibiting decreased penetration rate (Wang et al., 2003).

Biotrophic growth requires further reprogramming of fungal metabolism, towards the utilisation of plant-derived compounds. In the first place, pathogenic fungi need to get an access to these compounds. Obligate biotrophs, in contrast to hemibiotrophs, develop haustoria, specialized hyphae that mediate the direct uptake of nutrients. Furthermore, both hemi- and biotrophs modulate host metabolism to increase the nutrients availability (see chapter 1.3.3). Some phytopathogens like *Sclerotinia sclerotiorum* (Jobic et al., 2007) or rust fungus *Uromyces fabae* (Voegele et al., 2001) induce their own invertases to hydrolyse the host-derived sucrose to hexoses. Acquisition of hexoses is dependent on hexose transporters located in the fungal plasma membrane and the enhanced expression of hexose transporter genes was reported for fungi of all three life styles e.g. the biotrophic rust fungi *Melampsora larici-populina* and *Puccinia graminis* f. sp. *tritici* (Spanu, 2012), the hemibiotroph *Colletotrichum graminicola* (Lingner et al., 2011) or the necrotroph *S. sclerotiorum* (Jobic et al., 2007). Interestingly, it was shown that corn smut fungus *Ustilago maydis* can directly take up and utilise sucrose as a carbon source. Its sucrose transporter gene *Srt1* is exclusively expressed during infection and its deletion causes a severe reduction of virulence (Wahl et al., 2010).

Carbon sources utilisation is under tight control through the highly conserved process called carbon catabolite repression (CCR). When the preferred nutrient source is present in sufficient amount, the transcription of genes coding for the utilisation of alternative carbon sources, i.e. catabolic enzymes and uptake transporters, is repressed. Commonly, glucose is a favourable nutrient, which drives CCR (Divon and Fluhr, 2007). This process is well studied in yeast *Saccharomyces cerevisiae*, where in the absence of glucose, SNF1 protein kinase is

phosphorylating the transcriptional repressor Mig-1, which subsequently dissociates from promoters of the repressed genes (DeVit et al., 1997; Gancedo, 1998). It was shown in phytopathogenic fungi that disruption of SNF1 orthologue severely impairs fungal growth on complex carbon sources and leads to a reduction in virulence as in e.g. *Cochliobolus carbonum*, thus directly linking CCR and virulence (Tonukari et al., 2000).

1.2.2 Strategies for the identification of the virulence factors in *Colletotrichum graminicola*

Colletotrichum graminicola serves as a model organism to study plant-pathogen interactions due to its easy accessibility to transformation and random mutagenesis, allowing for the identification of virulence factors. Epstein et al. (1998) were able to generate a set of developmental mutants using restriction enzyme-mediated transformation (REMI). *Colletotrichum graminicola* can be also transformed with *Agrobacterium tumefaciens*, which reduces the rate of non-tagged mutations, as shown for transformation of *Fusarium* species (Covert et al., 2001; Mullins et al., 2001). Münch et al. (2007) generated a set of transformants with reduced virulence, resulting from mutants with reduced germination or appressoria formation, or with diminished melanisation rates *on planta*. Several described mutants were entirely hampered in germination or appressoria formation *on planta* and were completely apathogenic.

1.3 The plant defence response – an overview

Each plant possesses a system of an innate immunity (basal immunity) that determines the level of resistance to invading pathogens. This pre-penetration resistance is partially provided by the preformed, i.e. constitutive, components like epicuticular wax layers, rigid cell walls or phytoanticipins, i.e. secondary metabolites with antimicrobial properties (Nürnberger and Lipka, 2005). All these elements create a barrier that prevents the penetration of a broad range of pathogens into the plant tissue. However, some pathogens are able to overcome this preformed barrier, either in a passive or an active manner. This includes mechanisms like taking advantage of naturally occurring or induced cell wall weakening (stomata and wounds respectively), the secretion of cell wall degrading enzymes (Aparna et al., 2009) or the induction of enzymes degrading phytoanticipins, like e.g. avenacinase from oat pathogen *Gaeumannomyces graminis* (Freeman and Ward, 2004).

When the preformed defence is not sufficient to protect the plant from the attacking pathogens, induced defences are launched. The plant responds with cell wall reinforcement (callose appositions), programmed cell death and synthesis of pathogenesis- related (PR) proteins e.g. maize chitinases (PRm 1 and PRm 3) or glucanases (PRm 6a and PRm 6b) (Nasser et al., 1988, Lamb and Dixon, 1997, Balmer et al., 2012) and the production of antimicrobial secondary metabolites such as benzoxazinoids in maize (Ahmad et al., 2011). The induction of the induced defence response depends on the recognition of the invader. As the plants interact with many different microorganisms during their life cycle, this process needs to be on the one hand universal, relying on conserved components that allow the recognition of a broad spectrum of pathogens i.e. the recognition between self and non-self. On the other hand, it has some specificity, as during *R* gene-mediated defence. The broad range resistance is mediated by the pathogen recognition via set of receptors, so called *pattern recognition receptors* (PRRs). These receptors, localized in the plant cell surface, interact with highly conserved pathogen-derived molecules i.e. pathogen-associated molecular patterns (PAMPs). These molecules are derived from pathogens' cell wall or plasma membrane e.g. these can be fragments of chitin and ergosterol present in all fungi, flagellin from *Eubacteria*, lipopolysaccharide (LPS) from Gram-negative bacteria or peptidoglycans from Gram-positive bacteria. Moreover, secreted metabolites, lipids, proteins and peptides are also recognized as PAMPs (Nürnberger and Lipka, 2005). The *Arabidopsis thaliana* PAMP receptor FLS2 (FLAGELLIN SENSING 2) recognizes a 22 aa long peptide derived from flagellin (Chinchilla et al., 2006), while CHITIN ELICITOR RECEPTOR KINASE 1 (CERK1) binds chitooligosaccharides (Miya et al., 2007).The plant cell wall fragments that are products of pathogen cell wall degrading enzymes as for instance oligogalacturonides released from pectin by fungal endo-polygalacturonase (Brutus et al., 2010) or the endogenous peptides, not present under normal conditions in a plant tissue, e.g. ZmPEP1 (Huffaker et al., 2011, Yamaguchi and Huffaker, 2011), can also elicit defence response.

Plant cell surface-localised receptors belong to the families of receptor-like proteins (RLP) and receptor-like kinases (RLK), commonly containing extracellular domain with leucine-rich repeat (LRR) or LysM motifs (Beck et al., 2012), which are involved in ligand recognition. Upon elicitation, PAMP receptors induce a signalling cascade, either directly (RLKs) or indirectly (RLPs) through the interaction with another receptor-like kinases like BAK1. The signalling events involve reactive oxygen species (ROS; see chapter 1.3.1), nitric oxide (NO), changes in cytoplasmic Ca^{2+} levels, which lead to phosphorylation of mitogen-activated protein kinases (MAPK), a central component in plant stress signalling. As an

outcome, a set of genes conferring PAMP-triggered immunity (PTI) is induced (Jones and Dangl, 2006).

The induced defence responses are controlled by plant hormones, of which jasmonic acid (JA), ethylene (ET) and salicylic acid (SA) play a major role (Thomma et al., 2001). However, pathogens are able to modulate this signalling for their own advantages. As jasmonic and salicylic acid act antagonistically to each other, biotrophs prevent SA-dependent responses by up-regulating JA signalling e.g. bacteria from the genus *Pseudomonas* achieve this goal by producing coronatine which is a JA analogue (He et al., 2004).

The induced resistance can also be overcome by pathogens by other means. During the co-evolution of plants and pathogens, some pathogen races have gained the ability to produce specific effector molecules i.e. Avr proteins. These effectors make the selected plant cultivars susceptible for the infection. On the other side, host plants have acquired a set of resistance genes (*R* genes), whose products recognize corresponding Avr proteins, and gained specific resistance to the particular races called gene-for-gene resistance or effector-triggered immunity (ETI) (Dangl and Jones, 2001; Jones and Dangl, 2006). The largest class of *R* genes encodes proteins containing a nucleotide binding site (NB) and leucine-rich repeat domain (LRR) (Dangl and Jones, 2001). This class can be further divided into proteins that possess either coiled-coil (CC) or Toll-interleukin-1 receptor (TIR) domains at the N-terminal end. The NB-LRR receptors are located cytoplasmatically but there is also a class of R proteins which are plasma membrane-bound and possess extracellular LRR domains, i.e. Xa21 and Cf-X proteins. In tomato, Cf-2 and Cf-4 confer resistance to *Cladosporium fulvum* by recognizing the fungal effectors Avr2 and Avr4 respectively, and subsequently triggering hypersensitive response (Rivas and Thomas, 2005). The R proteins described above recognize their target effectors on protein level, by binding them as ligand. However, there is another class of effectors, called transcription-activator like (TAL) proteins, that bind to the promoter of the corresponding *R* gene, which drives its expression e.g. AvrBs3 from *Xanthomonas campestris* pv. *vesicatoria*, that specifically activates a transcription of *Bs3* gene from pepper (Römer et al., 2007).

1.3.1 Reactive oxygen species signalling during the plant defence response

One of the first events in plant defence is the accumulation of reactive oxygen species (ROS) during pathogen attack in the so called oxidative burst (Lamb and Dixon, 1997). Plasma membrane NADPH oxidases, homologous to mammalian respiratory burst oxidases

(RBO), are the main source of superoxide ($O^{\bullet 2-}$) in plants (Torres et al., 2006). Additionally, pH-dependent cell wall peroxidases, germin-like oxalate oxidases and amine oxidase, producing hydrogen peroxide (H_2O_2), may contribute to ROS accumulation in the apoplast (Wojtaszek, 1997; Mittler et al., 2004). The enhanced expression of cell wall peroxidases in response to bacteria and fungi was reported (Almagro et al., 2009). Subcellular compartments can also contribute to the oxidative burst. Hydrogen-peroxide and superoxide are side products of the glyoxylate cycle and fatty acid oxidation that both occur in glyoxysomes (Donaldson et al., 2001). Moreover, superoxide is generated during over-reduction of the electron transport chain in mitochondria and during the detoxifying activity of cytochromes in the cytoplasm and the endoplasmic reticulum (Mittler et al., 2004). During the light period, ROS are also produced in the chloroplasts, as by-products of photosynthesis (Apel and Hirt, 2004).

The generation of ROS is modulated by plasma membrane-bound G proteins i.e. *Rac2* homologs, which can act as both, activators (Ono et al., 2001) or negative regulators (Morel et al., 2004) of ROS accumulation. The soluble ROS scavenging system, consisting of ascorbate peroxidase, glutathione reductase, superoxide dismutases and catalases, serves as an important component to maintain ROS homeostasis (Mittler et al., 2004). This system facilitates a fine tuning of ROS-mediated defence events; e.g. tobacco plants exhibiting reduced activity of catalase and ascorbate peroxidase induce exaggerated responses to pathogens (Mittler et al., 1999).

A transient, low-amplitude ROS accumulation is induced directly after recognition of both avirulent and virulent pathogens, however, the second, prolonged phase of ROS accumulation is generated only in the interaction with avirulent strains (Lamb and Dixon, 1997). Virulent pathogens are able to dampen this second wave of ROS accumulation and thus to overcome this part of a defence response (Williams et al., 2011). Reactive oxygen species can be directly toxic to the invading pathogens (Lamb and Dixon, 1997) but primarily, they induce several components of the defence response such as the strengthening of cell walls by cross-linking of proline-rich proteins (Bradley, 1992) or by mediating programmed cell death of the host cells (hypersensitive response). It was reported that an Arabidopsis double mutant of the *NADPH oxidase* genes (*atrbohD atrbohF*) is not able to efficiently induce hypersensitive response (HR) following the recognition of the avirulent bacteria (Torres et al., 2002), likewise, programmed cell death in response to avirulent oomycete *Phytophtora infestans* is suppressed in *Nicotiana benthamiana* plants with silenced NADPH oxidase genes (Yoshioka et al., 2003). Furthermore, ROS act as signal molecules, which are

necessary for the induction of defence-associated genes (Levine et al., 1994). ROS signalling was also shown to be implicated, together with SA, in inducing systemic acquired resistance (Draper, 1997) and in ABA- and ET-mediated stomatal closure (Desikan et al., 2004; Desikan et al., 2005). Moreover, Arabidopsis *atrbohD atrbohF* double mutant fails to generate NO efficiently, thus ROS seem to be essential for nitric oxide production, which is also involved in plant defence signalling (Blume et al., 2000).

In general, ROS accumulation correlates with plant resistance to biotic stress, but some pathogens induce ROS production for their own benefits e.g. necrotrophic pathogens utilise ROS to kill the host cells. *Botrytis* species disturb the host peroxisomal ROS-scavenging system which leads to a collapse of this protective mechanism and finally kills the whole cell (Kuzniak and Sklodowska, 2005). Other pathogens interfere with chlorophyll-degradation and thereby induce ROS accumulation to enhance plant susceptibility (Kariola et al., 2005). Thus, reactive oxygen species are playing dual role in plant resistance both as positive and negative regulators.

1.3.2 Transcription factors mediating plant defence responses

Biotic stress caused by a pathogen attack is associated with an extensive transcriptional reprogramming, aiming to prioritize defence responses in the plant cells. As the response to the attempted infection must be quick, already pre-existing transcription factors are activated by posttranslational modifications (Moore et al., 2011). Transcription factors associated with defence response belong to different families. Many of the involved transcription factor families are unique to plants, e.g. ERF transcription factors, which are members of the APETALA2 (AP2)/ethylene-responsive-element-binding protein (EREBP) family. These proteins share the conserved ERF domain, binding to the GCC box, an element found in the promoters of *PATHOGENESIS-RELATED* genes. Most of the ERF transcription factors act as activators of defence-associated gene expression (Singh et al., 2002). The overexpression of ERF proteins enhances plant resistance through increased induction of defence-associated genes as shown for transgenic Arabidopsis plants overexpressing tomato PTO-INTERACTING 5 (PTI5) protein (He et al., 2001) or pepper CaPF1 (Yi et al., 2004).

Another class of defence-associated transcription factors, TGACG (TGA) motif-binding factors belong to a large family of basic leucine zipper (bZIP) proteins (Jakoby et al. 2002). TGA2, TGA5 and TGA6 were shown to interact with NON-EXPRESSOR OF PR1 (NPR1), a key component in the SA defence signalling pathway that, among others, activates

PR-1 gene expression (Zhang et al., 1999; Zhou et al., 2000). As expected, a triple knock-out mutant of these TGA genes abolishes SA analogue-mediated induction of the *PR-1* gene, however the basal level of *PR-1* gene expression are higher that in wild type plants (Zhang et al., 2003). Rochon et al. (2006) were able to show that TGA2 act as autonomous repressor of PR-1 gene expression in untreated plants, while after SA stimulation TGA2 is incorporated into the activating complex with NPR1.

Defence-associated gene expression is furthermore regulated by members of the WRKY transcription factor family, another gene family unique to plants (Eulgem et al., 2000). WRKY transcription factors are induced by a range of different pathogens and also by wounding (Eulgem et al., 2000). They bind to the W box in the promoters of many defence-associated genes, e.g. genes induced in systemic acquired resistance (Maleck et al., 2000) and can act as both, activators or repressors of gene transcription. WRKY70 is involved in positive regulation of SA-induced gene expression as well as in negative crosstalk to the JA pathway (Li et al., 2004). Some of the WRKY proteins were shown to modulate the expression of other WRKY genes or even their own expression. For instance, AtWRKY6 and AtWRKY18 serve as their own repressors, preventing their overaccumulation (Robatzek and Somssich 2002; Chen and Chen, 2002).

1.3.3 Plant primary metabolism on the level of photosynthesis and respiration during the defence response

Plant defence responses involve energetically costly events such as synthesis of a range of the new proteins e.g. PR proteins and antimicrobial secondary metabolites such as phenylpropanoids (Berger et al., 2007; Bolton, 2009). These processes generate an elevated demand for energy in form of ATP, reducing equivalents and carbon skeletons as building blocks (Bolton, 2009). Moreover, plants challenged with a particular pathogen launch a complete set of defence responses, even if these are not directly acting against the infectious agent, to make sure that at least part of them will be effective (Katagiri, 2004). Such a broad disease resistance response makes the whole mechanism even more costly and for that reason defence is provided mainly by induced responses, as the profit from a constitutive response would probably not cover its cost (Bolton, 2009). Upon induction of defence, energy and intermediates are redirected from primary metabolism into defence-associated pathways, and consequently, the availability of building blocks influences plant growth and development. This can be observed in an exaggerated manner it the mutants exhibiting constitutive or

elevated levels of defence. The Arabidopsis *constitutive PR gene expression* (*cpr*) mutants exhibit enhanced resistance through increased basal expression of *PR* genes, but are dwarfed compared to the wild type plants (Clarke et al., 1998). The same was observed in case of Arabidopsis *MAP kinase 4* (*mpk4*) (Petersen et al., 2000) and *lesion stimulating disease* (*lsd*) mutants (Dietrich et al., 1994).

One of the common reactions of primary metabolism to pathogen attack is the reduction of photosynthesis rate, observed in both compatible and incompatible interactions (Chou et al., 2000; Berger et al., 2004; Scharte et al., 2005; Bonfig et al., 2006; Scholes and Rolfe, 2006; Swarbrick et al., 2006), which may be due to several reasons. The observed reduction results probably from redirection of carbon skeletons into defence pathways (Somssich and Hahlbrock, 1998). Furthermore, a decline of photosynthesis rate might result from the oxidative damage caused by the oxidative burst or, from the other side, could serve as a protection mechanism against oxidative damage (Bolton, 2009). Another explanation for decline is cell death, which occurs locally, at the infection site. Finally, a reprogramming of the host primary metabolism takes place upon an infection. Reduced photosynthesis rate is associated with increased activity of invertase (see below) and subsequent accumulation of hexoses as shown e.g. for barley infected with powdery mildew (Swarbrick et al., 2006). A common event during pathogen attack is an increase of the photosynthesis rate in systemic leaves (Murray and Walters, 1992) or even in the cells directly surrounding the infection site, in order to support the infection site with extra nutrients (Chou, 2000; Berger, 2004). As a consequence of the lowered photosynthesis rate at the infection site and the concomitantly elevated demand for energy, an increase of cellular respiration could be commonly observed in plant pathogen interactions (Kangasjärvi et al., 2012). In this context, it is also possible that a dampened photosynthesis rate allows for an increased respiration rate (Scharte et al., 2005). Respiration supplies defence responses with energy and carbon skeletons. For instance, phosphoenolpyruvate can be redirected from glycolysis into the shikimate pathway leading to the biosynthesis of aromatic amino acids (phenylalanine, tyrosine and tryptophan), which in turn serve as precursors of antimicrobial secondary metabolites such as flavonoids, isoprenoids and phytoalexins (Dixon, 2001). Enhanced expression of phosphofruktokinase, catalysing a key regulatory step in glycolysis was observed in the interaction of *Puccinia triticina* with wheat (Bolton et al., 2008). Furthermore, the up-regulation of genes encoding rate-limiting enzymes of TCA cycle, citrate synthase and α-ketoglutarate dehydrogenase was occurring in the same interaction (Bolton, 2008). A pathway associated with TCA cycle, the GABA (γ-aminobutyrate) shunt, may also contribute to the plant defence response (Bolton et

al., 2008). This pathway sustains the TCA cycle in oxidative stress conditions (during oxidative burst), when aconitase, α-ketoglutarate dehydrogenase or succinyl-CoA ligase, which are oxidative stress-sensitive enzymes, are inactivated (Bolton, 2009). Another protection mechanism against excess cellular ROS is the up-regulation of alternative oxidase, a component of the mitochondrial electron transport chain (Yip and Vanlerberghe, 2001).

Inhibition of photosynthesis and the activation of respiratory metabolism induce a transition from source to sink in the infected tissue. Plant sink tissues have a high demand for nutrients (e.g. meristematic tissue) that need to be imported from the photosynthethically active organs of the plant called source. The infection-triggered transition from source to sink is accelerated by the induction of the plant cell wall invertase, whose activity is correlating with the sink strength (Roitsch et al., 2003). It was observed in different plant-pathogens interactions that host invertase is, probably actively, induced by invading pathogens for their own benefits i.e. for the uptake of hexoses released after cleavage of sucrose by invertase (Benhamou et al., 1991; Chou et al., 2000; Fotopoulos et al., 2003, Berger et al., 2004; Bonfig et al., 2006; Swarbrick et al., 2006). Hexoses can be utilised by the pathogen as nutrients (see chapter 1.2.1), but they are also important signalling molecules for the plant, regulating gene expression e.g. inducing defence genes (Herbers et al., 1996) or down-regulating photosynthetic genes (Scholes et al., 1994; Chou et al., 2000; Pego et al., 2000; Berger et al., 2004). Even in sink leaves, were the hexose content is high, a further increase in hexoses, leading to an increase in the hexose/sucrose ratio, could be observed in the infected tissue as part of the defence signalling (Benhamou et al., 1991; Berger et al., 2007). Thus, hexoses are directly linking primary metabolism to induced defence responses.

2 MATERIALS AND METHODS

2.1 Materials

2.1.1 Chemicals and enzymes

If not stated otherwise, enzymes and chemicals were ordered from Carl Roth GmbH + Co. KG (Karlsruhe), Fermentas (St. Leon Rot), New England Biolabs GmbH (Frankfurt am Main), Roche Diagnostics GmbH (Mannheim), Sigma-Aldrich (St. Louis, USA) and VWR (Darmstadt).

2.1.2 Oligonucleotides

All oligonucleotides were ordered from Metabion (Martinsried) and are compiled in the Table 1. Plasmid sequencing was conducted by GATC Biotech AG (Konstanz).

Table 1. Oligonucleotides used in the frame of this thesis.

Primer name	Primer description	Primer sequence (5'>3')
Primers for the verification of *C. graminicola* knock-out strains		
Clonat_prom_R	verififfcation of LF of KO strains (together with gene specific primers)	CAGCTCCTGGAAGCTTATCG
Clonat_term_F	verification of RF of KO strains (together with gene specific primers)	TCATTTGCACGAACGAAGAG
KOUbc8_LFcheck_F	verification of LF of *ubc8* KO strain (together with clonat_prom_R)	TACACTGTTCCCAGGTGCAA
KOUbc8_RFcheck_R	verification of RF of *ubc8* KO strain (together with clonat_term_F)	GCAGAACACGGCATACGTC
Ubc8_KOcheck_F	verififfcation of the deletion of ORF (*Ubc8*)	GCCGCCTTCTACGTTATTTG
Ubc8_KOcheck_R	verification of the deletion of ORF (*Ubc8*)	TTAATAATCCCGCCTGCTTG
KOKPHMT_LFcheck_F	verification of LF of *kphmt* KO strain (together with clonat_prom_R)	GGGACGAGGAGAAGGAGGT
KOKPHMT_RFcheck_R	verification of RF of *kphmt* KO strain (together with clonat_term_F)	GACGGCAGCTAGAGGTGAAT
KPHMT_KOcheck_F	verification of the deletion of ORF (*KPHMT*)	CCTTCTGCGAACCAGAGAAA
KPHMT_KOcheck_R	verification of the deletion of ORF (*KPHMT*)	ACATCGCCGTACCTCTTGAC
KO8447_LFcheck_F	verification of LF of *8447* KO strain (together with clonat_prom_R)	CGGGCATATCTACCCAGTGT
KO8447_RFcheck_R	verification of RF of *8447* KO strain (together with clonat_term_F)	ACAAGCAGGAGTTCCCAGTG
8447_KOcheck_F	verification of the deletion of ORF (*8447*)	ACCTTTAACGGCCAGAACCT
8447_KOcheck_R	verification of the deletion of ORF (*8447*)	GAGCCACAAACTGGCTTCTC
KO416hp_LFcheck_F	verification of LF of *416hp* KO strain (together with clonat_prom_R)	GCAATAGCACACGATTGTGAAG
KO416hp_RFcheck_R	verification of RF *416hp* the KO strain (together with clonat_term_F)	TCCCAAGTTCCACCTGTAGC
416hp_KOcheck_F	verification of the deletion of ORF (*416hp*)	ATTGAAGGGGGCATAAGATG
416hp_KOcheck_R	verification of the deletion of ORF (*416hp*)	CACGAGGACTCAGAAACAACT
Ubc8_LF_probe_F	generation of hybridisation probe for the promoter region of *Ubc8* gene	AATCTTCGGGTCCACCTTTC
Ubc8_LF_probe_R	generation of hybridisation probe for the promoter region of *Ubc8* gene	CCAGGACTTGGTTGTGGAGT
Ubc8_RF_probe_F	generation of hybridisation probe for the terminator region of *Ubc8* gene	TAAACTCCCAAACGCCAAAC
Ubc8_RF_probe_R	generation of hybridisation probe for the terminator region of *Ubc8* gene	TTGTCGGAAACACGAGAATG
KPHMT_RF_probe_F	generation of hybridisation probe for the promoter region of *KPHMT* gene	TACTCGTCGGAGAAGGTCGT
KPHMT_RF_probe_R	generation of hybridisation probe for the promoter region of *KPHMT* gene	GCCGCTTGAGTCTTTGAAAC
KPHMT_LF_probe_F	generation of hybridisation probe for the terminator region of *KPHMT* gene	AAACTACCCGTGGTGTTTCG
KPHMT_LF_probe_R	generation of hybridisation probe for the terminator region of *KPHMT* gene	GGTAGCGTACAGCACCGAAT
416hp_LF_probe_F	generation of hybridisation probe for the promoter region of *416hp* gene	GACGCAGAGGAAGTCTTTCG
416hp_LF_probe_R	generation of hybridisation probe for the promoter region of *416hp* gene	GTCTCTGCCAATGCGATACA
416RF/8447LF_probe_F	generation of hybridisation probe for the terminator region of *416hp* gene and the promoter region of *8447* gene	TTGGCTGCAACAGAGACAAC
416RF/8447LF_probe_R	generation of hybridisation probe for the terminator region of 416hp gene and the promoter region of *8447* gene	GGGAAACTTCTCAGGTTGGTG
8447_RF_probe_F	generation of hybridisation probe for the terminator region of *8447* gene	AGACTTCCGCGATAACAAGG
8447_RF_probe_R	generation of hybridisation probe for the terminator region of *8447* gene	TACATCACTGCTTGCGAACC

Maize primers for qRT-PCR

Zm_HMG_F	amplification of maize *high mobility group I/Y-2* transcript	GCTTGGTCTCCATGCTTCATCTAA
Zm_HMG_R	amplification of maize *high mobility group I/Y-2* transcript	CGGTGAAACTGAACTGAACACAAC
Zm_AOX2_F	amplification of maize *alternative oxidase 2* transcript	TCCAACCAGTTGTTTGAGAGTGAA
Zm_AOX2_R	amplification of maize *alternative oxidase 2* transcript	ACATTCGATATTAGCGAGCCCAAT
Zm_AOX3_F	amplification of maize *alternative oxidase 3* transcript	TTATCACTGACAAGTAGGCGTTGC
Zm_AOX3_R	amplification of maize *alternative oxidase 3* transcript	TAGTTCACCTCCGAGTAGCAAACC
Zm_NAC41_F	amplification of maize *NAC41* transcript	GATGAAGATGAGTGTCCACGAT
Zm_NAC41_R	amplification of maize *NAC41* transcript	CCAACCACATACGTATTATCTAACG
Zm_NAC100_F	amplification of maize *NAC100* transcript	TCTGAGAGTTGCTGTGATGGAA
Zm_NAC100_R	amplification of maize *NAC100* transcript	TAACCCTTACAAGACTACCAGCAAC
Zm_OPDR_F	amplification of maize *12-oxophytodienoate reductase 1* transcript	AAGATGGCAAGAATGAGGAGTCA
Zm_OPDR_R	amplification of maize *12-oxophytodienoate reductase 1* transcript	TGAAACAACACGACGCAATG

Arabidopsis primers for qRT-PCR

At_ACT_F	amplification of Arabidopsis *actin2* transcript	GCCAACAGAGAGAAGATGACCCAGA
At_ACT_R	amplification of Arabidopsis *actin2* transcript	ACACCATCACCAGAGTCCAACACAAT
At_AOX1a_F	amplification of Arabidopsis *alternative oxidase 1a* transcript	GCATCTGATATTCACTACCAAGGT
At_AOX1a_R	amplification of Arabidopsis *alternative oxidase 1a* transcript	AAAGCCGAATCCAAGTATGG
At_AOX1d_F	amplification of Arabidopsis *alternative oxidase 1d* transcript	GCTTCGGATATACAATTCAAAGG
At_AOX1d_R	amplification of Arabidopsis *alternative oxidase 1d* transcript	ATCCATATTGAGCTAATAAAAACGAA

C. graminicola **primers for qRT-PCR**

Cg_actin_RT_F	amplification of *C. graminicola actin* transcript	TGAGGCTCTCTTCGCTCCTT
Cg_actin_RT_R	amplification of *C. graminicola actin* transcript	GGTACCACCAGACATGACAATGTT
Cg_PAL_RT_F	amplification of *C. graminicola phenylalanine amonia-lyase* transcript	GCTGGGACAAGGCTCTTCAC
Cg_PAL_RT_R	amplification of *C. graminicola phenylalanine amonia-lyase* transcript	CCCTCTCGGATCGCTTCATA
Cg_Atg12_RT_F	amplification of *C. graminicola autophagy-related protein 12* transcript	TCCTCCACCCAGACATTTCA
Cg_Atg12_RT_R	amplification of *C. graminicola autophagy-related protein 12* transcript	GTCTTTGAAACAATTATGCAGGTTG
Cg_KPHMT_RT_F	amplification of *C. graminicola ketopantoate hydroxymethyltransferase* transcript	CCTTCACTGTCGGCGACTT
Cg_KPHMT_RT_R	amplification of *C. graminicola ketopantoate hydroxymethyltransferase* transcript	ATTGTGGGCGCCATCTC
Cg_E2_RT_F	amplification of *C. graminicola ubiquitin-conjugating enzyme E2 (Ubc8)* transcript	CGAGCTATCGGGATCCGTTT
Cg_E2_RT_R	amplification of *C. graminicola ubiquitin-conjugating enzyme E2 (Ubc8)* transcript	AAGCAGCAGCCTCTCCATTG
Cg_methyltransf_RT_F	amplification of *C. graminicola autophagy-related protein 12* transcript	GATCATCAGGACATGTCTTCAACC
Cg_methyltransf_RT_R	amplification of *C. graminicola autophagy-related protein 12* transcript	ACCCGGTGAATCAAGCTCAT
Cg_dTDPGlcdehyd_RT_F	amplification of *C. graminicola dTDP-glucose 4,6-dehydratase* transcript	CCCGAGAAAATTATCCCCAAG
Cg_dTDPGlcdehyd_RT_R	amplification of *C. graminicola dTDP-glucose 4,6-dehydratase* transcript	CCATCTGGCCCTTGTGTAAGA
Cg_8447_RT_F	amplification of *C. graminicola 8447 hypothetical protein* transcript	GGCCAGAGTTTGAGCAACAG
Cg_8447_RT_R	amplification of *C. graminicola 8447 hypothetical protein* transcript	GGAGGATCGTCCCTTGGTATC
Cg_416hypprot_RT_F	amplification of *C. graminicola 416 hypothetical protein* transcript	ATTGGTCACGCGACACTTTG
Cg_416hypprot_RT_R	amplification of *C. graminicola 416 hypothetical protein* transcript	CCCGCATCCACGATAATAGG

Primers for qPCR

CgH3-qPCR_F	amplification of *C. graminicola histone 3* gene	CGAGATCCGTCGCTACCAGA
CgH3-qPCR_R	amplification of *C. graminicola histone 3* gene	GGAGGTCGGACTTGAAGTCCT
Zm_SPS1_F	amplification of maize *sucrose-phosphate synthase 1* gene	TTGGGCCGAGGTTGGTGTTT
Zm_SPS1_R	amplification of maize *sucrose-phosphate synthase 1* gene	CGGCTTGTGAGGATTGGTTAGGA
Ch_Trpc_F	amplification of *C. higginsianum indol-3-glycerol phosphate synthase* gene	AAGTTCAGACTGCCGAAGAG
Ch_Trpc_R	amplification of *C. higginsianum indol-3-glycerol phosphate synthase* gene	TCAGCCTGCTTGTTGTGTTC
At_RbcS_F	amplification of Arabidopsis *ribulose-1,5-bisphosphate carboxylase/oxygenase small subunit* gene	TGATGGACGGTACTGGACAA
At_RbcS_F	amplification of Arabidopsis *ribulose-1,5-bisphosphate carboxylase/oxygenase small subunit* gene	GAAGCTTGGTGGCTTGTAGG
p19_F	amplification of internal standard DNA	CCATCATTGCGATAAAGGAAAGGC
p19_R	amplification of internal standard DNA	CGAAGGATAGTGGGATTGTGCGTC

Primers amplifying pPK2 vector sequence

PK2_1F	amplification of pPK2 core sequence	AAATCCTGGCCGGTTTGTCT
PK2_1R	amplification of pPK2 core sequence	CGGCACTTAGCGTGTTTGTG
PK2_2F	amplification of pPK2 core sequence	AAGAACCCGGACGTGCTGAC
PK2_2R	amplification of pPK2 core sequence	CCGCTATCGCTACGTGACTG
PK2_3F	amplification of pPK2 core sequence	CGGAAGGAATGTCTCCTGCT
PK2_3R	amplification of pPK2 core sequence	TCACTGCCCGCTTTCCAGTC
PK2_4F	amplification of pPK2 core sequence	CGACCTGGGAGACAGCAACA
PK2_5F	amplification of pPK2 core sequence	ACAGTTGCGCAGCCTGAATG
PK2_5R	amplification of pPK2 core sequence	CTGGTGCCGGTGATCTTCTC

TDNA_ 1F	amplification of T-DNA fragment derived from pPK2	CAATACGCAAACCGCCTCTC
TDNA_ 1R	amplification of T-DNA fragment derived from pPK2	TTCTTCTCGGCGTTCTGGAG
TDNA_ 2F	amplification of T-DNA fragment derived from pPK2	GGAAGACGGAGAAGCCACCT
TDNA_ 2R	amplification of T-DNA fragment derived from pPK2	TCAGCAGGTCGAGTGCAGAG
TDNA_ 3F	amplification of T-DNA fragment derived from pPK2	TTTCATATGCGCGATTGCTG
TDNA_ 3R	amplification of T-DNA fragment derived from pPK2	ATAGTCGCGTGGAGCCAAGA
TDNA_ 4F	amplification of T-DNA fragment derived from pPK2	TCTTGGCTCCACGCGACTAT
TDNA_ 4R	amplification of T-DNA fragment derived from pPK2	AAGGCGGGAAACGACAATCT

Genome Walker primers

GW_1R	Genome Walker primer for left border of T-DNA	CATACGAGCCGGAAGCATAAAGTGTAA
GW_2R	Genome Walker primer for left border of T-DNA	GCCTAATGAGTGAGCTAACTCACATTA
GW_3R	Genome Walker primer for left border of T-DNA	TATTGGCTAGAGCAATTCGGCGTTAAT
GW_1F	Genome Walker primer for right border of T-DNA	CTCTCAAGCCTACAGGACACACATTCA
GW_2F	Genome Walker primer for right border of T-DNA	TAGTGAATGCTCCGTAACACCCAATAC
GW_3F	Genome Walker primer for right border of T-DNA	ACCCAGAATGCACAGGTACACTTGTTT
AT036_GW_1R	Genome Walker primer for left border of T-DNA in AT036 strain	TATAGGAGGATCCAGGCACCGGTCAAC
AT036_GW_2R	Genome Walker primer for left border of T-DNA in AT036 strain	GTCGATTTGAGTCCACTTCCTCACTGG
AT036_GW_3R	Genome Walker primer for left border of T-DNA in AT036 strain	TGCCGAAATCCTTACAGCTTGTGTTGT
AT036_GW_1F	Genome Walker primer for right border of T-DNA in AT036 strain	TGTTCAAGACGATCTACGAACGCAGTG
AT036_GW_2F	Genome Walker primer for right border of T-DNA in AT036 strain	CGCCGGAGAGTTCAAGAAGTTCTGTTT
AT036_GW_3F	Genome Walker primer for right border of T-DNA in AT036 strain	ATGTACGGAGCAGATGCTAGGGCAAAT

Primers for confirmation of T-DNA insertion in *C. graminicola* ATMT mutants

Cg_01	control primer binding to *C. graminicola* genomic sequence	GTGGTCAGACAGCGGTATCC
Cg_02	control primer binding to *C. graminicola* genomic sequence	ACATACCCGTGGAGGCAGAC
HPH_F	amplification of hygromycin probe (for hybridisation) from vector pPK2 as template	CGTGCTTTCAGCTTCGATGTAGG
HPH_R	amplification of hygromycin probe (for hybridisation) from vector pPK2 as template	AAGATGTTGGCGACCTCGTATTG
633_GSP_RB_R	gene-specific primer for confirmation of T-DNA integration site in AT633 mutant	GAACCCGACAGAAACCTCATCCTTT
633_GSP_LB_F1	gene-specific primer for confirmation of T-DNA integration site in AT633 mutant	GAAATCAGATTAAGCAAGCAACCAACG
633_GSP_LB_F2	gene-specific primer for confirmation of T-DNA integration site in AT633 mutant	AGTGTACGGCGTAGTTCTGCATGCTAT
263_GSP_RB_R	gene-specific primer for confirmation of T-DNA integration site in AT263 mutant	TTCTCAACATAGCGGTCGAGGACTT
263_GSP_LB_F1	gene-specific primer for confirmation of T-DNA integration site in AT263 mutant	GGAGGATCTTACGACAAGACACTCCAA
263_GSP_LB_F2	gene-specific primer for confirmation of T-DNA integration site in AT263 mutant	TGTGCCTGTTGTATGTTGGTAGATTGC
263_GSP_LB_F	gene-specific primer for confirmation of T-DNA integration site in AT263 mutant	TAATCTTCGGGTCCACCTTTCCTCT
263_GSP_RB_R1	gene-specific primer for confirmation of T-DNA integration site in AT263 mutant	GTCAGTCCGTTATGGATGGTTTGTTGT
263_GSP_RB_R2	gene-specific primer for confirmation of T-DNA integration site in AT263 mutant	AGCTGCGCAGTGTCAATACAGTAAATG
416_GSP_LB_F	gene-specific primer for confirmation of T-DNA integration site in AT416 mutant	CACATGCCTGTGCGTTTATG
416_LB_TDNA_R	T-DNA-specific primer for confirmation of T-DNA integration site in AT416 mutant	GAGCTCACGAGTTCGTCACATT
Cg-AT-05-02	gene-specific primer for confirmation of T-DNA integration site in AT416 and AT399	TCAGAGGGCTCGGTAGGAAG
Cg-AT05-04	gene-specific primer for confirmation of T-DNA integration site in AT416 and AT399	AAGCCCTGGTCCAGCTTCTC
416 RB genom F1	gene-specific primer for assesing the range of genomic DNA deletion in AT416 and	CAAGTTCGCAGGTCTCAACA
416 RB genom R1	gene-specific primer for assesing the range of genomic DNA deletion in AT416 and	TCTCGGCTTGAGCGTGCTAAT

Primers for the generation of deletion casettes

Clonat_probe_F	amplification of *N-acetyl-transferase* gene	TCGTGGTCATCTCGTACTCG
Clonat_probe_R	amplification of *N-acetyl-transferase* gene	GGCATCGCAGTTATCCAAAT
KO_Ubc8_LF_F	amplification of LF of the deletion casette targeting *Ubc8* gene	CTGAGAGCTGGTGGTGTTGA
KO_Ubc8_LF_R	amplification of LF of the deletion casette targeting *Ubc8* gene (with overhang for	ACACAAGCATATCTCTGTGCTTATGCGAG
KO_Ubc8_RF_F	amplification of RF of the deletion casette targeting *Ubc8* gene (with overhang for	ACAGTTTCTTCAAGATGATGCGGCCAGAA
KO_Ubc8_RF_R	amplification of RF of the deletion casette targeting *Ubc8* gene	GGGTGAGGCTCTGAAAGACA
KO_Ubc8_nested_F	nested primer for an amplification of the deletion cassette targeting *Ubc8* gene	AAGGTTCCCCTTTGATCCAG
KO_Ubc8_nested_R	nested primer for an amplification of the deletion cassette targeting *Ubc8* gene	GCTAGCCTGGTGGACTTTGG
KO_KPHMT_LF_F	amplification of LF of the deletion casette targeting *KPHMT* gene	GGGAAGTCGGGAGTTCTCAG
KO_KPHMT_LF_R	amplification of LF of the deletion casette targeting *KPHMT* gene (with overhang	ACACAAGCATATCTCTGTGCTTATGGAGA
KO_KPHMT_RF_F	amplification of RF of the deletion casette targeting *KPHMT* gene (with overhang	ACAGTTTCTTCAAGATGATGCGGCCGATT
KO_KPHMT_RF_R	amplification of RF of the deletion casette targeting *KPHMT* gene	GTCGATGGCAGTTGGAAAGT
KO_KPHMT_nested_F	nested primer for an amplification of the deletion cassette targeting *KPHMT* gene	ACTCATGGAAGCCGCAAAG
KO_KPHMT_nested_R	nested primer for an amplification of the deletion cassette targeting *KPHMT* gene	GGAGTTGAAGGCCAACCTTTAG
KO_ 8447 _LF_F	amplification of LF of the deletion casette targeting *8447* gene	TCGTCTGACCGTTCTTCAGC
KO_ 8447 _LF_R	amplification of LF of the deletion casette targeting *8447* gene (with overhang for	ACACAAGCATATCTCTGTGCTTATGTGTG
KO_8447_RF_F	amplification of RF of the deletion casette targeting *8447* gene (with overhang for	ACAGTTTCTTCAAGATGATGCGGCCGGA
KO_8447_RF_R	amplification of RF of the deletion casette targeting *8447* gene	CAGGTGCACACACAGAAACG
KO_8447_nested_F	nested primer for an amplification of the deletion cassette targeting *8447* gene	AAGCGGCTTTCTCCTGGAT
KO_8447_nested_R	nested primer for an amplification of the deletion cassette targeting *8447* gene	GTCATGAGGGACAAGAATGCTC
KO_ 416hyppr _LF_F	amplification of LF of the deletion casette targeting *416hp* gene	CACGCTGCCCGTATAAGTGT
KO_ 416hyppr _LF_R	amplification of LF of the deletion casette targeting *416hp* gene (with overhang for	ACACAAGCATATCTCTGTGCTTATGTTTC
KO_416hyppr_RF_F	amplification of RF of the deletion casette targeting *416hp* gene (with overhang for	ACAGTTTCTTCAAGATGATGCGGCCTTCG
KO_416hyppr_RF_R	amplification of RF of the deletion casette targeting *416hp* gene	CAAACTGGCTTCTCCCAGGT
KO_416hyppr_nested_F	nested primer for an amplification of the deletion cassette targeting *416hp* gene	CGCTGCTGATCAACGCATA
KO_416hyppr_nested_R	nested primer for an amplification of the deletion cassette targeting *416hp* gene	GCGCGTTGAGTGGATGTTAC

Primers for genotyping of Arabidopsis lines

SALK_084897_LP	primer for wild type allele of *AOX1a* gene (together with SALK_084897_RP)	ATGTTCCAACGACGTTTCTTG
SALK_084897_RP	primer for wild type allele of *AOX1a* gene (together with SALK_084897_LP) and	AAAGCCCATTGACAGGAAAAG
LBb1.3	primer for mutant allele of *AOX1a* gene (together with SALK_084897_RP)	ATTTTGCCGATTTCGGAAC
GK-529D11_LP	primer for wild type allele of *AOX1d* gene (together with GK-529D11_RP)	CATCATAAACCCTCCAATTTCACT
GK-529D11_RP	primer for wild type allele of *AOX1d* gene (together with SALK_084897_LP) and	CGAAGCATAGTGGTTAATATCACG
GK-T-DNA	primer for mutant allele of *AOX1d* gene (together with GK-529D11_RP)	ATATTGACCATCATACTCATTGC

2.1.3 List of vectors

Vectors used in this work are presented in Table 2.

Table 2. Vectors used in the frame of this thesis.

Vector Name	Application / Resistance	Reference
pGEM®-T Easy	*E.coli* Cloning vector / ampicillin	Promega Corporation (Madison, WI, USA)
pPN	In this work: template for nourseothricin N-acetyl-transferase gene amplification (construction of a deletion cassette for the generation of knock-out mutants of *C. graminicola*) / nourseothricin	Korn et al., 2015
pPK2	Binary vector for *Agrobacterium tumefaciens*-mediated transformation of *C. graminicola* / hygromicin	Covert et al., 2001

2.1.4 Strains

2.1.4.1 Bacterial strains

For the amplification of plasmids, chemical competent cells of *E. coli* from strain XL1-Blue (La Jolla, CA, USA) were used.

2.1.4.2 *Colletotrichum* strains

Colletotrichum graminicola (Cesati) Wilson [teleomorph *Glomerella graminicola* (Politis)] wild type strain CgM2 and T-DNA insertion mutant strains generated by

Agrobacterium tumefaciens-mediated transformation were kindly provided by Steffen Münch and Holger Deising (Martin-Luther-Universität Halle-Wittenberg). *Colletotrichum higginsianum* strain MAFF 305635 was obtained from the Ministry of Agriculture, Forestry and Fisheries (Tokio, Japan).

2.1.5 Plant material

2.1.5.1 Maize seed material

Maize kernels (*Zea mays* cv. Nathan) were kindly provided by Steffen Münch and Holger Deising (Martin-Luther-Universität Halle-Wittenberg), while kernels of *Zea mays* cv. Mikado were a gift of Philip Jung (KWS Saat AG, Einbeck). For the central experiment (trancriptome-metabolome analysis) performed at Max-Planck-Institut for terrestrial microbiology (Marburg), *Zea mays* cv. Early Golden Bantam was used.

2.1.5.2 Arabidopsis seed material

Wild type Arabidopsis seeds (*Arabidopsis thaliana* cv. Col-0) and the knock-out, anti-sense and overexpressing lines were ordered from Nottingham Arabidopsis Stock Center (NASC, Nottingham, UK) (see Table 3).

Table 3. *Arabidopsis thaliana* lines used in the frame of this thesis.

Name of the line	NASC Name	NASC Code
Aox1a anti-sense line	Anti-sense line *Aox1a* (At3g22370)	N6707
Aox1a overexpressing line	*Aox1a* (At3g22370)	N6593
Aox1a T-DNA insertion line	SALK_084897	N584897
Aox1b T-DNA insertion line	SALK_011992C	N664429
Aox1c T-DNA insertion line	SAIL_12_H10	N800585
Aox1d T-DNA insertion line	GK-529D11	N450735
Aox2 T-DNA insertion line	SALK_059351	N559351

2.2 Methods

2.2.1 Cultivation of plant material

2.2.1.1 Cultivation of maize plants

Maize plants (*Zea mays*) cvs. Nathan and Mikado were cultivated in phytochamber (Plant Master, CLF Plant Climatics, Weilburg) at a PFD (photon flux density) of 400 $\mu E \cdot m^{-2} \cdot s^{-1}$ in a 14h / 10h light / dark cycle and 28°C, 60% rH (light phase) / 20°C, 70-80% rH (dark phase) temperature and humidity cycle including 1 hour long ramping period at the beginning and the end of the light phase. Maize seeds were first soaked for 4 hours in tap water and afterwards, sown individually in pots (12 cm in diameter) with P-type soil (Frühstorfer Erde, www.hawita-gruppe.de).

Maize plants (*Zea mays*) cv. Early Golden Bantam for the central experiment (trancriptome-metabolome analysis) were cultivated in phytochambers at the Max-Planck-Institut for terrestrial microbiology (Marburg). Conditions were as follows: PFD of about 1100 $\mu E \cdot m^{-2} \cdot s^{-1}$, 15h / 9h light / dark cycle, temperature 28°C / 20°C and relative humidity of 40% rH/ 60% rH during the light / dark phase respectively. The light intensity, temperature and relative humidity changed gradually between dark / light phase values during the first and last hour of the light phase. Seeds were sown as described for cv. Nathan (see paragraph above).

2.2.1.2 Cultivation of Arabidopsis plants

Arabidopsis seeds were sown in the pots containing 65% P-type soil (Frühstorfer Erde, www.hawita-gruppe.de), 25% sand and 10% expanded clay (Liadrain, Pautzfeld) and stratified in the dark at 8°C for 48h to synchronise germination. Plants were grown for 2 weeks in short day conditions (8h/16h light/dark cycle at 22°C/20°C), transferred to single pots and further grown in 12h/12h light/dark cycle at 22°C/20°C in the phytochamber (GroBank Bright Boy XXL, CLF, Wertingen).

2.2.2 Microbiological methods

2.2.2.1 Cultivation of fungal material

If not stated otherwise, *C. graminicola* and *C. higginsianum* were grown on oatmeal agar (OMA) plates (see below) at 22°C in 16h/8h light/dark cycle. Plates were initially inoculated with 10 µl of the respective conidia stock and fungus was grown for one (*C. higginsianum*) or two weeks (*C. graminicola*). Afterwards, conidia were washed off with 100 µl of Milli-Q water (from one spot on the plate) and transferred to the following plate. To prepare a stock, conidia were harvested with 0.5 ml of Milli-Q water from 2 cm^2 area and mixed with the equal volume of NSY-Medium (see below) and stored at -80°C.

Oatmeal agar (OMA) Medium	
50 g/l	shredded oatmeal
12 g/l	agar
	sterilised in autoclave for 45 min. at 121°C

	NSY- Medium
0.8% (w/v)	Nutrient Broth (peptone and meat extract 5:3)
0.1% (w/v)	yeast extract
0.5% (w/v)	sucrose
70% (v/v)	glycerol
	sterilised in autoclave for 20 min. at 121°C

2.2.2.2 Testing the influence of *n*-propyl gallate and salicylhydroxamic acid on the growth of *C. graminicola*

The growth of *C. graminicola* in the presence of salicylhydroxamic acid (SHAM) and *n*-propyl gallate (nPG) was tested on Fries complete medium plates (see below). Plates were supplemented with SHAM or nPG (see below), both dissolved in DMSO (final concentration of DMSO in the medium was 0.005% (v/v)). Control plates were supplemented with 0.005%

(v/v) DMSO. Plates were inoculated with 10^3 conidia in 30 µl Milli-Q water and incubated at 23°C for 2 weeks.

Fries complete medium	
3% (w/v)	sucrose
0.5% (w/v)	ammonium tartrate
0.1% (w/v)	potassium dihydrogen phosphate
0.1% (w/v)	ammonium nitrate
0.048% (w/v)	magnesium sulphate
0.1% (w/v)	sodium chloride
0.013% (w/v)	calcium chloride
0.1% (w/v)	yeast extract
1.5% (w/v)	agar

Fries complete medium supplemented with (final concentration given):

SHAM	1 µM	10 µm	0.1 mM	10 mM
nPG	5 µM	50 µM	0.5 mM	5 mM

2.2.2.3 Transformation of *C. graminicola*

C. g*raminicola* conidia were harvested from the culture grown in 100 ml of 0.5 M sucrose suplemented with 0.1% (w/v) yeast extract for 7 days at room temperature by filtering through a nylon cloth and following centrifugation at 2 500 rpm in a large bench top centrifuge for 10 minutes at 4°C. The conidia pellet was resuspended in 20 ml of protoplastation solution (see below) and incubated for 4 hours at 30°C with rotary shaking at 100 rpm. The resulting protoplasts were collected by centrifugation at 1 200 rpm for 10 minutes at 4°C, washed with 10 ml STC buffer (see below), centrifuged as before and resuspended in 1 ml of STC buffer. To protoplast aliquots of 100-200 µl, 1-5 µg of deletion cassette (see chapter 2.2.4.8) was added, followed by incubation for 30 minutes on ice, addition of 1 ml of PEG buffer (see below) and incubation for 20 minutes at room temperature. Each aliquot was mixed with 3-4 ml of liquid regeneration medium (see below) preheated to 45°C and streaked on a transformation plate (see below). To test the vitality of the protoplasts and the effectiveness of selection, two aliquots of protoplasts were handled as described above except the addition of deletion cassette DNA and these aliquots were streaked on transformation plates with and without nourseothricin respectively. Transformants

were grown at room temperature for 4-6 days and resulted individual colonies were inoculated on potato dextrose agar (PDA) plates (see below) supplemented with nourseothricin. After 14 days of growth at room temperature, cubic block were taken with an inoculation loop from mycelium-containing parts of the transformation plates. Fresh (small or 6-well) PDA plates supplemented with nourseothricin were inoculated by agitating the "bottom" side of the cube (i.e. this which had a contact with a bottom part of the first plate) on the surface of the following plate. The cubes were discarded afterwards. After 2 days of growth at room temperature, the first single-spore colonies were visible. These colonies were then transferred with inoculation loop to 24-well OMA plates. After 14 days of growth, following new set of 24-well OMA plates was inoculated with conidia freshly taken with an inoculation loop from the previous plate. No water was used for transferring the conidia, to avoid cross-contamination. Conidia from the OMA plates from the previous step were washed off with 1 ml of Milli-Q water and used for gDNA isolation (see chapter 2.2.4.2 in Methods). Following OMA plates were incubated for 14 days and subjected for preparation of spore-stocks (see chapter 2.2.2.1).

Protoplastation solution	
0.7 M	sodium chloride
0.1% (v/v)	2-mercaptoethanol
400 mg	lysing enzyme from *Trichoderma harzianum*

STC buffer	
1 M	sorbitol
50 mM	$CaCl_2$
10 mM	Tris-HCl pH 8.0

PEG buffer	
40% (w/v)	PEG 4 000
50 mM	Tris-HCl pH 8.0
0.6 M	KCl
50 mM	$CaCl_2$

Regeneration medium	
1 M	sucrose
0.1% (w/v)	yeast extract
0.1% (w/v)	casein hydrolysate
0.6% (w/v)	agar

Transformation medium	
1 M	sucrose
0.1% (w/v)	yeast extract
0.1% (w/v)	casein hydrolysate
1.5% (w/v)	agar
0.01% (w/v)	nourseothricin

Potato dextrose agar (PDA) medium supplemented with nourseothricin	
2.4% (w/v)	potato dextrose
1.2% (w/v)	agar
0.1% (w/v)	nourseothricin

All buffers/solutions/media were sterilised in an autoclave for 20 min. at 121°C. Nourseothricin was added to media after autoclaving and cooling down the medium to approximately 37°C.

2.2.2.4 Infection of maize plants with *C. graminicola*

Conidia of *C. graminicola* were washed off from a 2 weeks old oatmeal agar (OMA) plate (see chapter 2.2.2.1) with 1ml Milli-Q water and diluted to a final concentration of $2x10^4$ (low titer) or $2x10^6$ (high titer) conidia / ml. Fully expanded fourth leaves of two weeks old maize plants were either sprayed with a conidia suspension of a high titer ($2x10^6$conidia / ml) containing additionally 0.02 % (v/v) Tween-20 or dipped in a conidia suspension of a low titer ($2x10^4$ conidia / ml) for 24 h. Sprayed plants were kept in 100% relative humidity conditions for the next 24 h. Mock-treated leaves were sprayed with 0.02% (v/v) Tween-20 in Milli-Q water or dipped in pure Milli-Q water, respectively. Leaves were collected at the respective time points after inoculation, frozen immediately in liquid nitrogen and subjected to further analysis.

2.2.2.5 Infection of *A. thaliana* plants with *C. higginsianum*

Conidia of *C. higginsianum* were washed off from a 7-days old oatmeal agar (OMA) plate (see chapter 2.2.2.1) with 1ml Milli-Q water and diluted to a final concentration of $2x10^6$ conidia / ml. Five weeks after sowing, plants were sprayed with conidia suspension additionally containing 0.02 % (v/v) Tween-20 at the end of the light period. High humidity conditions were ensured for 60h after inoculation by covering the plants with a plastic dome that was sprayed with water in the inside. Control plants were sprayed with 0.02 % (v/v) Tween-20 and afterwards treated as infected plants.

2.2.3 Microscopic analysis

Segments of infected leaves were fixed in ethanol/acetate (v/v 3:1) over night at room temperature. The following day, the fixing solution was replaced with the staining solution (10 g phenol, 10 ml water, 10 ml glycerine, 10 ml lactic acid and 0.01% (w/v) acid fuchsin) and samples were incubated at 60ºC for 20 min. Afterwards samples were analysed by light microscopy with a Leica DMR fluorescence microscope (Leica, Wetzlar). Epifluorescence of the cell walls was analysed in the unstained leaves using UV light.

2.2.4 Molecular biology methods

Standard techniques like agarose gel electrophoresis, DNA amplification via PCR, restriction enzyme digestion and Southern blot were carried out as described in Sambrook et al. (1989). RNA was isolated according to the method described by Chomczynski and Sacchi, 1987. Ligation and transformation of *E.coli* was performed with pGEM®–T Easy Vector System (see chapter 2.1.3), isolation of plasmid DNA with the QIAprep® MiniPrep Kit (QIAGEN, Hilden), isolation of fungal RNA with the RiboPure^{TM}-Yeast Kit (Life Technologies, Carlsbad, CA, USA), PCR products purification with QIAquick® PCR Purification Kit (QIAGEN) and gel extraction with QIAquick® Gel Extraction Kit (QIAGEN) according to manufacturers protocols.

2.2.4.1 Quick isolation of plant DNA for genotyping

Arabidopsis leaf samples were frozen in liquid nitrogen immediately after harvesting and afterwards homogenised in the extraction buffer (200 mM Tris/HCl pH 7.5; 250 mM NaCl; 25 mM EDTA; 0.5% (w/v) SDS) with a homogeniser (RZR1; Heidolph, Schwabach). Cell debris were separated by centrifugation of samples in a microcentrifuge for 5 minutes at 13,000 rpm. The DNA pellet was precipitated by mixing the entire supernatant with 1 volume of isopropanol, incubation for 2 minutes at room temperature and subsequent centrifugation (as described above). Air-dried DNA-pellets were dissolved in TE buffer.

TE buffer	
1 mM	EDTA
10 mM	Tris-HCl pH 7.5

2.2.4.2 Quick isolation of fungal DNA for genotyping

Fungal conidia were washed off from oatmeal agar plate (2 cm^2 area) (see chapter 2.2.2.1) with Milli-Q water and sedimented by centrifugation in a microcentrifuge for 5 minutes at 2,000 rpm. Afterwards, the conidia pellet was resuspended in 200 µl of lysis buffer (see below), mixed with 200 µl of glass beads and 200 µl of phenol/chloroform/isoamyl alcohol (v/v/v 25:24:1) and centrifuged in a microcentrifuge for 5 minutes at 13,000 rpm. DNA was purified from the resulted supernatant by centrifugation (as before) in 1 volume of phenol/chloroform/isoamyl alcohol and subsequently precipitated with 2 volumes of 100% ethanol for 15 minutes at -20°C. The DNA pellet was sedimented by centrifugation in a microcentrifuge for 15 minutes at 13,000 rpm, washed with 70% ethanol, air-dried and dissolved in TE buffer (see chapter 2.2.4.1).

Lysis buffer	
2% (v/v)	Triton X-100
1% (w/v)	SDS
100 mM	NaCl
100 mM	Tris-HCl pH 8.0
1 mM	EDTA

2.2.4.3 Isolation of fungal DNA in large scale for Southern blot and GenomeWalker™

Fungal conidia (up to $4x10^8$ conidia) were washed off from one oatmeal (see chapter 2.2.2.1) agar plate 1 ml with Milli-Q water and sedimented by centrifuging in a microcentrifuge for 5 minutes at 2,000 rpm. The conidia pellet was resuspended in 200 µl of SCE buffer (see below) supplemented with 0.8% (v/v) 2-mercaptoethanol and 0.3% (w/v) zymolyase T20 (AMS Biotechnology (Europe) Ltd, Abingdon, UK) and incubated for 60 minutes at 37°C to generate spheroplasts. Afterwards, 200 µl of SDS buffer (see below) was added and the sample was incubated for 10 minutes at 75°C to break the cells. Subsequently, 200 µl of 2 M potassium acetate was added and cell debris were separated by incubation on ice for 20 minutes and following centrifugation in a microcentrifuge for 20 minutes at 13,000 rpm. The nucleic acid pellet was precipitated with 1 ml isopropanol and 200 µl of 2 M ammonium acetate, incubation for 30 minutes at -20°C and centrifugation in a microcentrifuge for 10 minutes at 13,000 rpm. The resulted pellet was air-dried and treated with RNase A (500 µg/ml) in 200 µl of TE buffer (see chapter 2.2.4.1.) for 10 minutes at 37°C. DNA was purified twice by centrifugation in 1 volume of phenol/chloroform/isoamyl alcohol (v/v/v 25:24:1). The DNA pellet was precipitated by incubation in 2 volumes of 100% ethanol and 1/10 volume of 3 M sodium acetate pH 5.2 for 15 minutes at -20°C and centrifugation in a microcentrifuge for 15 minutes at 13,000 rpm. The pellet was washed twice with 70% ethanol and dissolved in 100 µl of Milli-Q water.

SCE buffer	
1 M	sorbitol
0.1 M	sodium citrate
0.06 M	EDTA pH 7.0

SDS buffer	
2% (w/v)	SDS
0.5 M	EDTA
0.1 M	Tris-HCl pH 9.0

2.2.4.4 Radioactive labelling and hybridisation of DNA probes

Pre- and hybridisation were performed in Church buffer (see below) with 1% (w/v) bovine serum albumin at 65°C for 2 hours and over night, respectively. Membrane (Gene Screen™ Hybridisation Transfer Membrane, Perkin Elmer, Rodgau) with UV-cross-linked DNA (UV-Crosslinker, Stratagene) was hybridised with 150 ng of the probe, labelled with 40 µCi [α^{32}P]dCTP (Hartmann Analytic, Braunschweig) using High Prime DNA Labelling Kit (Roche Diagnostics GmbH, Mannheim) according to manufacturer's protocol. Subsequently, the membrane was washed with 6xSSC buffer (see below) supplemented with 0.1% (w/v) SDS at 65°C, until the radiation level of 1-5 Bq/cm^2 was reached, and exposed to an X-ray film (Kodak) in cassettes with photomultiplier lining at -80°C for 2-3 days.

	Church buffer
0.5 M	phosphate buffer pH 7.2
7% (w/v)	SDS
10 mM	EDTA

	6x SSC buffer
2.7% (w/v)	tri-sodium citrate
5.3% (w/v)	NaCl

2.2.4.5 Evaluation of relative transcript amounts by qRT-PCR

An aliquot of 1 µg of total RNA was treated with 1U DNase I (Fermentas, St. Leon-Rot) for 30 min at 37°C. The reaction was stopped adding 1 µl of DNA Stop Solution and following incubation for 10 min at 65°C. RT reaction was performed with oligo(dT)$_{18}$ and Revert Aid™ H Minus Reverse Transcriptase (Fermentas) in a total volume of 40 µl according to the manufacturer's protocol. qRT-PCRs were performed with 1 µl of cDNA from the respective RT reaction (as described above) using 2x Brilliant II SYBR® Green QPCR Master Mix (Stratagene, Waldbronn) and 200 nM of upstream and downstream primer. Primers used for evaluation of relative transcript amounts are compiled in Table 1. The total volume of the reaction was 20 µl. The following PCR programme was used: initial denaturation for 10 min at 95°C, afterwards 40 cycles of denaturation for 30 sec at 95°C, annealing for 30 sec at 59°C and elongation for 1 min at 72°C. The qRT-PCRs were run on

Mx3000P™ System and analysed with MxPro QPCR Software (Stratagene – Agilent Technologies Company, La Jolla, CA, USA). Target maize, Arabidopsis and *C. graminicola* and gene transcript amounts were normalised to *ZmHMG*, *AtACT2* and *CgACT*, respectively. Normaliser reactions were performed with 1 µl of the respective cDNA (as described above) during the same run as target gene reactions. Afterwards, relative transcripts amounts were calibrated to the reference samples as indicated in the respective figure legends in the Results part.

2.2.4.6 Evaluation of relative fungal DNA quantity by qPCR

Three leaf punches (1 cm^2 in total) per sample were frozen in liquid nitrogen immediately after harvesting and afterwards, ground with mortar and pestle under liquid nitrogen. As an internal standard, 1 ng of p19 DNA (Vogel, 2009) was added to the sample. Genomic DNA was isolated with the DNeasy Plant Mini Kit (QIAGEN, Hilden) according to the manufacturer's protocol. qPCRs were performed with 1 µl of genomic DNA using 2x Brilliant II SYBR® Green QPCR Master Mix (Stratagene, Waldbronn) and 200 nM of upstream and downstream primer (see primer list in Table 1). The total volume of the reaction was 20 µl. The following PCR programme was used for the amplification of *CgH3* and *ZmSPS1*: initial denaturation for 10 min at 95°C, afterwards 40 cycles of denaturation for 30 sec at 95°C, annealing for 30 sec at 59°C and elongation for 1 min at 72°C. For *ChTrpC* reactions, the following PCR programme was used: initial denaturation for 10 min at 95°C, afterwards 40 cycles of denaturation for 30 sec at 95°C, annealing for 30 sec at 60°C and elongation for 1 min at 72°C. The qPCRs were run on the Mx3000P™ System and analysed with MxPro QPCR Software (Stratagene –Agilent Technologies Company, La Jolla, CA, USA). The amount of *C. graminicola* DNA was determined with *CgH3* primers relative to the maize *SPS1* gene or the internal standard p19, while the quantity of *C. higginsianum* DNA was evaluated with *ChTrpC* primers and normalised to the leaf area.

2.2.4.7 Determination of T-DNA integration sites in ATMT-generated mutants of *C. graminicola* via adaptor-mediated PCR

In ATMT-generated mutants, a T-DNA fragment between left (LB) and right (RB) border (Fig. 1; Fig. 13 in chapter 3.1.3) should have integrated into the genome of the target organism. In fungal insertion mutants, this is not always the case and the inserted T-DNA

may be truncated or contain adjacent vector sequence. Thus, the exact determination of the integrated T-DNA fragment was conducted for each analysed *C. graminicola* mutant prior to adapter mediated PCR (GenomeWalker™ Kit, Clontech, Mountain View, CA, USA) procedure. For this purpose, PCRs with a set of primers (see Table 1 and Figure 13 in chapter 3.1.3) amplifying fragments distributed throughout the whole vector sequence were performed on genomic DNA of analysed mutant strains . Primer pairs PK2_1-5 F/R were amplifying five regions of the vector core sequence. These regions of the vector should not integrate into genomic DNA of ATMT-generated mutants and thus, should not be detected by PCR with these primer pairs. Primer pairs TDNA_1-4 F/R were amplifying four regions spread throughout the T-DNA fragment of the vector sequence. This is the region which should integrate into genomic DNA of transformants and should be detected during PCR with these primers.

Subsequently, after the closer characterisation of the actual left and right borders of each *C. graminicola* insertion mutant, a set of primers (GW_1-3F/R) for adapter mediated PCR were designed (see Table 1 and Fig. 1) according to the protocol of GenomeWalker™ Universal Kit (Clontech Laboratories, Inc, Mountain View, CA, USA).

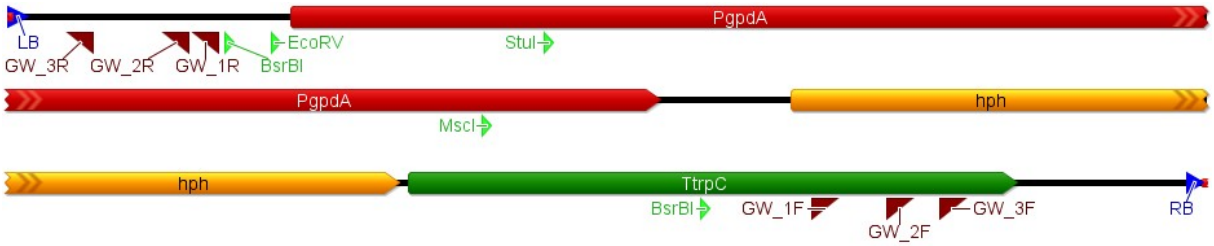

Fig. 1. Positions of GenomeWalker™ primers (GW_1-3F/R) within T-DNA fragment. Restriction sites of BsrBI, MscI, StuI and EcoRV, relevant for GenomeWalker™ strategy, are marked. LB / RB – left / right border, hph – hygromicin phosphotransferase gene under the control of the gpdA promoter (PgpdA) and with TrpC (TtrpC) terminator.

The further GenomeWalker™ procedure was performed as described by the manufacturer (see Fig. 2 for the scheme summarizing the procedure). Genomic DNA (10µg) of *C. graminicola* mutants was digested with BsrBI, EcoRV or StuI restriction enzymes for the determination of T-DNA integration sites at the left border and with BsrBI or MscI restriction enzymes for determination of the junction site at the right border. Digested gDNA was used as a template for first round of PCRs with adaptor primer A1 (provided with the kit) and primers GW_1R or GW_2R for the left border junction and GW_1F or GW_2F for the right border junction. Products of the first round of PCRs served as a template for the second round of PCRs (nested PCRs) with adaptor primer AP2 (provided with the kit) and GW_2R

or GW_3R primer for the left border junction and GW_2F or GW_3F primer for the right border junction, respectively (please also refer to the description in the legend of Fig. 2). In case of mutant AT036, a different set of T-DNA specific primers and another set of enzymes were used (see below) as it could be concluded from the first set of GenomepWalker™ PCRs that the integrated PK2 vector sequence did not exactly cover the T-DNA sequence. Genomic DNA of mutant AT036 was digested with HaeIII or MscI restriction enzymes for the determination of T-DNA integration site at the left border and with BmgBI or NaeI restriction enzymes for determination of the junction site at the right border. First round of PCRs was performed with adaptor primer A1 (provided with the kit) and primers AT036_GW_1R or AT036_GW_2R for the left border junction and AT036_GW_1F or AT036_GW_2F for the right border junction. Nested PCR was performed with adaptor primer AP2 (provided with the kit) and AT036_GW_2R or AT036_GW_3R primer for the left border junction and AT036_GW_2F or AT036_GW_3F primer for the right border junction.

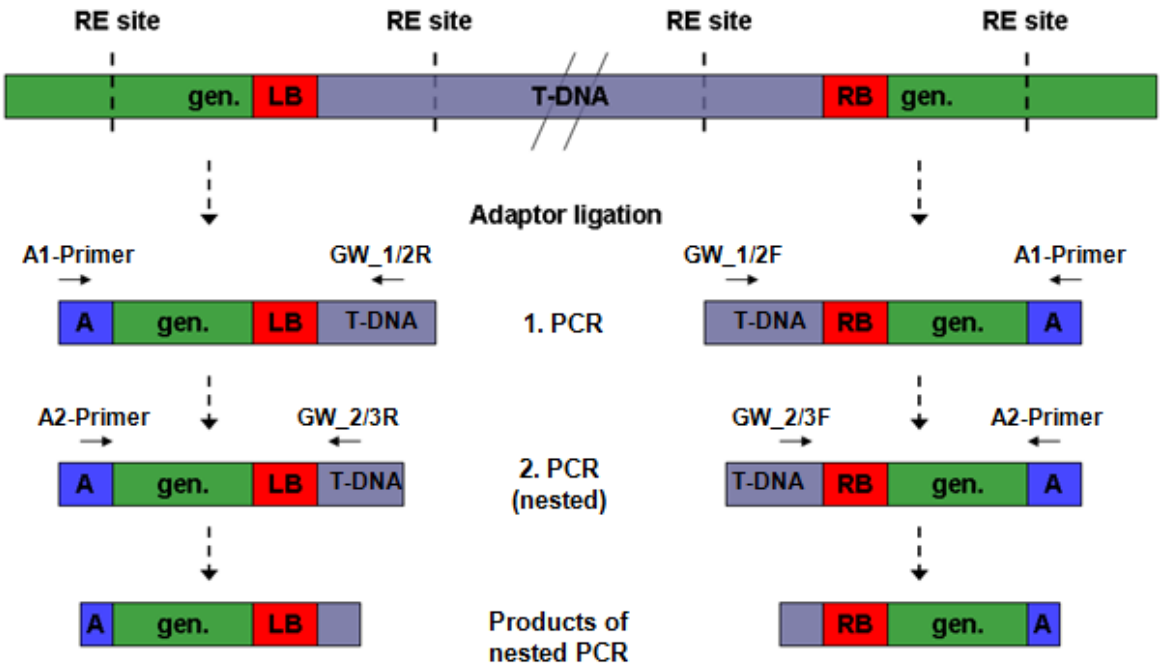

Fig. 2. Scheme summarizing the strategy of GenomeWalker™ approach. Genomic DNA is digested with restriction enzymes that cut both within and adjacent to T-DNA insertion (RE sites – exemplary positions of restriction enzymes sites) and then ligated to GenomeWalker™ Adaptor (A) provided in the kit (Clontech). Genomic regions flanking T-DNA insertion (gen.) are amplified within two rounds of PCR. First round is performed with adaptor primer (A1-Primer, provided by the manufacturer) and innermost T-DNA-specific primer: GW_1R or GW_2R for the junction at the left border (LB) and GW_1F or 2F for the junction at the right border (RB). Subsequent nested PCR is performed with nested adaptor primer (A2-Primer, provided by the manufacturer) and outermost T-DNA-specific primer: GW_2R or GW_3R for the junction at the LB and GW_2F or 3F for the junction at the RB.

Junction sites of T-DNA and adjacent genomic sequence were identified by sequencing of the products amplified by secondary (nested) GenomeWalker™ PCR (see Table 1 for details on primers used for these reactions). Products were first separated on 1.5% agarose gel and extracted with QIAquick® Gel Extraction Kit (Qiagen, Hilden). Subsequently, they were ligated to the pGEM®-T Easy vector (Promega Corporation (Madison, WI, USA) and cloned according to the manufacturer's protocol. Resulting plasmids were purified with QIAprep® MiniPrep Kit (QIAGEN, Hilden) and served as a template for sequencing performed by GATC (Konstanz).

2.2.4.8 Construction of deletion cassettes for the generation of knock-out mutants of *C. graminicola*

Knock-out mutants of *C. graminicola* were generated through a method employing a homologous recombination event, where the whole open reading frame of a target endogenous gene is replaced with a selectable marker gene, in this case nourseothricin N-acetyl-transferase, conferring resistance to nourseothricin. The selectable marker gene was introduced into protoplasts of *C. graminicola* (see chapter 2.2.2.3) as a part of linear DNA deletion cassette. This deletion cassette was generated by overlap PCR in the way that nourseothricin N-acetyl-transferase gene was flanked from both sides by approx. 1 kb of the 5' and 3' region adjacent to the target open reading frame. A schematic view of a deletion cassette and positions of primers used for its construction is depicted in the Fig. 3. Primers used for the construction of specific deletion cassettes were compiled in Table 1. Nourseothricin N-acetyl-transferase gene sequence was amplified from the plasmid pPN (kindly provided by Martin Korn, Lehrstuhl für Biochemie, Erlangen) with Phusion polymerase (New England Biolabs GmbH, Frankfurt am Main) according to manufacturer's protocol. Flanking regions of the deletion cassette were amplified using Phusion polymerase on 100 ng of *C. graminicola* genomic DNA, e.g. with primers KO_Ubc8_LF_F/R and KO_Ubc8_RF_F/R for the amplification of the promoter (left flank) and terminator (right flank) region of the *Ubc8* gene respectively. Reverse primer for the generation of the left flank i.e. promoter region (KO_Ubc8_LF_R for Ubc8 deletion cassette) and forward primer for the generation of the right flank i.e. terminator region (KO_Ubc8_RF_F respectively) contained overhangs on their 5' ends, which were complementary to the border sequence of the nourseothricin N-acetyl-transferase gene, The amplified left and right flanks (10 ng each) served as primers for the double-joint PCR (DJ-PCR) on the nourseothricin N-acetyl-

transferase gene sequence (30 ng) as a template, using Phusion polymerase. This step allowed for the joining of all three fragments (left flank, right flank and resistance gene) into one fragment to generate a deletion cassette. The following programme was used: initial denaturation for 30 sec at 98°C, afterwards 10 cycles of denaturation for 15 sec at 98°C, annealing for 15 sec at 60°C and elongation for 1 min at 72°C, afterwards 25 cycles of denaturation for 15 sec at 98°C and annealing/elongation for 90 sec at 72°C and final elongation for 5 min at 72°C. To obtain suitable amount of linear DNA for transformation (see chapter 2.2.2.3), the deletion cassette was amplified during PCR with nested primers. The following programme was used: initial denaturation for 30 sec at 98°C, afterwards 30 cycles of denaturation for 20 sec at 98°C and annealing/elongation for 2 min at 72°C and final elongation for 10 min at 72°C. PCR products obtained after each step (flanks and resistance gene sequence amplification, DJ-PCR and nested PCR) were purifired with QIAquick® PCR Purification Kit (Qiagen, Hilden).

A. Amplification of promoter (LF) and terminator (RF) of a target gene on genomic DNA of *C. graminicola* and *NatR* gene on pPN template

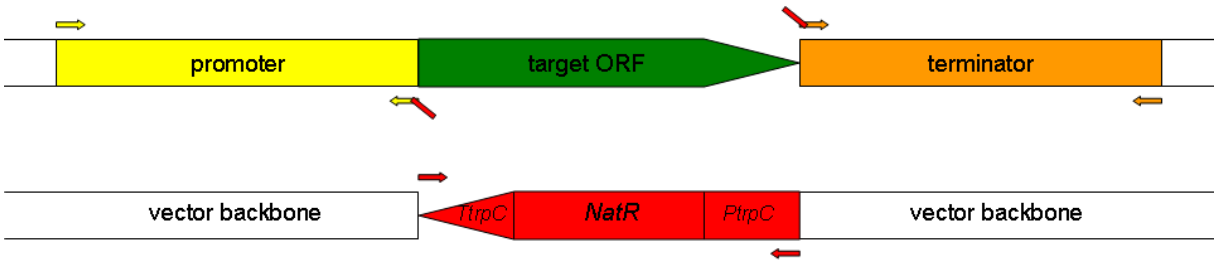

B. Generation of a deletion cassette on NatR gene as a template with left and right flank as primers

C. Amplification of the deletion cassette with nested primers

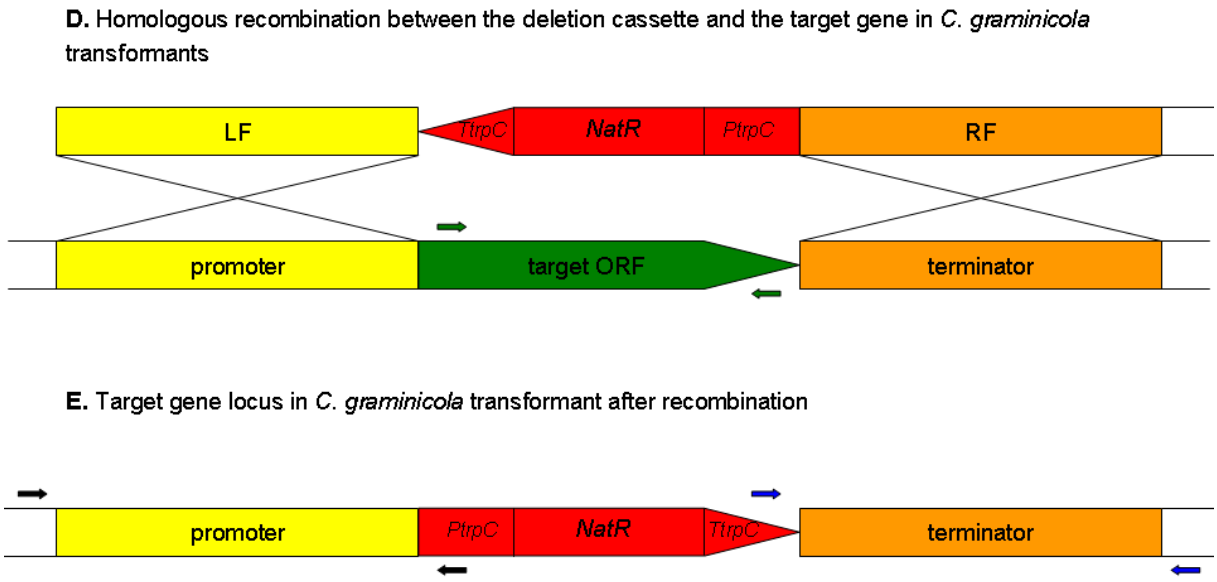

Fig. 3. Schematic overview of deletion cassette generation and disruption of target gene open reading frame (ORF) through homologous recombination.
(A) Promoter (left flank in a deletion cassette, LF) and terminator (right flank in a deletion cassette, RF) regions of a target gene were amplified with KO_[gene name]_LF_F/R and KO_[gene name]_ RF_F/R primers respectively (represented as yellow and orange arrows), containing 25-nucleotide overhang (represented as a red portion of the respective primer) complementary to the resistance gene. Nourseothricin N-acetyl-transferase gene (*NatR*) was amplified with clonat_probe_F/R primers. The deletion cassette was generated through PCR on *NatR* gene as a template and with left and right flank as primers (B) and amplified with nested primers KO_[gene name]_nested_F/R (represented as yellow and orange dashed lines (C). The deletion cassette was eventually transformed to protoplasts of *C. graminicola* as linear DNA and the disruption of the target ORF by homologous recombination event was verified with primers [gene name]_KOcheck_F/R (green arrows) amplifying target ORF (D) and with primers KO[gene name]_LFcheck_F/R (black arrows) and KO[gene name]_RFcheck_F/R (blue arrows), amplifying left and right flank respectively (E). Primers used were compiled in Table 1.

2.2.5 Biochemical methods

2.2.5.1 Quantitation of glycogen

C. graminicola conidia ($2x10^6$) were harvested from two weeks old cultures from oatmeal agar plates (see chapter 2.2.2.1) with Milli-Q water, centrifuged in a microcentrifuge for 3 minutes at 2,000 rpm and the condia pellet was resuspended in 400 µl of 20% (w/v) potassium hydroxide. Glycogen was extracted as described in Gunja-Smith et al., 1977. In brief, samples were boiled for 1 hour at 99°C and cooled on ice afterwards. Twenty µl of 1 M potassium phosphate buffer pH 7.2 was added and pH of the sample was adjusted with 5 N hydrochloric acid to pH 6-7. Samples were then mixed with two volumes of 100% ethanol and centrifuged in a microcentrifuge for 13,000 rpm for 15 min. Afterwards, samples were washed 3 times with 1 ml of 67% ethanol and centrifuged as in the previous step. The glycogen pellet was dried for 5 min at 37°C and resuspended in 600 µl of Milli-Q water.

Glycogen was quantified via the determination of glucose monomers, which were released upon enzymatic glycogen breakdown. For this purpose pH, of the samples was adjusted to pH 5.5 – 6 with 0.1 M sodium acetate buffer pH 6.0. Per sample, 7.3 U of α-amylase and 5 U of amyloglucosidase, both dissolved in 50 µl of 0.1 M sodium acetate buffer pH 5.5, were added. The samples were incubated over night at room temperature and the reaction was stopped by incubation for 10 min at 95°C and sample was centrifuged for 5 min at 13,000 rpm in a microcentrifuge. Glucose quantity was determined as described in chapter 2.2.5.2.

2.2.5.2 Quantitation of soluble sugars and starch

Soluble sugars were extracted from maize leaf segments (30-50 mg) twice with 1 ml of 80% ethanol for 20 minutes at 80°C. Combined ethanol extracts were dried in a vacuum concentrator and were redissolved in 400 µl Milli-Q water and subjected for soluble sugars quantitation (see below). The extracted leaf segments were homogenised in 0.2 M KOH with a homogeniser (RZR1; Heidolph, Schwabach) and incubated for 45 minutes at 95°C to solubilise starch. Afterwards, the pH value of the sample was adjusted to 5.5 with 1 M sodium acetate and subjected for enzymatic starch hydrolysis with 7.3 U of amylase and 5 U of amyloglucosidase at room temperature overnight. The following day, samples were incubated at 95 ºC for 10 minutes to stop the reaction and centrifuged in a microcentrifuge 5 minutes at 13,000 rpm to separate the glucose-containing supernatant from the leaf debris.

Glucose, fructose and sucrose quantity was determined spectrophotometrically in 10 µl of ethanol extract in a total reaction volume of 200 µl in a microtiter plate (BioTek, Bad Friedrichshall) as described by Bergmeyer, 1972. Starch quantity was determined as glucose content (as described above) in 5 µl of the extract from ethanol-insoluble fraction.

2.2.5.3 Quantitation of amino acids

Ethanol extracts from maize leaves segments (the same as for soluble sugar measurements – see chapter 2.2.5.2) were used for quantitation of amino acids. Per sample 10 µl of extract were derivatised with the fluorescent dye AQC (6-aminoquinolyl-N-hydroxysuccinimidylcarbamate) (Mohammad Hajirezaei, IPK Gatersleben) and the contents of free amino acids were determined on a Dionex Summit HPLC system as describe by Cohen and Mischaud; 1993 and Abbasi et al., 2009.

2.2.5.4 Quantitation of glutathione

Maize leaves were ground in liquid nitrogen with mortar and pestle. Aliquots of 50 mg were extracted in 0.1 M HCl according to Abbasi et al., 2009. To determine total and oxidised glutathione, 50 µl of extract was used for quantitation. To evaluate total glutathione content, extracts were first reduced with dithiothreitol and derivatised with monobromobimane to fluorescent derivates, which were separated and quantified by HPLC. To measure oxidised glutathione content, reduced thiol groups were first blocked irreversibly with N-ethylmaleimide, so that only oxidised form was further derivitised with dithiothreitol and monobromobimane. The quantity of total and oxidised glutathione was determined on a Dionex Summit HPLC system as described by Abbasi et al., 2009.

2.2.5.5 Quantitation of ascorbate

Maize leaves were ground in liquid nitrogen and 50 mg aliquots were used for extraction with 1.1 ml of sulfosalicylic acid. Ascorbate was quantified spectrophotometrically as decribed by Law et al., 1983. The assay is based on the reduction of Fe^{3+} (provided as $FeCl_3$) to Fe^{2+} by ascorbic acid in acidic solution, by adding trichloroacetic acid. Fe^{2+} forms coloured complexes with provided bipyridyl, which can be measured spectrophotometrically at a wavelength of 525 nm. To determine total and reduced ascorbate, 200 µl of extract was used for derivatisation and quantitation. To measure total ascorbate content, extract containing ascorbate and dehydroascorbate (oxidised form of ascorbate) was first reduced with dithiothreitol. Excess of dithiothreitol was removed by adding N-ethylmaleimide and extract was afterwards subjected for the spectrophotometric assay.

2.2.5.6 Quantitation of phosphorylated intermediates and organic acids

Maize leaves were ground with liquid nitrogen and 50 mg aliquots were subjected for extraction with mortar and pestle in 500 µl of ice-cold 1 M perchloric acid. Extract was transferred to a tube. The mortar and pestle were rinsed with 500 µl of cold 0.1 M perchloric acid and the two extracts were combined. Samples were centrifuged for 2 min at 4°C and 13,000 rpm in a microcentrifuge. Supernatants were neutralised with 2x 25 µl of 5 M K_2CO_3 and incubated for 1h on ice. Perchlorate was precipitated by centrifuging (as before). Supernatants were transferred to fresh tubes and stored at -80°C for further use.

Directly before measurements of the metabolites content, 200 µl aliquots of extracts were filtered with AcroPrep™ Omega 10K filter plates (Pall Corporation, East Hills, USA) according to manufacturer's protocol. Phosphorylated intermediates and organic acids were quantified in 10 µl aliquots of the filtered extracts on an ICS3000 HPLC System (Dionex) connected to a QTrap 3200 Triple-Quadrupole mass spectrometer with turboV ion source (Applied Biosystems). The HPLC System consisted of a guard column AG11HC (2x 50 mm, Dionex) and a series of two IonPac AS11HC columns (2x 250 mm, Dionex). The elution gradient was generated by mixinig water (eluent A) and 100 mM KOH (eluent B) at a flow rate of 0.25 ml/min for 80 min and column temperature 35°C according to the following programme:

Time	Eluent A	Eluent B
0-1 min.	96%	4%
1-6 min.	85%	15%
6-12 min.	91%	19%
12-22 min.	80%	20%
22-24 min.	77%	23%
24-27 min.	65%	35%
27-37 min.	62%	38%
37-39 min.	55%	45%
39-71 min.	0%	100%
71-80 min.	96%	4%

Ion scans were performed in ranges 87-606 and 59-385 of mass-to-charge ratio for precursor and product ions respectively. The electrospray ionization source was adjusted to -4,500 eV at 600°C. Nitrogen gas pressure values were as follows: 20 p.s.i. for curtain gas and gas 2, 30 p.s.i. for gas 1 and "medium" for collision gas. Dwell time for ions was set to 75 ms and scan time per cycle to 3.7 s. The system was controlled by combination of Chromeleon VS 6.8, DCMS-Link VS1.1 (both Dionex) and Analyst 1.4.1 (Applied Biosystems) software. Metabolite contents were calculated based on standard solutions.

2.2.5.7 Evaluation of hydrogen peroxide formation in the elicited leaf explants

Arabidopsis leaves were cut into small pieces (2-2.5 mm^2) and five explants per sample were incubated floating on water over night in the dark. Afterwards, water was replaced with 195 µl of assay buffer solution (0.02 mM luminol (5-amino-2,3-dihydro-1,4-

phthalazinedione); 1 mM sodium hydroxide; 0.02 U/ml horseradish peroxidase) and 5 µl of 200 mM phosphate buffer pH 8.0. The background luminescence was measured with a Bechthold luminometer in a white microtiter plate (BioTek, Bad Friedrichshall) for 5 min in 30 sec intervals with maximum gain settings and no absorbance filter. To elicit H_2O_2 production, flg22 (kindly provided by PD Dr. Frederik Börnke, Lehrstuhl für Biochemie, Erlangen) peptide was added to a final concentration of 1 µM and the luminescence was recorded in thirty second intervals for 30-40 mins. Maximal luminescence value was identified for each sample. Mean maximal luminescence was calculated from 3 technical replicates for each biological replicate.

2.2.5.8 Measurement of enzyme activities

Conidia of *C. graminicola* for the extraction of enzyme activities were grown for two weeks on oatmeal agar plates (see chapter 2.2.2.1) with and without 2% glucose, inoculated with $2x10^4$ conidia in 20 µl of Milli-Q water. Conidia ($1x10^6$) were harvested as described in chapter 2.2.5.1, sonicated in 500 µl of extraction buffer (50 mM Hepes/KOH pH 7.0; 5 mM $MgCl_2$; 0.5 mM EDTA; 0.5% (v/v) Triton X-100) for thirty seconds and centrifuged in a microcentrifuge for thirty seconds at 13,000 rpm. The enzyme-containing supernatant was diluted with glycerol to a final glycerol concentration of 50% (v/v). For the extraction of pyruvate kinase, PEP carboxykinase and NADP malic enzyme, dithiothreitol was added to the extraction buffer to a final concentration of 5 mM. Enzyme activities were determined spectrophotometrically at a wave length of 340 nm in 200 µl of assay buffer (see Table 4 for the individual composition) in a microtiter plate reader (BioTek, Bad Friedrichshall) and were measured as the change in absorbance. The measurements were performed with 5 µl (for pyruvate kinase, GAPDH, UGPase) or 10 µl (for the other enzymes) of extract in two replicate reactions including the substrates: glucose (for hexokinase), PEP (for pyruvate kinase and PEP carboxykinase), fructose-1,6-bisphosphate (for fructose-1,6-bisphosphatase), isocitrate (for isocitrate lyase), 3-PGA (for GAPDH), UDP-glucose (for UGPase) and L-malate (for NADP malic enzyme), and one control replicate each, in which the respective substrates were omitted.

Table 4. Composition of assay buffers for spectrophotometrical measurements of enzyme activities.

	Hexo-kinase	**Pyruvate kinase**	**Fructose -1,6-bis-phospha-tase**	**Isocitrate lyase**	**PEP carboxy-kinase**	**GAPDH**	**UGPase**	**NADP malic enzyme**
Hepes/ KOH pH 7.5	100 mM	50 mM	100 mM	50 mM	100 mM	80 mM	100 mM	80 mM
ATP	2 mM					5 mM		
ADP		2 mM			10 mM			
NAD^+	0.8 mM							0.6 mM
$NADP^+$			0.06 mM				0.3 mM	
NADH		0.2 mM		0.5 mM	0.32 mM	0.2 mM		
$MgCl_2$	5 mM	10 mM	5 mM	5 mM	16 mM	10 mM	5 mM	10 mM
KCl		50 mM						
$KHCO_3$					35 mM			
EDTA			1 mM					
3-PGA					1.6 mM	4 mM		
PPi							1 mM	
DTT		2 mM			1 mM			2 mM
BSA		0.2 mM						
G6PDH	1 U		1 U					
LDH		2.8 U		45 U				
PGI			5 U					
PGK					2 U	20 U		
GAPDH					2 U		5 U	
PGM							5 U	
glucose	5 mM							
PEP		2 mM			5 mM			
F16BP			1 mM					
isocitrate				4 mM				
UDP-Glc							0.8 mM	
L-malate								25 mM

2.2.6 Physiological methods

2.2.6.1 Photosynthetic performance measurements

Photosynthetic parameters: effective and maximum photosystem II quantum yield (Y(II) and Fv/Fm respectively), electron transport rate (ETR) and non-photochemical quenching (NPQ) were evaluated with a combined infrared gas exchange/chlorophyll fluorescence imaging system (GFS-3000 and MINI-Imaging-PAM Chlorophyll Fluorometer, Heinz Walz GmbH, Effeltrich). Infected leaves were dark adapted for 20 min and then placed in the cuvette (24x32 mm) of the device. A saturation pulse was applied to determine maximal fluorescence ($Fv/Fm_)$. Afterwards, absorptivity was measured by illuminating the sample first with red (R=660 nm) and then with near infra-red (NIR=780 nm) light and R- and NIR-images were recorded. Finally, the leaf was illuminated with 400 μE m^{-2} s^{-1} of actinic

light and chlorophyll fluorescence was determined by applying saturated light pulses every 60 s. Ambient CO_2 and H_2O concentration were set to 350 ppm and 10,000 ppm respectively, temperature to 28°C. Measurements were continued until yield of PSII has reached its maximum. Y(II) and Fv/Fm were calculated as described in Genty et al. (1989) and NPQ as in Bilger and Bjorkman (1990). ETR was calculated as:

ETR = Y(II) x PFD x 0.5 x Absorptivity

with PFD (photon flux density) = 400 μE m^{-2} s^{-1}. Absorptivity was calculated as Abs = 1-R/NIR, where R was a signal density for reflected red light (R) and NIR – signal density for reflected near infra-red light (NIR).

2.2.6.2 Respiration measurements

2.2.6.2.1 Respiration measurements of maize leaves

Respiration rate was evaluated with a combined infrared gas exchange/chlorophyll fluorescence imaging system (GFS-3000 and MINI-Imaging-PAM Chlorophyll Fluorometer, Heinz Walz GmbH, Effeltrich). Infected leaves were dark adapted for 12 hours and then placed in the cuvette (24x32 mm) of the device covered with aluminium foil. Ambient CO_2 and H_2O concentration were set to 350 ppm and 10,000 ppm respectively, temperature to 24°C. Measurements were continued for ca. 1 h in the dark until respiration rates were stable.

2.2.6.2.2 Respiration measurements on Arabidopsis leaves

Harvested Arabidopsis leaves were cut into 1 mm wide strips (approx. 70-80 mg) and incubated in 3 ml of assay buffer (see below) in the dark for 10 min, to get rid of wound-induced respiration

assay buffer	
10 mM	Tricine
0.2 mM	$CaCl_2$ pH 7.0

Total leaf respiration (oxygen uptake) was recorded in 3 ml of fresh assay buffer using Clark-type oxygen electrode (Hansatech Instruments, Pentney, Norfolk, UK) darkened with the aluminium foil. After 20 min, potassium cyanide was added to a final concentration of 2.5

mM to assess alternative respiration. After the next 20 min, salicylhydroxamic acid was added to a final concentration of 10 mM and records were conducted for 20 min to assess residual respiration.

2.2.6.3 Hormone treatment

Hormone treatments were performed with 1 mM jasmonic acid (JA) (Biomol GmbH, Hamburg), 1.3 mM of the SA analogue 2,6-dichloroisonicotinic acid (INA), and 5 mM of the ethylene precursor 1-aminocyclopropane-1-carboxylic-acid (ACC). Fourth leaves of two weeks old maize plants were cut submerged in Milli-Q water and incubated in 15 ml 0.2% ethanol containing the indicated hormone concentrations or Milli-Q water for mock controls. Leaves were collected after 0, 10 or 24 h of treatment, frozen immediately in liquid nitrogen and subjected for RNA extraction (see chapter 2.2.4).

2.2.6.4 Abiotic stress assay

Maize plants were grown with regular watering to 100% soil capacity every other day. Three weeks old plants were subjected to drought and high salinity by withholding water or continuing irrigation with 200 ml of 200 mM sodium chloride for one week, respectively. Mock-treated plants were watered as before. After one week of stress treatment, all leaves of each plant were harvested, pooled and subjected to RNA extraction (see chapter 2.2.4).

2.2.7 Microarray analysis

For transcript profiling, the microarray data described by Voll et al., 2011 was employed. Transcriptome data from *C. graminicola*-infected leaves were obtained by Gunther Döhlemann (MPI Marburg) und Jörg Kämper (TU Karlsruhe) with Genechip® Maize Genome Array (Affymetrix, Santa Clara, USA). The experiment was performed in three biological replicates, using standard Affymetrix protocols (Midi Euk2V3 protocol on GeneChip Fluidics Station 400; scanning on Affymetrix GSC3000). Expression data were deposited in the Gene Expression Omnibus (http://www.ncbi.nlm.nih.gov/geo/), with the accession number GSE31188. Transcriptome data were analysed using Affymetrix Micro Array Suite 5.1, bioconductor (http://www.bioconductor.org/) and dChip1.3

(http://biosun1.harvard.edu/complab/dchip/), as described by Eichhorn et al., 2006. Changes greater than twofold with a corrected P-value <0.001 were considered as significant.

2.2.8 Phylogenetic analyses

Maize sequences were downloaded from http://www.maizesequence.org (Release 5b.60) and from the Grassius Grass Regulatory Information Server (http://www.grassius.org/index.html). Arabidopsis sequences were obtained from the Arabidopsis Information Resource (TAIR) (http://www.arabidopsis.org/) and rice sequences were downloaded from GreenPhylDB (http://greenphyl.cirad.fr/v1/cgi-bin/greenphyl.cgi).

Multiple alignments of protein sequences were performed with the program ClustalW 2.0 (Thompson et al., 1994) and phylogenetic trees were build using the UPGMA method implemented in the program Geneious Pro 5.4.3 (Drummond et al., 2011) with 100 replicates for bootstrap assessment. Protein sequences were screened for common motifs with MEME Multiple Em for Motif Elicitation (http://meme.sdsc.edu/meme/cgi-bin/meme.cgi) (Bailey and Elkan, 1994).

2.2.9 Statistical data analyses

All statistical data analyses were performed with a two-tailed, unpaired Student's t-test (p-value < 0.05) available within Microsoft Excel programme.

Cluster analysis of metabolites and differentially regulated maize transcripts was performed with Cluster 3.0 (similarity metric – Spearman Rank Correlation) (de Hoon et al., 2004) and displayed with TreeView programme (Page, 2002).

3 RESULTS

3.1 Identification and characterisation of *C. graminicola* pathogenicity mutants

3.1.1 Pathogenicity mutants of *C. graminicola* – evaluation of virulence

C. graminicola T-DNA insertion mutants were used to study the infection process on the functional level in order to identify novel virulence factors. Insertion mutants were generated by *Agrobacterium tumefaciens*-mediated transformation and screened for reduced virulence (Münch et al., 2007 and 2011). Two independent transformants AT399 and AT416, that prove to be apathogenic when tested on detached maize leaves by S. Münch (Martin-Luther University Halle-Wittenberg, Table 5), have been re-examined in the frame of this thesis on living plants by a spray inoculation assay. Both strains exhibited strongly reduced virulence and were affected already at the early stages of development (Fig. 4 and 5). Germination rate, appressoria formation and melanisation rates were reduced when compared to the wild type strain CgM2. No penetration structures of mutant strains could be observed at both analysed time points, i.e. during the biotrophic phase at 24 hpi and in the early necrotrophic phase at 72 hpi.

Table 5. Development of infection structures of *C. graminicola* mutants AT399 and AT416 compared to the wild type (WT) strain CgM2. Infection assays were performed by droplet inoculation on detached maize leaves cv. Nathan (data provided by S. Münch, Martin-Luther University Halle-Wittenberg). Infection structures are given as a percentage of the preceding structure at 24 and 72 hpi (hours post infection).

Rate of	24 hpi			72 hpi		
	WT	**AT399**	**AT416**	**WT**	**AT399**	**AT416**
germination	68%	35%	49%	85%	49%	49%
appressoria formation	95%	23%	7%	99%	48%	7%
appressoria melanisation	95%	10%	33%	97%	76%	33%
penetration	4%	0%	0%	81%	1%	0%

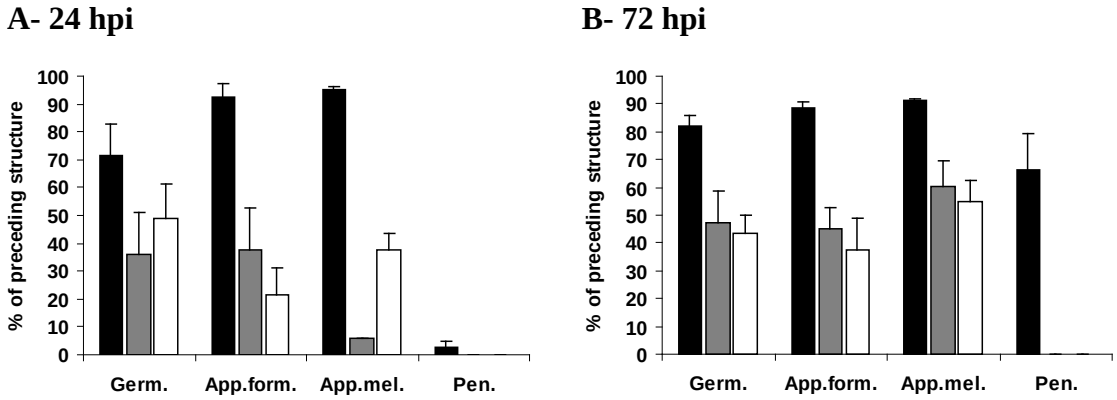

Fig. 4. Development of the infection structures of two *C. graminicola* mutants AT399 (grey bars) and AT416 (white bars) compared to the wild type strain CgM2 (black bars). Infection assays were performed on living, two-weeks old, maize plants (cv. Nathan) by spray-inoculation (titer $2x10^6$ conidia / ml). Infection structures are given as a percentage of the preceding structure. Data are shown as mean values with standard deviation as error bars (n=8). Germ.: germination rate, App. Form.: appressoria formation rate ; App. Mel.: appressoria melanisation rate , Pen.: penetration rate.

Fig. 5. Phenotype of maize leaves (cv. Nathan) infected with wild type *C. graminicola* CgM2 and two mutant strains AT416 and AT399 six days after spray-inoculation with a fungal titer of $2x10^6$ conidia / ml.

Moreover, microscopic observation revealed that both mutant strains induced specific plant defence responses i.e. formation of callose papilla beneath the appressoria, which most probably prevented the penetration of the fungus into the host cells and was reflected by lack of penetration events. Compared to the wild type strain CgM2, where only 8% of all appressoria induced weak papilla formation, 32% and 29% of AT399 and AT416 appressoria, respectively, elicited strongly fluorescent papilla (Fig. 6 and Fig. 7). Thus, these two mutants may serve as a good model to study the induction of host defence responses during early stages of the *C. graminicola*-maize interaction.

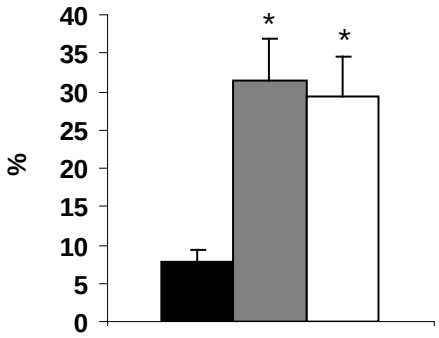

Fig. 6. Induction of papilla formation by *C. graminicola* mutant strains AT399 (grey bars) and AT416 (white bars) appressoria compared to wild type CgM2 appressoria (black bars). Number of appressoria accompanied by papilla is presented as percentage of total number of appressoria observed at 2.5 days after dip-inoculation of maize plants (cv. Nathan) into a conidia solution with a titer of $2x10^6$ conidia / ml. Mean values are shown (n=8). Asterisks indicate a significant difference (t-test, p-value < 0.05) to the wild type CgM2 appressoria. Error bars represent the standard error.

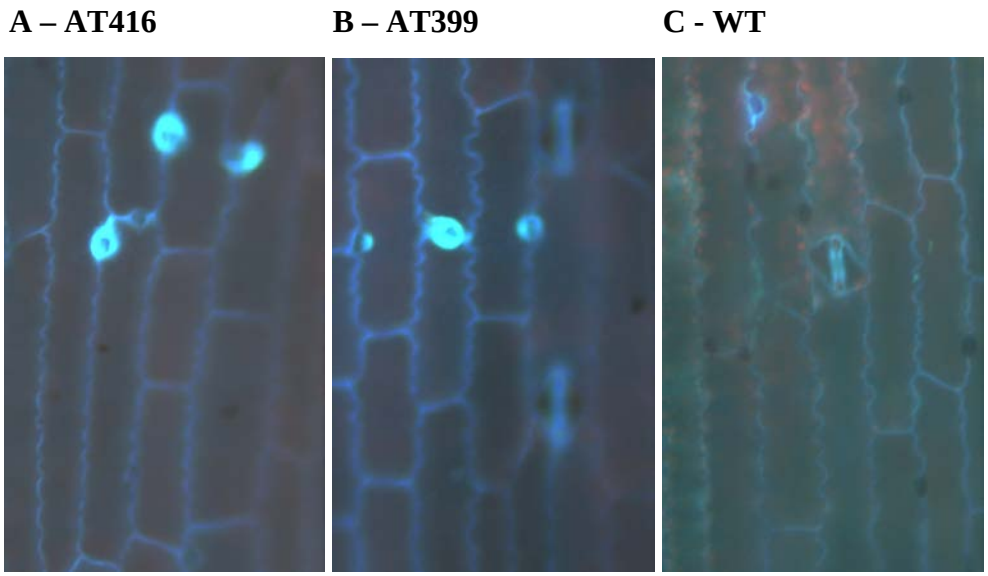

Fig. 7. Papilla (seen as autofluorescent spots) formation underneath appressoria (visible as black dots) of *C. graminicola* mutant strains AT416 and AT399 and wild type (WT) strain CgM2 at 5 dpi. Maize plants (cv. Nathan) were spray-inoculated with a conidia titer of $2x10^6$ conidia / ml . Magnification - 200x.

To further confirm the reduced virulence of mutant strains *on planta*, the photosynthetic performance of infected leaves was followed from 4 dpi to 6 dpi. Compared to mock-treated control leaves, a decrease of effective PSII quantum yield (Y(II)) and electron transport rate (ETR) was typically observed within a distance of 250 µm to anthracnose lesions on leaves inoculated with the wild type strain CgM2 (Fig. 8A, 8B and Fig. 9). At these sites, nonphotochemical quenching (NPQ) was increased, which is a measure for absorbed light energy that is dissipated in the antenna complexes and that cannot be utilised for photosynthesis (Fig. 8C). However, these effects on the photosynthetic performance were

not observed at a distance greater than 250 µm to the anthracnose lesions of CgM2 wild type infected leaves (Fig. 8 and 9). Interestingly, a decline of the effective PSII quantum yield was less pronounced in the leaves inoculated with the mutants AT416 and AT399 compared to the leaves infected with the wild type strain CgM2 and was observed only at the later stages of the infection, i.e. 6 dpi (Fig. 8). These data demonstrate that level of virulence of these *C. graminicola* strains correlates with decline in effective PSII quantum yield and electron transport rate and allows for evaluation of the fungal pathogenicity via chlorophyll fluorescence measurements.

A – Y(II)

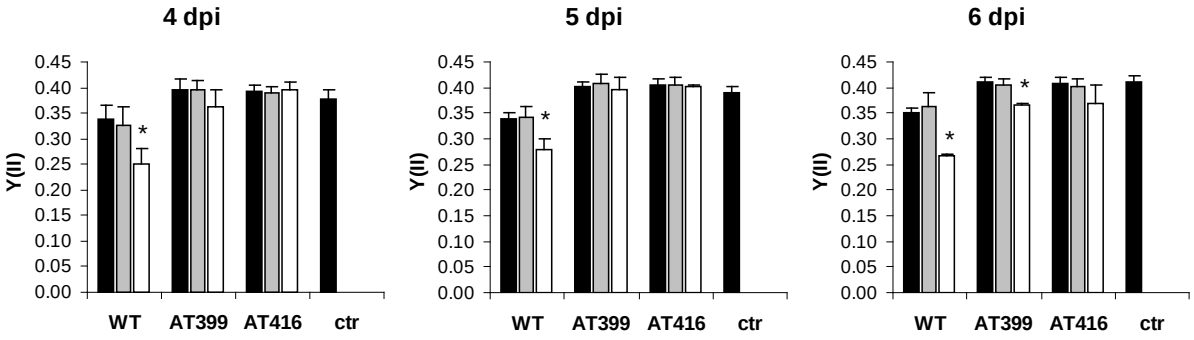

B - ETR

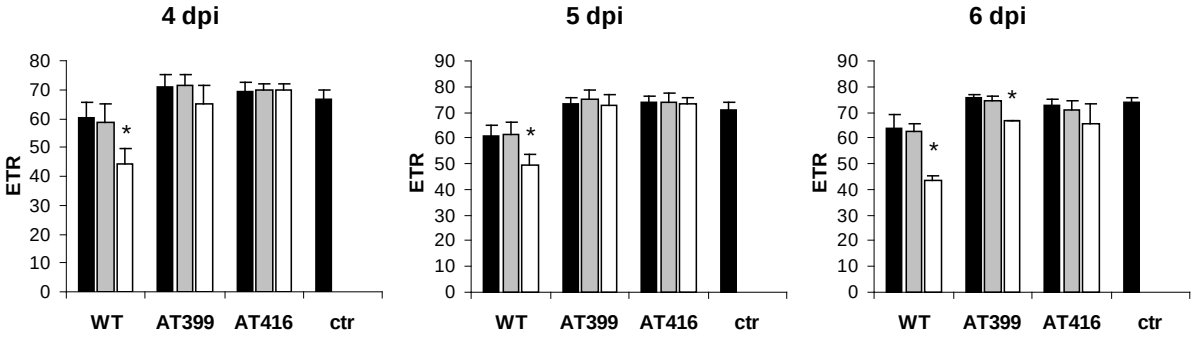

C – NPQ/4

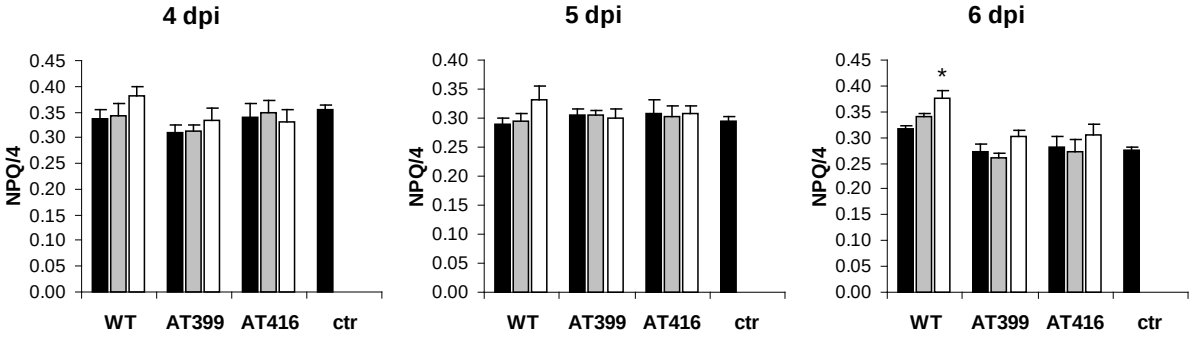

Fig. 8. Effective PSII quantum yield (A), electron transport rate (B) and nonphotochemical quenching (C) in spray-inoculated maize leaves cv. Nathan at 4-6 dpi (titer $2x10^6$ conidia / ml). WT – leaves infected with wild type *C. graminicola* CgM2, AT399/AT416 – leaves infected with the respective ATMT mutant strain, ctr – mock-treated control leaves. Mean values are shown (n=4), which represent the healthy area of the leaf (black bars), the area remote to the lesion at a distance > 250 µm (grey bars) and the area adjacent to the lesion at the distance < 250 µm (white bars). Asterisks indicate a significant difference (t-test, p-value < 0.05) to the healthy area of the respective leaf. Error bars represent the standard error.

A – 4 dpi

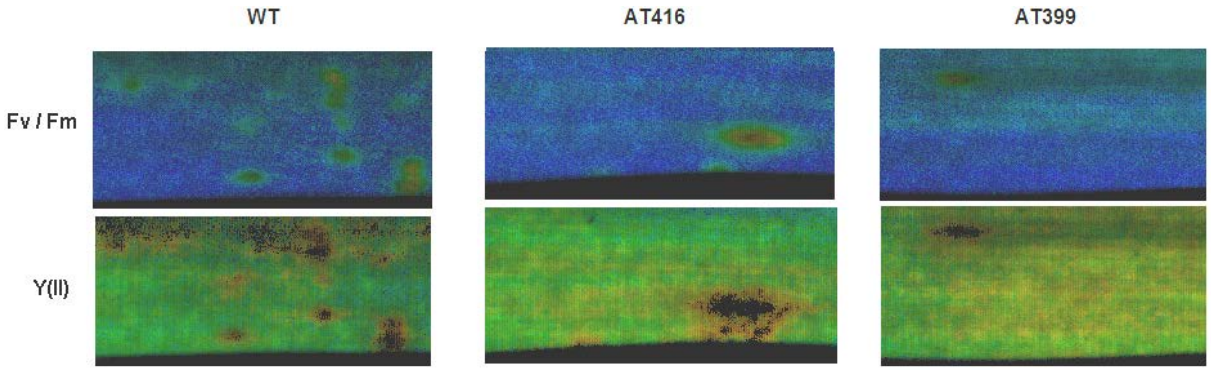

B – 5 dpi

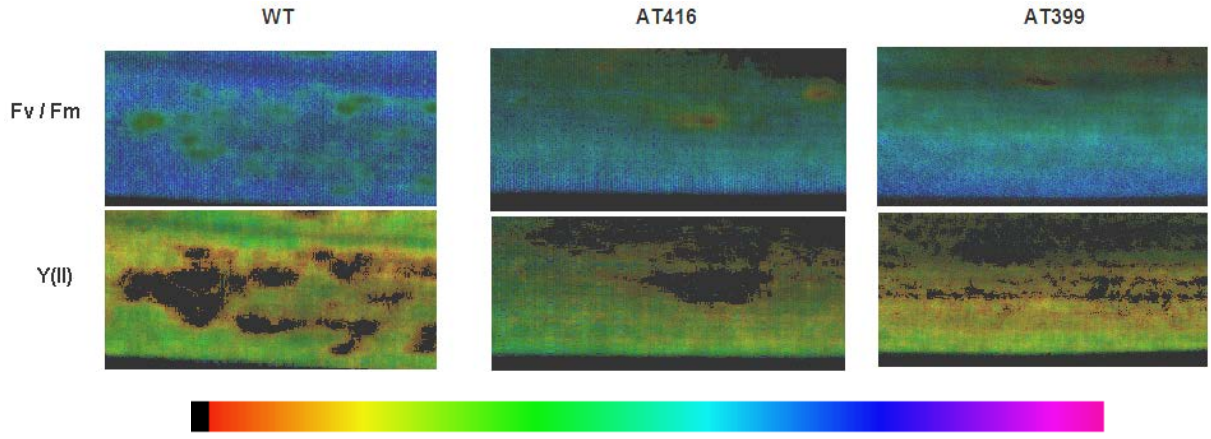

Fig. 9. Photosynthetic performance of maize leaves cv. Nathan at 4 (A) and 5 (B) days after spray-inoculation with a conidia titer of $2x10^6$ conidia / ml , measured as maximum (Fv/Fm, upper panels) and effective (Y(II) PSII, lower panels) quantum yield; Fv/Fm and Y(II) images represent the same area of the leaf. The false colour scale ranging from black (0, left end) to pink (1) is depicted at the bottom. WT – leaves infected with wild type *C. graminicola* CgM2, AT399/416 – leaves infected with the respective ATMT mutant strain.

3.1.2 Partial re-screening of the collection of *C. graminicola* ATMT mutants

Some of *C. graminicola* ATMT mutants exhibited reduced pathogenicity on detached leaves but not on living plants when tested by S. Münch (Martin-Luther University Halle-Wittenberg). In the frame of this thesis 6 genotypes from this subgroup were re-screened on

living plants in order to identify mutants that are only weakly affected in pathogenicity, which makes them especially interesting for further experiments that aim at investigating compatibility. Plants were spray-inoculated with a titer of $2x10^6$ conidia / ml and disease symptoms were scored at 8 dpi due to the following classification into five groups:

- group I: no symptoms,
- group II: small lesions (size up to 0.5 cm),
- group III: some big lesions (up to 5 lesion per leaf, size > 0.5 cm),
- group IV: many big lesions (more than 5 lesion per leaf, size > 0.5 cm),
- group V: necrosis of the leaf (more than 50% of leaf area).

In a first experiment, three mutant strains were tested: AT176, AT177 and AT633 together with wild type *C. graminicola* CgM2 as a reference, using 10 plants per genotype. Phenotypes of infected leaves are summarized in Fig. 10A and Fig. 11A. All three mutant genotypes showed reduced pathogenicity, compared to wild type strain CgM2. The strain AT633 was most strongly reduced in virulence, as none of the infected leaves exhibited severe disease symptoms (group IV or V). In a second experiment, three other mutant strains were tested: AT036, AT263 and AT286, using 14 plants per genotype. The strain AT286 exhibited only a slightly reduced pathogenicity; the two other mutant strains, AT263 and AT036, were more strongly affected than AT286, if the number of plants with the weakest symptoms (group II) is considered (Fig. 10B and 11B). The strains AT036, AT263, AT633 were selected and tested in a second round of infection experiments and the moderate reduction of virulence could be confirmed for all three strains (Fig. 12).

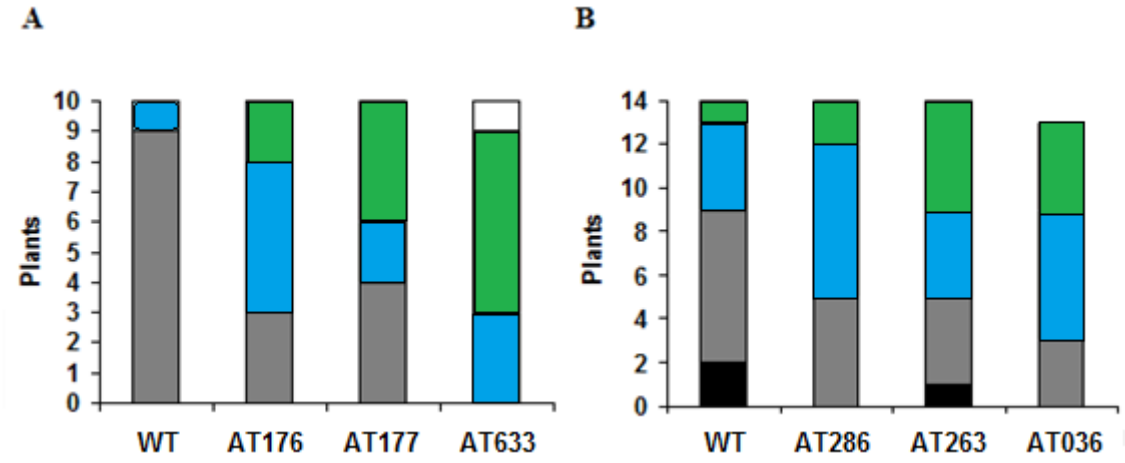

Fig. 10. Re-screening of the *C. graminicola* ATMT mutant collection for mutants with weakly reduced pathogenicity. Maize plants cv. Nathan were spray-inoculated with a conidia titer of $2x10^6$ conidia / ml and symptoms were scored at 8 dpi. White bars – group I: no symptoms, green bars – group II: small lesions (up to 0,5 cm), blue bars – group III: up to five big lesions (more than 0.5 cm) per leaf, grey bars – group IV: more than five big lesions (more than 0.5 cm) per leaf, black bars – group V: necrosis of more than 50% of leaf area. WT –

plants infected with wild type strain CgM2, ATxxx – plants infected with the respective ATMT mutant strain. Part A and B show results of two independent experiments.

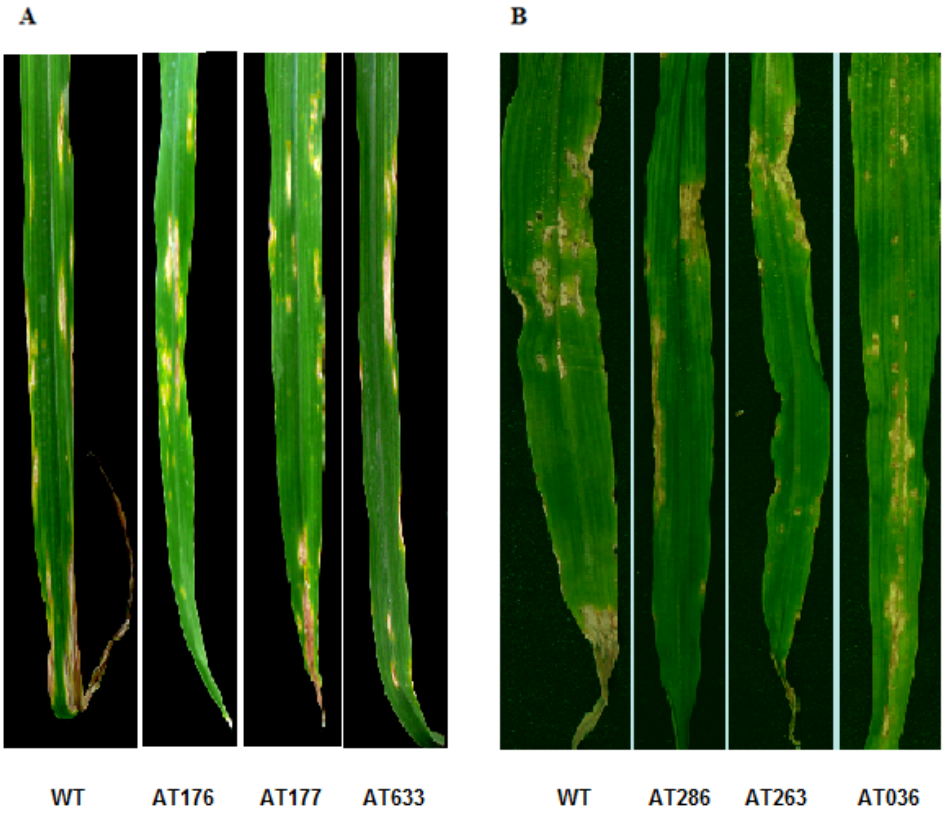

Fig. 11. Phenotype of the infected leaves (plants from the same experiments as presented in Fig. 10) classified into group III (up to five big lesions, greater than 0.5 cm, per leaf) in case of AT633 or in group IV (more than five big lesions, greater than 0.5 cm, per leaf) in case of other strains. Part A and B show results of two independent experiments.

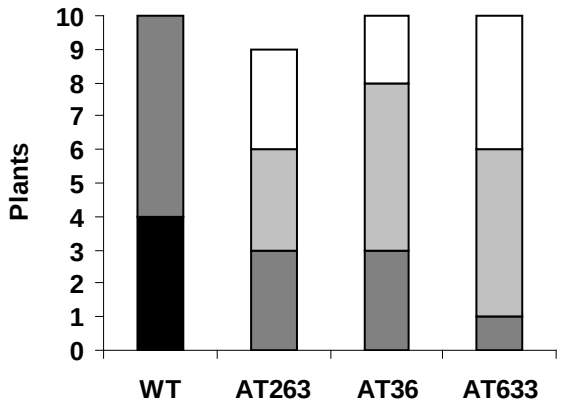

Fig. 12. Second re-screening of three *C. graminicola* ATMT mutants selected for weakly affected pathogenicity. Maize plants cv. Nathan were spray-inoculated with a fungal titer $2x10^6$ conidia / ml and symptoms were scored at 8 dpi. White bars –small lesions (up to 0.5 cm), grey bars – up to five big lesions (more than 0,5 cm) per leaf, dark grey – more than five big lesions (more than 0.5 cm) per leaf, black bars – necrosis of more than 50% of leaf area.

3.1.3 Identification of T-DNA integration sites of *C. graminicola* mutants

To identify T-DNA integration sites and the corresponding genes that are required for full pathogenicity, the selected fungal ATMT strains were subjected to GenomeWalker™ analysis. From the two virulence mutants AT399 and AT416 that had been selected by S. Münch (Martin-Luther University Halle-Wittenberg), the T-DNA integration site was already identified only for strain AT399. The T-DNA integration sites of the strains AT036, AT263, AT633, that were selected during the re-screening of the collection, were also unknown.

The exact characterisation of the integrated T-DNA fragment was conducted for each analysed mutant prior to the GenomeWalker™ procedure, as a truncation of the T-DNA or a read through across the left or right border can occur (personal communication with S. Münch). Genomic DNA of each mutant was subjected for PCR analysis (as described in Materials and methods chapter 2.2.4.7, see also Fig. 13) which revealed that most probably the entire T-DNA sequence had integrated into the genome of two strains, AT263 and AT633 (Fig. 14). In strain AT416, the right border of the T-DNA probably was missing, as no product was obtained with T-DNA amplicon #4, which is specific for the predicted right border of the T-DNA sequence (Fig. 15). The strain AT036 seems to have a T-DNA insertion truncated at the left border, as no product specific for the predicted left border sequence was obtained from the T-DNA specific amplicon #1. However, part of the vector DNA was integrated adjacent to the right border, as the product with amplicon #V, specific to the vector backbone sequence adjacent to predicted right border of T-DNA, was obtained (Fig. 15).

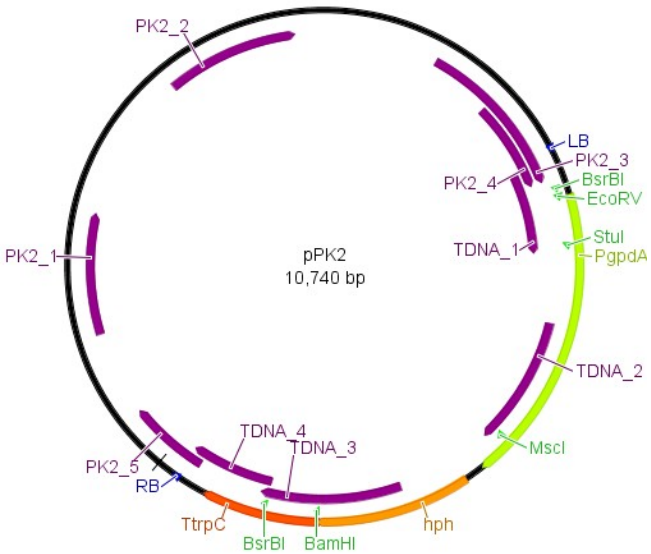

Fig. 13. Vector pPK2 used for *Agrobacterium tumefaciens*-mediated transformation of *C. graminicola*. T-DNA fragment contains *hygromycin B phosphotransferase* gene (hph) under the control of the *gpdA* promoter (PgpdA) and *TrpC* terminator (TrpC), conferring tolerance to hygromicin. The position of left (LB) and right border (RB) is marked. PK2_1-5 - amplicons specific for the pPK2 vector backbone, TDNA_1-4 - amplicons specific to the predicted T-DNA sequence (see Table 1 for primers used to generate the amplicons). Restriction sites of BsrBI, MscI, StuI and EcoRV, relevant for GenomeWalker™ strategy are labelled.

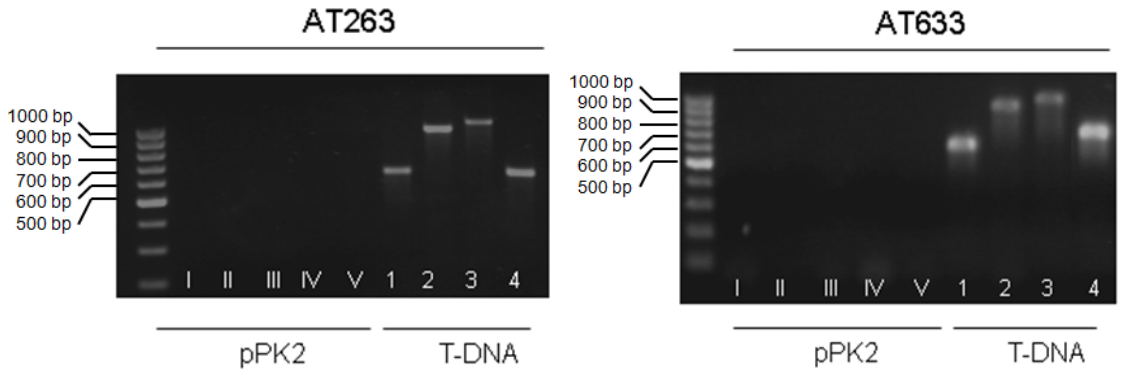

Fig. 14. Results of PCR analysis of pPK2 vector sequence integrated in the genome of *C. graminicola* mutant strains AT263 and AT633. Arabic numbers represent amplicons specific to the predicted T-DNA sequence (T-DNA_1-4 in Fig. 13), while roman numbers represent amplicons specific for the pPK2 vector backbone (PK2_1-5 in Fig. 13). Ladder – Gene Ruler™ 100 bp DNA ladder (Fermentas).

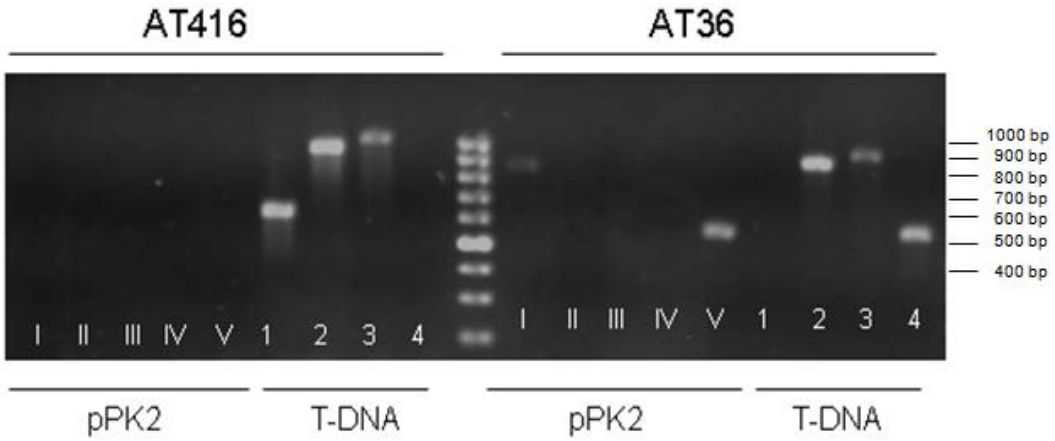

Fig. 15. Results of PCR analysis of pPK2 vector sequence integrated in the genome of *C. graminicola* mutant strains AT416 and AT36. Arabic numbers represent amplicons specific to the predicted T-DNA sequence (T-DNA_1-4 in Fig. 13), while roman numbers represent amplicons specific for the pPK2 vector backbone (PK2_1-5 in Fig. 13). Ladder – Gene Ruler™ 100 bp DNA ladder (Fermentas).

The analysis described above allowed to verify, which fragment of pPK2 vector had integrated into the genome of the individual ATMT mutants, however it was not possible to evaluate the number of distinct T-DNA fragments present in the genome as the obtained PCR products may have been amplified from more than one copy of T-DNA template. Thus, subsequent PCR analysis and Southern blot analysis of genomic DNA of each mutant was performed to determine the number of T-DNA insertions per genome. PCR analysis allowing to test for tandem T-DNA integrations was conducted with two primers, TDNA_1R binding

at the left border and TDNA_4F binding at the right border, facing outward direction from the T-DNA insertion (Fig. 16A). Such combination of primers could amplify the product only when two integrations "head-to-tail" (right border to left border) occurred (Fig. 16D). When using only the left border primer, TDNA_1R a product could be amplified in case of a "head-to-head" integration (Fig. 16C), while right border primer TDNA_4F only could produce a PCR fragment from "tail-to-tail" integrations (Fig. 16B). A specific product of a size around 900 bp was obtained only on genomic DNA isolated from the mutant AT416 during the PCR with left and right border primers, revealing that a tandem integration "head-to-tail" occurred in this mutant (Fig. 17).

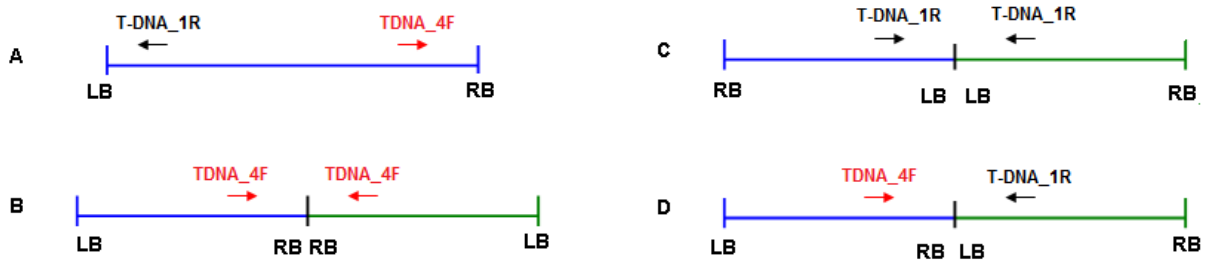

Fig. 16. Primer combinations to detect tandem T-DNA insertions. TDNA_1R specific for the left border (black arrow) and forward primer TDNA_4F specific for the right border (red arrow) were used to detect tandem T-DNA insertions in ATMT mutants in the situation if only one T-DNA integration occurred (A), two integrations "tail-to-tail" (B), two integrations "head-to-head" (C) and two integrations "head-to-tail" (D) occurred.

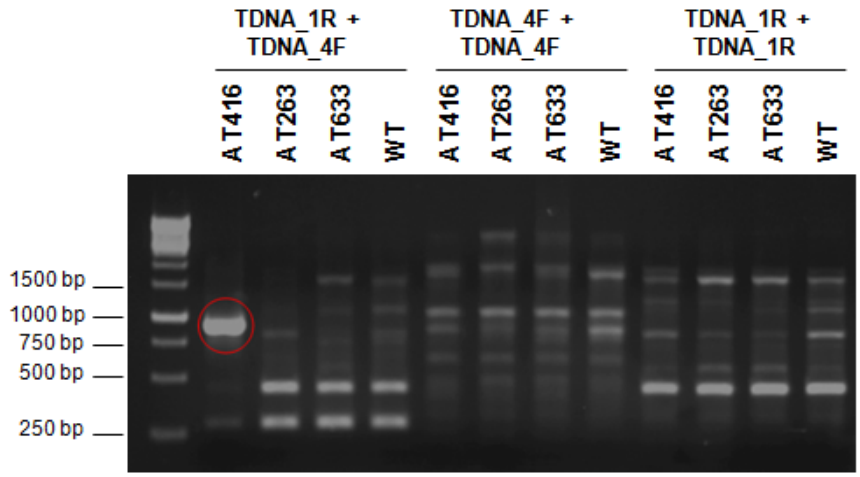

Fig. 17. PCR analysis on genomic DNA of *C. graminicola* insertion mutants: AT416, AT263, AT633 and wild type strain CgM2 (WT) as a control for primer specificity with left border TDNA_1R and right border TDNA_4F primers (see Fig. 16D), two right border TDNA_4F primers (see Fig. 16B) and two left border TDNA_1R primers (see Fig. 16C). The only specific product obtained was marked with a red circle. Ladder – Gene Ruler™ 1 kb DNA ladder (Fermentas).

A Southern blot analysis was conducted on genomic DNA digested with BamHI and hybridised with a hygromycin probe to investigate the number of T-DNA insertions per

genome. The position of the BamHI restriction sites and the probe binding site in the T-DNA are presented in Fig. 18. Based on the Southern blot results, one T-DNA insertion per genome occured in the mutants AT036, AT263, AT633, as only a single hybridisation signal was observed (Fig. 19). The sizes of hybridised bands are greater than the predicted distance of the BamHI restriction sites to the left border, so it can be assumed that the hybridised fragments also contain a portion of adjacent genomic DNA. For the strain AT416, hybridisation to two different fragments was observed, which is consistent with previous PCR analysis (Fig. 17) that suggested the presence of two concatemeric T-DNAs in the mutant genome. The presence of the second T-DNA fragment introduced one additional BamHI site (see Fig. 18B), at a distance of 4.12 kb to the BamHI site of the first T-DNA insertion, producing an additional signal in Southern blot analysis (Fig. 19). The other signal probably represents T-DNA insertion with part of adjacent genomic sequence.

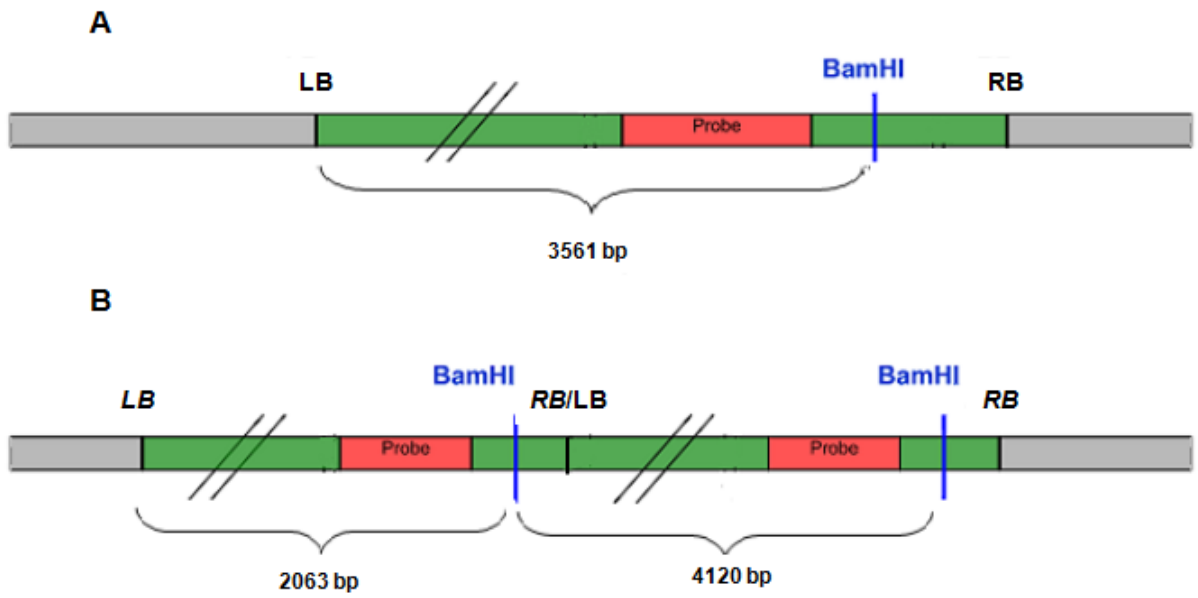

Fig. 18. Schematic view of T-DNA integration sites in the genome of *C. graminicola* insertion mutants AT263 and AT633 (A) and AT416 (B). Genomic sequence is marked with grey bars, T-DNA sequence with green bars, binding sequence of the hygromycin probe as a red bar, BamHI restriction sites are marked with blue lines. RB/LB – right/left border of T-DNA insertion. *LB*/*RB* – truncated borders in AT416: both right borders (labelled as *RB*) and outer left border (labelled as *LB*); as predicted by PCR analysis (Fig. 15) and sequencing of PCR products obtained during GenomeWalkter^{TM} analysis (see below). The inner left border (LB) is not truncated. Sizes of DNA fragments are based on PCR analysis shown in Figs. 15 and 17.

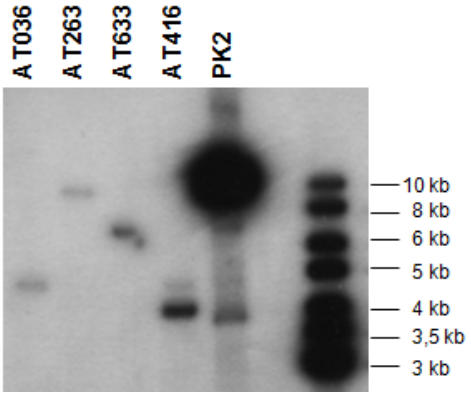

Fig. 19. Southern blot analysis of T-DNA copy number in the *C. graminicola* insertion mutants. Genomic DNA of mutant strains (AT036, AT263, AT633, AT416) was digested with BamHI and hybridised with hygromycin probe. As a positive control, the vector pPK2 digested with BamHI was used. M- 1 kb DNA ladder (PeqLab).

After estimating the number and the topology of T-DNA integration sites, a GenomeWalker™ analysis (Clontech) was conducted to sequence the T-DNA flanking sequences and to identify the insertion sites in the genome. In the first step of the GenomeWalker™ approach, genomic DNA is digested with blunt end cutters to produce DNA fragments containing T-DNA and genomic flanking regions. In the next step, fragments are ligated to adaptor molecules and are amplified by PCR using primers specific to T-DNA and adaptor sequence (Fig. 2 in Materials and Methods chapter 2.2.4.7.). The resulting PCR products consist of a part of T-DNA sequence and of the genomic region adjacent to the T-DNA, which can then be identified by sequencing.

Digestion of genomic DNA, ligation with an adaptor to create GenomeWalker™ libraries and subsequent two rounds of PCRs with primers binding to adaptor and T-DNA insertion were performed as described in Materials and Methods (chapter 2.2.4.7). As revealed by sequencing, PCR products (Suppl. Fig. 1) were specific and contained adjacent genomic sequence at the T-DNA junctions in case of AT263, AT633 and AT416. Sequencing of products obtained on the AT36 library revealed that they were amplified due to unspecific primer binding and it was not possible to identify the insertion site. For the mutants AT263 and AT633, products of the second nested PCR were sequenced, while products of primary PCR on GenomeWalker™ library created for AT416 strain were subjected for further analysis as the products obtained during nested PCR arose from unspecific primer binding. Sequencing of products generated on AT416 GenomeWalker™ library revealed not only that both right borders were truncated, as already indicated by PCR analysis (Fig. 15), but also that part of the outer left border was deleted, so that all binding sites for T-DNA specific GenomeWalker™ primers were missing on the left border side.

In summary, the genomic sequence adjacent to the right border in the genome of AT633, genomic sequence adjacent to the left border in the genome of AT416 and genomic sequence adjacent to the left and right border in the genome of AT263 were retrieved by the GenomeWalker™ approach. Retrieved genomic sequences were used for BLAST search against the *C. graminicola* genome, available at http://genome.jgi.doe.gov/pages/blast-query.jsf?db=Colgr1. This allowed for identification of T-DNA integration sites (Fig. 20 and 21).

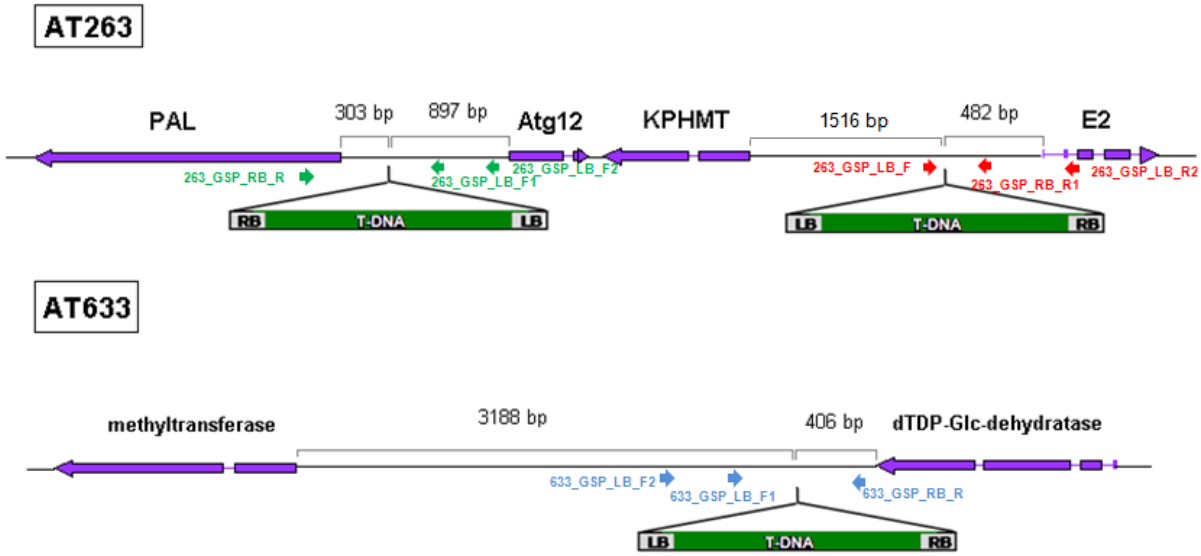

Fig. 20. Sketch summarizing the molecular characterisation of the T-DNA integration sites in *C. graminicola* insertion mutants: AT263 and AT633. Coding sequences are marked with purple bars/arrows (exons) and lines between (introns), rest of genomic sequence as black lines, T-DNA sequence is represented as green bars, LB/RB – left/right border. Position of primers used for genotyping (see Fig. 22 and 23) are marked (arrows not in scale with scheme of the genomic sequence). PAL – *phenylalanine ammonia-lyase*, Atg12- *ubiquitin-like autophagy protein 12*, KPHMT - *ketopantoate hydroxymethyltransferase*, E2 – *ubiquitin-conjugating enzyme (E2 ligase / GLRG_08803.1)*.

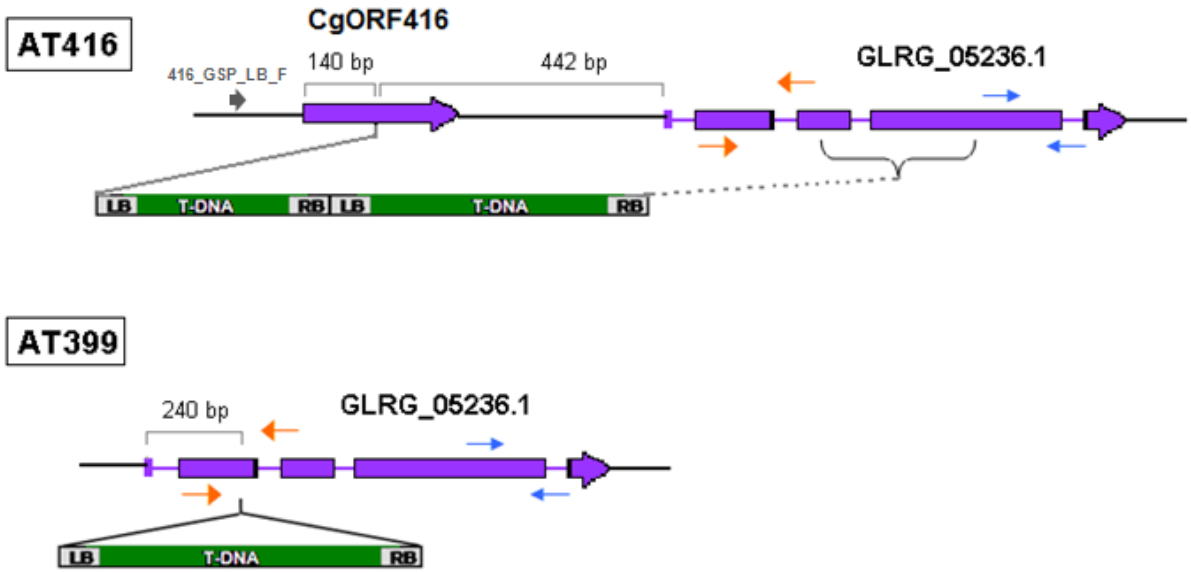

Fig. 21. Sketch summarizing the molecular characterisation of the T-DNA integration sites in *C. graminicola* insertion mutants: AT416 and AT399. Coding sequences are marked with purple bars/arrows (exons) and lines between (introns), rest of genomic sequence as black lines, T-DNA sequence is represented as green bars. LB/RB – left/right border. As the exact T-DNA junction at the right border in AT416 is not known, due to a deletion of adjacent genomic DNA, the region of the potential RB insertion (based on PCR analysis presented in Fig. 24) is marked with a bracket. Rough positions of primers used for genotyping (see Fig. 22 and 24) are marked (arrows not in scale with scheme of the genomic sequence): grey arrow – 416_GSP_LB_F, orange arrows - Cg-AT-05-02 and Cg-AT-05-04, blue arrows - 416_RB_genom F1/R1, CgORF416 and GLRG_05236.1 - genes coding for hypothetical proteins.

Surprisingly, two genomic sequences, identified for the AT263 junction site at the left and right border respectively, aligned to the same contig but about 4kb apart from each other (Fig. 20). It was not possible to detect these two independent T-DNA insertions by PCR analysis (Fig. 17) as these are not tandem insertions. They are also located close to each other, so they give just one band in Southern blot (Fig. 19), as no BamHI site is present between them. One of the two T-DNA insertions of AT263 integrated 303 bp upstream from the ATG of *phenylalanine ammonia-lyase* (*PAL*) gene, encoding an enzyme involved in phenylalanine biosynthesis, and 897 bp upstream of the start codon of *ubiquitin-like autophagy protein 12* (*Atg12*) gene, whose product is involved in autophagy. The other T-DNA integrated 482 bp upstream from the ATG of *ubiquitin-conjugating enzyme* (*E2 ligase/GLRG_08803.1*) gene. Between two insertions, a *ketopantoate hydroxylmethyltransferase* gene is located, whose product is involved in pantothenoate and CoA biosynthesis.

In AT633, the right border coding sequence of *dTDP-Glc-dehydratase* gene was located 406 bp apart from the T-DNA fragment, while the left border coding sequence of *methyltransferase* gene was located more than 3 kb downstream from the T-DNA insertion (Fig. 20). The analysis of this 3 kb fragment of genomic sequence in ORF Finder

(http://www.ncbi.nlm.nih.gov/projects/gorf/) revealed the presence of short open reading frames with no significant homology.

In the mutant AT416, T-DNA integrated into the coding sequence of a hypothetical protein predicted by program ORF Finder (http://www.ncbi.nlm.nih.gov/projects/gorf/), 140 bp downstream from its start codon (Fig 21). The protein, called from now CgORF416, has no conserved domains (Conserved Domain Search; http://www.ncbi.nlm.nih.gov/Structure/cdd/wrpsb.cgi) but a signal peptide for the secretory pathway is predicted (signal peptide probability: 0,711, SignalP prediction; http://www.cbs.dtu.dk/services/SignalP/). Closer PCR analysis of AT416 (see Fig. 24) showed that probably a deletion of some part of genomic region occurred at the junction with the outward facing right border, resulting in a partial deletion of a gene coding a hypothetical protein annotated as *GLRG_05236.1* (http://www.broadinstitute.org/ annotation/genome/colletotrichum_group/MultiHome.html). Interestingly, this gene is also affected in AT399, which carries a T-DNA insertion within the second exon of *GLRG_05236.1* (Fig. 21). Amplification of a genomic region with primers located in the 5' end of the *GLRG_05236.1* coding sequence (orange arrows on Fig. 21) gave no product in case of AT416 and in AT399 (Fig. 24). PCR with another set of primers (blue arrows on Fig. 21), designed to bind to the 3' end of the hypothetical transcript, yielded a product in both WT and both mutants AT399 and AT416, which allowed to restrict the deleted region in AT416 (Fig. 24). As shown in Fig. 5, phenotype of the leaves infected with AT399 resembles that of AT416. The protein GLRG_05263.1 is predicted to be a non-secretory protein (SignalP prediction), has no conserved domains but seems to be conserved in *Colletotrichum* species as revealed by blasting this protein against the *C. higginsianum* proteome (Suppl. Fig. 2).

The T-DNA integration sites were confirmed by PCR with specific primers binding to the genomic sequence potentially adjacent to the T-DNA insertion and the GW_3F/GW_3R primer, respectively (Fig. 22). An attempt to confirm junction sites at the other T-DNA borders failed for all mutants. Products, obtained during PCR with primers specific to genomic DNA at the other side of the insertion and T-DNA specific primers, were generated by unspecific primers binding as revealed by sequencing. However, when PCR was performed on genomic DNA with primer pairs, binding to the flanking genomic sequence at the both sides of T-DNA insertion site, products were obtained only on CgM2 wild type genomic DNA, but not on that of the respective mutant, confirming the integration of T-DNA at this region (Fig. 23).

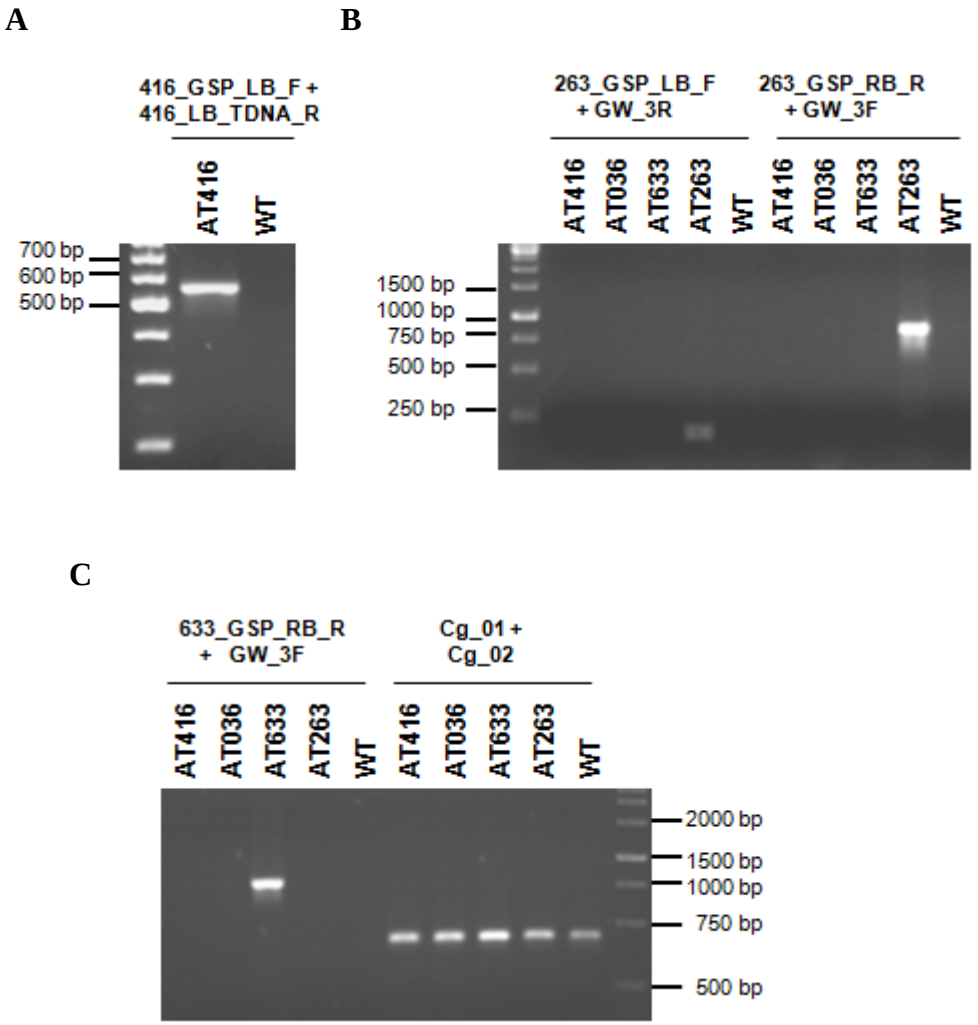

Fig. 22. Confirmation of T-DNA flanking sequences in *C. graminicola* insertion mutants by PCR with genome specific primer (GSP) and T-DNA primer. (A) Amplification of left border flanking sequence in AT416; (B) amplification of left border (left panel) and right border (right panel) flanking sequence in AT263; (C – left panel) amplification of right border flanking sequence in AT633. See Fig. 1 in chapter 2.2.4.7 and Fig. 20 and 21 for the position of primers. Primer specificity was tested by performing respective PCR reaction on gDNA from all mutant strains and wild type strain. Positive control of gDNA quality was performed with Cg_01 and Cg_02 primers (C – right panel). Ladder – Gene Ruler™ 100 bp DNA ladder in (A), Gene Ruler™ 1 kb DNA ladder (Fermentas) in (B and C).

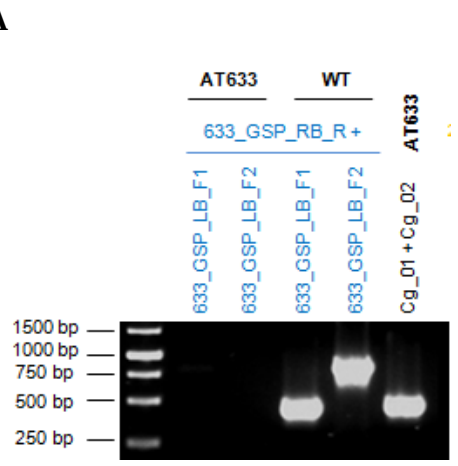

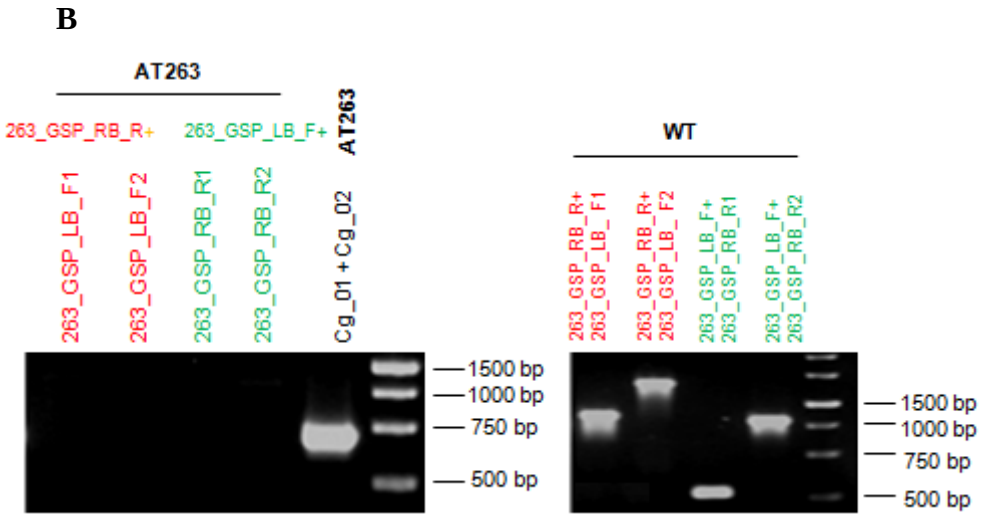

Fig. 23. Genotyping of *C. graminicola* insertion mutants: (A) AT633 and (B) AT263 with gene-specific primers binding adjacent to the T-DNA on both sides of the insertion (see Fig. 20 for the position of primers). As a primer-control, all reactions were also performed on CgM2 wild type (WT) DNA. Positive control of mutants' DNA was performed with Cg_01 and Cg_02 primers. Ladder - Gene Ruler™ 1 kb DNA ladder (Fermentas).

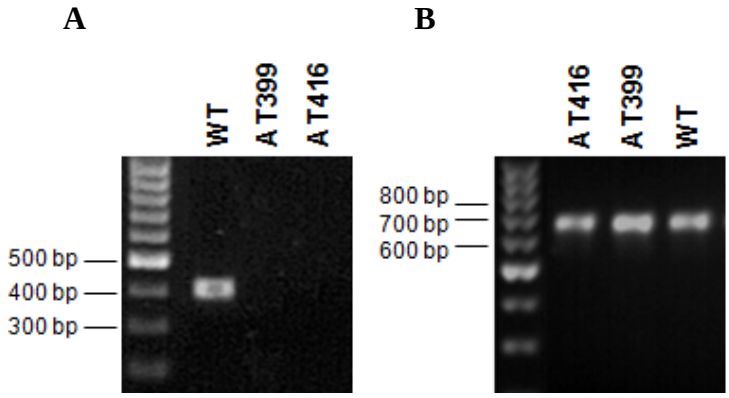

Fig. 24. Result of PCR performed on genomic DNA of the *C. graminicola* insertion mutants AT416 and AT399 and the wild type strain CgM2 (WT) with primers designed to sequence coding for a hypothetical protein GLRG_05236.1. (A) PCR with primers binding to 5' end of the gene (primers Cg-AT-05-02 and Cg-AT-05-04, marked with orange arrows on Fig. 21) or (B) 3' end of the gene (primers 416_RB_genom F1/R1, marked with blue arrows on Fig. 21). Ladder – Gene Ruler™ 100 bp DNA ladder.

To narrow down the candidate genes in the individual mutant strains, the expression of all genes adjacent to respective T-DNA insertions was examined during pathogenesis. A regular RT-PCR was done on cDNA extracted from maize leaves infected with wild type *C. graminicola* CgM2 at 3 dpi (Fig. 25). A strong signal for *phenylalanine ammonia-lyase, ubiquitin-conjugating enzyme (E2 ligase/GLRG_08803.1), methyltransferase,* and *dTDP-glucose-dehydratase* transcripts was obtained. Weak signals were observed for *ubiquitin-like autophagy protein 12, ketopantoate hydroxymethyltransferase* and two genes coding for hypothetical proteins GLRG_05236.1 and CgORF416, located adjacent to the T-DNA insertion site of AT416. In summary, all candidate genes were expressed *in planta*. No signal

was obtained when primers for *C. graminicola* genes were tested on cDNA from mock-treated leaves, meaning that these primers are specific for fungal DNA.

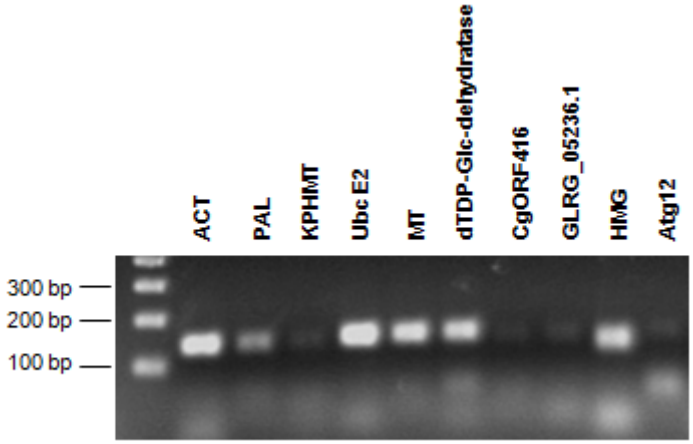

Fig. 25. RT-PCR to determine expression of candidate genes *in planta*. RT-PCR was performed on cDNA from leaves infected with WT *C. graminicola* (3 dpi), using primers designed for *C. gramincola actin* as a quality control of fungal cDNA (ACT), *phenylalanine ammonia-lyase* (PAL), *ketopantoate hydroxymethyltransferase* (KPHMT), *ubiquitin-conjugating enzyme E2* (Ubc E2), *methyltransferase* (MT), *dTDP-glucose-dehydratase* (dTDP-Glc-dehydratase), *CgORF416*, *GLRG_05236.1*, gene coding for *Zea mays* high mobility group protein as a quality control of maize cDNA (HMG) and *ubiquitine-like autophagy protein 12* (Atg12). Ladder – Gene Ruler^{TM} 100 bp DNA ladder.

In order to determine which genes were affected in their expression by the T-DNA insertion, a RT-PCR or, if necessary, a qRT-PCR of candidate genes was performed on cDNA isolated from leaves infected with respective mutant and wild type strain CgM2 as a control (see chapter 3.1.4, 3.1.5 and 3.1.6).

3.1.4 Identification and verification of affected genes in AT263 mutant

The ATMT mutant AT263 was shown to contain two tightly linked T-DNA insertions that potentially affect the expression of four genes (see Fig. 20). qRT-PCR analysis of AT263 mutant revealed that transcript level of *phenylalanine ammonia-lyase* was up-regulated two times in the mutant compared to wild type strain CgM2, while level *of ubiquitin-conjugating enzyme E2* (*E2 ligase/GLRG_08803.1*) transcript was down regulated 32 times in the mutant compared to CgM2 wild type (Fig. 26). This result shows that the expression of ubiquitin-conjugating enzyme gene is strongly suppressed in the mutant AT263. Thus, this gene was chosen for the generation of targeted knock-out strains. Structure of this gene and its predicted protein structure are presented in a Fig. 27. The predicted protein sequence contains all catalytic sites of E2 ligases and shows the highest similarity to ubiquitin-conjugating

enzymes from other species. Comparison of the affected E2 ligase from *C. graminicola* with ubiquitin-conjugating enzymes from *S. cerevisiae* showed that sequence of *C. graminicola* protein is most similar to yeast ubiquitin-conjugating enzyme 8 (Ubc8) (Fig. 28). Yeast Ubc8 is a negative regulator of gluconeogenesis, labelling fructose-1,6-bisphosphatase, a key enzyme of this pathway, for degradation (Schüle et al., 2000). Due to the strong similarity to yeast Ubc8, the E2 ligase affected in AT263 is designated *CgUbc8* from now on.

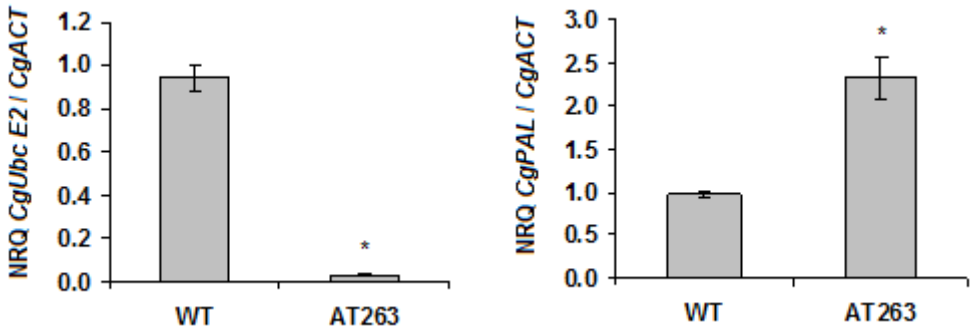

Fig. 26. qRT-PCR analysis of *ubiquitin-conjugating enzyme E2/GLRG_08803.1* (*CgUbc E2*) and *phenylalanine ammonia- lyase* (*CgPAL*) transcript amount in *C. graminicola* AT263- and WT-infected maize leaves (cv. Nathan). Leaves were dip-inoculated with a fungal titer of 10^4 conidia / ml and harvested for RNA isolation at 4dpi. Mean values of relative transcript levels (NRQ) normalised to *histone H3* (*CgH3*) are shown (n=4). Asterisks indicate a significant difference (t-test, p-value < 0.01) to the leaves infected with wild type strain CgM2. Error bars represent the standard error.

A – coding sequence of *CgUbc E2/ GLRG_08803.1*

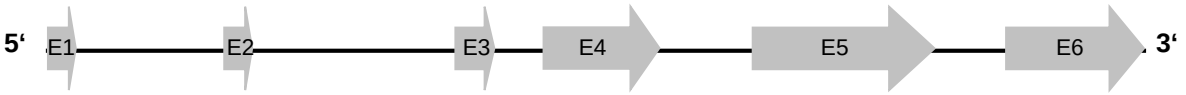

B – Cg Ubc E2/GLRG_08803.1 protein structure

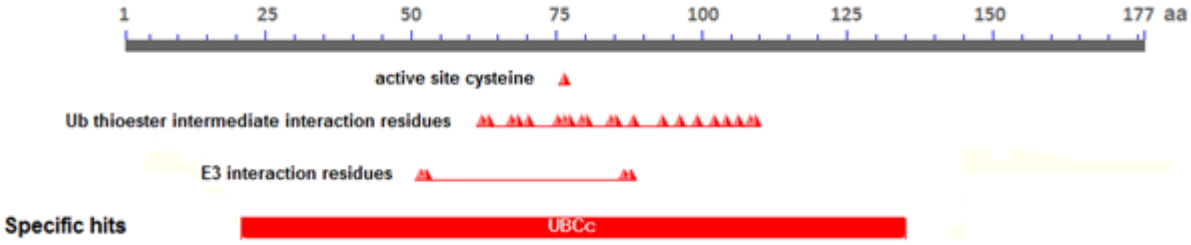

Fig. 27. Gene and predicted protein structure of *C. graminicola ubiquitin-conjugating enzyme E2/GLRG_08803.1*. (A) Exon-intron structure of the gene. Exons (E1-E6) are represented by grey arrows, intron sequence with a black line. The genomic sequence is 1.061 bp in length with introns, the coding sequence is 531 bp long. (B) Predicted functional residues of the CgUbc E2 protein. Protein sequence is represented by a grey bar, the position of ubiquitin-conjugating enzyme E2 catalytic domain (UBCc) is marked with a red bar, the positions of conserved catalytic cysteine residue forming a thiol-ester linkage with ubiquitin (active site

cysteine), Ub thioester intermediate interaction residues and residues interacting with E3 ligase are marked with red triangles. Scheme was generated by Conserved Domain Search programme (http://www.ncbi.nlm.nih.gov/cdd).

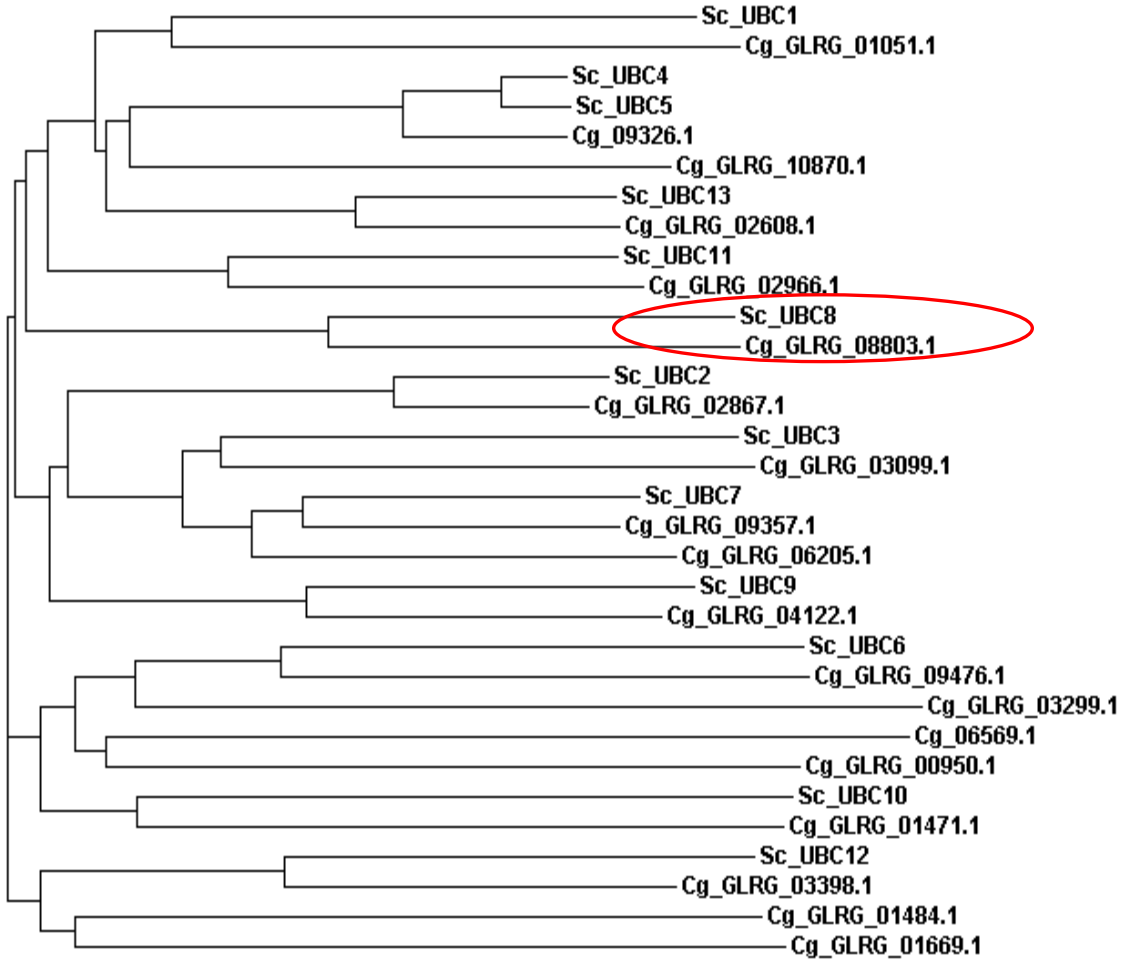

Fig. 28. Comparison of ubiquitin-conjugating enzymes from *C. graminicola* (Cg) and yeast (Sc) reveals that *C. graminicola* ubiquitin-conjugating enzyme GLRG_08803.1 shows the highest similarity to yeast Ubc8 which is a negative regulator of gluconeogenesis, targeting fructose-1,6-bisphosphatase for degradation (Schüle et al., 2000). Phylogenetic tree was generated with the programme ClustalW.

Furthermore, the expression of two other genes, *ubiquitin-like autophagy protein 12* (*CgAtg12*) and *ketopantoate hydroxymethyltransferase* (*CgKPHMT*), located between the two T-DNA insertions in the mutant AT263 was evaluated by qRT-PCR. *CgAtg12* transcript amounts were not affected in AT263, while the expression of *CgKPHMT* was diminished four times in the mutant strain compared to CgM2 wild type (Fig. 29). The weak suppression of the *CgKPHMT* transcription probably did not significantly affect the mutant phenotype, however to exclude this possibility, the gene was also chosen for a targeted knock-out approach.

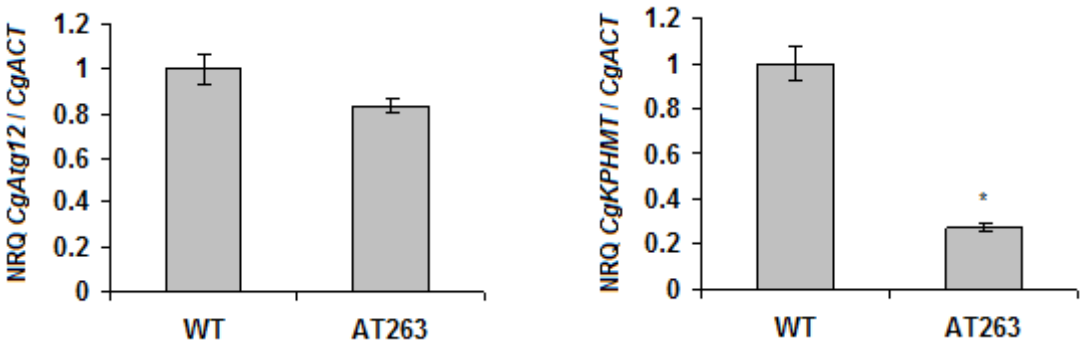

Fig. 29. qRT-PCR analysis of the expression levels of *ubiquitin-like autophagy protein 12* gene (*CgAtg12*) and *ketopantoate hydroxymethyltransferase* gene (*CgKPHMT*) in mutant AT263-infected maize leaves (cv. Nathan). Leaves were dip-inoculated with a fungal titer of 10^4 conidia / ml and harvested for RNA isolation at 4 dpi. Mean values of relative transcript levels (NRQ) normalised to *histone H3* (*CgH3*) are shown (n=4). Asterisk indicates a significant difference (t-test, p-value < 0.01) to the leaves infected with wild type strain CgM2. Error bars represent the standard error.

Following selection of the genes affected by the T-DNA insertions in the AT263 mutant, knock-out strains targeting *ubiquitin-conjugating enzyme 8* (*CgUbc8*) and *ketopantoate hydroxylmethyltransferase* (*CgKPHMT*) were generated as described in chapter 2.2.4.8). The results of the amplification of the deletion cassettes for the transformation of *C. graminicola* protoplasts are presented in Suppl. Fig. 3 and 4, while the numbers of generated transformants are summarized in Table 6. To confirm a homologous recombination event, left and right flanks of the respective deletion cassette were successfully amplified by PCR for both knock-out mutant strains (Suppl. Fig. 5). However, PCR analysis with primers designed for the respective target gene gave no product only in case of CgUbc8-knock-out-strains. A PCR on genomic DNA isolated from all putative *KPHMT* knock-out strains with primers specific to the target gene produced a specific product of the same size like for CgM2 wild type DNA, indicating that *KPHMT* has not been deleted.

Table 6. Statistics for the generation of targeted knock-out strains for the genes: *ubiquitin-conjugating enzyme 8* (*Ubc8*) and *ketopantoate hydroxymethyltransferase* (*KPHMT*). Number (No.) of independent transformants represents the number of independent colonies on the transformation plate, number of analysed transformants and number of confirmed knock-out strains represents the strains screened and confirmed by PCR respectively, isolated from single spores. Percentage of knock-out strains was calculated from the number of confirmed knock-out strains and the number of analysed transformants.

Target gene	No. of independent transformants	No. of analysed transformants	No. of confirmed knock-out strains	Percentage of knock-out strains
CgUbc8	25	21	18	86 %
CgKPHMT	21	19	0	0 %

Following PCR analysis, selected transformants were verified by Southern blot approach with probes targeting left and right flank of the respective gene/deletion cassette. Sketches of the knock-out and corresponding wild type loci, including fragments detected on Southern blots, are shown in Fig. 30 and 31, together with the results of the hybridisation. All selected putative *CgUbc8* knock-out transformants were confirmed by both left and right flank probe hybridisation. The analysis of putative *CgKPHMT* knock-out strains revealed that both the knock-out and wild type locus were present in all analysed strains. This suggests that the deletion of *CgKPHMT* is lethal and only transformants generated by the fusion of wild type and transformed protoplasts could be regenerated on the selection medium. Fusion of protoplast was already shown to be induced by min. 30% PEG (Peberdy, 1979), thus it is possible that the transformation buffer used in this study may cause fusion events.

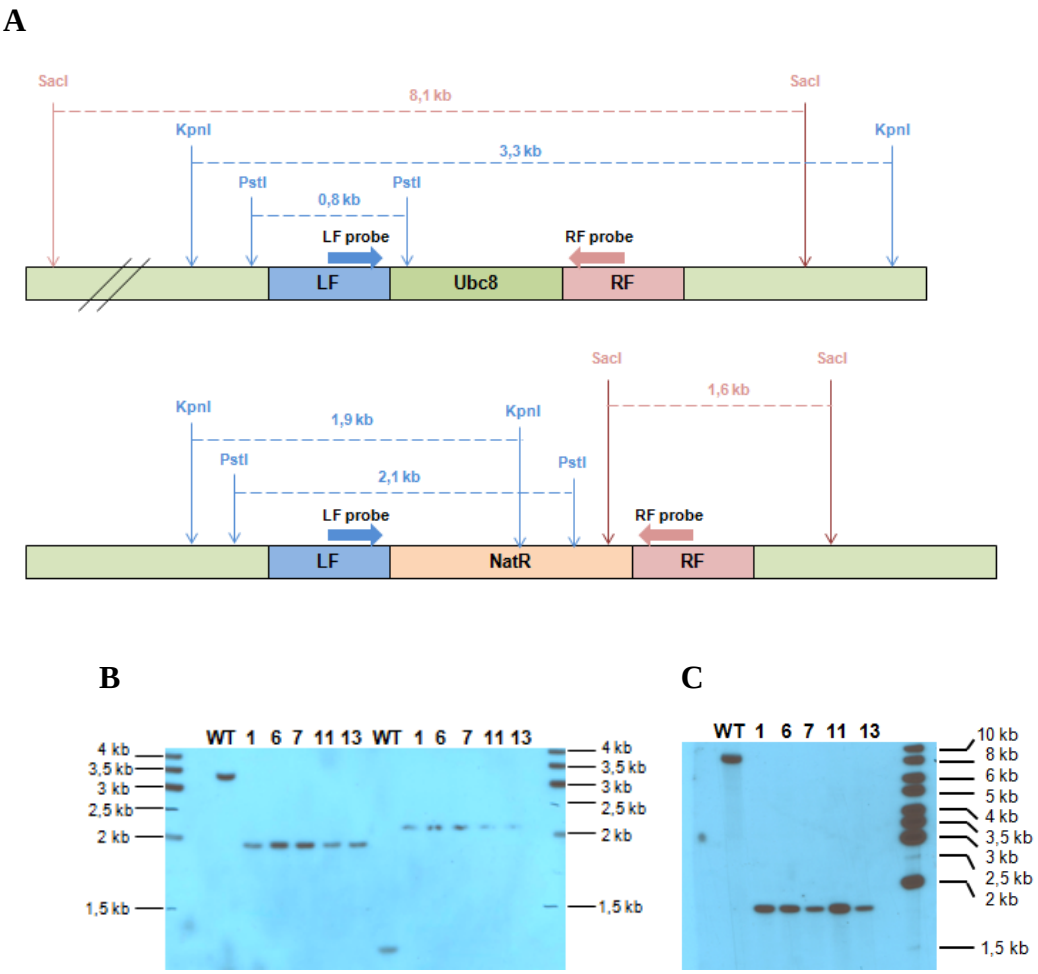

Fig. 30. Southern blot analysis of *CgUbc8* knock-out transformants. (A) Scheme of wild type (upper part) and knock-out (lower part) *CgUbc8* locus. LF/RF – left/right flank, Ubc8 – *CgUbc8* coding sequence, NatR – *nourseothricin N-acetyl-transferase* coding sequence, position of left/right flank probe binding, sites of restriction enzymes used for DNA digestion and resulting DNA fragments are marked. (B) and (C) – results of Southern probe hybridisation with the probe targeting the left flank (B) and right flank (C). gDNA of wild type strain CgM2 and putative knockout mutant strains (lanes 1, 6, 7, 11, 13) was digested with KpnI (B left part of the blot) or PstI (B - right part) or SacI (C). Ladder – 1 kb DNA ladder (PeqLab).

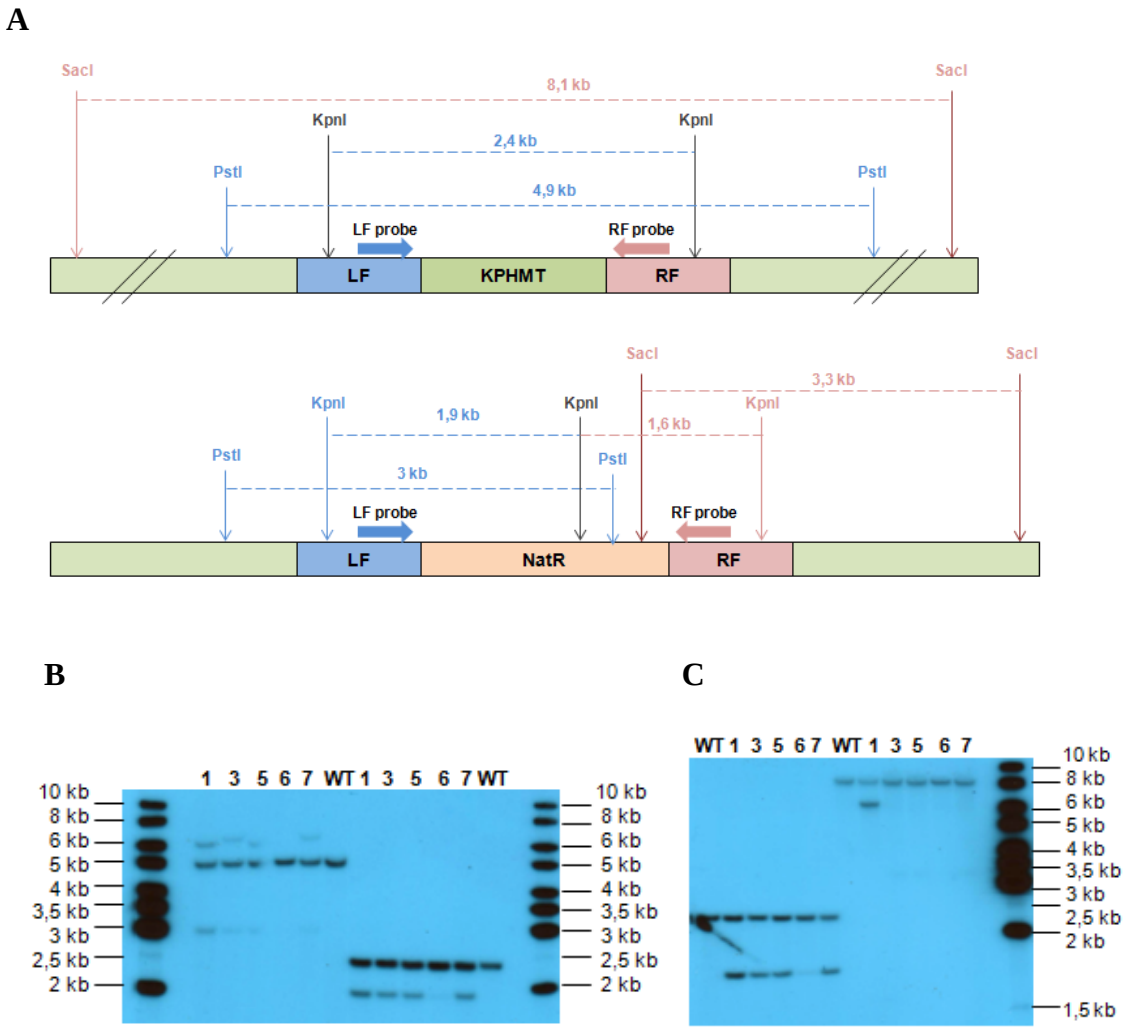

Fig. 31. Southern blot analysis of *CgKPHMT* knock-out transformants. (A) Scheme of wild type (upper part) and knock-out (lower part) *KPHMT* locus. LF/RF – left/right flank, KPHMT – *KPHMT* coding sequence, NatR – *nourseothricin N-acetyl-transferase* coding sequence, position of left/right flank probe binding, sites of restriction enzymes used for DNA digestion and resulting DNA fragments are marked. (B) and (C) – results of Southern probe hybridisation with the probe targeting the left flank (B) and right flank (C). gDNA of wild type strain CgM2 and putative knockout mutant strains (lanes: 1, 3, 5, 6, 7) was digested with PstI (B – left part of the blot) or KpnI (B – right side, C – left side) or SacI (C – right part of the blot). Ladder – 1 kb DNA ladder (PeqLab).

Knock-out strains generated for the *CgUbc8* gene that were confirmed by PCR and Southern blot analysis were subsequently tested for reduced virulence. Maize plants were inoculated with two transformant lines. As a reference, maize plants were also infected with the AT263 insertion mutant strain and the wild type strain CgM2. A reduced pathogenicity was observed in case of both tested *CgUbc8* knock-out transformant lines; with the phenotype of the infected leaves similar to that observed for the leaves infected with AT263 insertion mutant (Fig. 32 and Fig. 33). Furthermore, the photosynthetic performance of the infected leaves was measured by chlorophyll fluorescence imaging, which was previously been shown to serve as a good indicator for the virulence of the strain (chapter 3.1.1.). The effective PSII

quantum yield (Y(II)) and the electron transport rate (ETR) of the leaves infected with AT263 insertion mutant and the two *CgUbc8* knock-out strains were significantly higher compared to the leaves infected with the wild type strain CgM2 (Fig. 34) There was no significant difference between the Y(II) and ETR values of the ATMT insertion mutant and the targeted knock-out strains.

These results confirm that down-regulated expression of *CgUbc8* accounts for the pathogenicity phenotype of AT263 and that altered expression of the other genes (*PAL*, *Atg12* and *KPHMT*), adjacent to the identified T-DNA integration sites, does not substantially contribute to the phenotype of AT263.

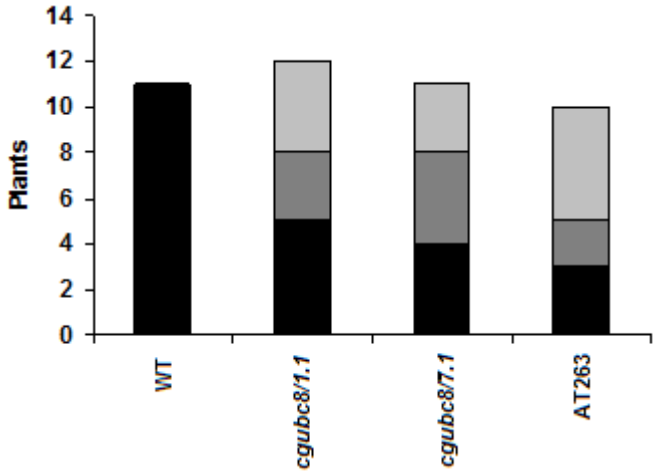

Fig. 32. Verification of reduced virulence of *CgUbc8* knock-out strains. Maize plants cv. Mikado were dip-inoculated with a fungal titer of $2x10^4$ conidia / ml and scored at 5 dpi, according to the classification described in chapter 3.1.2. Light grey bars – group III: up to five big lesions (more than 0.5 cm) per leaf, dark grey bars – group IV: more than five big lesions (more than 0.5 cm) per leaf, black bars – group V: necrosis of more than 50% of leaf area. WT - plants infected with the wild type strain CgM2, *cgubc8/1.1* and *cgubc8/7.1* - plants infected with *CgUbc8* knock-out strains (line 1.1 and 7.1), AT263 - plants infected with the AT263 insertion mutant strain.

Fig. 33. Phenotype of representative maize leaves (cv. Mikado) infected with wild type *C. graminicola* CgM2 (WT), two *CgUbc8* knock-out strains (*cgubc8/1.1*and *cgubc8/7.1*) and AT263 insertion mutant 5 days after dip-inoculation (same experiment as shown in Fig. 32). Representative leaves falling into group V (necrosis of more than 50% of leaf area) are shown.

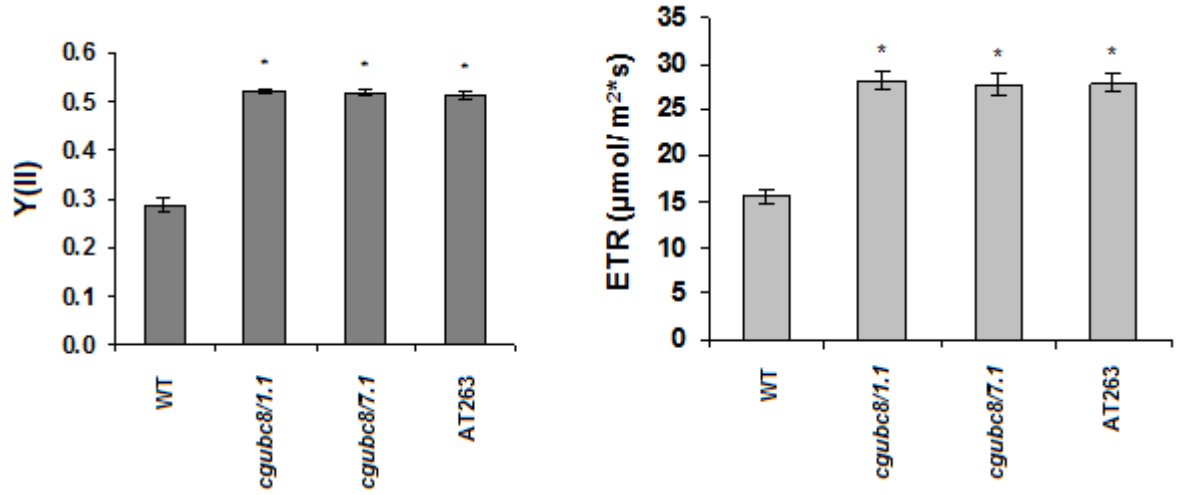

Fig. 34. Levels of effective PS(II) quantum yield (Y(II)) and electron transport rate (ETR) of maize leaves (cv. Mikado) infected with the wild type *C. graminicola* CgM2 (WT), *CgUbc8* knock-out strains (*cgubc8/1.1* and *cgubc8/7.1*) or insertion mutant strain (AT263) at 2dpi. Mean values are shown (n=7). Plants were dip-inoculated with a fungal titer of $2x10^4$ conidia / ml. Asterisks indicate a significant difference (t-test, p-value < 0.01) to the leaves infected with wild type strain CgM2. Error bars represent the standard error.

3.1.5 Identification and verification of affected genes in AT416 mutant

As described above, T-DNA integration in AT416 insertion mutant caused a deletion of adjacent genomic region where two hypothetical proteins (CgORF416 and GLRG_05236.1) are located (see Fig. 21), which should abolish their expression. To confirm this effect, RT-PCR analysis was conducted with primers amplifying the sequence of a *CgORF416* and primers specific for cDNA sequence at the 3' end of a coding sequence of *GLRG_05236.1*, i.e. the reverse primer spanning an exon-exon junction. No products were obtained on cDNA of AT416 mutant-infected leaves, meaning that both genes are not expressed in the mutant (Fig. 35). Thus, they were chosen as targets for the generation of knock-out strains (as described in chapter 2.2.4.8), see also Suppl. Fig. 3 and 4 for the results of the amplification of the deletion cassettes).

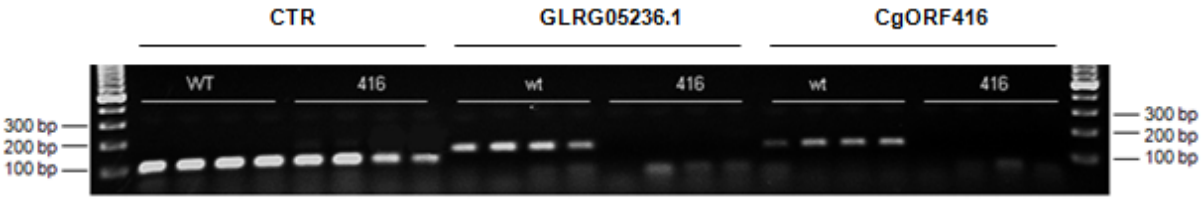

Fig. 35. RT-PCR analysis of two genes coding for hypothetical proteins: *GLRG_05236.1* and *CgORF416* on wild type CgM2 (WT) and AT416 mutant strain (416). CTR – control of cDNA quality with primers for *C. graminicola histone 3* gene. Ladder – Gene Ruler™ 100 bp DNA ladder.

Transformants were confirmed by amplification of left and right flanks of the respective deletion cassette and by PCR with primers binding to target gene. No product could be produced with primers designed for the respective target gene (see Table 7 and Suppl. Fig. 5).

Table 7. Statistics for the generation of targeted knock-out strains for two genes coding for hypothetical proteins affected in the AT416 strain: *GLRG_05236.1* and *CgORF416*. Number (No.) of independent transformants represents the number of independent colonies on the transformation plate, number of analysed transformants and number of confirmed knock-out strains represents the strains isolated from single spores and screened and confirmed by PCR, respectively. Percentage of knock-out strains was calculated from the number of confirmed knock-out strains and the number of analysed transformants.

Target gene	No. of independent transformants	No. of analysed transformants	No. of confirmed knock-out strains	Percentage of knock-out strains
GLRG_05236.1	24	18	9	50 %
CgORF416	29	17	12	71 %

Subsequently, Southern blot analysis with probes targeting left and right flank of the deletion cassette was performed for selected transformants (see Fig. 36 and 37). Four out of five putative knock-out transformants per deleted gene were confirmed by this approach.

A

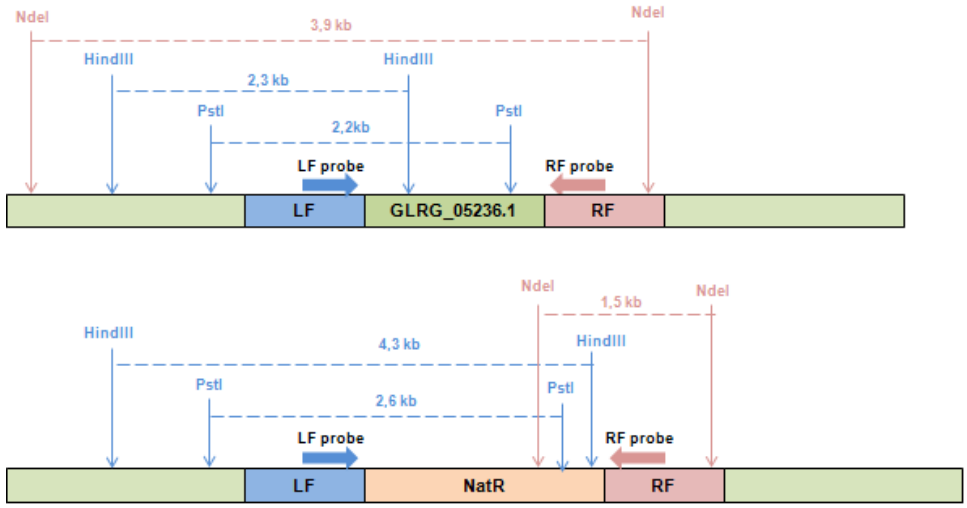

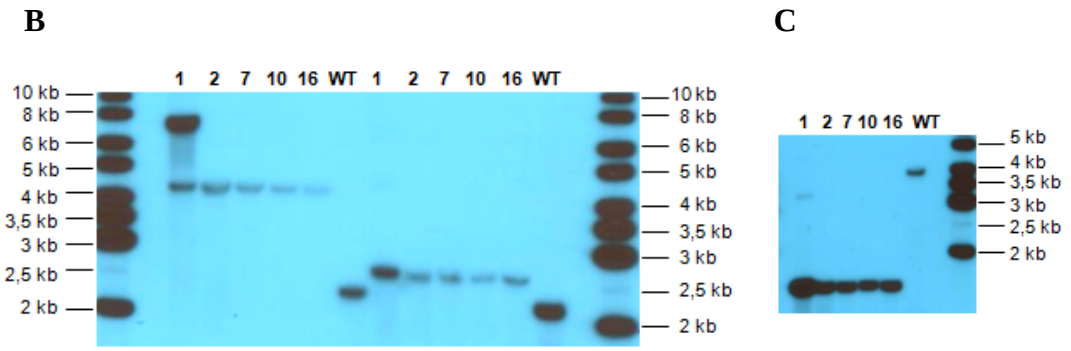

Fig. 36. Southern blot analysis of *GLRG_05236.1* knock-out transformants. (A) Scheme of wild type (upper part) and knock-out (lower part) *GLRG_05236.1* locus. LF/RF – left/right flank, GLRG_05236.1 – *GLRG_05236.1* coding sequence, NatR – *nourseothricin N-acetyl-transferase* coding sequence, position of left/right flank probe binding, sites of restriction enzymes used for DNA digestion and resulting DNA fragments are marked. (B) and (C) – results of Southern probe hybridisation with the probe targeting the left flank (B) and right flank (C). gDNA of wild type strain CgM2 (WT) and putative knockout mutant strains (lanes 1, 2, 7, 10, 16) was digested with HindIII (B – left part) or PstI (B – right part) or NdeI (C). Ladder – 1 kb DNA ladder (PeqLab).

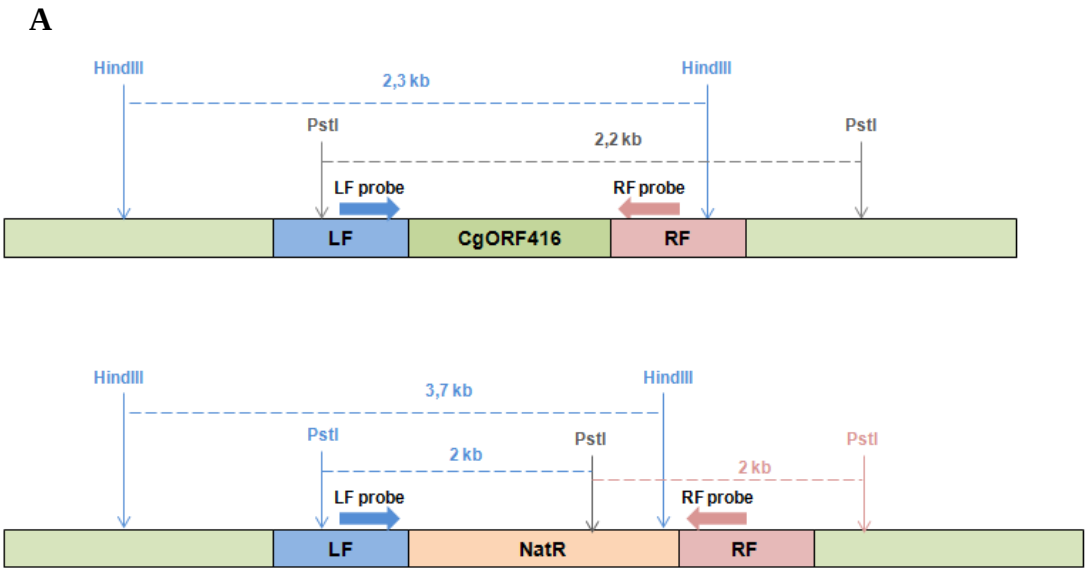

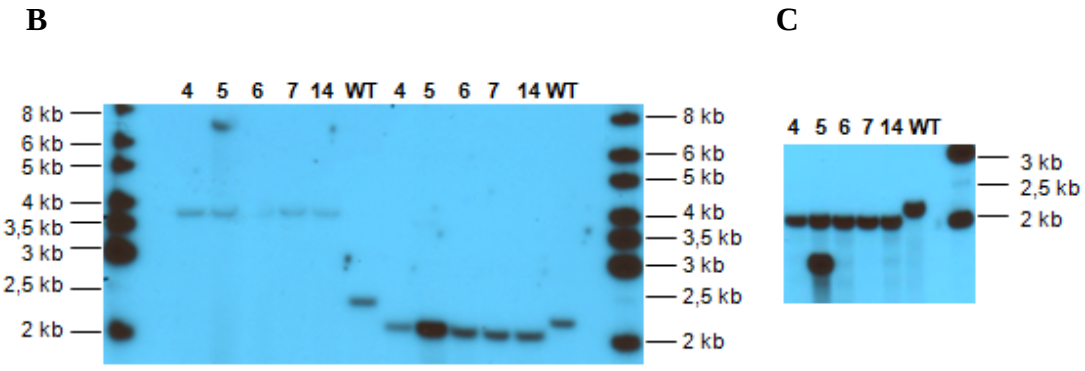

Fig. 37. Southern blot analysis of *CgORF416* knock-out transformants. (A) Scheme of wild type (upper part) and knock-out (lower part) *CgORF416* locus. LF/RF – left/right flank, CgORF416 – *CgORF416* coding sequence, NatR – *nourseothricin N-acetyl-transferase* coding sequence, position of left/right flank probe binding, sites of restriction enzymes used for DNA digestion and resulting DNA fragments are marked. (B) and (C) – results of Southern probe hybridisation with the probe targeting the left flank (B) and right flank (C). gDNA of wild type strain CgM2 and putative knockout mutant strains (lanes: 4, 5, 6, 7, 14) was digested with Hind III (B – left part of the blot) or PstI (B - right part of the blot and C). Ladder – 1 kb DNA ladder (PeqLab).

Confirmed knock-out strains were subjected for virulence assessment on maize plants. Inoculation was performed with two transformant lines per knock-out target and with the AT416 insertion mutant and the wild type strain CgM2 for reference. Knock-out strains carrying the deletion of *GLRG_05236.1* gene exhibited strongly reduced pathogenicity, but not to a comparable extent as observed for the AT416 insertion mutant (Fig. 38 and 39). This result suggests that some other, not yet identified, gene that is required for pathogenicity might be also affected by the T-DNA insertion site in the strain AT416. The virulence of the *CgORF416* knock-out strains was not reduced (Fig. 38 and 39) meaning that lack of expression of *CgORF416* in AT416 does not influence the T-DNA mutant's pathogenicity phenotype substantially.

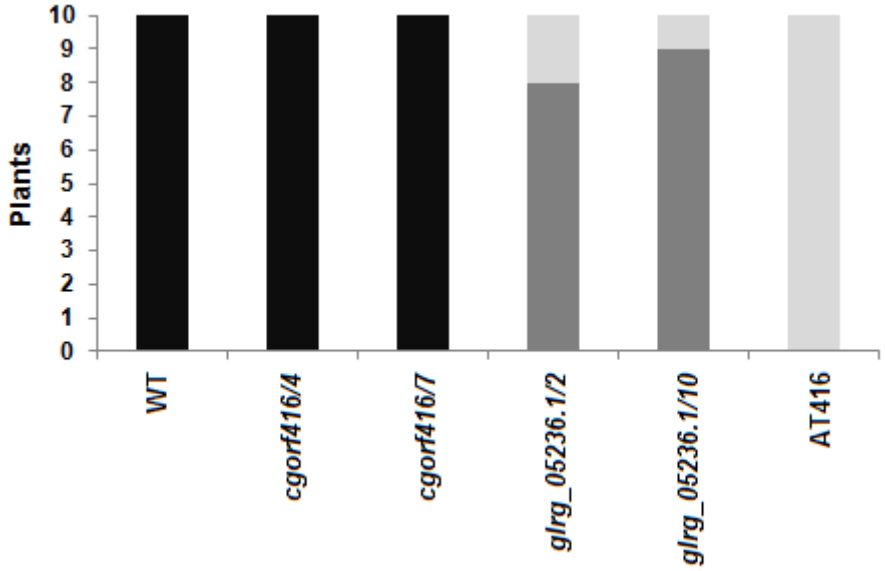

Fig. 38. Phenotype of maize leaves cv. Mikado infected with the wild type strain CgM2 (WT), *CgORF416* knock-out strains (*cgorf416/4* and *cgorf416/7*), *GLRG_05236.1* knock-out strains (*glrg_05236.1/2* and *glrg_05236.1/10*) and AT416 insertion mutant. Plants were dip-inoculated with a fungal titer of $2x10^4$ conidia / ml and scored at 8 dpi, according to the classification described in chapter 3.1.2. Grey bars – group III: up to five big lesions (more than 0.5 cm) per leaf, dark grey bars – group IV: more than five big lesions (more than 0.5 cm) per leaf, black bars – group V: necrosis of more than 50% of leaf area.

Fig. 39. Phenotype of representative maize leaves (cv. Mikado) infected with wild type *C. graminicola* CgM2 (WT), *CgORF416* knock-out strains (*cgorf416/4* and *cgorf416/7*), *GLRG_05236.*1 knock-out strains (*glrg_05236.1/2* and *glrg_05236.1/10*) and AT416 insertion mutant 8 days after dip-inoculation. Plants were inoculated with a fungal titer of $2x10^4$ conidia / ml. Leaves falling into group V (WT and *CgORF416* knock-out strain), group IV (*GLRG_0536.1* knock-out strain) and group III (AT416) are shown (plants from the same experiment as shown in Fig. 38).

3.1.6 T-DNA insertion in AT633 mutant has no influence on adjacent genes

Transcript levels of two genes located most proximal to T-DNA integration in the mutant AT633 (Fig. 20) were also evaluated by qRT-PCR. There was no change in the expression level of the *methyltransferase* gene compared to the CgM2 wild type strain, while *dTDP-glucose dehydratase* was expressed five times stronger on the transcript level in the mutant AT633 compared to the wild type strain CgM2 (Fig. 40). As the T-DNA insertion did not lead to reduced transcript amounts of both target genes, mutant AT633 was not further analysed.

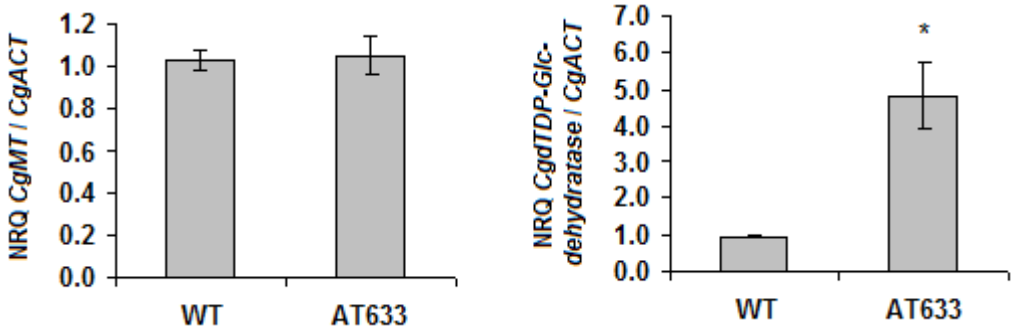

Fig. 40. qRT-PCR analysis of *methyltransferase* (*CgMT*) and *dTDP-glucose dehydratase* transcripts amount in mutant AT633-infected maize leaves (cv. Nathan). Leaves were dip-inoculated with a fungal titer of 10^4 conidia / ml and harvested for RNA isolation at 4 dpi. Mean values of relative transcript levels (NRQ) normalised to *histone H3* (*CgH3*) are shown (n=4). Asterisk indicates a significant difference (p-value < 0.02) to the leaves infected with wild type strain CgM2 (t-test, p-value < 0.02). Error bars represent the standard error.

3.1.7 Evaluation of *CgUbc8* knock-out strain development *on planta*

Development of *CgUbc8* knock-out (see chapter 3.1.4) and AT263 insertion mutant strains *on planta* was evaluated to specify which stage of the infection process is affected in these strains. Microscopic observation of acid fuchsin-stained leaves revealed that all mutant lines were impaired at the stage of penetration into the host tissue (Fig. 41). However, closer microscopic analysis showed that developmental defects can be already observed at the stage of appressoria formation. Down regulation or deletion of *CgUbc8* hampered melanisation of appressoria as compared to CgM2 wild type appressoria (Fig. 42).

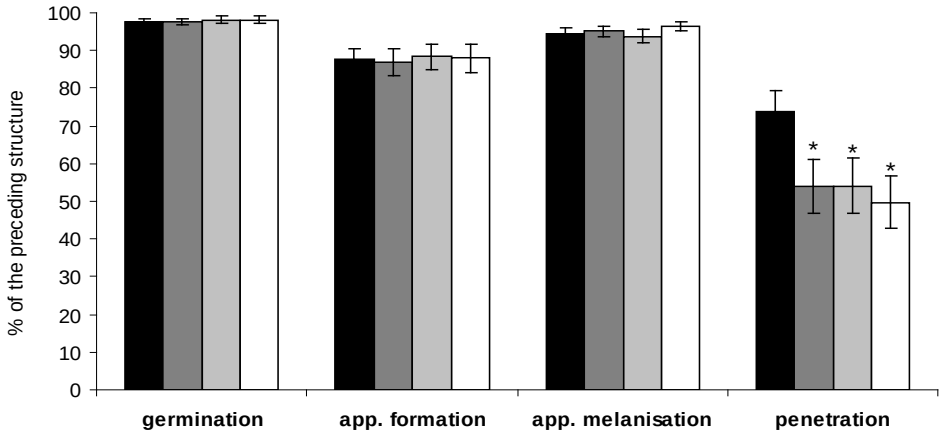

Fig. 41. Development of fungal infection structures *on planta* at 2.5 days post dip-inoculation of maize leaves (cv. Mikado) with a fungal titer of 10^4 conidia / ml. Dark bars – wild type strain CgM2, dark grey bars – *CgUbc8* knock-out strain 1.1, light grey bars - *CgUbc8* knock-out strain 7.1, white bars – AT263 mutant strain. Infection structures are given as a percentage of the preceding structure (100 structures per strain were counted). Mean values are shown (n=6). Asterisks indicate a significant difference to the leaves infected with wild type strain CgM2 (t-test, p-value < 0.05). Error bars represent the standard error.

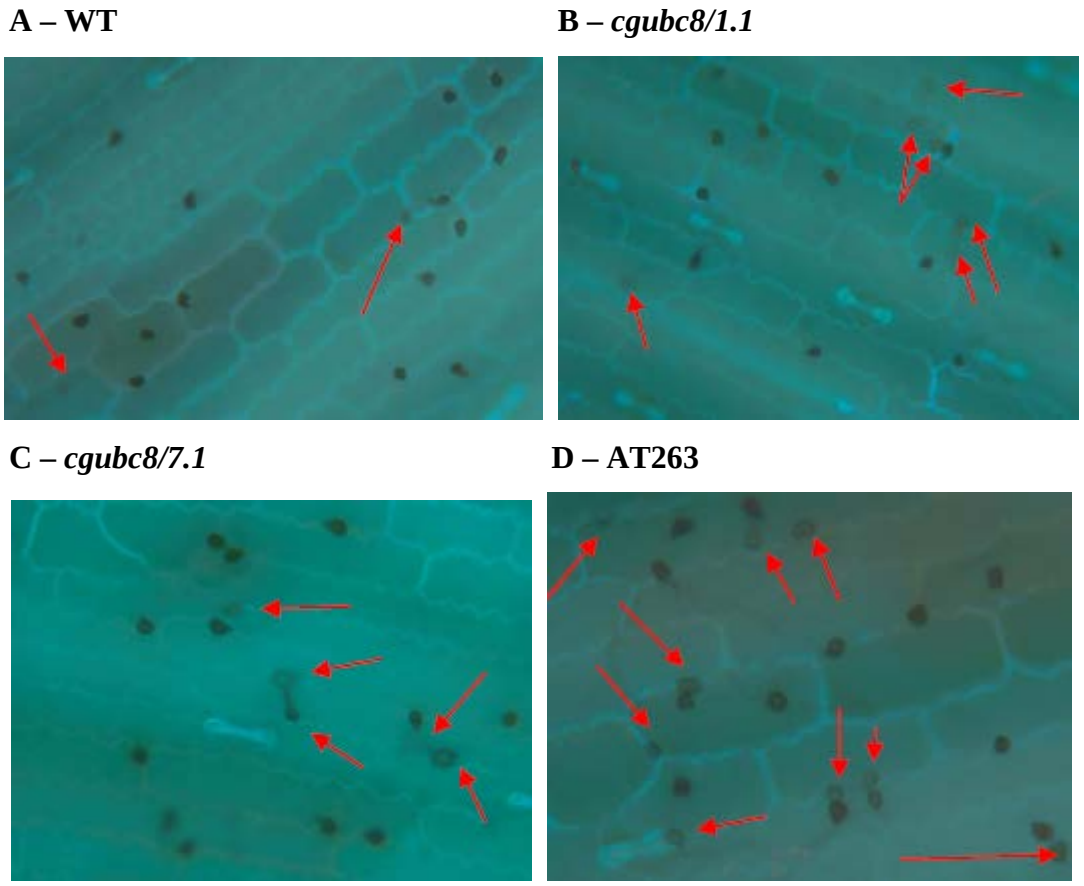

Fig. 42. Melanisation of appressoria formed on the surface of maize leaves (cv. Mikado) at 2 days after dip-inoculation with a fungal titer of 10^4 conidia / ml of wild type *C. graminicola* CgM2 (A), two *CgUbc8* knock-out strains 1.1 (B) and 7.1 (C) and AT263 insertion mutant (D). Appressoria which did not completely melanise are marked with red arrows.

3.1.8 *CgUbc8* deletion depletes a glycogen pool in the spores of *C. graminicola*

Ubiquitin-conjugating enzyme 8 (Ubc8) was shown to negatively regulate gluconeogenesis in yeast by mediating the glucose-induced ubiquitination of fructose-1,6-bisphosphatase (FBPase) and subsequent targeting of FBPase to degradation by the proteasome. As observed for *Ubc8* knock-out yeast cells, lack of Ubc8 protein leads to nearly complete stabilisation of FBPase in the presence of glucose and inhibition of ubiquitin conjugation onto the enzyme (Schüle et al., 2000). Thus, in the continuous presence of FBPase, the gluconeogenesis pathway would constantly be active (Fig. 43), which would lead to elevated glycogen content in the *Ubc8* knock-out cells. To test this hypothesis, glycogen content was evaluated in the *C. graminicola* conidia, where glycogen represents a main carbon storage compound. The result clearly shows that the glycogen content in conidia with down regulation or deletion of *CgUbc8* gene was reduced to less than a half of the content in CgM2 wild type conidia (Fig. 44.). Such a severe reduction of storage compounds could be a

potential cause for defects in spore development i.e. spore melanisation and penetration observed for AT263 insertion mutant and *CgUbc8* knock-out strain (Fig. 41 and 42).

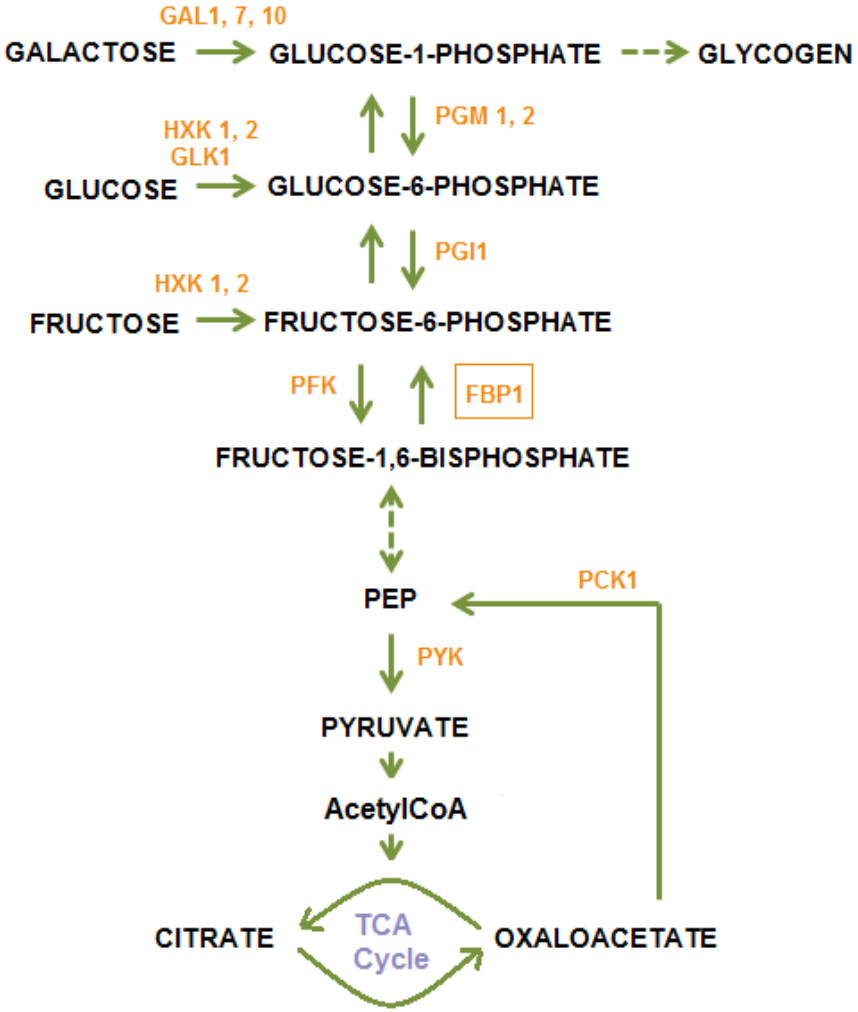

Fig. 43. Major anabolic (gluconeogenesis) and catabolic routes (glycolysis) for sugars in yeasts. Gluconeogenesis is regulated by the degradation of fructose-1,6-bisphosphatase (Fbp1) in proteasome, the enzyme which catalyses rate-limiting step in the pathway. GAL1, 7, 10 – galactokinase 1, 7, 10; HXK1, 2 – hexokinase 1, 2; GLK1 – glucokinase 1; PGM1, 2 – phosphoglucomutase 1, 2; PGI1 - glucose-6-phosphate isomerase 1; PFK – phosphofructokinase 1; FBP1 – fructose-1,6-bisphosphatase 1; PYK – pyruvate kinase; PCK1 – PEP carboxykinase 1. Adapted from Ronne (1995).

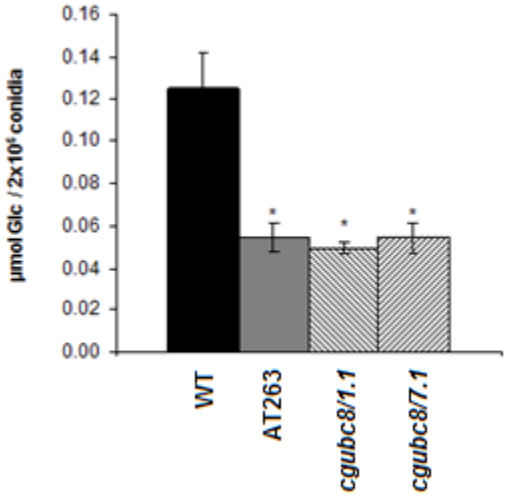

Fig. 44. Glycogen content in $2x10^6$ conidia of *C. graminicola* wild type CgM2 (WT), AT263 insertion mutant (AT263) and *CgUbc8* knock-out mutant strains 1.1 and 7.1 (*cgubc8/1.1* and *cgubc8/7.1*). Mean values are shown (n=4). Asterisks indicate a significant difference to leaves infected with wild type strain CgM2 (t-test, p-value < 0.02). Error bars represent the standard error.

Furthermore, this result indicates that *CgUbc8* influences glycogen synthesis in the opposite way as *ScUbc8* controls yeast gluconeogenesis (Schüle et al., 2000, Fig. 43). In yeast cells, deletion of *ScUbc8* and the concomitant stabilisation of Fbp1 activate gluconeogenesis and subsequently increase the glycogen pool. The possible explanation for the effects of *CgUbc8* deletion in *C. graminicola* is that the ubiquitin ligase may possibly stabilise FBPase by targeting its negative regulator to degradation or that CgUbc8 may target another enzyme of gluconeogenesis pathway. Thus, the activities of the enzymes involved in glycolysis and gluconeogenesis were determined in CgM2 wild type and mutant *C. graminicola* conidia.

3.1.9 *CgUbc8* deletion influences the activity of glycolytic and gluconeogenetic enzymes in the spores of *C. graminicola*

The activity of glycolytic and gluconeogenetic enzymes was determined in conidia of *C. gramicinola* wild type CgM2, AT263 insertion mutant and *CgUbc8* knock-out strains (*cgubc8/1.1* and *cgubc8/7.1*) as described in chapter 2.2.5.8. When comparing enzyme activities of conidia grown on medium with and without glucose, it was observed that a decrease in activity of most of the enzymes (phosphofructokinase, pyruvate kinase, hexokinase, isocitrate layse, malate dehydrogenase and UGPase) upon glucose was greater in wild type strain CgM2 compared to the insertion mutant and knock-out strains. Phosphofructokinase activity was higher in the AT263 insertion mutant and both *CgUbc8* knock-out strains upon addition of glucose compared to the wild type CgM2 (Fig. 45).

Similarly, AT263 insertion mutant and one of two *CgUbc8* knock-out strains exhibited higher hexokinase activity on medium with glucose than wild type CgM2 and the other *CgUbc8* knock-out strain (Fig. 45). On medium without glucose, downregulation of hexokinase was observed in AT263 and both *CgUbc8* mutant strains compared to wild type CgM2. Such downregulation was observed also in the activities of pyruvate kinase and phosphophfuctokinase (Fig. 45).

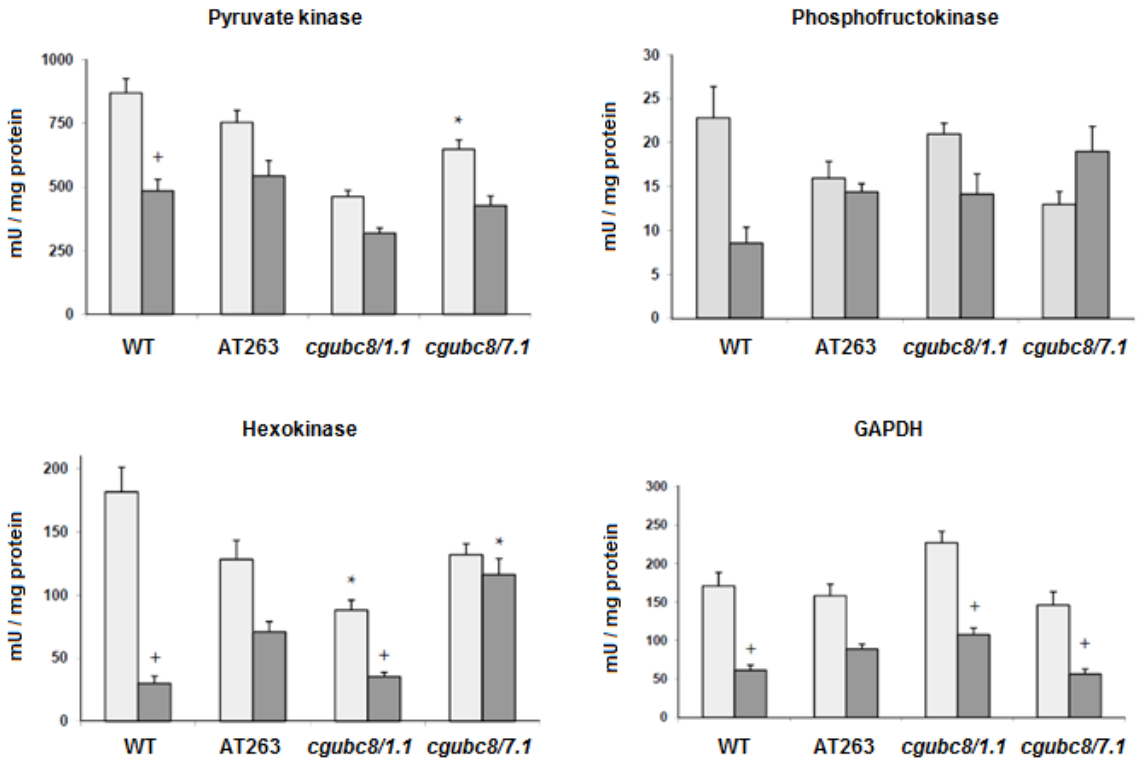

Fig. 45. Activities of glycolytic and gluconeogenetic enzymes in the conidia of the wild type strain CgM2 (WT), T-DNA insertion mutant (AT263) and two *CgUbc8* knock-out lines (*cgubc8/1.1* and *cgubc8/7.1*) on the medium without additional glucose (light grey bars) and with 2 % glucose (dark grey bars). Significant differences (t-test, p-value < 0.05) to the wild type strain CgM2 on the respective medium are marked with asterisks. Significant differences (t-test, p-value < 0.05) in enzyme activities of each strain on the medium with additional glucose compared to the medium without glucose are marked with a cross. GAPDH - glyceraldehyde 3-phosphate dehydrogenase.

The activity of malate dehydrogenase (Fig. 46) was lower in the AT263 insertion mutant and both *CgUbc8* knock-out strains compared to the wild type CgM2 on medium without glucose. Isocitrate lyase was downregulated on medium without glucose in AT263 mutant and one of two *CgUbc8* knock-out strains (Fig. 46). The acitivities of fructose-1,6-bisphosphatase and phosphoenolpyruvate carboxykinase were constant in wild type CgM2 irrespective of glucose addition to the medium (Fig. 46). While, glucose did influence the activities of both enzymes in AT263 mutant and knock-out strains, however, the observed

changes were not consistent. UDP-glucose pyrophosphorylase (UGPase) was strongly inhibited by glucose in wild type CgM2 and to a lesser extent in both *CgUbc8* knock-out lines (Fig. 46). UGPase activity was not altered upon glucose in AT263 insertion mutant.

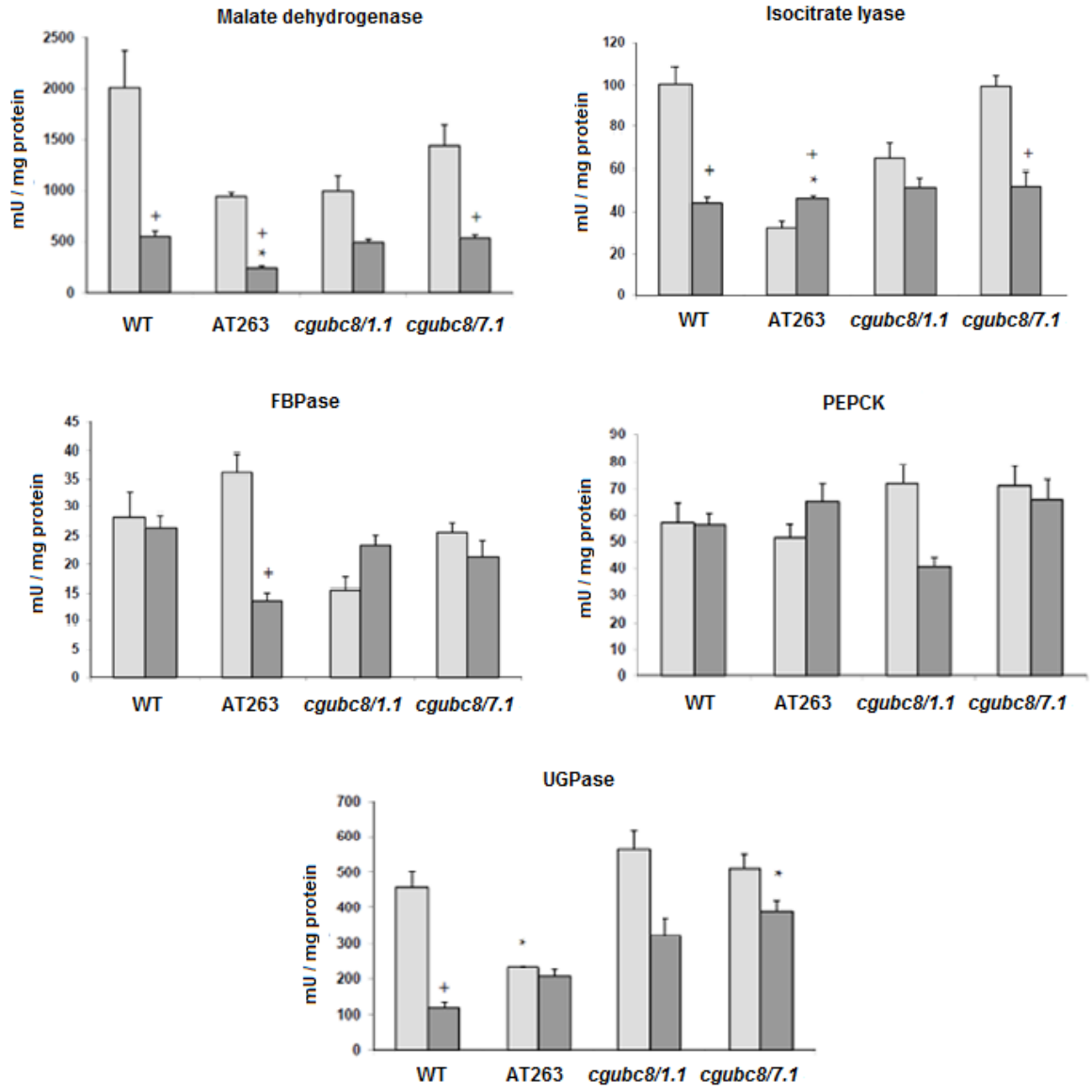

Fig. 46. The activities of the gluconeogenetic enzymes in the conidia of the wild type strain CgM2 (WT), T-DNA insertion mutant (AT263) and two knocked-out lines (*cgubc8/1.1* and *cgubc8/7.1*) on the medium without additional glucose (light grey bars) and with 2 % glucose (dark grey bars). The significant difference (t-test, p-value < 0.05) to the wild type strain CgM2 on the respective medium was marked with an ansterisk. The significant difference (t-test, p-value < 0.05) in enzyme activities of each strain on the medium with additional glucose compared to the medium without glucose was marked with a plus. FBPase – fructose-1,6-bisphosphatase, UGPase – UDP-glucose pyrophosphorylase, PEPCK – phosphoenolpyruvate carboxykinase.

3.2 Analysis of the combined metabolome-transcriptome data from wild type *C. graminicola* CgM2- infected leaves

3.2.1 Global analysis of maize trancriptome and metabolome during the infection with wild type *C. graminicola* CgM2

In order to assess the maize response to the infection with wild type *C. graminicola* CgM2, a combined transcriptome-metabolome analysis was performed in cooperation with partners from the research consortium DFG-FOR666. For this approach, a fourth leaf of two week old plants was sprayed with a conidiospore suspension with a fungal titer of $2x10^6$ conidia / ml and infected leaves were harvested at three time points; 36 hpi – when the fungus was in the biotrophic stage, 72 hpi – when the switch to necrotrophic growth occured and 96 hpi – when the fungus grew necrothrophically. Collected samples were used for microarray hybridisation and metabolome analysis. The experiment (central experiment, CET) was repeated independently three times.

Transcriptome analysis was performed with Affymetrix chip, harbouring 17 555 features representing 13 339 maize genes (12 113 of them were represented in distinct UniGene clusters). Features expressed differentially upon wild type *C. graminicola* CgM2 infection at any of the analysed time points (fold change >=2, when transcriptome of infected leaves was compared to that of mock treated control leaves), served as a template for a cluster analysis (Fig. 47). The transcrits profiles from the 36 hpi time point formed their own cluster and were separated from the other two time points, as not many changes in transcriptome could be observed at this early stage. This was probably caused by the relative small number of the infected host cells, diluted by the bigger portion of non-infected cells. At 96 hpi, there was a clear separation of the infected- and mock treated-leaves-derived sets of features, which indicates strong dynamics of host metabolism during the later stages of the infection. The data obtained for 72 hpi were not coherent as neither data from mock treated leaves nor data from infected leaves formed clearly separated clusters. Probably, the progression of the infection was not perfectly synchronised in all three repetitions of the experiment, which was mostly noticeable at 72 hpi as this time point reflects the transition from biotrophy to necrotrophy. Thus, the set of data obtained for 72 hpi was not further analysed.

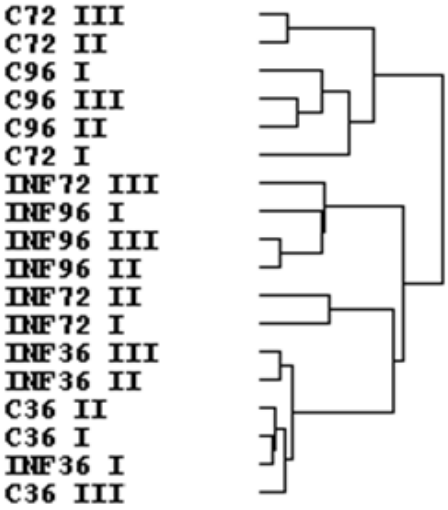

Fig. 47. Hierarchical Cluster Analysis (HCA) of differentially regulated maize transcripts, performed with Cluster 3.0 (using Spearman Rank Correlation as similarity metric) and displayed with TreeView programme. C – represents set of transcripts of mock treated leaves, INF – represents set of transcripts of wild type C. *graminicola* CgM2-infected leaves. Arabic numbers represent time points, at which the samples were harvested (hours post infection), Roman numbers – repetitions of central experiment.

At the early stages of the infection, minor effect on the transcriptome level could be observed, less than two percent of total number of features on the chip was identified as being differentially regulated in the two treatments (mock vs. infected leaves) (Table 8). Necrotrophic stage of the infection was associated with the greater alterations of the host transcription.

Table 8. Number of differentially expressed features based on microarray analysis of maize leaves (mock vs. wild type *C. graminicola* CgM2-infected) at 36 hpi and 96 hpi. Percentage given in brackets was calculated based on differentially regulated features relative to total number of features on the Affymetrix chip.

Differentially expressed features	**36 hpi**	**96 hpi**
Induced	251 (1.4%)	1 257 (7%)
Repressed	62 (0.34%)	692 (3.9%)

At 36 hpi, predominantly an accumulation of biotic stress-related transcripts and transcripts associated with secondary metabolism, i.e. metabolism of defence-related metabolites such as phenylpropanoids, could be observed (Fig. 48). Furthermore, changes in the expression of cell wall transcripts suggest a re-modeling of the cell wall as a part of

induced defence response. Induction of some transcripts involved in transport and signalling, including hormone signalling, was observed. However, it needs to be emphasised that in general, the portion of differentially regulated transcripts compared to the total number of transcripts in the respective functional category was low (see Table 8). Similarly, the result of cluster analysis of host metabolites indicate that host metabolism is almost not affected during the biotrophic stage of the infection (Supp. Fig. 7).

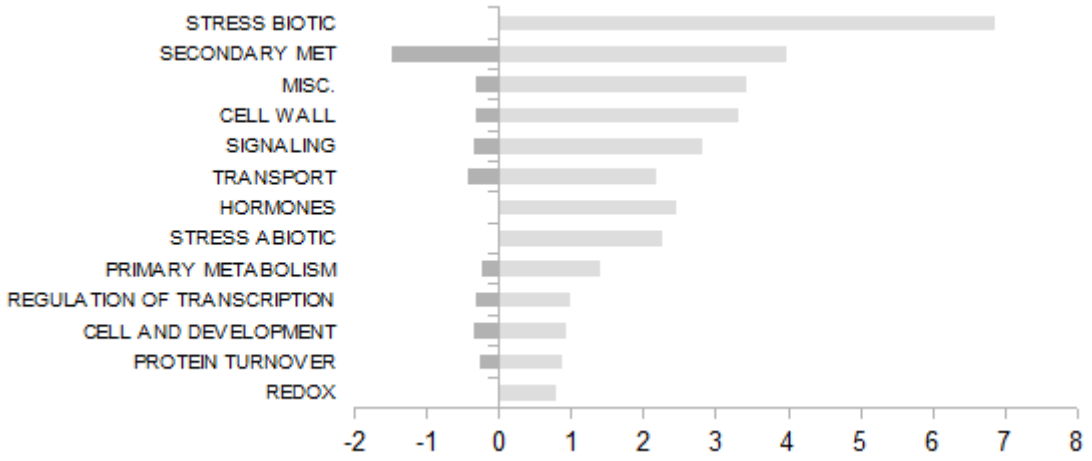

Fig. 48. Differentially expressed features 36 hours post wild type *C. graminicola* CgM2-infection, grouped into functional categories. Contribution of each functional category was calculated as a percentage of the total number of features belonging to the respective category on the chip. Bars of induced categories face to the right side and bars of repressed categories face to the left side. Secondary met – secondary metabolism, misc – miscellaneous i.e. all transcripts not belonging to any other category.

At 96 hpi however, massive changes in transcription of genes involved in secondary metabolism and genes associated with biotic stress, hormone signalling and redox status were detected (Fig. 49). Furthermore, an expression profile of genes involved in primary metabolism was altered, suggesting that host metabolism is strongly altered during the necrotrophic infection phase (Fig. 50).

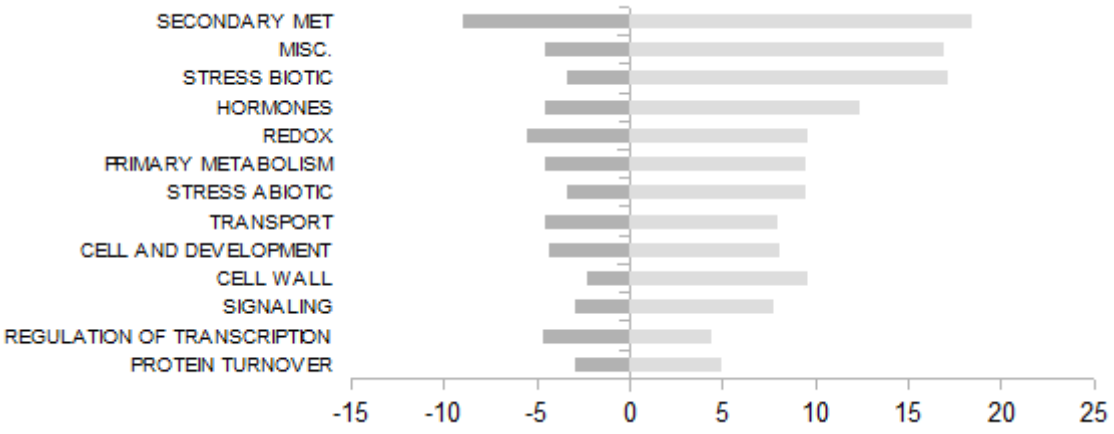

Fig. 49. Differentially expressed features at 96 hours post wild type *C. graminicola* CgM2-infection grouped into functional categories. Contribution of each category was calculated as a percentage of the total number of features belonging to the respective category on the chip. Bars of induced categories face to the right side and bars of repressed categories face to the left side. Secondary met – secondary metabolism, misc – miscellaneous i.e. all transcripts not belonging to any other category.

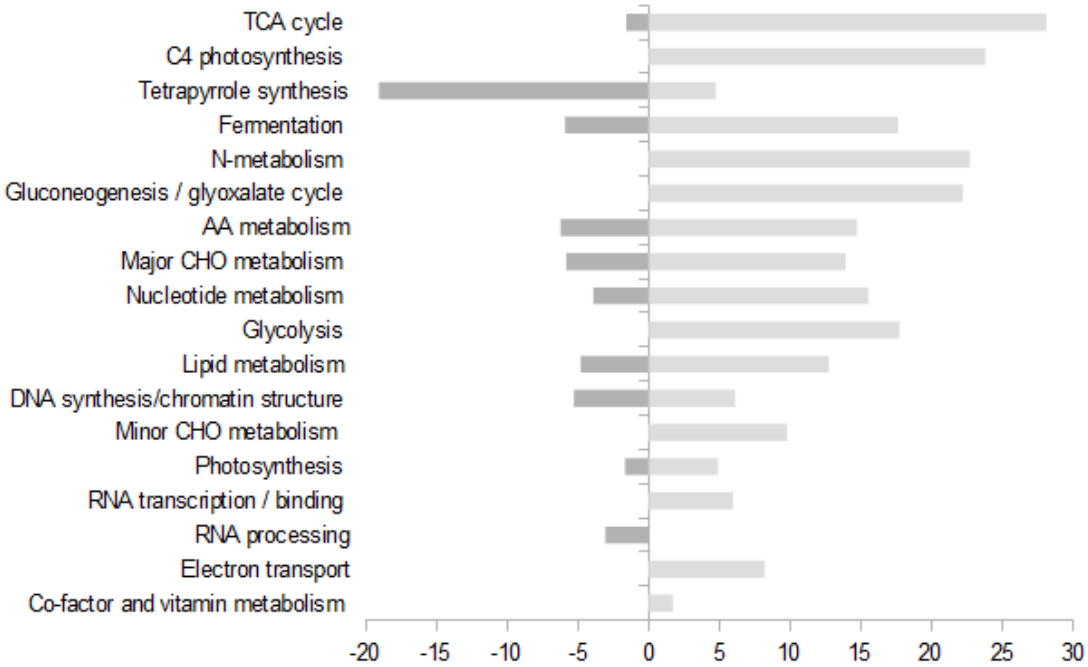

Fig. 50. Differentially expressed features involved in primary metabolism at 96 hours post wild type *C. graminicola* CgM2-infection and grouped into functional categories. Contribution of each category was calculated as a percentage of the total number of features from to the respective category on the chip. Bars of induced categories face to the right side and bars of repressed categories face to the left side.

3.2.2 Pathway-specific analysis of maize trancriptome and metabolome during the infection with wild type *C. graminicola* CgM2

Transcriptome analysis (see chapter 3.2.1) revealed changes in the expression of genes involved in primary metabolism in the wild type *C. graminicola* CgM2-infected leaves. A strong induction of genes of respiratory metabolism (TCA cycle and glycolysis), major N- and C-metabolism but also C4 photosynthesis was observed. Thus, steady state contents of metabolites, involved in pathways affected on the transcriptional level, were evaluated in the samples collected during the central experiment.

3.2.2.1 Host glycolysis and TCA cycle are induced on the trancriptome level and metabolome level during the necrotrophic growth of wild type *C. graminicola* CgM2

Genes coding for glycolytic enzymes were affected mainly at 96 hpi. Two genes coding for irreversible steps of this pathway; phosphofructokinase and pyruvate kinase were moderately induced (fold change = 3-5). On the metabolome level, only contents of glucose-6-phosphate and fructose-6-phosphate as well as fructose-1,6-bisphosphate were significantly higher in the infected leaves (Fig. 51). However, these metabolites are also involved in the competing anabolic pathway, i. e. sucrose synthesis, which was concomitantly upregulated at 96 hpi (see chapter 3.2.2.2.). On the other hand, in the illuminated leaves, the activity of Calvin cycle strongly contributes to fructose-6-phosphate and fructose-1,6-bisphosphate content.

Microarray analysis revealed that the *α-ketoglutarate dehydrogenase* gene, coding for a regulated enzyme of the TCA cycle, is up-regulated 11 times during the necrotrophic stage of the infection (Fig. 52). Transcripts for another key regulatory enzyme of the cycle, citrate synthase, were three times more abundant in infected leaves. The other enzymes of the TCA cycle were slightly induced on the transcript level (fold change 2-6). Similar to transcripts of the TCA cycle genes, intermediates of the TCA cycle were also accumulating in infected leaves at later stages of infection (at 96 hpi) (Fig. 52). A massive, 37-fold increase in isocitrate content was observed, accompanied by significantly elevated contents of malate, α-ketoglutarate and succinate. This result might suggest that induction of respiratory pathway occurs first during the necrotrophic growth phase of *C. graminicola*. However, lack of pronounced changes in the metabolite profile during the early stage of infection could result from the fact that just a small portion of the cells was penetrated by the fungus at 36 hpi, when compared to non-infected cells. Like in case of transcriptome data, as discussed above, it could mask the influence of the fungus on the host metabolism.

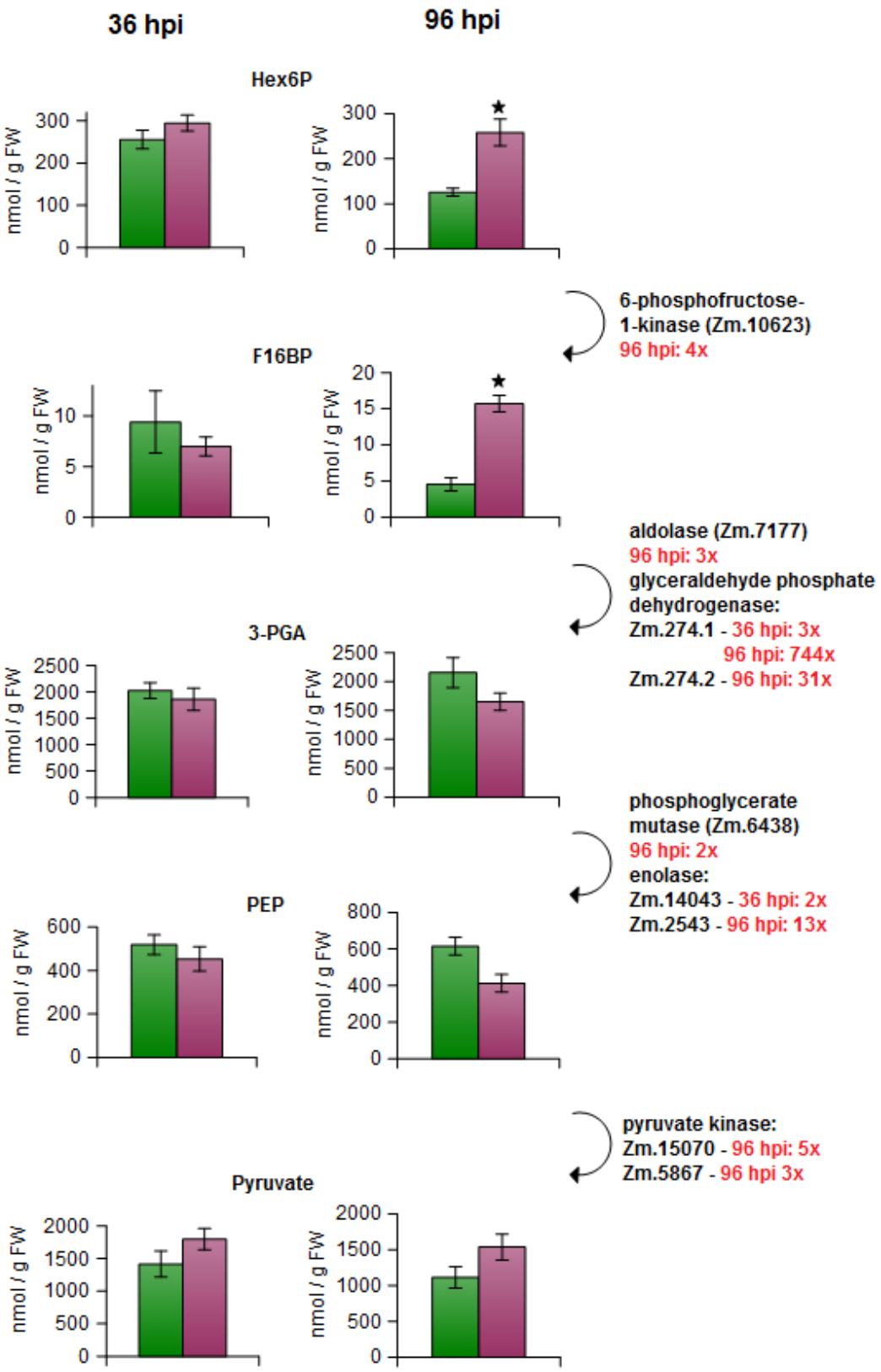

Fig. 51. Combined transcriptome-metabolome analysis of glycolysis in maize leaves at 36 and 96 hours post infection with wild type *C. graminicola* CgM2. Contents of metabolites were shown as mean values of all three repetitions of the CET with the error bars representing the standard error (n =9-12). Green bars represent mock-treated leaves, purple bars – leaves infected with *C. graminicola*. Significant differences (t-test, p-value < 0.05) between the contents in the mock-treated and infected leaves are marked with an asterisk. Up-regulation of the genes coding for glycolytic enzymes based on microarray analysis is shown as fold change (infected vs. mock-treated leaves).

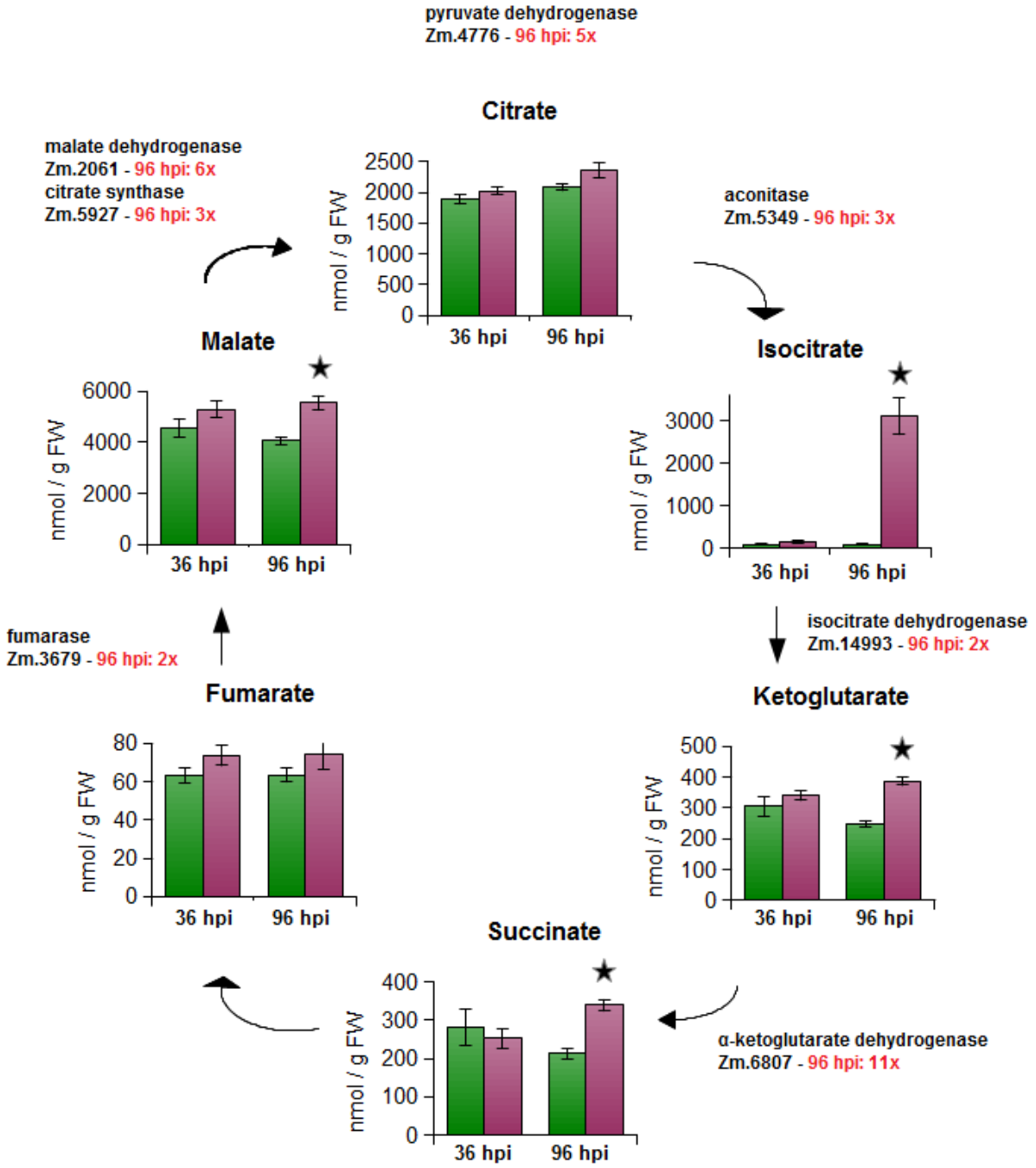

Fig. 52. Combined transcriptome-metabolome analysis of TCA cycle in maize leaves at 36 and 96 hours post infection with wild type *C. graminicola* CgM2. Contents of metabolites were shown as mean values of all three repetitions of CET with the error bars representing the standard error (n =9-12). Green bars represent mock-treated leaves, purple bars – leaves infected with *C. graminicola*. Significant differences (t-test, p-value < 0.05) between the contents in the mock-treated and infected leaves were marked with an asterisk. Up-regulation of the genes coding for enzymes of tricarboxylic acid cycle based on microarray analysis was shown as fold changes (infected vs. mock-treated leaves).

These results inspired to study the influence of *C. graminicola* infection on host respiration on the physiological level. Dark respiration rate of maize leaves, assessed by gas exchange measurements, was elevated upon infection when compared to mock treated control plants already at 3 dpi, but there was no significant difference in the transpiration rate

between the treatments (Fig. 53). This observed increase in dark respiration rate correlated with a decrease of the photosynthesis efficiency. The effective PSII quantum yield (Y(II)) of infected leaves was lower compared to mock treated control plants (Fig. 8 in chapter 3.1.1.).

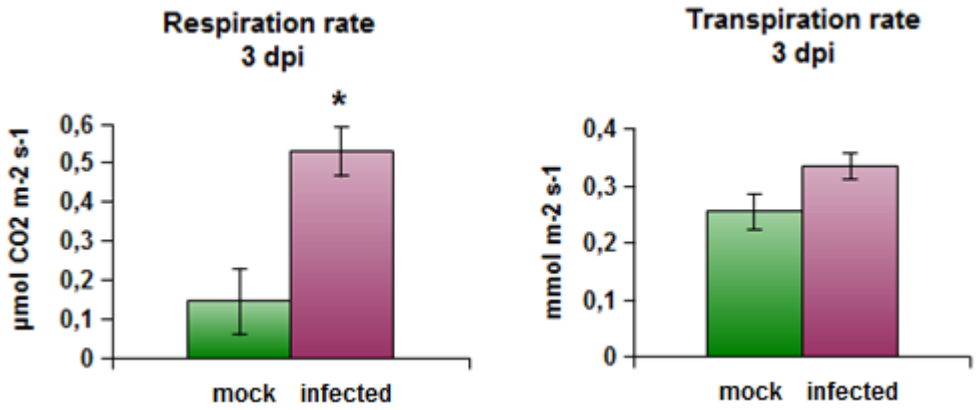

Fig. 53. Respiration and transpiration rates of wild type *C. graminicola* CgM2-infected maize leaves at 72 hpi, compared to mock-treated leaves. Data represents means of values determined for three replicate leaves with the error bars representing the standard error. Significant difference (t-test, p-value < 0.05) between the treatments is marked with an asterisk.

3.2.2.2 Interaction with wild type *C. graminicola* CgM2 leads to the accumulation of hexoses in maize leaves

Inhibition of photosynthesis and induction of respiratory metabolism may indicate a transition from source to sink metabolism in infected maize leaves. As this process is commonly accompanied by the induction of cell wall invertases in variety of plant-pathogen interactions, activities of maize cell wall and soluble acid invertase were evaluated. Activity of the former enzyme was increased 1.5 times in infected leaves at 96 hpi, while that of the latter enzyme three times (Fig. 54). No significant change in activity of both enzymes was observed during early interaction at 36 hpi (data not shown).

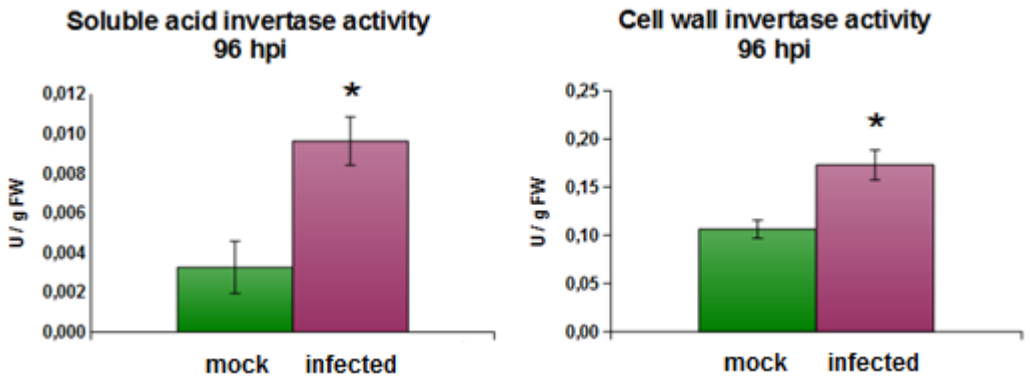

Fig. 54. Soluble acid invertase and cell wall invertase activities in wild type *C. graminicola* CgM2-infected maize leaves at 96 hpi, compared to mock-treated leaves. Mean values of all three repetitions of the CET are shown with the error bars representing the standard error (n =9-12). Significant differences (t-test, p-value < 0.05) between the contents in the mock-treated and infected leaves are marked with asterisks.

Transcripts of the genes coding for these two enzymes accumulated during the necrotrophic stage of the infection 2.4 times (*cell wall invertase 1* – Zm.409) and 2.3 times (*soluble acid invertase* - Zm.81096). A 10-fold increase in *sucrose synthase* (Zm.84048) transcripts at 96 hpi suggests that sucrose is degraded in the infected leaves not only by invertases but also by sucrose synthase. Moreover, accumulation of hexoses and elevated hexose to sucrose ratio were observed already at 36 hpi and were even more pronounced at 96 hpi, during the necrotrophic stage of fungal growth (Fig. 55).

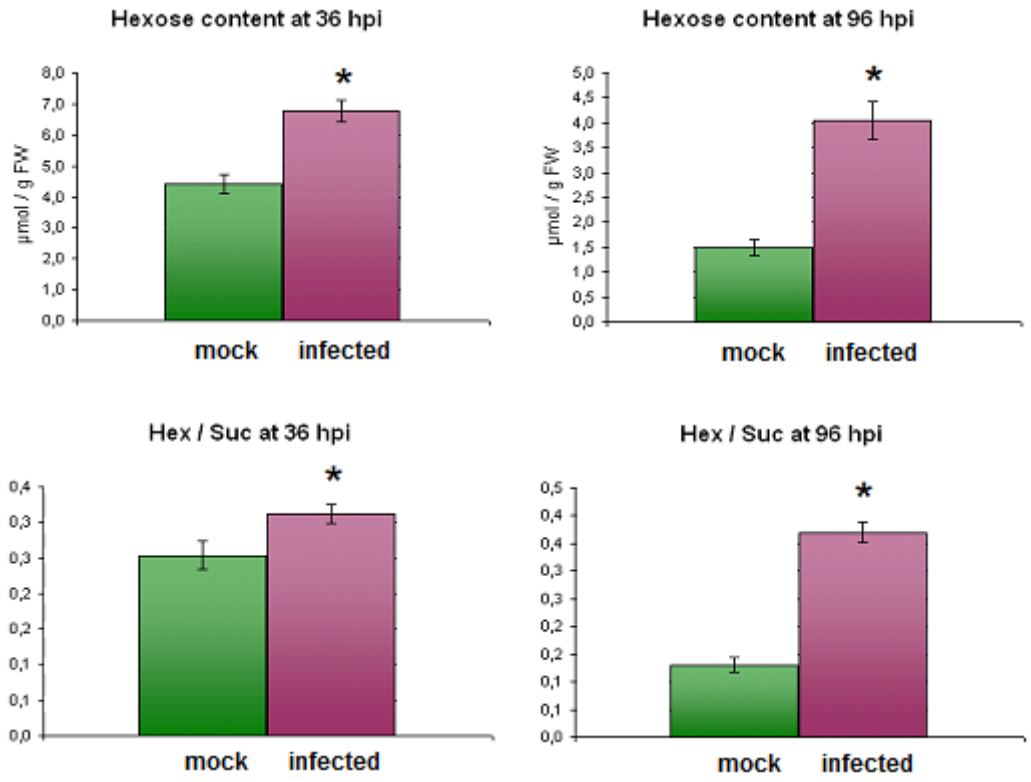

Fig. 55. Hexose content and hexose to sucrose ratio in wild type *C.graminicola* CgM2-infected maize leaves at 36 and 96 hpi, compared to mock-treated leaves. Mean values of all three repetitions of the CET are shown with the error bars representing the standard error (n =9-12). Significant differences (t-test, p-value < 0.05) between the contents in the mock-treated and infected leaves are marked with asterisks.

Interestingly, despite the activation of sucrose degrading enzymes, sucrose content was not altered in the infected leaves (Fig. 56). This could suggest that both sucrose degradation and synthesis are enhanced upon *C. graminicola* infection. Indeed, contents of the intermediates of sucrose synthesis were elevated at 96 hpi when compared to mock-treated control plants (Fig. 57). No significant changes in content of sucrose synthesis

intermediates were observed at 36 hpi (data not shown). Furthermore, expression of the gene coding for *sucrose phosphate phosphatase* (Zm.8470), catalyzing last step of sucrose synthesis, was induced 4.5 times at 96 hpi.

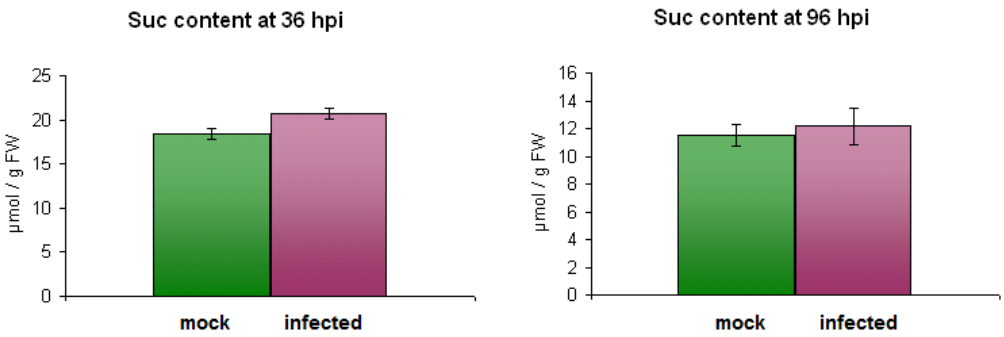

Fig. 56 Sucrose content in wild type *C. graminicola* CgM2-infected maize leaves at 36 and 96 hpi, compared to mock-treated leaves. Mean values of all three repetitions of the CET are shown (n =9-12).

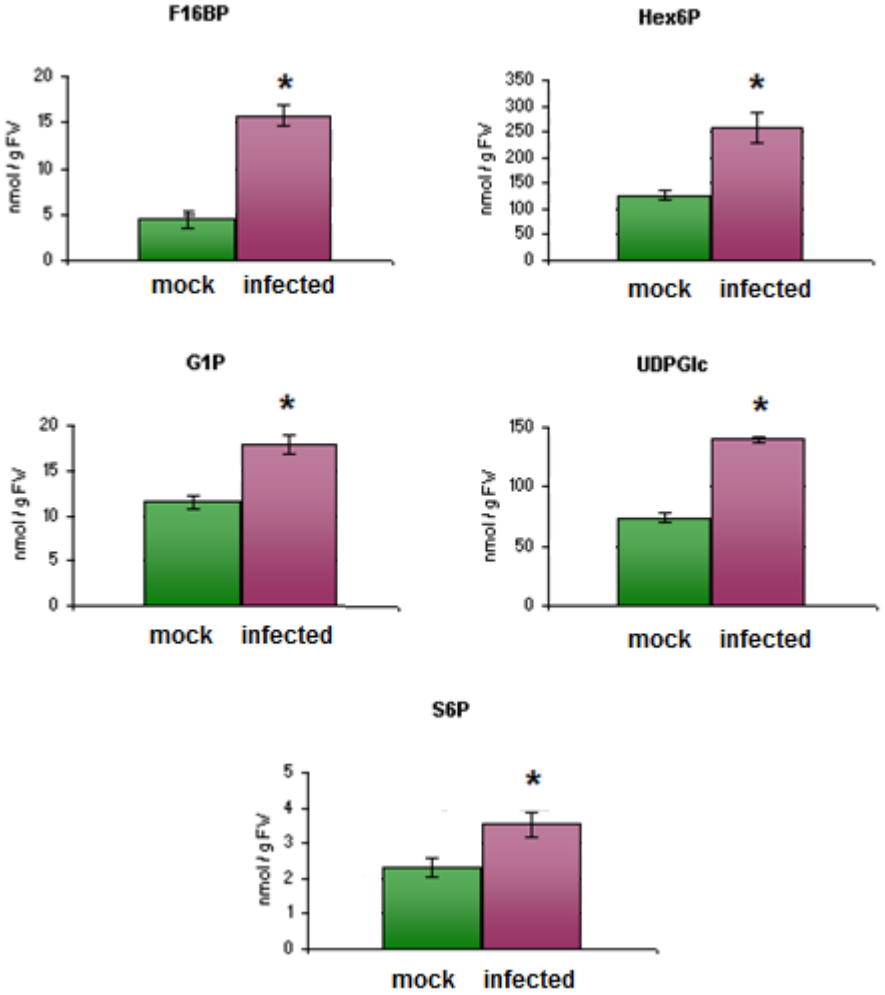

Fig. 57. Contents of phosphorylated intermediates of sucrose synthesis in *C. graminicola* CgM2-infected maize leaves at 96 hpi, compared to mock-treated leaves. Mean values of all three repetitions of the CET are shown with the error bars representing the standard error (n =9-12). Significant differences (p-value < 0.05) between the contents in the mock-treated and infected leaves are marked with asterisks.

On transcriptome level, starch degradation was induced with concomitant repression of starch synthesis. Two *beta-amylase* genes were induced 2-fold (Zm.3883) and 3-fold (Zm.80), while *ADP-glucose pyrophosphorylase* (Zm.12726) and *starch synthase* (Zm.423) were repressed 2-fold, as revealed by microarray analysis. The infection with wild type *C. graminicola* CgM2 did, however, not have an influence on starch content in maize leaves (Fig. 58).

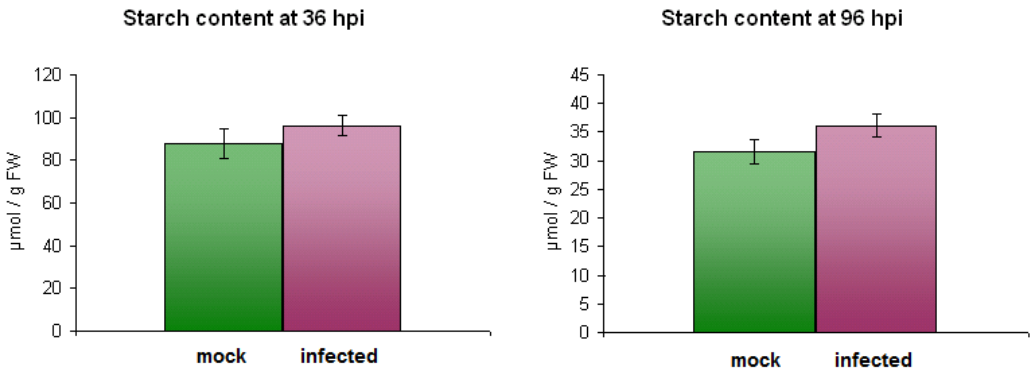

Fig. 58. Starch content in wild type *C. graminicola* CgM2-infected maize leaves at 36 and 96 hpi, compared to mock-treated leaves (mock). Mean values of all three repetitions of the CET are shown with the error bars representing the standard error (n =9-12).

3.2.2.3 Contents of free aromatic amino acids are elevated in leaves infected with wild type *C. graminicola* CgM2 at 96pi

Microarray analysis revealed an accumulation of transcripts involved in nitrogen metabolism during the necrotrophic stage of the infection (Fig. 50). An accumulation of free amino acids was observed at 36 hpi, while the total content of free amino acids was not affected at 96 hpi when compared to mock-treated leaves (Fig. 59). However, the infection with wild type *C. graminicola* CgM2 strongly influenced the composition of the free amino acid pool, but only at 96 hpi (Fig. 60). No significant changes in relative content occurred at 36 hpi (data not shown).

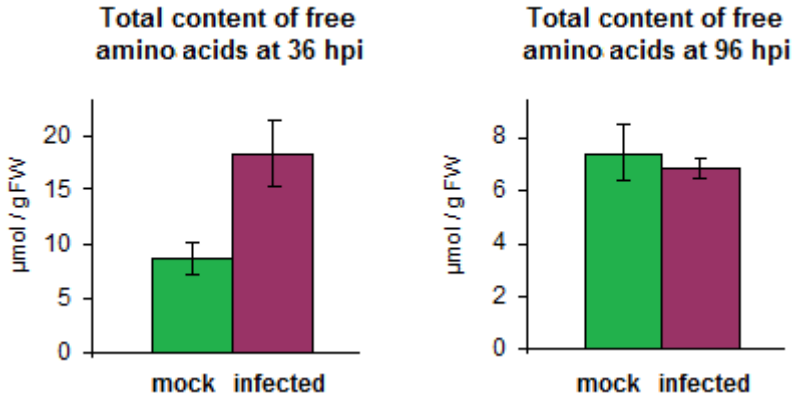

Fig. 59. Total content of free amino acids in wild type *C. graminicola* CgM2-infected maize leaves at 36 hpi (left) and 96 hpi (right), compared to mock-treated leaves. Mean values of all three repetitions of the CET are shown with the error bars representing the standard error (n =9-12).

Contents of aspartate and alanine were reduced. An increase in contents of glycine and serine, intermediates of photorespiratory pathway, and resulting two-fold increase in glycine/serine ratio were observed in infected leaves compared to mock control leaves. Infection with wild type *C. graminicola* CgM2 led also to increased contents of histidine, lysine, proline, branched-chain amino acids (valine, alanine, leucine) and aromatic amino acids (tyrosine and phenylalanine). Elevated levels of phenylalanine and tyrosine might indicate an induced defence response, as these amino acids are substrates for phenylpropanoid biosynthesis that produces major phytoalexins in maize.

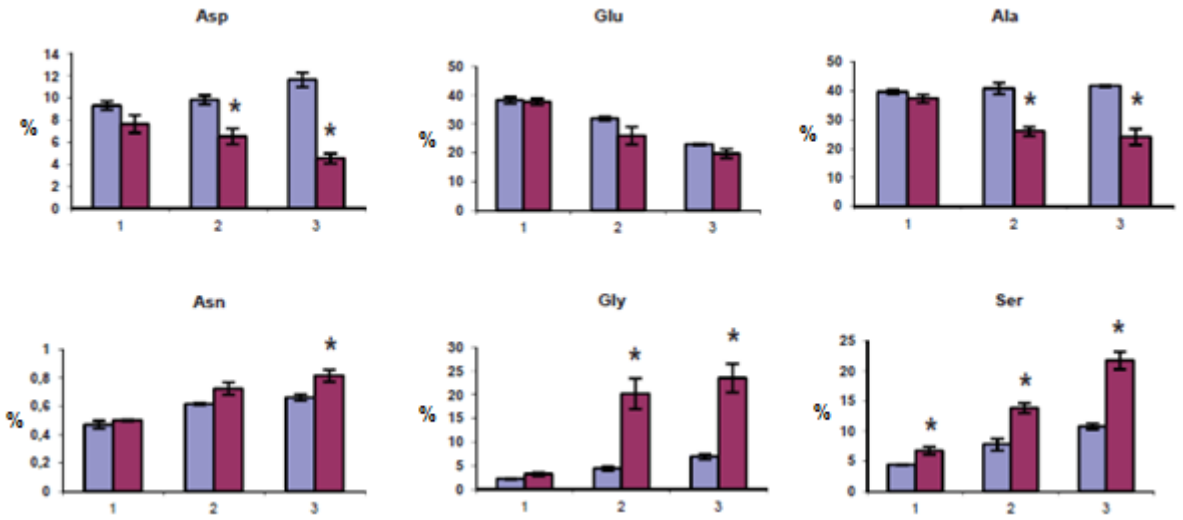

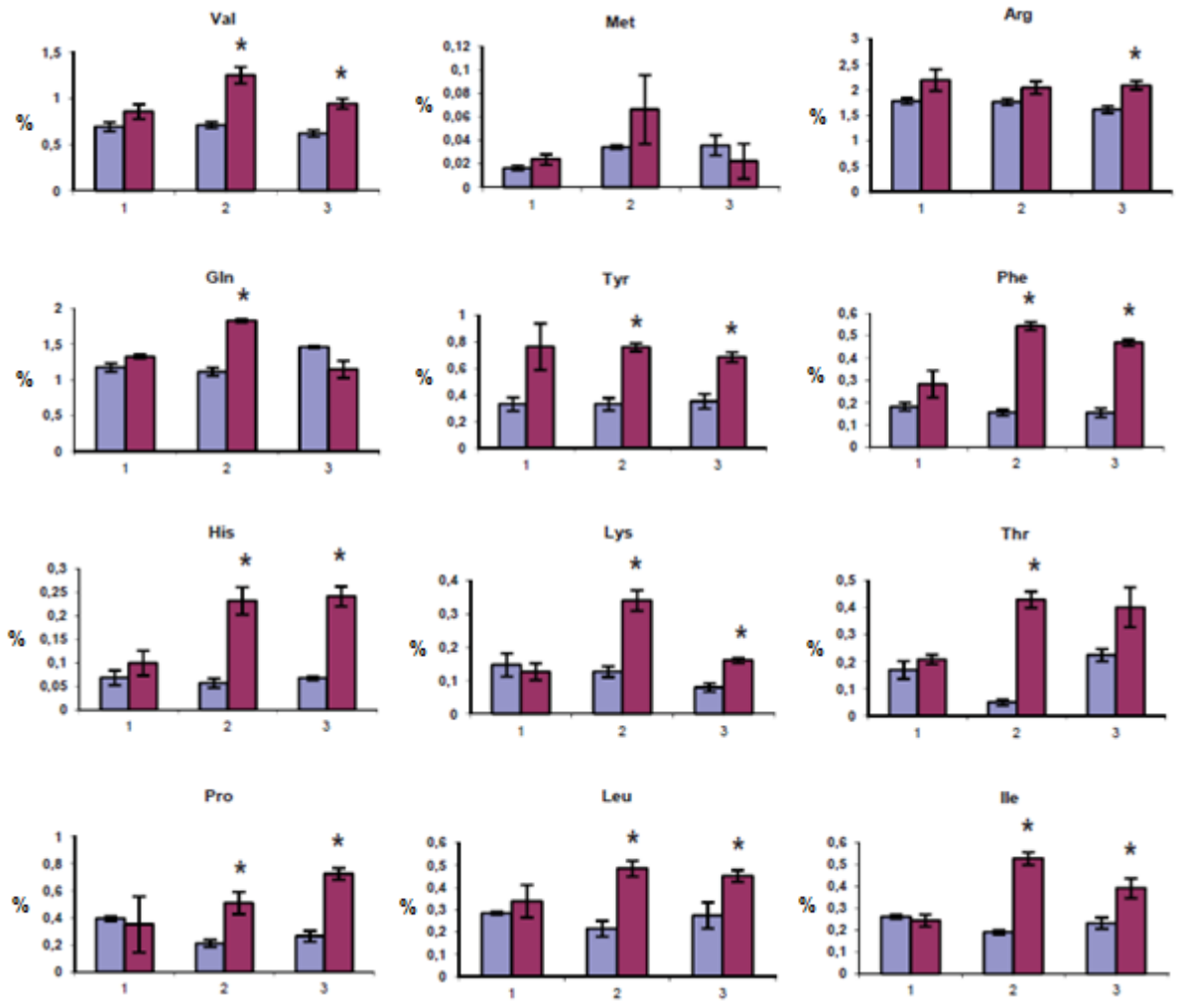

Fig. 60. Free amino acid pool composition in maize leaves infected with wild type *C. graminicola* CgM2 at 96 hpi. Relative contents of free amino acids, evaluated as a percentage of total amino acid content are depicted for *C. graminicola*-infected (purple bars) and mock-treated leaves (blue bars). Amino acids are abbreviated according to three letter code. The results from three experimental replicates of the CET (1-3) are shown with the error bars representing the respective standard error. Significant differences (t-test, p-value < 0.05) between mock-treated and infected leaves in the respective experimental replicate are marked with an asterisk.

Microarray data corroborate that aromatic acid biosynthesis through the shikimate pathway was up-regulated on transcriptome level in infected leaves at 96 hpi, as transcripts for 10 of the 17 unigenes of the pathway that were represented on the array were found to be induced on the transcriptional level (Table 9). The greatest induction was observed for 3-*dehydroquinate dehydratase* (311-fold) and *prephenate dehydratase* (Zm.81014, 58-fold). *Shikimate kinase* (Zm.85349, 14-fold), *tyrosine aminotransferase* (14-fold) and *EPSP synthase* (12-fold) were moderately up-regulated, while *chorismate synthase* (Zm.18081) and *chorismate mutase* (Zm.5976) were both induced 5-fold. Moreover, *phenylalanine ammonia-lyase* (Zm.15903), gene coding for an enzyme deaminating phenylalanine to cinnamic acid, a

precursor of all phenylpropanoids, was up-regulated on the transcriptome level 33-fold at 96 hpi.

Table 9. Transcriptional regulation of genes of aromatic amino acid biosynthesis in wild type *C. graminicola* CgM2-infected maize leaves at 96 hpi. Annotated unigenes that were up-regulated compard to mock-treated control leaves (fold change >=2) are highlighted in green. Dotted line in the "localisation" means that sub-cellular localisation could not be predicted with TargetP 1.1 (available at http://www.cbs.dtu.dk/services/TargetP/)

Gene	UniGene	Fold change	Localisation	Rice homolog localisation
phospho-2-dehydro-3-deoxyheptonate aldolase	Zm.10517	0,7x	chloroplast	chloroplast
3-dehydroquinate dehydratase	Zm.6257	311x	----- (partial sequence)	----- (partial sequence)
shikimate dehydratase	Zm.2709	1x	chloroplast	chloroplast
shikimate kinase	Zm.85349 Zm.3954 Zm.4535	14x 2x 0,5x	mitochondrial chloroplast chloroplast	chloroplast chloroplast chloroplast
EPSP synthase	Zm.98	12x	-----	chloroplast
chorismate synthase	Zm.18081 Zm.13401	5x 1x	chloroplast chloroplast	chloroplast chloroplast
chorismate mutase	Zm.5976 Zm.10652 Zm.5976	5x 1,5x 1x	----- ----- -----	----- ----- chloroplast
prephenate dehydratase	Zm.81014 Zm.118787 Zm.82666 Zm.12272	58x 5x 1x 1x	chloroplast chloroplast chloroplast chloroplast	chloroplast chloroplast chloroplast chloroplast
tyrosine aminotransferase	Zm.118031	14x	-----	-----

3.2.2.4 Antioxidant content in maize leaves infected with wild type *C. graminicola* CgM2 is not altered.

Enhanced generation of reactive oxygen species is an early component of the plant defence response and serves as signal that drives downstream defence mechanisms. Due to the fact that reactive oxygen species are destructive to the cell constituents, it is important to control intracellular ROS levels. Soluble antioxidants such as glutathione and ascorbate play an important role in this process. Thus, glutathione and ascorbate content and the redox status of these two antioxidants were analysed in maize leaves upon *C. graminicola* infection. No

significant difference in glutathione content and its reduction status could be observed between infected and mock treated maize leaves at both analysed time points (36 hpi and 96hpi) (Supp. Fig. 7). The ascorbate content was lower in infected tissue only at 96 hpi in one repetition of the experiment; however its reduction status remained unaltered (Supp. Fig. 8).

It can be concluded that infection of maize with wild type *C. graminicola* CgM2 does not alter host soluble antioxidant status.

3.3 Investigating the role of selected, strongly induced host genes for the maize – *Colletotrichum graminicola* interaction

3.3.1 Role of maize alternative oxidase AOX3 for the interaction with *C. graminicola*

3.3.1.1 Two genes coding for alternative oxidases are induced in maize leaves colonised with *Colletotrichum graminicola*

Maize transcriptome analysis revealed that cellular respiration, was induced in maize leaves (cv. Nathan) infected with *C. graminicola* at 96 hpi. The greatest up-regulation of expression of respiratory chain genes was observed for *alternative oxidase 2* (*AOX2*, 17-fold), *AOX3* (339-fold) and *NADPH dehydrogenase* (90-fold). Moreover, the expression of *AOX2* and *AOX3* was enhanced 2.3-fold and 25-fold, respectively, already during the biotrophic stage of interaction (at 36 hpi) (Fig. 61). To confirm these results, relative quantity of *AOX2* and *AOX3* transcript amounts was determined by qRT-PCR.

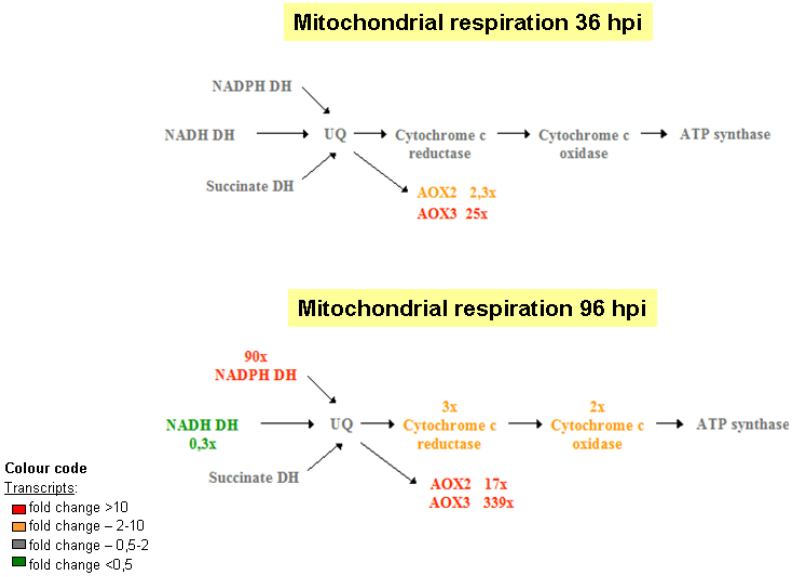

Fig. 61. Induction of structural genes of mitochondrial respiration in maize leaves (cv. Early Golden Bantam) infected with wild type *C. graminicola* CgM2 at 36 hpi (top) and 96 hpi (bottom). The components of the mitochondrial electron transport chain, their positions in the chain and the direction of electron transport (marked with arrows) are presented in the scheme. The genes with unaltered expression level upon infection are marked in grey while genes weakly/moderately/strongly induced were marked in green/orange/red, according to the colour code depicted in the figure. NAD(P)H DH – *NAD(P)H dehydrogenase*, succinate DH – *succinate dehydrogenase*, UQ – *ubiquinone*, AOX2/3 – *alternative oxidase 2/3*. Data shows the fold change in expression (infected vs. mock-treated leaves, n=3).

A strong 14-fold increase in *AOX3* transcript amounts was observed at 2 dpi (Fig. 62). The induction of *AOX3* expression was even more pronounced at 4 dpi (875-fold). Interestingly, transcript level of *AOX2* accumulated moderately only during the necrotrophic stage of the infection (14-fold at 4 dpi) (Fig. 62). This result corroborates the microarray data and suggests that only AOX3 can play a role during early stages of the interaction with *C. graminicola* and might be associated with basal defence response. To test this hypothesis, the induction of *AOX3* in the interaction with two insertion mutant strains of *C. graminicola* with reduced pathogenicity was determined. AT171 is a strain with weakly affected virulence, due to decreased penetration rate (Münch et al. 2011), while AT416 is affected at all steps of *in planta* development, which leads to severely reduced virulence (as presented in Fig. 4 in chapter 3.1.1). *AOX3* transcript amounts were determined by qRT-PCR at 24, 36 and 44 hours post infection.

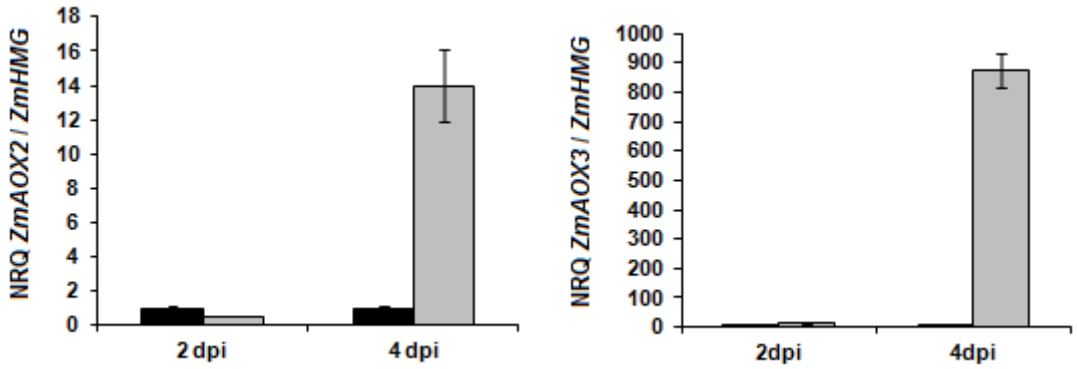

NRQ *ZmAOX2 / ZmHMG*	$NRQ_{infected}$/ NRQ_{mock}
2 dpi	0.5
4 dpi	14

NRQ *ZmAOX3 / ZmHMG*	$NRQ_{infected}$/ NRQ_{mock}
2 dpi	14
4 dpi	875

Fig. 62. Induction of maize *alternative oxidase 2* and *3* in maize leaves (cv. Nathan) infected with wild type *C. graminicola* CgM2, as analysed by qRT-PCR. Leaves were spray-inoculated with a fungal titer of 10^6 conidia / ml. Mean values (n=4) of quantity of transcripts relative to the housekeeping gene *ZmHMG (high mobility group I/Y-2*), calibrated to respective mock control (NRQ_{mock} = 1) are shown (upper panel). Black bars – mock-treated control leaves, grey bars – infected leaves. Asterisks indicate a significant difference to mock controls (t-test, p-value < 0.05). Error bars represent the standard error. Respective NRQ fold changes are presented in the lower panel.

Induction of *AOX3* expression occurred already at 24 hpi and increased with infection progress, which was more pronounced in leaves infected with wild type strain CgM2 (Fig. 63). Moderate accumulation of *AOX3* transcript during pre-penetration stage (24 hpi) and very strong accumulation at the time point after the establishment of biotrophic interaction (44 hpi) suggests that *AOX3* may rather be involved in induced defence response events than in basal defence. This idea is supported by the observation that the level of *AOX3* transcript in leaves infected with the mutant strain AT416 was relatively stable at all tested time points. AT416 exhibits delayed development compared to the wild type strain CgM2, meaning that even at 44 hpi no penetration events commonly occur in AT416-inoculated leaves (Fig. 4). Moreover, a positive correlation between *AOX3* induction and the virulence of the used strain (see right panel in Fig. 63), was possibly reflecting the number of penetrating appressoria and the amount of fungal hyphae within the host tissue.

The differences in transcript accumulation in leaves two days after inoculation with wild type *C. graminicola* CgM2 that was observed between the two experiments (Fig. 62 and 63) most probably resulted from two different inoculation strategies that were used. During the second experiment, leaves were inoculated by dipping into spore suspension instead of spraying with spore suspension, which increased the number of infected cells per leaf area and thus enriched the analysed leaf samples for infected cells.

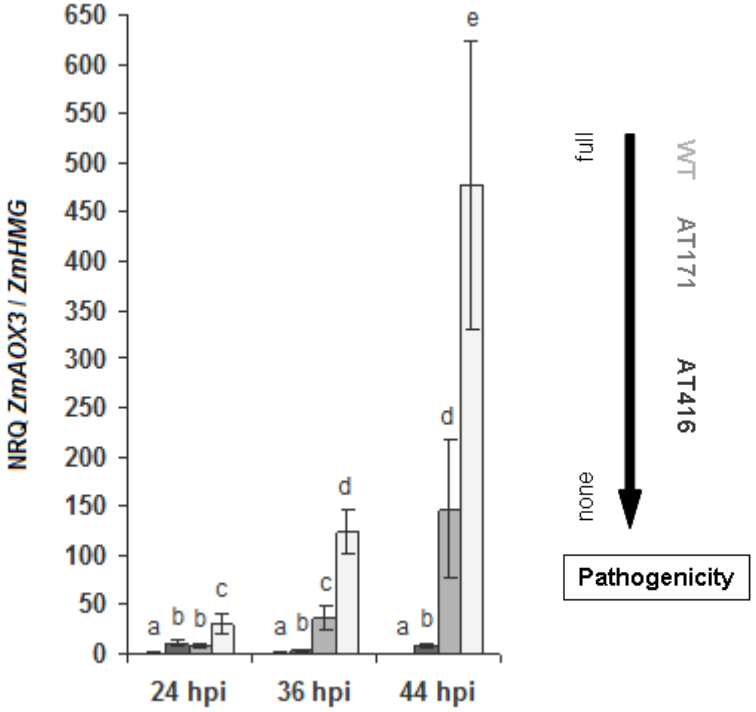

NRQ *ZmAOX3* / *ZmHMG*	NRQ_{AT416}/ NRQ_{mock}	NRQ_{AT171}/ NRQ_{mock}	$NRQ_{wild\ type}$/ NRQ_{mock}
24h	11	8	30
36h	3	36	125
44h	8	147	478

Fig. 63. Induction of maize *alternative oxidase 3* in maize leaves (cv. Nathan) infected with *C. graminicola* wild type strain CgM2 (pale grey bars) and pathogenicity mutants strains AT171 (grey bars) and AT416 (dark grey bars), as analysed by qRT-PCR. Leaves were dip-inoculated with a fungal titer of 10^4 conidia / ml. Mean values (n=4) of quantity of transcripts relative to housekeeping gene *ZmHMG* (*high mobility group I/Y-2*), calibrated to respective mock control (black bars) (NRQ_{mock} = 1), are shown (upper panel). Different letters (a, b, c, d) represent significant differences (t-test, p-value<0.005). Error bars represent the standard error. Respective NRQ fold changes are presented in the lower panel.

3.3.1.2 *AOX3* gene responds to the hormones regulating plant defence responses

To further elucidate the role of AOX3 in plant defence response, *AOX3* gene expression after treatment with plant hormones and their analogues was tested. Both jasmonic acid and 2,6-dichloroisonicotinic acid (INA), an analogue of salicylic acid, induced the accumulation of *AOX3* transcript; with the influence of JA being more pronounced (Fig. 64). The treatment with 1-aminocyclopropane-1-carboxylic-acid (ACC), a precursor of ethylene, did not alter the level of *AOX3* expression (Fig. 64). Commonly, JA and ethylene act synergistically in plant defence response, but *AOX3* seems to not respond to ethylene.

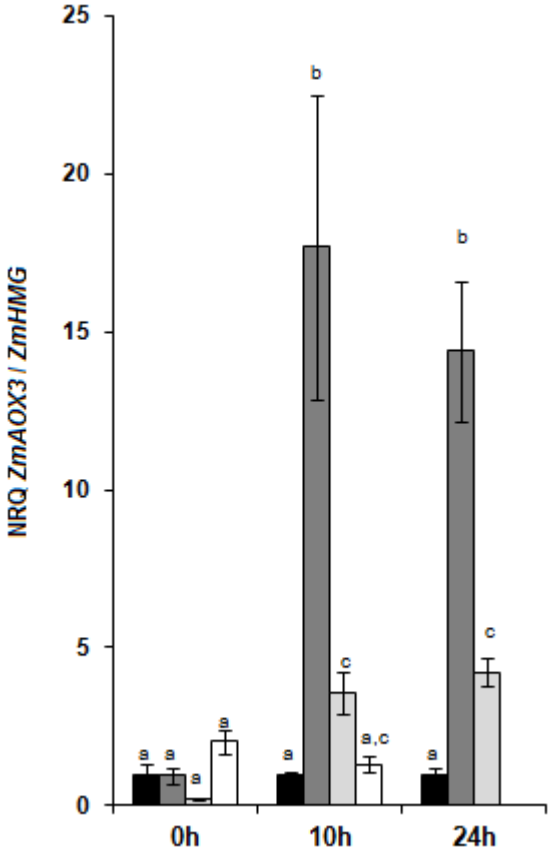

NRQ *ZmAOX3* / *ZmHMG*	NRQ_{JA}/ NRQ_{mock}	NRQ_{INA}/ NRQ_{mock}	NRQ_{ACC}/ NRQ_{mock}
0h	1	0.2	2
10h	18	4	1
24h	14	4	--

Fig. 64. Induction of maize *alternative oxidase 3* in maize leaves (cv. Nathan) treated with 1 mM jasmonic acid (JA) (dark grey bars), 1.3 mM 2,6-dichloroisonicotinic acid (INA, an analogue of salicylic acid) (pale grey bars) or 5 mM 1-aminocyclopropane-1-carboxylic-acid (ACC, a precursor of ethylene) (white bars) as analysed by qRT-PCR. Mean values (n=4) of quantity of transcripts relative to the housekeeping gene *ZmHMG* (*high mobility group I/Y-2*), calibrated to respective mock control (black bars) (NRQ_{mock} = 1), are shown (upper panel). Different letters (a, b, c) represent significant differences (t-test, p-value < 0.005). Error bars represent the standard error. Respective NRQ fold changes are presented in the lower panel.

3.3.1.3 Treatment with inhibitors of alternative oxidase restricts *C. graminicola* growth *on planta*

As presented in chapters 3.3.1.1 and 3.3.1.2, the *alternative oxidase 3* is induced in maize leaves colonised by *C. graminicola* and its expression can be triggered by hormones associated with the defence response. These results raise the question for the role of alternative oxidase in the interaction of maize with *C. graminicola*. Is the expression of *alternative oxidase* enhanced in response to the fungus in the frame of the plant defence

response or does the pathogen actively induce *AOX3* expression as part of its infection strategy. To clarify if host or pathogen benefit from *AOX* induction, fungal proliferation in maize leaves treated with inhibitors of alternative oxidase was evaluated. Treatment with both tested inhibitors, *n*-propyl gallate (nPG) and salicylhydroxamic acid (SHAM), reduced *C. graminicola* colonisation by more than half when compared to water-treated control leaves (Fig. 65).

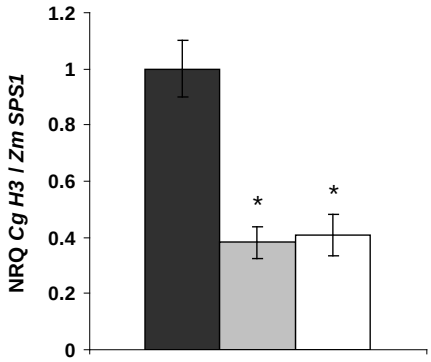

Fig. 65. Proliferation of wild type *C. graminicola* CgM2 three days after infection of maize leaves (cv. Nathan) pre-treated with water (black bar) or inhibitors of alternative oxidase – 10 mM salicylhydroxamic acid (pale grey bar) and 5 mM *n*-propyl gallate (white bar) for 24 hours prior to pathogen inoculation. Leaves were dip-inoculated with a fungal titer of 10^4 conidia / ml. The experiment was performed in three biological replicates and data from one representative replicate are presented. Mean values of relative amounts of fungal genomic DNA (*CgH3*) normalised to maize genomic DNA (*ZmSPS1*) are shown (n=4). All values were calibrated to water-pre-treated leaves (NRQ_{mock} = 1). Asterisks represent significant differences to water-treated control (t-test, p-value < 0.01). Error bars represent the standard error.

To exclude the possibility that nPG and SHAM are toxic to *C. graminicola* and directly inhibit its proliferation, fungal growth was tested on media containing different amounts of the inhibitors. Only the highest SHAM concentration tested was inhibiting *C. graminicola* growth; in case of nPG, concentrations of 0.5 mM and 5 mM had such effect (Fig. 66 and 67). Since these were the solutions which were fed to maize leaves via the transpiration stream, it can be assumed that *in planta* concentrations of the inhibitors were much lower.

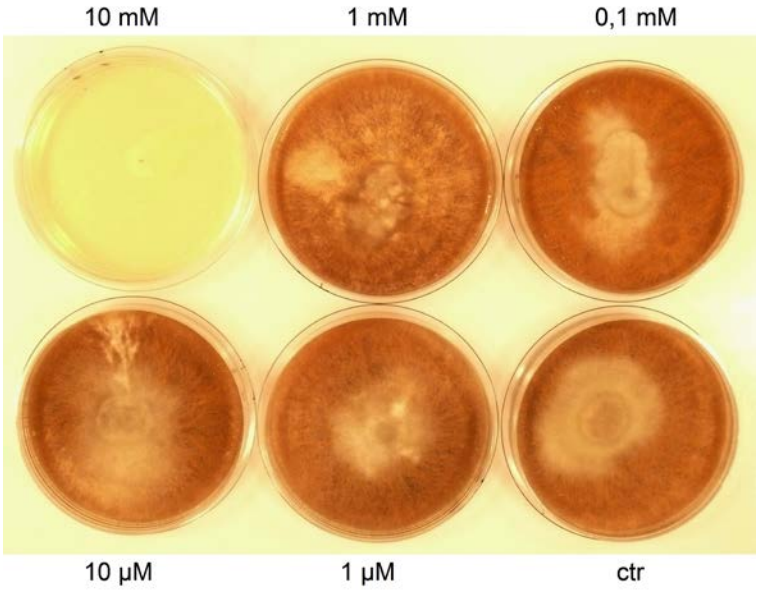

Fig. 66. Growth of wild type *C. graminicola* CgM2 on Fries complete medium plates supplemented with indicated concentration of salicylhydroxamic acid dissolved in dimethyl sulfoxide (DMSO). Control plate (ctr) was supplemented with DMSO only. Photo was taken 2 weeks after plate inoculation.

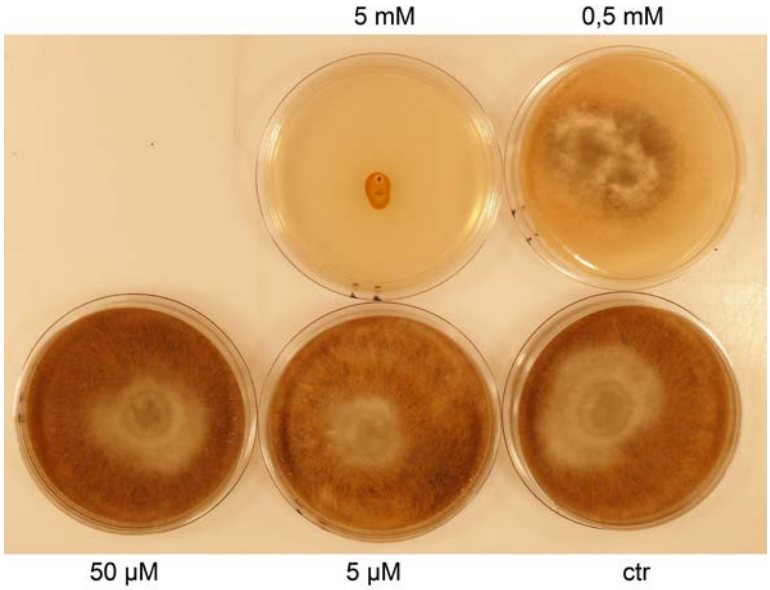

Fig. 67. Growth of wild type *C. graminicola* CgM2 on Fries complete medium plates supplemented with the indicated concentration of *n*-propyl gallate dissolved in dimethyl sulfoxide (DMSO). Control plate (ctr) were supplemented with DMSO only. Photo was taken 2 weeks after plate inoculation.

Since pre-treatment of maize leaves with AOX inhibitors resulted in diminished colonisation with *C. gramincola*, it can be hypothesised that induction of host alternative oxidase is beneficial for *C. graminicola.* ROS are important signalling molecules mediating plant defence responses (see chapter 1.3.1). Thus, enhanced activity of alternative oxidase would prevent ROS accumulation in maize leaves in response to *C. graminicola* infection and concomitantly interfere with defence events. To test this hypothesis, the expression of two maize defence-associated genes, *12-oxophytodienoate reductase 1* and *pathogenesis-related*

protein 5, was evaluated in leaves pre-treated with AOX inhibitors by qRT-PCR. Transcripts of these two genes accumulated much stronger in leaves treated with the inhibitors of alternative oxidase compared to water-treated control leaves (Fig. 68).

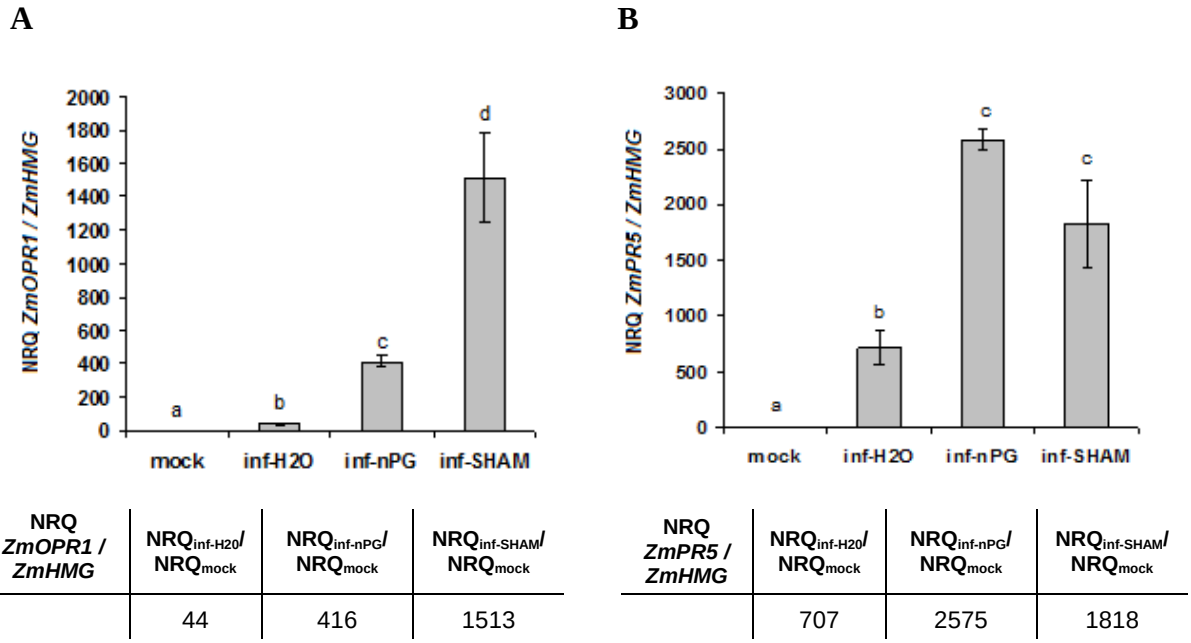

NRQ *ZmOPR1* / *ZmHMG*	$NRQ_{inf\text{-}H2O}$ / NRQ_{mock}	$NRQ_{inf\text{-}nPG}$ / NRQ_{mock}	$NRQ_{inf\text{-}SHAM}$ / NRQ_{mock}
	44	416	1513

NRQ *ZmPR5* / *ZmHMG*	$NRQ_{inf\text{-}H2O}$ / NRQ_{mock}	$NRQ_{inf\text{-}nPG}$ / NRQ_{mock}	$NRQ_{inf\text{-}SHAM}$ / NRQ_{mock}
	707	2575	1818

Fig. 68. Transcript accumulation of maize *12-oxophytodienoate reductase 1* (A) and *pathogenesis-related protein 5* (B) in maize leaves (cv. Nathan) three days after dip-inoculation with 10^4 conidia / ml of wild type *C. graminicola* CgM2 (inf). Leaves were either pre-treated with water or inhibitors of alternative oxidase – 10 mM salicylhydroxamic acid (SHAM) and 5 mM *n*-propyl gallate (nPG) for 20 h prior to pathogen inoculation. Mean values (n=4) of quantity of transcripts relative to the housekeeping gene *ZmHMG* (*high mobility group I/Y-2*), calibrated to mock control (NRQ_{mock} = 1) are shown. Different letters (a, b, c, d) represent significant differences (t-test, p-value < 0.005). Error bars represent the standard error. Respective NRQ fold changes are presented in the lower panel.

Interestingly, the expression of *AOX3* gene was also enhanced in inhibitor treated leaves (Fig. 69). It was already reported that inhibition of alternative oxidase leads to hydrogen peroxide accumulation (Popov et al., 1997) which was shown to induce AOX transcript accumulation in tobacco (Vanlerberghe and Mclntosh, 1996). The less pronounced effect of nPG on *AOX* expression compared to SHAM can be explained by a direct influence of nPG on ROS homeostasis, as it was shown before that *n*-propyl gallate can directly quench superoxide ions (Reddan et al., 2003).

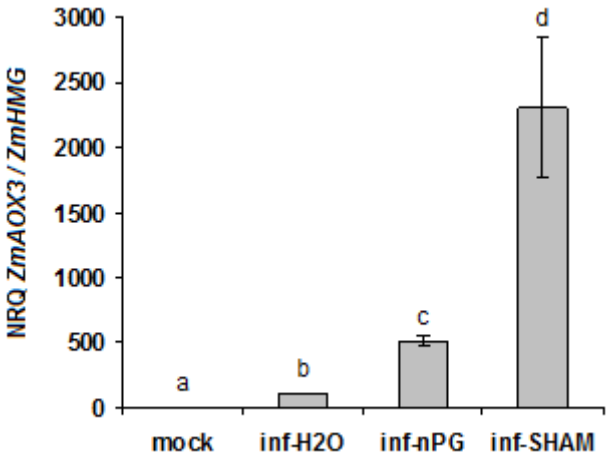

NRQ *ZmAOX3* / *ZmHMG*	$NRQ_{inf\text{-}H2O}$/ NRQ_{mock}	$NRQ_{inf\text{-}nPG}$/ NRQ_{mock}	$NRQ_{inf\text{-}SHAM}$/ NRQ_{mock}
	110	516	2309

Fig. 69. Transcript accumulation of maize *alternative oxidase 3* in maize leaves (cv. Nathan) three days after dip-inoculation with with 10^4 conidia / ml of wild type *C. graminicola* CgM2 (inf). Leaves were either pre-treated with water or inhibitors of alternative oxidase – 10 mM salicylhydroxamic acid (SHAM) and 5 mM *n*-propyl gallate (nPG) for 20 h prior to pathogen inoculation. Mean values (n=4) of quantity of transcripts relative to the housekeeping gene *ZmHMG* (*high mobility group I/Y-2*), calibrated to mock control (NRQ_{mock} = 1) are shown. Different letters (a, b, c, d) represent significant differences (t-test, p-value < 0.005). Error bars represent the standard error. Respective NRQ fold changes are presented in the lower panel.

Taken together, obtained data suggest that inhibition of alternative oxidase might lead to ROS accumulation which in turn could induce the expression of AOX and defence-associated genes. Thus, it is possible that *C. graminicola* benefits from enhanced AOX expression, which may prevent the induction of defence responses through insufficient ROS accumulation. In such a situation, alternative oxidase would serve as potential compatibility factor in maize – *C. graminicola* interaction. To finally prove this hypothesis, the interaction of *C. graminicola* with maize plants lacking alternative oxidase should be analysed. However, maize *AOX* deletion mutants are not available and maize plants with silenced *AOX* gene could not be generated as the virus-induced gene silencing procedure could not be established. Thus, further research on the influence of host alternative oxidase on the interaction with the pathogenic fungus was conducted in the *Arabidopsis thaliana – Colletotrichum higginsianum* pathosystem.

3.3.1.4 Transcripts of *Aox1a* and *Aox1d* accumulate in Arabidopsis leaves in response to *Colletotrichum higginsianum* infection

To elucidate if alternative oxidase is also induced in the *Arabidopsis thaliana – C. higginsianum* interaction, relative transcript levels of all five isoforms were quantified by qRT-PCR. *Aox1a* gene was induced in infected leaves, starting from two days post inoculation. However, a stronger accumulation of *Aox1a* transcripts was observed during necrotrophic colonisation (Fig. 70).

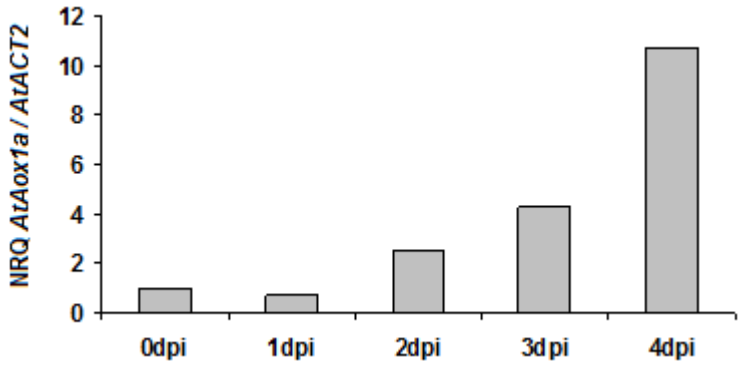

Fig. 70. Transcript accumulation of *Arabidopsis thaliana alternative oxidase 1a* in Arabidopsis leaves (cv. Col-0) in the course of *C. higginsianum* infection between 0 and 4 dpi. Relative quantities of transcripts were normalised to *AtACT2* (*Actin2*) and calibrated to mock control (NRQ_{0dpi} = 1). Each sample (a single replicate per time point) was prepared from pooled leaves of eight plants.

Transcripts of *Aox1d* also accumulated in infected leaves, already from the first day after inoculation, but expression level of this gene was much lower compared to *Aox1a*, even at later stages of the infection (Fig. 71, 72). Transcripts of the other three alternative oxidase isoforms (*Aox1b*, *Aox1c* and *Aox2*) could not be detected throughout the experiment.

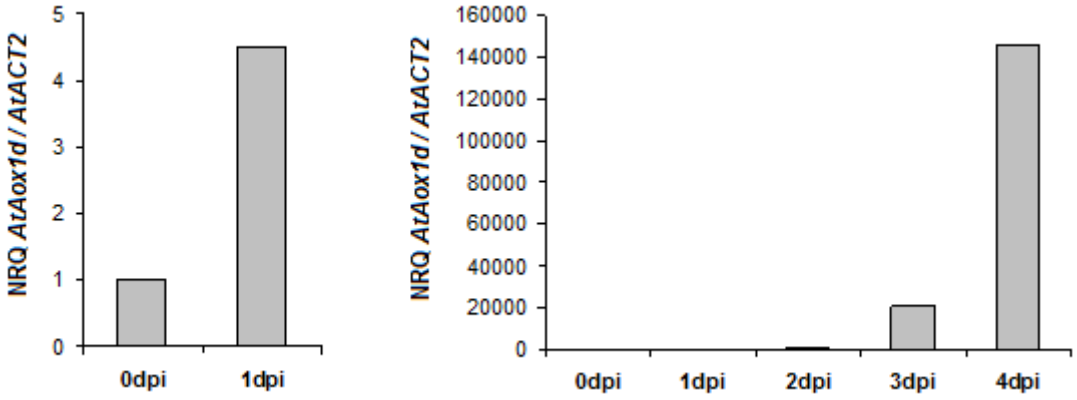

NRQ *AtAox1d* / *AtACT2*	NRQ_{1dpi}/ NRQ_{0dpi}	NRQ_{2dpi}/ NRQ_{0dpi}	NRQ_{3dpi}/ NRQ_{0dpi}	$NRQ4_{dpi}$/ NRQ_{0dpi}
	4.5	651	21 024	146 252

Fig. 71. Transcript accumulation of *Arabidopsis thaliana alternative oxidase 1d* in Arabidopsis leaves (cv. Col-0) in the course of *C. higginsianum* infection between 0 and 4 dpi. Relative quantities of transcripts were normalised to *AtACT2* (*Actin2*) and calibrated to mock control (NRQ_{0dpi} = 1). Each sample (a single replicate per time point) was prepared from pooled leaves of eight plants. At the left side only data obtained at 0 and 1 dpi were depicted, to present the induction at early stages of the interaction. Respective NRQ fold changes are presented in the lower panel.

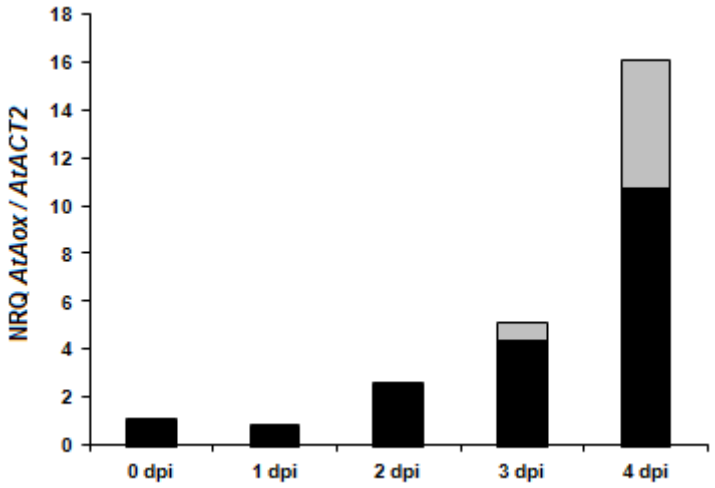

NRQ *AtAox* / *AtACT2*	NRQ_{0dpi}	NRQ_{1dpi}/ NRQ_{0dpi}	NRQ_{2dpi}/ NRQ_{0dpi}	NRQ_{3dpi}/ NRQ_{0dpi}	$NRQ4_{dpi}$/ NRQ_{0dpi}
AtAox1a	1	0.7	2.5	4.3	10.7
AtAox1d	0	0	0.02	0.7	5.3

Fig. 72. Combined chart showing the relative expression level of *Arabidopsis thaliana alternative oxidase 1a* (black, see also Fig. 70) and *alternative oxidase 1d* (grey, see also Fig. 71) in Arabidopsis leaves (cv. Col-0) in the course of *C. higginsianum* infection between 0 and 4 dpi. Values were calibrated to *Aox1a* mock control ($NRQ_{Aox1a\ 0dpi}$ = 1). Respective NRQ fold changes are presented in the lower panel.

3.3.1.5 Alternative respiration rate reflects the expression level of *Arabidopsis thaliana Aox1a* gene

Plants with altered levels of *Aox* expression can serve as a tool to study the role of host alternative oxidase activity in the *A. thaliana – C. higginsianum* interaction. *Aox1a* overexpressing and anti-sense lines as well as *Aox1a* and *Aox1d* knock-out plants were ordered from Nottingham Arabidopsis Stock Center (Nottingham, UK). Unfortunately, no homozygous *Aox1a* knock-out plants could be identified, thus further experiments were performed with the other lines. In a first step, transcript levels of the respective *Aox1* gene was evaluated in order to prove that *Aox* expression is indeed altered in these lines. As

presented in Fig. 73A, plants overexpressing *Aox1a* accumulated significantly more *Aox1a* transcripts compared to wild type Arabidopsis (cv. Col-0) in both mock- and *C. higginsianum*-infected leaves. The silencing of the *Aox1a* gene in *Aox1a* anti-sense plants could not be verified as the used qRT-PCR primers also detected the anti-sense transcripts. However, most probably it was solely anti-sense and not endogenous transcript as the full-length cDNA was used to create *Aox1a* anti-sense line (Umbach et al., 2005). Interestingly, mutated *Aox1d* transcript accumulated in *Aox1d* knock-out plants (Fig. 73B), genotyping results confirmed that endogenous transcript is not present in these plants (Suppl. Fig 9). However, Aox1d protein might be not functional in *Aox1d* knock-out plants, as the T-DNA insertion is located in an exon of the *Aox1d* gene. This could, however, not be proved as all attempts for the immunological detection of Aox1d protein in wild type Col-0 plants and knock-out plants with an antibody raised against alternative oxidase of *Chlamydomonas reinhardtii* failed.

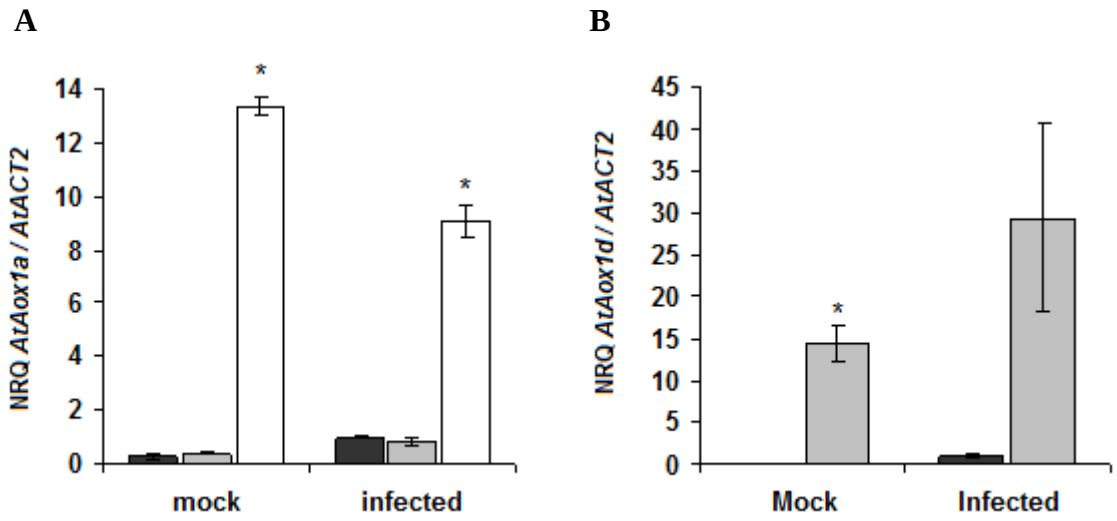

Fig. 73. Transcript level of *A. thaliana alternative oxidase 1a* (A) and *d* (B) in Arabidopsis leaves. (A) Col-0 (black bars), *Aox1a* anti-sense (grey bars), *Aox1a* overexpressing (white bars) and (B) Col-0 (black bars) and *Aox1d* knock-out (grey bars) plants three days after infection with *C. higginsianum*. Control plants were sprayed with water (mock). Mean values of relative transcript amounts normalised to *AtACT2* (*Actin2*) were calibrated to infected Col-0 ($NRQ_{infected\ Col\text{-}0} = 1$). Asterisks represent significant differences to the respective Col-0 values (t-test, p-value < 0.01). Error bars represent the standard error.

Subsequently, it was verified if altered *Aox* gene expression caused changes on the functional level, i.e. if respiration characteristics were altered in any of the genotypes. Alternative respiration of mock-treated and *C. higginsianum*-infected leaves was measured with Clark-type oxygen electrode after inhibition of the cytochrome pathway with potassium cyanide. In Col-0 wild type, an increase in alternative respiration rate upon infection with *C.*

higginsianum was observed (Fig. 74), confirming that enhanced expression of *Aox* genes leads to enhanced activity of alternative oxidase. This effect was also clearly seen in plants overxpressing *Aox1a* gene, which showed increased alternative respiration in both mock-treated and *C. higginsianum*-infected leaves compared to Col-0 wild type.

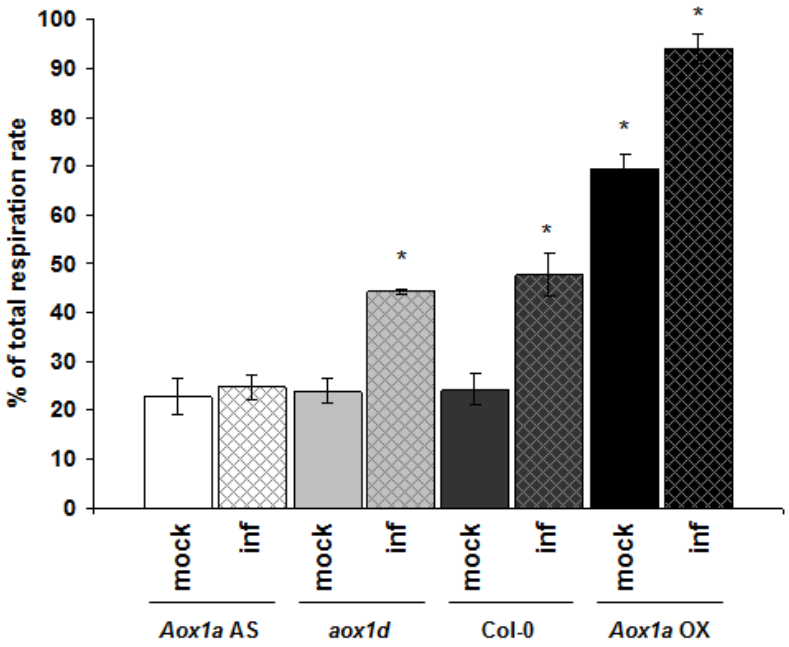

Fig. 74. Alternative respiration rates expressed as percentage of total respiration rate in mock-treated (mock) and C. *higginsianum*-infected leaves (inf) of wild type Arabidopsis (cv. Col-0), *Aox1a* anti-sense (*Aox1a* AS), *Aox1d* knock-out (*aox1d*) and *Aox1a* overexpressing (*Aox1a* OX) Arabidopsis plants at 3 dpi. Mean values from four replicate leaves were shown. Asterisks indicate significant difference to infected Col-0 plants (t-test, p-value < 0.05). Error bars represent the standard error.

Interestingly, putative *Aox1d* knock-out plants exhibited unaltered alternative respiration rates compared to Col-0 plants, meaning that indeed contribution of Aox1d protein to alternative respiration is limited. Otherwise, it is possible that *Aox1d* knock-out plants compensate a lack of this isoform by enhancing the activity of other leaf isoform i.e. *Aox1a*. Indeed, an increase by 25% in *Aox1a* transcript amount was observed in *Aox1d* knock-out plants (Fig. 75). In addition, plants with silenced *Aox1a* gene exhibited no increase in alternative respiration upon *C. higginsianum* infection, indicating that *Aox1a* is the major AOX isoform in Arabidopsis leaves that enables respiration through alternative pathway.

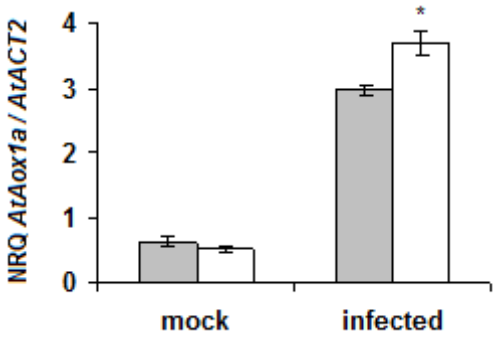

Fig. 75. Transcript level of *Arabidopsis thaliana alternative oxidase 1a* in Arabidopsis leaves. Wild type Col-0 (grey bars) and *Aox1d* knock-out (white bars) plants three days after infection with *C. higginsianum*. Control plants were sprayed with water (mock). Mean values (n=4) of relative transcript amounts were normalised to *AtACT2* (*Actin 2*). Asterisk represents significant difference to the respective Col-0 values (t-test, p-value < 0.02). Error bars represent the standard error.

3.3.1.6 Enhanced activity of alternative oxidase does not lower reactive oxygen species production in *A. thaliana* leaves

As presented above, altered expression of *Aox1a* gene influenced the activity of the alternative respiration pathway in *A. thaliana* plants. Thus, it was assumed that the homeostasis of reactive oxygen species was altered in the *Aox* overexpressors as alternative oxidase quenches ROS. To verify this hypothesis, ROS production after elicitation with the PAMP elicitor flg22 was evaluated in wild type Col-0 and *Aox1a* anti-sense and overexpressing plants. Although the activity of alternative oxidase was enhanced in *Aox1a* overexpressing plants, no decrease in ROS production could be observed (Fig. 76). However, the accumulation of ROS occurred in *Aox1a* anti-sense plants, which may suggests that activity of alternative oxidase influences oxidative burst released by elicitation.

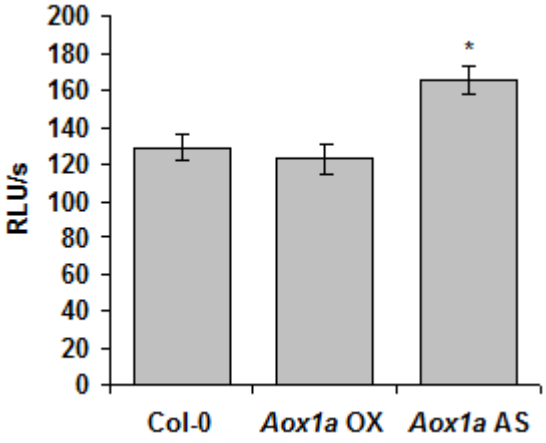

Fig. 76. Reactive oxygen species production in *A. thaliana* Col-0 leaves and *Aox1a* overexpressing (*Aox1a* OX) and *Aox1a* anti-sense (*Aox1a* AS) line after elicitation with 1 µM flg22 peptide. Mean (n=10) of maximal ROS

production rates (measured as relative luminescence units per second (RLU/s)) are shown. Asterisk represent significant difference to Col-0 plants (t-test, p-value < 0.001). Error bars represent the standard error.

3.3.1.7 Susceptibility of *A. thaliana* to the infection with *C. higginsianum* could not be linked to *Aox1* expression level

As described above (Fig. 65), inhibition of alternative oxidase in maize leaves restricted the proliferation of *C. graminicola*, suggesting that alternative oxidase may act as a compatibility factor in this interaction. If this mechanism is conserved between the species, this should also be observed in the *A. thaliana – C. higginsianum* interaction. To solve this question, *A. thaliana* plants with altered levels of *Aox1a* expression were challenged with *C. higginsianum* and relative fungal quantity in infected leaves was evaluated by qPCR at 3.5 dpi. This experiment was repeated independently six times. Unfortunately, no consistent results could be obtained (Fig. 77). *Aox1a* overexpressing plants showed significantly increased susceptibility to *C. higginsianum* in two replicate experiments but this result could not be confirmed in four other experiments. No significant change in susceptibility of *Aox1a* anti-sense plants compared to Col-0 plants could be observed. Thus, it can be concluded that alternative oxidase has no significant effect on compatibility in the *A. thaliana – C. higginsianum* interaction.

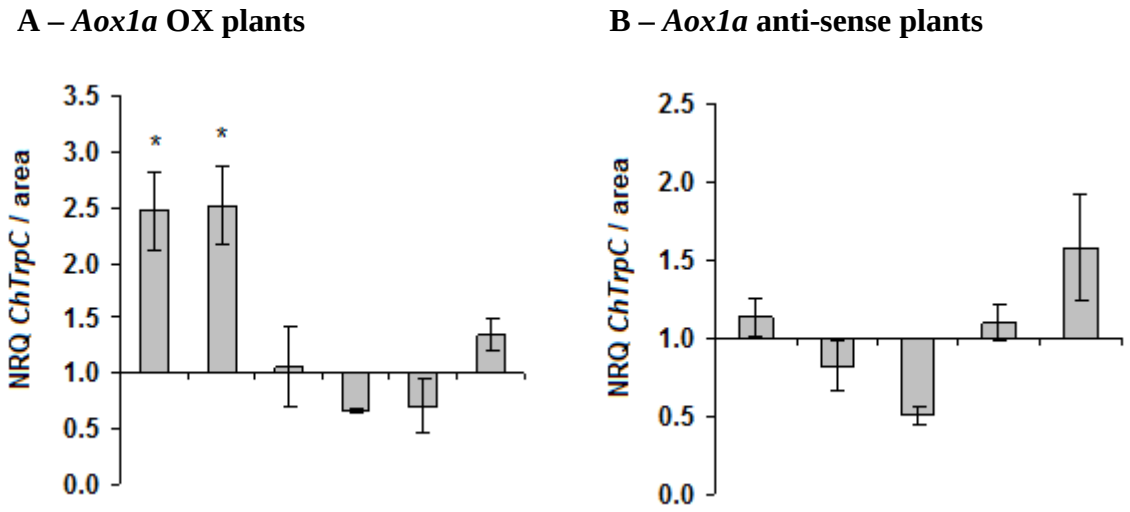

Fig. 77. Relative degree of *C. higginsianum* colonisation 3.5 days after the infection of *A. thaliana Aox1a* overexpressing (A) and *Aox1a* anti-sense (B) plants in comparison to Col-0 wild type. Results collected from six (in A) and five (in B) independent experiments are presented. Mean values (n=4) of relative *C. higginsianum* genomic DNA quantity per leaf area are shown that are normalised to the Col-0 value from the respective replicate experiment; therefore, NRQ = 1 corresponds to relative *C. higginsianum* DNA quantity in Col-0 plants, bars above the abscissa indicate stronger fungal colonisation compared to Col-0 wild type, bars below the abscissa indicate weaker fungal colonisation relative to Col-0 wild type. Asterisks represent significant differences to Col-0 wild type control (t-test, p-value < 0.05). Error bars represent the standard error.

3.4.2 Role of two maize NAC transcription factors, ZmNAC41 and ZmNAC100, for the interaction with *Colletotrichum graminicola*

3.4.2.1 Two maize NAC transcription factors are induced in the leaves infected with *C. graminicola*

The transcriptome analysis revealed that there are two genes coding for putative NAC transcription factors - *ZmNAC41* and *ZmNAC100* - induced in maize leaves infected with *C. graminicola.* Following analysis by qRT-PCR confirmed the microarray data. Transcript of *ZmNAC100* accumulated in the course of the infection from 14-fold at 2 dpi to more than 33-fold if control level at 4 dpi, while *ZmNAC41* transcript level was induced 129-fold and 119-fold compared to mock controls at 2 dpi and 4 dpi, respectively (Fig. 78)

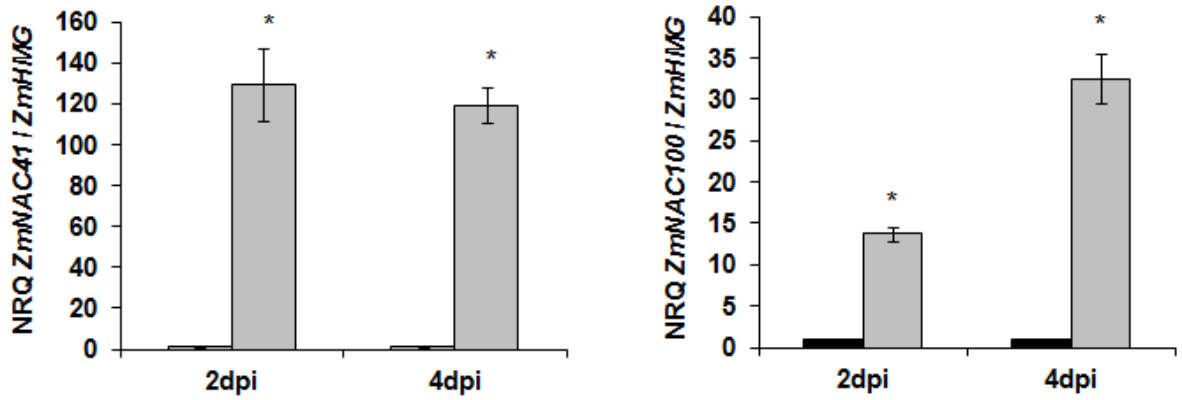

NRQ *ZmNAC41* / *ZmHMG*	NRQ_{inf} / NRQ_{mock}
2 dpi	129
4 dpi	119

NRQ *ZmNAC41* / *ZmHMG*	NRQ_{inf} / NRQ_{mock}
2 dpi	14
4 dpi	33

Fig. 78. Induction of two *NACs* in maize leaves (cv. Nathan) upon infection with *C. graminicola* wild type CgM2. Relative quantities of *ZmNAC41* (left side chart) and *ZmNAC100* (right side chart) transcripts were analysed by qRT-PCR and are expressed relative to *ZmHMG* on a log2 scale as means ± SE (n = 4). Black bars – mock-treated control leaves, grey bars – infected leaves. Error bars represent the standard error. Asterisks indicate significant differences (t-test, p-value < 0.05) to the respective mock control. Respective NRQ fold changes are presented in the lower panel.

However, it seems likely that the induction of both *NACs* transcripts is even higher in infected cells than the results of the qRT-PCR suggest. Leaves subjected for transcript quantification were spray-inoculated which, especially at the early time point of infection, may lead to a dilution of infected cells by healthy cells whose transcripts prevail in the RNA pool. To better assess the early time points after infection, the analysis was performed with

dip-inoculated leaves, in which the proportion of infected tissue should be greater compared to spray-inoculated leaves. Weak transcriptional induction *ZmNAC41* was observed in CgM2 wild type *C. graminicola*-infected leaves already at 24 hpi, i.e. the pre-penetration stage, but a massive accumulation of *ZmNAC41* transcript was associated around the time point of host penetration (36 hpi). The accumulation of the *ZmNAC100* transcript was also associated with the successful penetration of the wild type strain CgM2 into the host tissue, however, the induction was much weaker compared to *ZmNAC41* (Fig. 79).

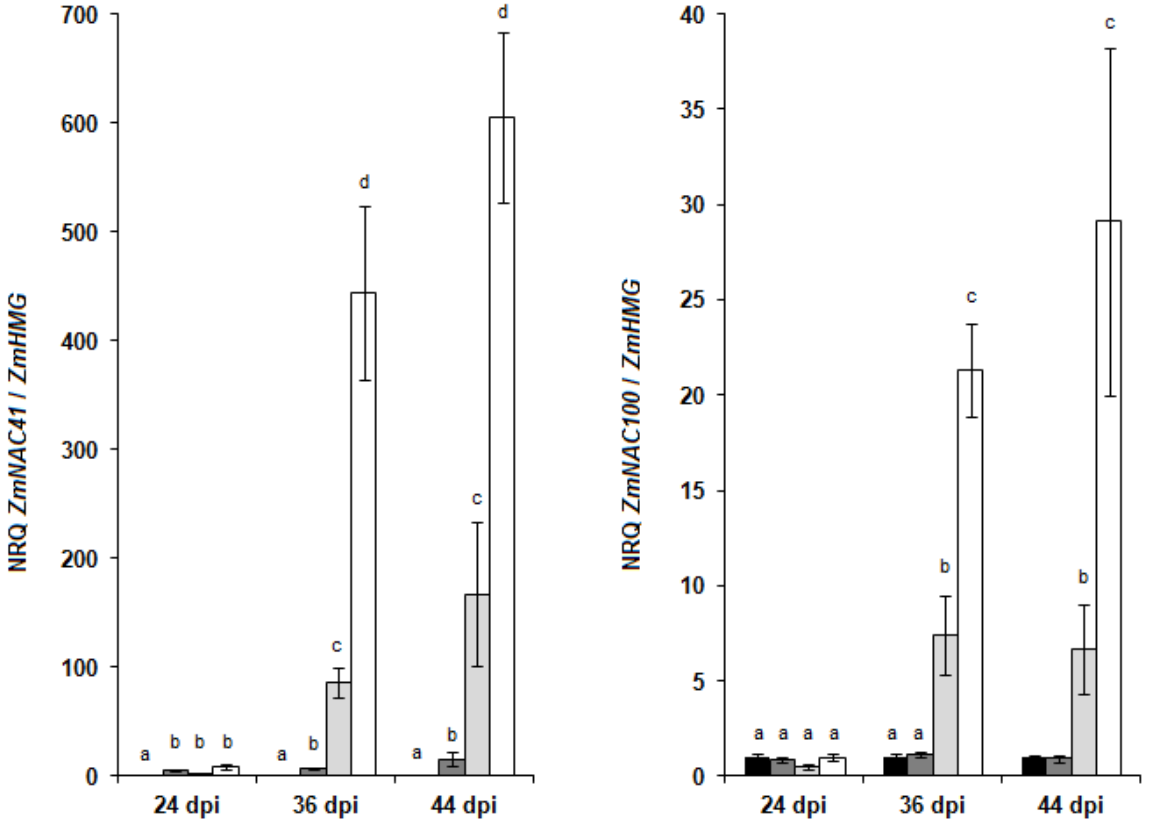

NRQ *ZmNAC41 / ZmHMG*	NRQ_{AT416}/ NRQ_{mock}	NRQ_{AT171}/ NRQ_{mock}	NRQ_{WT}/ NRQ_{mock}
24 dpi	5	3	9
36 dpi	7	86	443
44 dpi	16	167	605

NRQ *ZmNAC100 / ZmHMG*	NRQ_{AT416}/ NRQ_{mock}	NRQ_{AT171}/ NRQ_{mock}	NRQ_{WT}/ NRQ_{mock}
24 dpi	1	0.5	1
36 dpi	1	7	21
44 dpi	1	7	29

Fig. 79. Relative quantities of *ZmNAC41* (left side chart) and *ZmNAC100* (right side chart) transcripts in maize leaves (cv. Nathan) were analysed by qRT-PCR and are expressed relative to *ZmHMG* on a log2 scale as means (n = 4). Error bars represent the standard error. Mock-treated leaves - black bars, leaves infected with *C. graminicola* mutant AT416 strain – dark grey bars, *C. graminicola* mutant AT171 strain – pale grey bars, *C. graminicola* wild type strain - white bars. Dissimilar letters indicate significant differences (t-test, p-value < 0.05) between the treatments. Respective NRQ fold changes are presented in the lower panel.

To scrutinise if both *NAC* genes respond to the infection with mutant strains of *C. graminicola* which are affected in pathogenicity, two mutant strains, AT171 displaying weakly affected virulence (Münch et al., 2011) and AT416 (see chapter 3.1.1), strongly affected in virulence, were also investigated in this experiment (Fig. 79). *ZmNAC41* was induced in all three interactions over the course of infection, with the level of induction correlating with the virulence of the fungus. The accumulation of *ZmNAC100* transcript was stronger in wild type CgM2 interaction compared to AT171 strain, while infection with the AT416 strain had no influence on *ZmNAC100* gene expression. Interestingly, the colonisation of the host tissue by the mutant AT416 was delayed compared to AT171 and wild type strain CgM2; even at 72 hpi no fungal structures of AT416 could be observed in the host cells beneath the appressoria (Fig. 80). This result indicates that expression of the *ZmNAC100* gene is enhanced in maize tissue upon penetration events, suggesting that product of this gene may play a role in induced defence response. Taken together, both genes may serve as potential compatibility factors in the analysed interaction, as their expression levels were positively correlated with the virulence of the strains.

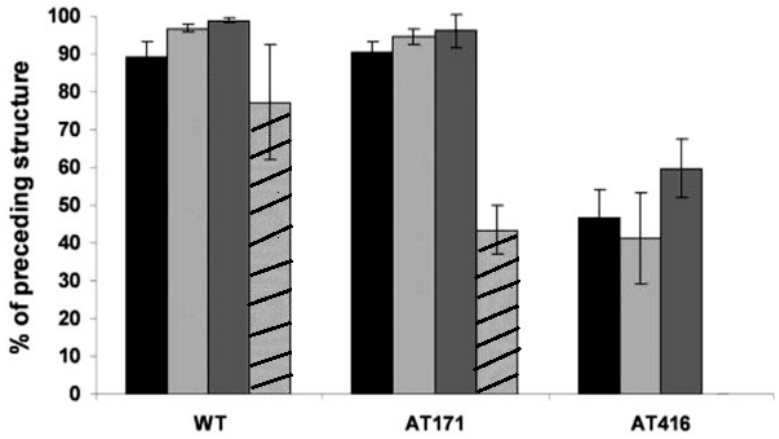

Fig. 80. Germination rates (black bars), appressoria formation (light grey bars), melanisation rates (dark grey bars) and penetration rates (hatched bars) of *C. graminicola* wild type strain CgM2 (left bracket) and the ATMT mutant strains AT171 (middle bracket) and AT416 (right bracket) were assessed at 72 hpi. Four replicate samples per genotype with approx. 100 conidia were assessed and are given as means. Error bars represent the standard error. The data for every developmental stage is given in percent relative to the total number of infection events that exhibited the preceding developmental stage.

3.4.2.2 *ZmNAC41* and *ZmNAC100* are induced by stimuli associated with the defence response and by senescence

As transcription of both *NAC* genes was induced during biotic stress, the response of these two *NAC* genes to phytohormones that coordinate the plant defence response was

subsequently analysed. The level of both transcripts was evaluated by qRT-PCR in leaves upon treatment with one of the following; 1 mM jasmonic acid (JA) or 1.3 mM 2,6-dichloroisonicotinic acid (INA), an analogue of the defence messenger salicylic acid (SA), or 5 mM 1-aminocyclopropane-1-carboxylic-acid (ACC), a precursor of the phytohormone ethylene. The result shows that transcription of both genes was enhanced by 1mM jasmonic acid after 10 and 24 hours of treatment and that transcripts of *ZmNAC100* accumulated within this period (Fig. 81). Moreover, exogenous application of INA induced the transcription of *ZmNAC100*, while treatment with 5 mM ACC did not affect transcript amounts of both genes. These results suggest that the two NAC transcription factors may play a role in JA-dependent defence response and in case of *ZmNAC100* also in the SA-dependent defence response.

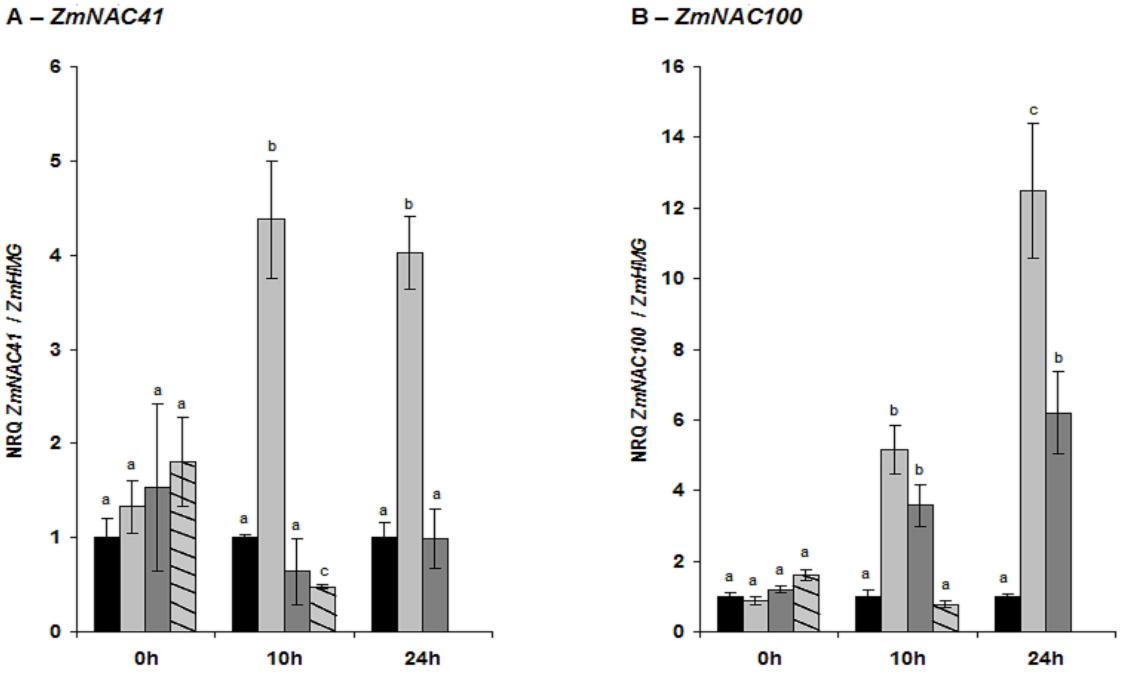

Fig. 81. Induction of *ZmNAC41* and *ZmNAC100* nin maize leaves (cv. Nathan) in response to phytohormone and hormone analogue treatments. Relative quantities of *ZmNAC41* (A) and *ZmNAC100* (B) transcripts in mock-treated control leaves (black bars) and after 0 h (left bracket), 10 h (middle bracket) and 24 h (right bracket) of treatment with 1 mM JA (light grey bars) or 1.3 mM INA (dark grey bars) and after 0 h and 10 h of treatment with 5 mM ACC (hatched bars) were analysed by qRT-PCR and are expressed as means (n =4) relative to *ZmHMG* and calibrated to respective mock control (NRQ_{mock} = 1). Error bars represent the standard error. Dissimilar letters indicate significant differences (t-test, p-value < 0.05) between the treatments.

It is known that the induction of defence-related genes occurs not only upon biotic stress but also as a part of the senescence process (e.g., as reviewed by Quirino et al., 2000). Thus, the expression of *ZmNAC41* and *ZmNAC100* was evaluated during leaf development (Fig. 82). *ZmNAC41* was expressed throughout the seedling and mature leaf stages and

ZmNAC41 induction was observed in senescencent leaves. A similar expression profile was observed for *ZmNAC100*.

3.4.2.3 The transcription of *ZmNAC41* and *ZmNAC100* is down-regulated during abiotic stress

It is reported that some *NAC* genes, e.g. rice *OsNAC6*, play overlapping roles in response to both biotic and abiotic stress (Nakashima et al., 2007). To test if the same applies to *ZmNAC41* and *ZmNAC100*, the transcriptional response of both genes to drought and high salinity was assessed. A decrease of transcript amount of both genes was observed in leaves upon salt stress, while transcript accumulation of only *ZmNAC100* was repressed by drought conditions (Fig. 82). These results show that both genes are negatively regulated by abiotic stress such as salt stress.

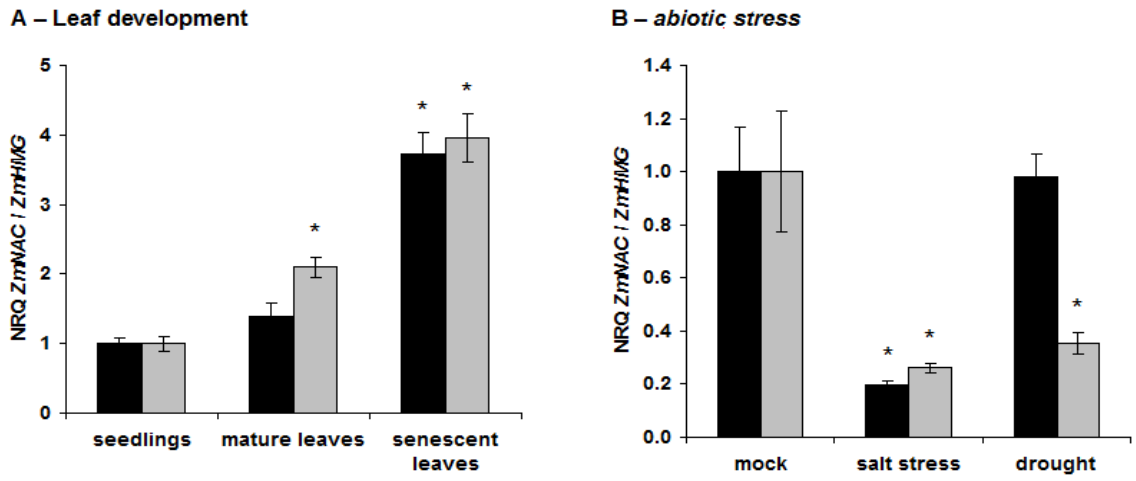

Fig. 82.Transcript amounts of *ZmNAC41* and *ZmNAC100* in maize leaves (cv. Nathan) during leaf development and in response to abiotic stress treatments. Relative quantities of *ZmNAC41* (black bars) and *ZmNAC100* (grey bars) were analysed in seedlings (one week old seedlings), mature (4th leaf of three weeks old plants) and senescent leaves (2nd or 3rd leaf of three weeks old plants) (A) and in leaves upon drought (withholding water irrigation for one week) or high salinity (irrigation with 200 ml of 200mM NaCl for one week) conditions (B). Relative transcript amounts were determined by qRT-PCR and are expressed as means (n = 4) relative to *ZmHMG* and calibrated to seedlings ($NRQ_{seedlings}$ = 1) in (A) or mock control (NRQ_{mock} = 1) in (B). Error bars represent the standard error. Asterisks indicate significant differences (t-test, p-value < 0.05) of mature and senescent leaves to seedlings (A) or stress-treated leaves to the respective mock-treated control (B).

3.4.2.4 Additional maize NAC transcription factors are differentially regulated during the interaction with fungal pathogens

Transcriptome analysis revealed that the expression of two other *NAC* genes, *ZmNAC15* and *ZmNAC97*, was up-regulated in leaves colonised with *C. graminicola*, once the fungus switched to necrotrophic growth (Table 10). *ZmNAC38* was induced along with *ZmNAC41* in maize leaves 12 hours after infection with the biotrophic fungus *Ustilago maydis*. However, transcript level of *ZmNAC38* dropped 2.7-fold at late stage of the infection (192 hpi). The other gene, *ZmNAC36*, was repressed 2.4-fold at 96 hpi upon this interaction. Promoter regions of all abovementioned *NAC* genes, *ZmNAC15*, *ZmNAC36*, *ZmNAC38* and *ZmNAC97*, including *ZmNAC41* and *ZmNAC100*, were analysed to identify potential promoter elements that may mediate the response to challenge with pathogenic fungi. All promoter regions comprised the consensus NAC transcription factor binding motif, which was described for *ANAC019* and *ANAC092* (Olsen et al., 2005), and for most of the analysed *NAC* genes, the consensus motif was repeated multiple times (Table 11). Moreover, binding sites of ERF and TGA transcription factors, regulating the transcription of ethylene- and salicylic acid responsive genes, respectively, were identified in all promoter regions except for *ZmNAC41* and *ZmNAC97*. Binding sites for the transcription factor Myc2, which is involved in regulating the jasmonic acid-dependent defence response, were present in *ZmNAC38*, *ZmNAC15* and *ZmNAC41*. Two latter NAC genes also contained WRKY-binding motifs, which were also found in promoter regions of *ZmNAC36* and *ZmNAC100*. Interestingly, the promoter region of *ZmNAC41* and *ZmNAC100*, the only NACs up-regulated during the early stages of the interaction with *C. graminicola*, contained a Whirly-binding site. In summary, the *NAC* genes responsive to *C. graminicola* and *U. maydis* contained a similar set of defence-associated promoter elements.

Table 10. Maize *NAC* genes differentially regulated in the interaction with *C. graminicola* and *Ustilago maydis*. Linear fold change values (f.c.) of gene expression are given; negative values represent a down regulation. Only fold changes > 2 are displayed. Data were extracted from the microarray analysis of the maize transcriptome (Voll et al., 2011) and p-values (p-val) were calculated using bioconductor (http://www.bioconductor.org).

	Colletotrichum graminicola				*Ustilago maydis*					
NAC gene	**36 hpi**		**96 hpi**		**12 hpi**		**96 hpi**		**192 hpi**	
	f.c.	p-val	**f.c.**	p-val	**f.c.**	p-val	**f.c.**	p-val	**f.c.**	p-val
ZmNAC100	**3.3**	0.19	**204**	$2.8 \cdot 10^{-6}$						
ZmNAC41	**3.4**	0.02	**45**	$3.5 \cdot 10^{-4}$	**7.0**	0.08				
ZmNAC15			**3.2**	0.05						
ZmNAC97			**2.2**	0.006						
ZmNAC38					**3.7**	0.09			**−2.7**	0.003
ZmNAC36							**−2.4**	0.07		

Table 11. Presence of binding motifs for defence-associated transcription factors in the promoter regions of maize *NAC* genes up-regulated in response to *C. graminicola* and *U. maydis*. The distance of each promoter element from the respective start codon is given in base pairs, followed by the identified sequence motif in brackets.

NAC gene	Myc2	Whirly	ERF	WRKY	TGA	NAC
ZmNAC100		−582 bp (GTCAAAA)	−691 bp (GCCGCC)	**−464 bp (TTGACC)**	−556 bp (TGACG)	−833 bp (AGACGTG)
		−1737 bp (GTCAAAT)			- 1471 bp (TGACG)	−920 bp (TGTCGTG)
						−963 bp (ATGCGTG)
ZmNAC41	−1284 bp (CATGTG)	−1155 bp (GTCAAAT)		**−348 bp (TTGACC)**		−1166 bp (TAGCGTGAT)
						−1615 bp (TAACGTATA)
ZmNAC15	−795 bp (CATGTG)		**−364 bp (AGCCGCC)**	**−349 bp (TTGACC)**	−530 bp (TGACG)	−906 bp (TTGCGTA)
	−1445 bp (CATGTG)		- 592 bp (GCCGCC)			−945 bp (TTTCGTA)
			−1333 bp (GCCGCC)			−1023 bp (AGCCGTA)
			−1464 bp (GCCGCC)			−1319 bp (TTGCGTG)
			−1566 bp (GCCGCC)			
			−1569 bp (GCCGCC)			
ZmNAC97						−1718 bp (TTACGTG)
						−1825 bp (TTGCGTG)
ZmNAC38	−1604 bp (CATGTG)		**−351 bp (GCCGCC)**		−857 bp (TGACG)	**−254 bp (TGACGTA)**
			−369 bp (GCCGCC)		−952 bp (TGACG)	**−399 bp (ATCCGTA)**
			−384 bp (GCCGCC)		−1101 bp (TGACG)	−915 bp (ATTCGTA)
			−482 bp (GCCGCC)			−1051 bp (AGGCGTG)
						−1106 bp (AGGCGTG)
ZmNAC36			−1343 bp (GCCGCC)	−510 bp (TTGACC)	−1153 bp (TGACG)	−761 bp (TGGCGTG)
			−1346 bp (GCCGCC)		−1211 bp (TGACG)	

3.4.2.5 The family of maize NAC transcription factors

A first attempt to describe the maize NAC family was done by Shen at al. (2009), who identified 177 putative maize *NAC* genes. However, only the preliminary, unassembled version of maize genome was available to the authors to search for the *NAC* coding sequences. Using the recently assembled genome of maize B73 (release 5b.60, available at http://maizesequence.org), both the number and the phylogeny of maize NAC transcription factors was revised in this work. The N-terminal part (NAC domain) of ZmNAC41 and ZmNAC100 was used as a query to screen the peptide database (http://maizesequence.org). Furthermore, the assembled genome was screened with gene models of putative maize NAC transcription factors available at Grassius Grass Regulatory Information Server (http://www.grassius.org/index.html). As a result, 116 sequences (excluding alternative splice variants) could be retrieved from the assembled genome, which were named as *ZmNAC*s with ascending Arabic numbers based on their chromosomal localisation (starting from the tip of the short arm of chromosome 1, see Suppl. Table 1). A phylogenetic tree generated from all sequences revealed that the NAC members cluster into 12 major clades (Fig. 83).

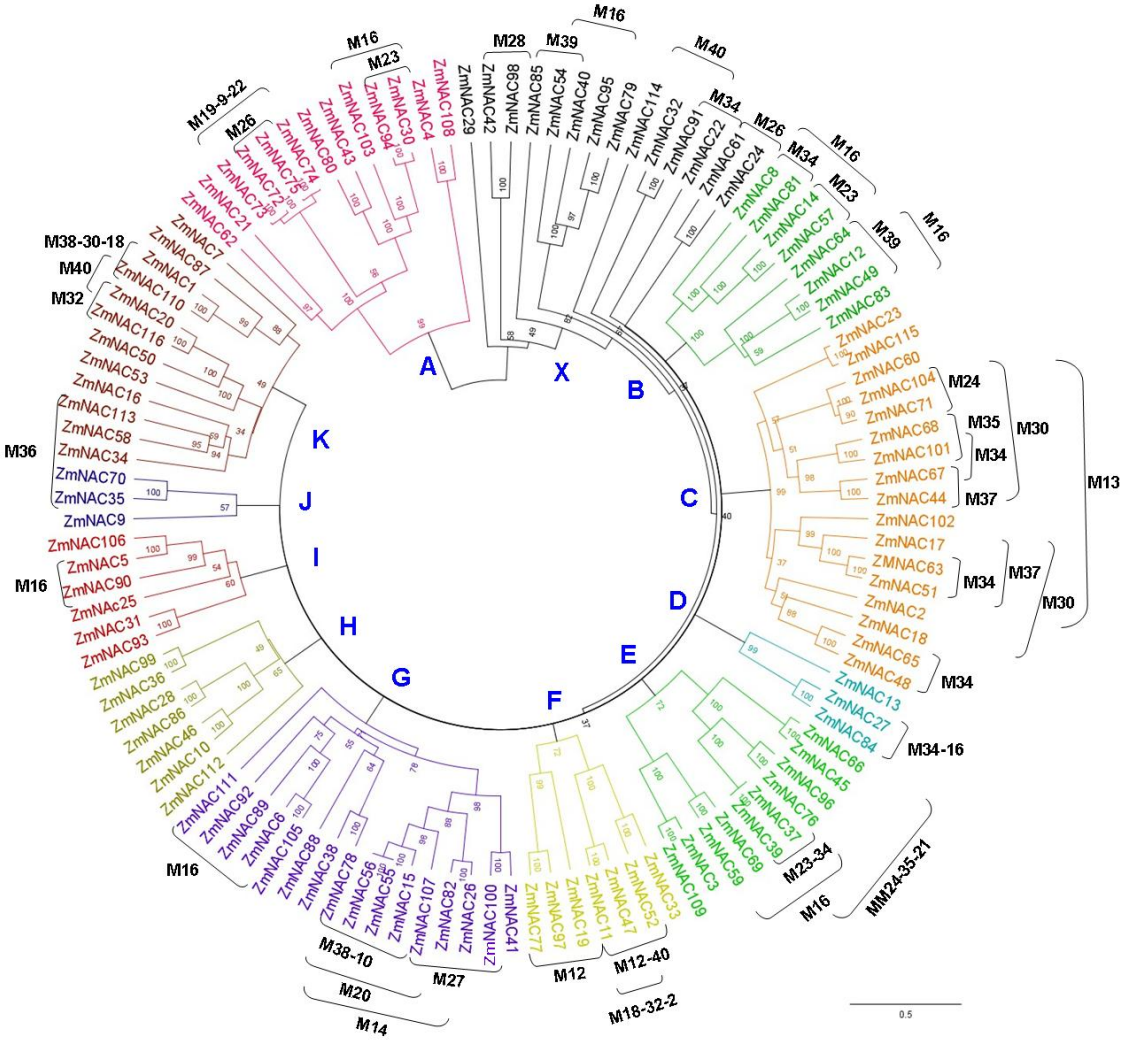

Fig. 83. Phylogenetic analysis of maize NAC proteins. The 116 maize NAC proteins were extracted from the published B73 genome sequence as described in the text and were numbered according to position in the genome (starting with the short arm of chromosome 1, see Suppl. Table 1). Bootstrap values are indicated at the nodes, the bar at the bottom of the figure depicts the distance scale for branch length. Proteins with identical C-terminal motifs are indicated by brackets including the respective motif number (see Supp. Table 2).

The sequences clustered due to the similarities within the NAC domain; therefore, the clade structure was almost the same in trees built with NAC domain only and with the whole protein sequence (data not shown). The high level of conservation in the N-terminal region, comprising the NAC domain, was confirmed by the alignment of the consensus sequences of each clade (Fig. 84). In contrast, the C-terminal part of the NAC proteins was highly divergent, even between family members clustering to the same clade (Supp. Fig. 11). Based on an alignment of the N-terminal regions, five highly conserved subdomains (A-E) were identified within the NAC domain (Fig. 84), which showed high similarity between family members across the clades.

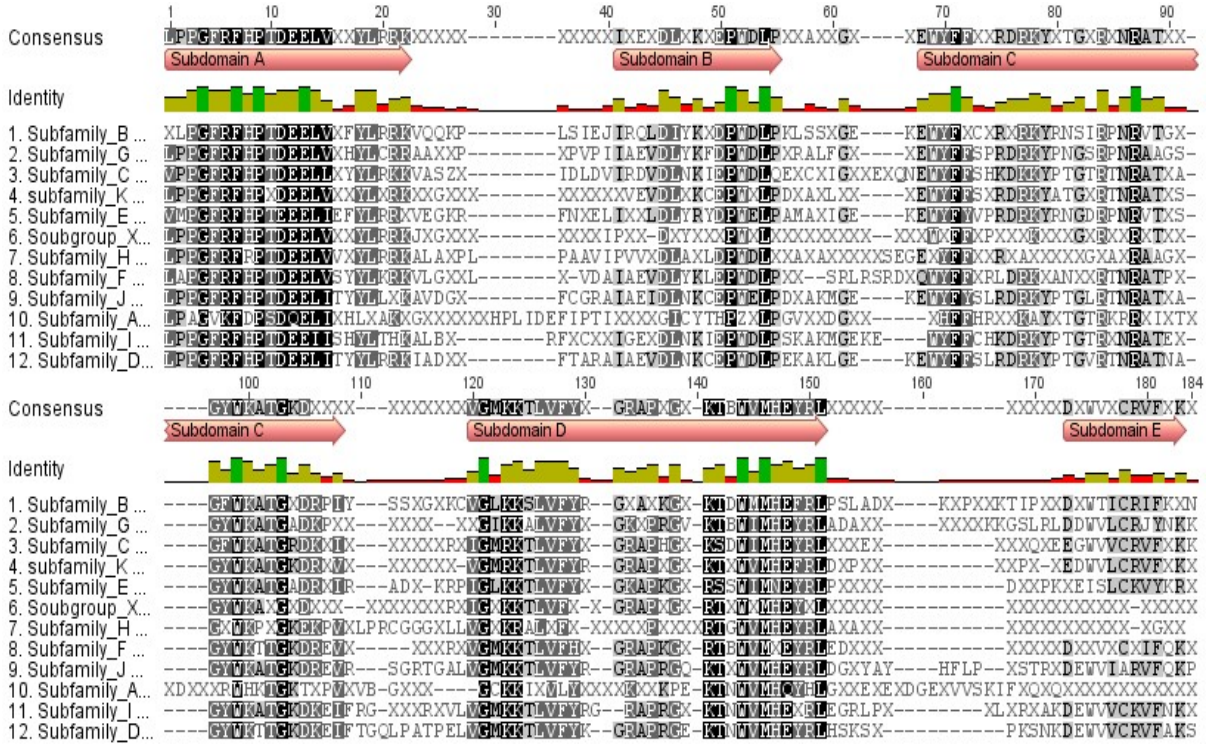

Fig. 84. Architecture of maize NAC domains. A multiple alignment of the consensus sequences of the NAC domains from each clade was compiled using ClustalW 2.0. Amino acid residues present in at least 50% of the subfamiliy members are displayed in the consensus sequences. For a complete alignment, please see Supp. Fig. 10.

Closer analysis, performed with MEME (http://meme.sdsc.edu/meme/cgi-bin/meme.cgi), identified common motifs (cut off p-value 1e-10) within the N-terminal part of the protein sequences (Fig.85 and Suppl. Table 2). The sequence patterns within the NAC domain were well conserved even between the clades, with just single divergent amino acids, as shown by the analysis of subdomain D as an example (Fig. 86). The motifs at the N-terminus, in front of the NAC domain, were more divergent and only present in some clades. The only common motif in this region was shared between the members of clades C, E, G and I. However, clade-specific sequences at the start of the N-terminus were identified in members of clade A, C and G.

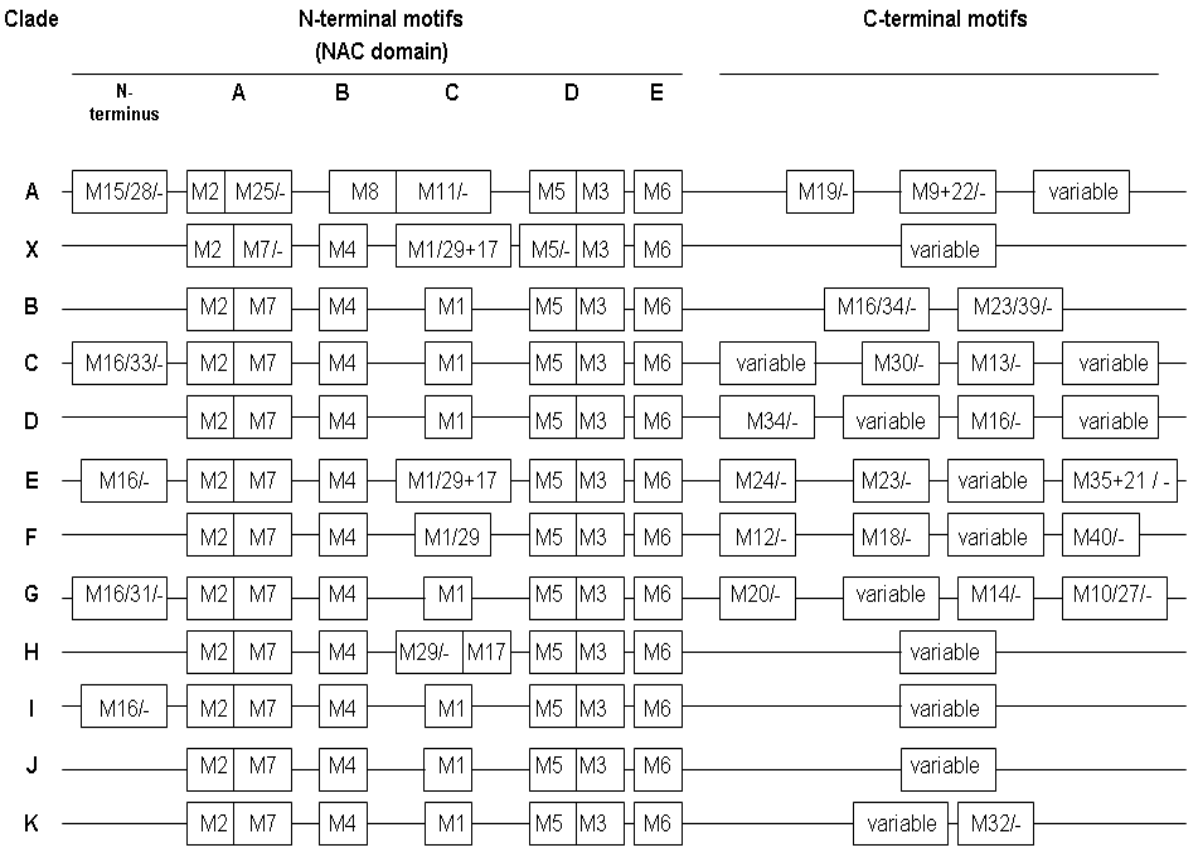

Fig. 85. Positions of the motifs detected within the N- and C-terminus of maize NAC proteins. The motifs detected with MEME (Multiple Em for Motif Elicitation, http://meme.nbcr.net/meme/cgi-bin/meme.cgi) are marked. For a complete list of motifs, please see Suppl. Table 2. For simplicity reasons, all proteins are aligned to one length. The term "variable" is used if more than three variants of the sequence are present at the respective spot, while the absence of a given motif is marked with a dash.

Similar analysis performed for C-terminus of maize NACs revealed the presence of twenty four motifs with a cut off p-value of 1e-10 (Supp. Table 2). Most of them were clade-specific, but some were also found in NAC homologues from other species. Pattern QYGAPF (motif 12), identified in the sequences from clade F, was identical to motif 39 (in Fang et al., 2008) that was found in six rice NACs. Maize motif 30 (LPLE) was also found in the C-terminal parts of Arabidopsis and rice members, as motif iii (in Ooka et al., 2003). Another motif identified in Arabidopsis NACs (motif ix/x in Ooka et al., 2003) corresponded to maize motif 36 (CFS) in members of clades K and J.

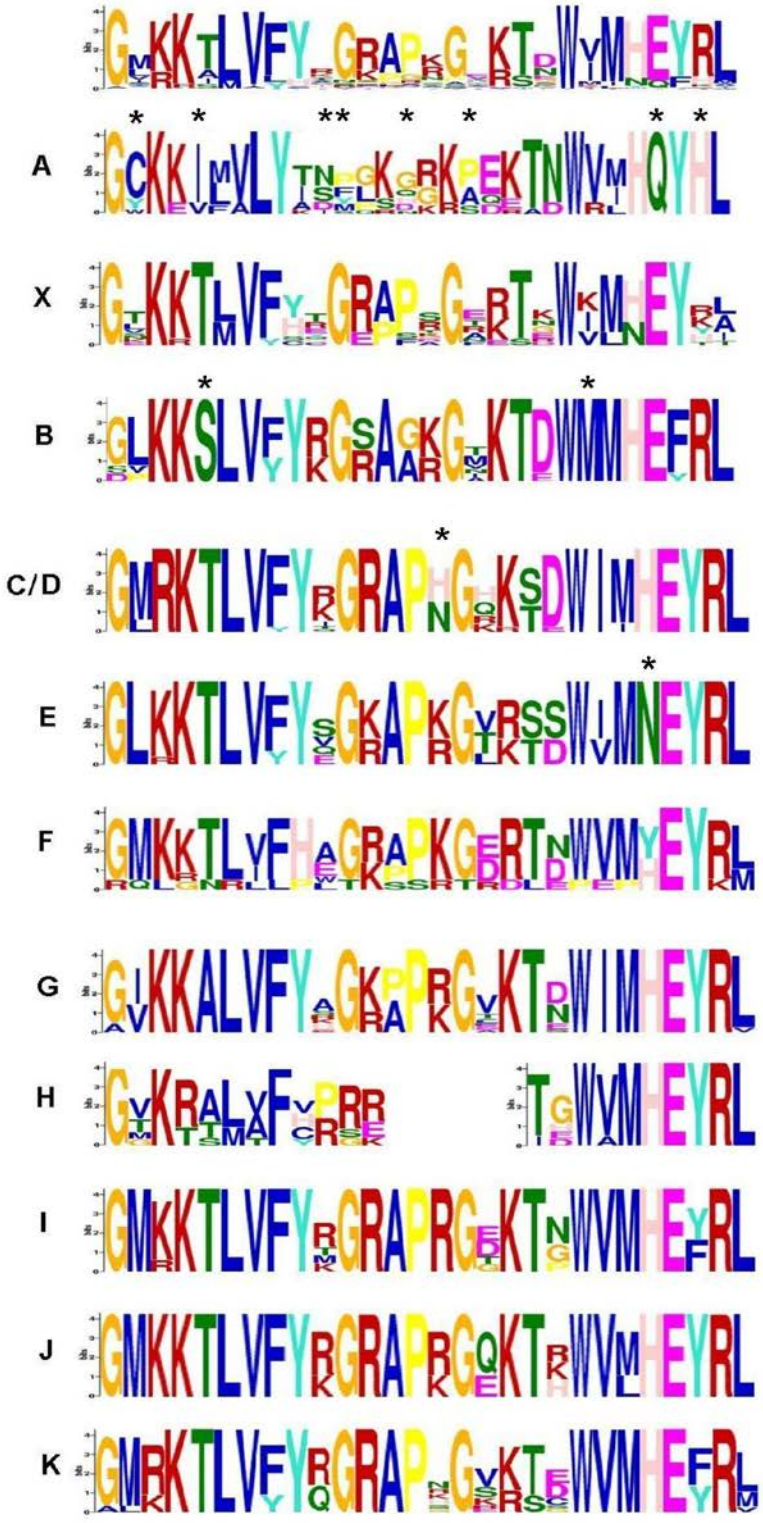

Fig. 86. Divergence of the NAC subdomain D consensus sequence between clades. Comparison of the subdomain D amino acid consensus sequences from individual NAC clades after analysis with MEME (Multiple Em for Motif Elicitation, http://meme.nbcr.net/meme/cgi-bin/meme.cgi). Amino acid incidences at individual positions are represented by letter size. At the top, the subdomain D consensus amino acid sequence for all 116 NAC sequences is given and below consensus sequences for the indicated clades are listed. Clades are indicated by the letter left to the motifs. For clade H, the middle part of subdomain D consists of a stretch of variable amino acid residues Amino acid residues specific for individual clades are highlighted by asterisks.

3.4.2.6 ZmNAC41 and ZmNAC100 belong to a clade enriched in defence-associated NAC transcription factors

The above described phylogenetic analysis revealed that ZmNAC41 and ZmNAC100 both belong to clade G (Fig. 83). These two transcription factors are closely related and their protein sequences are 78% similar over the entire sequence, while similarity is increased to 87% in the region of the NAC domain. Analysis of maize gene duplication data (Schnable et al. 2009) showed that segmental duplication event within long arms of chromosome 3 and 8 gave rise to the creation of *ZmNAC41* and *ZmNAC100*, respectively. Moreover, phylogenetic analysis showed that ZmNAC15 and ZmNAC38, two members also induced during the biotic stress response, clustered to clade G as well. In contrast, two other defence-related NAC proteins, ZmNAC36 and ZmNAC97, were divergent from each other and from the other four proteins mentioned above, clustering to clades H and F, respectively (Fig. 83). When phylogenetic analysis was performed with all maize NACs along with all functionally characterised members from Arabidopsis and rice, four Arabidopsis proteins, playing role in defence response, were also located in clade G (Fig. 87). These were two pairs of closely related and co-regulated transcription factors. ATAF1, associated with defence against pathogenic bacteria and necrotrophic fungi (Wang et al., 2009), was clustering together with ATAF2, known to regulate *PR* gene transcription (Delessert et al. 2005). ANAC019 and ANAC05, both regulating JA-responsive defence genes (Bu et al. 2008), clustered as the other pair. In contrast, the only rice members known to be associated with biotic stress responses, *OsNAC6 and OsNAC19*, were not clustering to clade G (Fig. 87). Taken together, eight defence-associated NACs from the three species were clustering to clade G, whereas four other NACs involved in microbial defence were found in different clades. Thus, it can be concluded that clade G is enriched in proteins playing a role in the response to biotic stress and the ancestor of the members of this clade most probably may have had a defence-associated function.

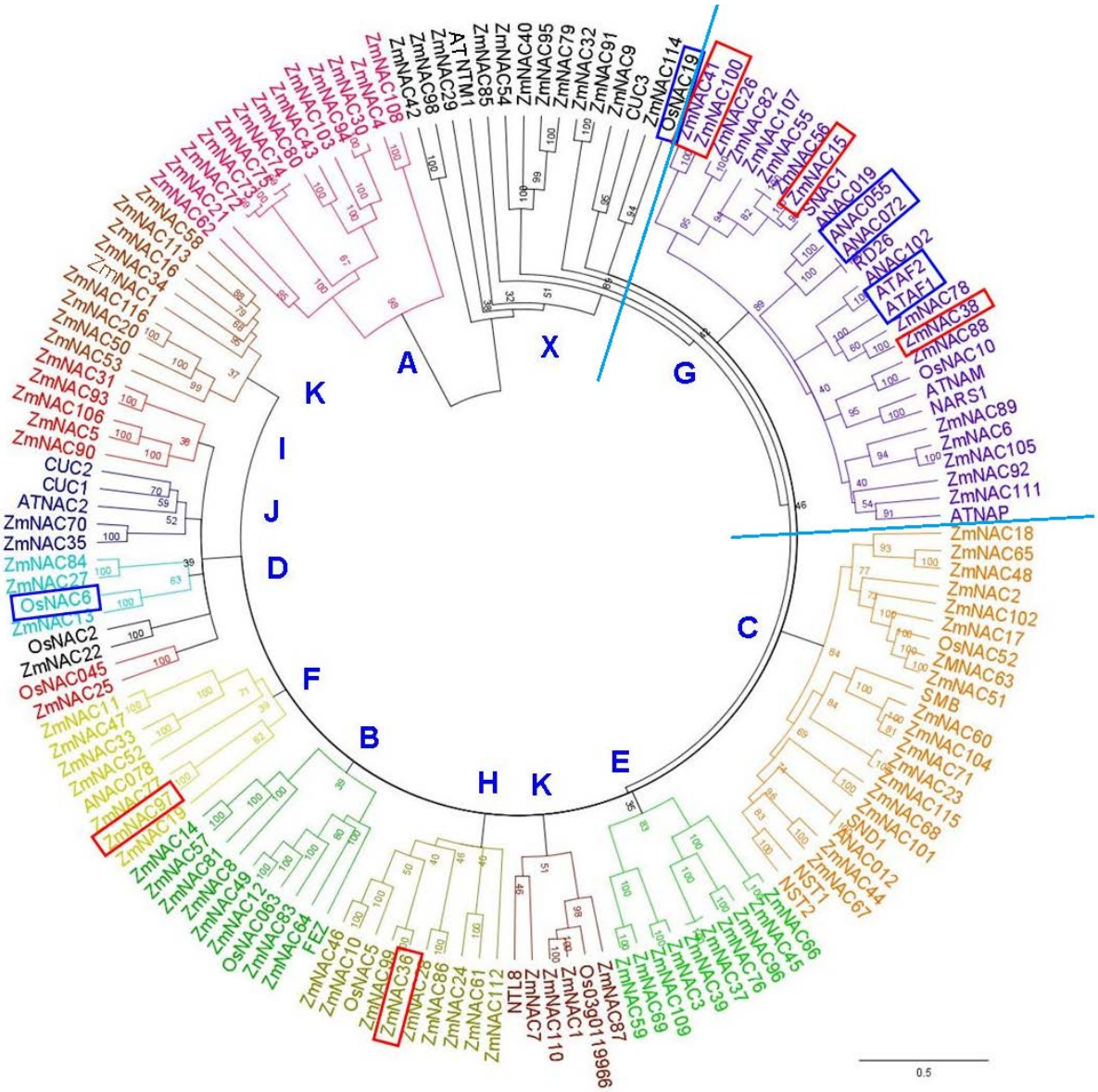

Fig. 87. Phylogenetic relationship of NAC proteins associated with the plant defence response. In comparison to the pedigree shown in Fig. 83, all Arabidopsis and rice NAC proteins with known function were included. Defence-associated NAC proteins are labelled with red (maize) and blue (Arabidopsis, rice) boxes. Clade G was enclosed by blue lines. Bootstrap values are indicated at the nodes, the bar depicts the distance scale for branch length.

4 DISCUSSION

4.1 Reprogramming of the transcriptome and metabolome in maize during the infection with *C. graminicola*

Most pronounced changes in primary metabolism, observed in maize leaves infected with *C. graminicola*, were transcriptional up-regulation of the enzymes of TCA cycle and the accumulation of carboxylic intermediates. Elevated contents of α-ketoglutarate, succinate and malate and most prominently of isocitrate were typical for the necrotrophic stage of the infection. Similar effect on the carboxylates like malate and citrate were described for the hemibiotrophic interaction of *Magnaporthe grisea* with their susceptible hosts (barley, rice and grass *Brachypodium distachyon*). Accumulation of malate was even occurring during the early, pre-symptomatic, phase of the infection (Parker et al., 2009). Microarray analysis of maize leaves colonised with *C. graminicola* revealed that most of the TCA cycle enzymes were induced on the transcriptional level. Most pronounced was the accumulation of *α-ketoglutarate dehydrogenase* and *malate dehydrogenase* transcripts. *Malate dehydrogenase* was also shown to be up-regulated in the biotrophic interaction of *Ustilago maydis* with maize (Voll et al., 2011). Moreover, the induction of two rate-limiting enzymes of TCA cycle, citrate synthase and α-ketoglutarate dehydrogenase occurred during the response of wheat to leaf rust fungus *Puccinia triticina* (Bolton et al., 2008). Enhanced metabolic flux into the TCA cycle might provide carbon skeletons as well as reducing equivalents and ATP to fuel biosynthetic pathways that are engaged during the plant defence reaction.

Furthermore, as revealed by microarray analysis, the induction of maize glycolytic pathway occurred already at early stages of the infection with *C. graminicola* and increased with the course of the infection. Intermediates of the first step of the pathway, hexose-6-phosphate and fructose-1,6-bisphosphate, accumulated at 96 hpi, however concomitant upregulation of sucrose synthesis also strongly influences contents of these metabolites. Moreover, the activity of Calvin cycle also contributes to fructose-6-phosphate and fructose-1,6-bisphopshate pool in illuminated leaves, rendering a clear assignment of hexose phosphates impossible. Concomitant up-regulation of transcripts for two rate-limiting glycolytic enzymes, *phosphofructokinase* and *pyruvate kinase*, was observed in maize leaves infected with *C. graminicola* at 96 hpi. Induced transcription of *6-phosphofructokinase* was also shown to occur in the biotrophic interaction between wheat and *P. triticina* (Bolton et al., 2008).

This induction of respiration on the cellular level was accompanied by enhanced respiration and reduced photosynthesis rate on the physiological level. Such a decline in photosynthesis rate could enhance respiratory flux into glycolysis and TCA cycle in a feedback loop. Similar reduction in photosynthesis rate was observed in plant interactions with different pathogens, e.g. Arabidopsis and the bacterial pathogen *Pseudomonas syringae* pv. *tomato* (*Pst*) (Bonfig et al., 2006). Both, virulent and avirulent strains of *Pst* affected host photosynthesis. However, the response showed different timing; the response to the avirulent strain occured already 3h post inoculation, while that to the virulent strain first 48h after inoculation (Bonfig et al., 2006). Also infection with viruses led to decline of photosynthesis as observed for the interaction of tobacco plants with potato virus Y (Herbers et al. 2000). Likewise, such response was induced in the interactions with fungal pathogen, e.g. with biotrophic white blister rust *Albugo candida*. More detailed analysis using chlorophyll fluorescence imaging revealed that reduction in photosynthesis rate was restricted to the infected areas of Arabidopsis leaves (Chou et al., 2000). Only at late infection stages this decline in photosynthesis spread across the whole leaf area, including uninfected parts. Swarbrick et al. (2006) showed that photosynthesis was negatively impacted not only in the susceptible interaction of barley and powdery mildew but also when infection was performed on resistant *Mla12* and *mlo* barley lines. However, the effect on photosynthesis was greater in susceptible leaves than in both resistant lines, as observed at 7 days post infection.

Decline in photosynthesis rate and induction of respiratory metabolism in *C. graminicola* infected leaves might indicate a transition from source to sink during the infection. Concomitant induction of cell wall invertase, which determines the sink strength (Roitsch et al., 2003), supports source-sink transition. Such induction, observed in various pathosystems and more pronounced in incompatible interactions (Bonfig et al., 2006; Swarbrick et al., 2006; Horst et al., 2008; Kocal et al., 2008; Siemens et al., 2011), may rather serve as a resistance and not as a susceptible factor. However, in maize infected with *C. graminicola* or powdery mildew (*Blumeria graminis* f.sp. *hordei*) the increase of the enzyme activity was slower than in other species and occurred at later infection stages (Voll et al., 2011). On the other hand, a significant increase in hexose content and hexose to sucrose ratio could be observed already during the biotrophic phase of *C. graminicola*-maize interaction. Taken together, analysis of respiration on transcriptome and metabolome level revealed changes that occur at very early stages of the interaction.

Furthermore, substantial changes in amino acid metabolism were observed in maize leaves during the infection with *C. graminicola*. Accumulation of aromatic amino acids like

phenylalanine and tyrosine could serve as substrate for phenylpropanoids biosynthesis and support induced defence response. Concomitant transcriptional induction of the seven enzymes of shikimate pathway seems to confirm this scenario. Such transcriptional activation of the enzymes of this pathway, e.g. chorismate synthase was also reported for the interaction of Arabidopsis with the bacterium *Pseudomonas syringae* (Truman et al., 2006). In the interaction of rice with the hemibiotrophic fungus *Magnaporthe oryzae*, a couple of enzymes of the shikimate pathway were also induced transcriptionally (Wei et al., 2013). Moreover, transcript of phenylalanine-ammonia lyase, converting phenylalanine to cinnamic acid which is the substrate for phenylpropanoid synthesis, accumulated in infected plants (Wei et al., 2013). These changes were observed early in the interaction (24 h post inoculation) and were more prominent in the response of two resistant lines (IRBL18 and IRBL22) than that of a susceptible line (LTH). Thus, the enhanced induction of aromatic amino acid and phenylpropanoid biosynthesis can be considered as a resistance factor.

Elevated glycine/serine ratio could indicate increased flux through photorespiration, resulting from elevated oxygenation activity of RubisCO due to a decline in its carboxylation efficiency. Photorespiration was shown to play a role in defence response against plant pathogens. This pathway is a major source of hydrogen peroxide, which is produced by O_2-dependent glycolate oxidase (GOX) in peroxisomes. Down-regulation of GOX in Arabidopsis resulted in disease symptoms formation and pathogen proliferation upon inoculation with non-host *Pseudomonas syringae* pv. syringae strain B728 and *Pseudomonas syringae* pv. tabaci (Rojas et al., 2012). When GOX was silenced in *Nicotiana benthamiana*, the onset of hypersensitive response was delayed, making the plants susceptible to non-host *P. syringae* pv. tomato T1, *P. syringae* pv. glycinea and *Xanthomonas campestris* pv. vesicatoria (Rojas et al., 2012). Sørhagen et al. (2013) showed transcriptional down-regulation of photorespiratory genes, along with photosynthetic genes, in the compatible interactions of Arabidopsis with two *P. syringae* strains (pv. tomato and pv. maculicola) as well as with the necrotrophic fungus *Botrytis cinerea*. Furthermore, some photorespiratory enzymes are the target for pathogen-derived compounds. Syringolide, a bacterial elicitor of *P. syringae* pv. tomato binds to soybean hydroxypyruvate reductase, resulting in the inhibition of this enzyme and consequently, causing an onset of hypersensitive response (Okinaka et al., 2002). Whereas a fungal toxin victorin from *Cochliobolus victoriae* was proposed to target a protein P from glycine decarboxylase complex in susceptible oat genotypes (Navarre and Wolpert, 1995).

It appears likely, that identified changes reflect redirection of host metabolism towards the induced defence response pathways but may also be targeted by *C. graminicola* in order to

match its nutritional requirements (see chapter 4.3. for model of redirection of host metabolism). Thus, the observed changes of host metabolism may comprise both resistance and compatibility mechanisms.

4.2 Changes on the metabolome level do not consistently match reprogramming on the transcriptome level

Analysis of maize primary metabolism revealed that there was no generally consistent match between changes in transcriptome and metabolome. Strong correlation could be shown for TCA cycle and amino acid metabolism. Whereas glycolysis represented rather weak accordance of changes on both levels. Most of the glycolytic enzymes were induced on transcriptome level, but only contents of the intermediates involved in the entry steps of the pathway, hexose-6-phosphate and fructose-1,6-bisphosphate, were altered during the infection. Genes coding for enzymes of major carbohydrate metabolism were differentially regulated on the transcriptome level and accompanied by acumulation of phosphorylated sugars like glucose-1-phosphate, UDP-glucose and sucrose-6-phopsphate. However, there were no significant changes in sucrose or starch content in infected leaves. This could be explained with the fact that both, biosynthethic and degrading enzymes were transcriptionally induced and thus steady state content of respective metabolites were not altered. As contents of all metabolites analysed in this work were measured as steady states contents, no conclusions on metabolic flux can be made. Obtained results represent only accumulation of individual metabolites. However, if the steady state content is not altered, it is still possible that metabolic flux is affected. Moreover, the changes on post-transcriptional and post-translational level need to be taken into account. Such regulation, which is significant e. g. for central carbon metabolism (Gibon et al., 2004), could cause a discrepancy between transcript amounts of respective enzymes and their activity *in vivo*.

Similar weak match of transcriptome and metabolome profile was observed for compatible and incompatible interaction of rice with *Xanthomonas oryzae* pv. o*ryza*e (Sana et al., 2010). Whereas, aligning of the transcriptome data available for *Arabidopsis-Pseudomonas syringae* interaction (Truman et al., 2006) with the respective metabolome data revealed substantial accordance (Ward et al., 2010), especially for glucosinolate and phenylpropanoid metabolism.

4.3 Model for the redirection of host primary metabolism during maize - *C. graminicola* interaction

Based on the results of combined transcriptome-metabolome analysis, a model of host metabolism during the interaction with *C. graminicola* can be proposed (Fig. 88). At the early, biotrophic, stage of the infection, just a few changes on both transcriptome and metabolome level were observed, while the ensuing necrotrophic phase was associated with substantial metabolic reprogramming. As discussed above, most prominent events upon fungal colonisation were induction of respiratory metabolism via up-regulation of glycolysis and TCA cycle, down-regulation of photosynthesis and changes in major carbohydrates and free amino acid metabolism. Higher flux through TCA cycle may have anaplerotic function to provide building blocks, reducing equivalents and energy in form of ATP for the biosynthesis of defence compounds. Concomitant up-regulation of biosynthesis of branched-chain and aromatic amino acids might support phenylpropanoids biosynthesis, which is also induced on the transcriptional level. Increased glycine/serine ratio suggests that photorespiration is induced upon fungal colonisation, which will lead to a stronger accumulation of hydrogen peroxide in addition to the oxidative burst. Reduction of photosynthetic performance and concomitant induction of cell wall invertase can lead to transition from source to sink in the infected tissue. This might be beneficial for the host, as imported compounds can serve as substrates for defence biosynthetic pathways. Moreover, elevated hexoses act as signalling molecules inducing defence gene expression (Biemelt and Sonnewald, 2006; Herbers et al., 2000) and down-regulating photosynthetic genes (Chou et al., 2000; Berger et al., 2004) which further supports the idea of a source-sink transition. On the other hand, accumulating hexoses can also be utilised by *C. graminicola* from the apoplast as preferred carbon source.

Similar changes in primary metabolism were also observed in another maize pathosystem i.e. during the interaction with *Ustilago maydis* and in barley colonised with powdery mildew (Voll et al., 2011). As such reprogramming of host primary metabolism is not specific to given pathosystem, it presumably represents a common response of cereal plants to infection on the metabolic level.

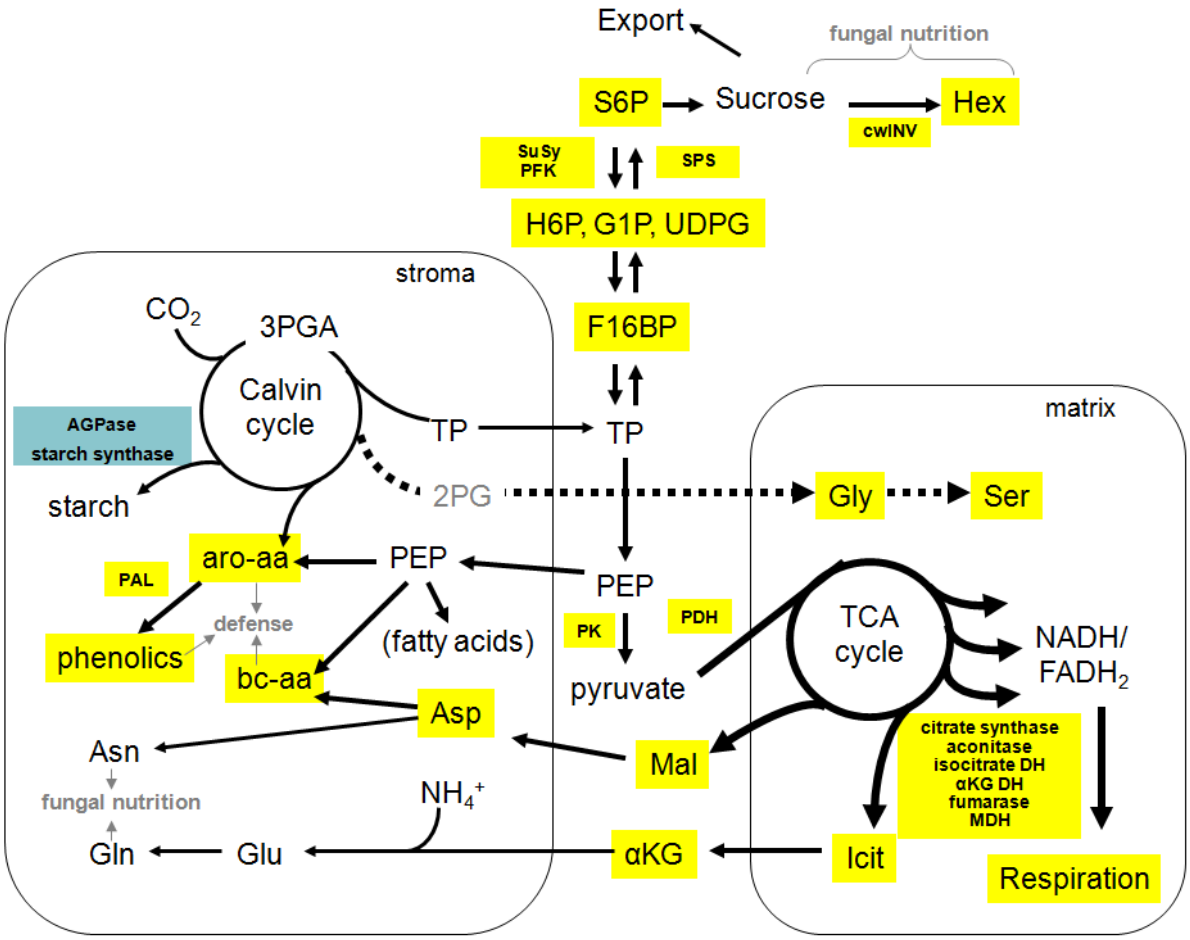

Fig. 88. Model of reprogramming of leaf metabolism during the maize – *C. graminicola* interaction, based on the results of the combined metabolome-transcriptome analysis at 96 hours post infection. Please note that for simplicity, C4 metabolism has been omitted. Yellow – up-regulation/accumulation compared to mock control; blue – decline compared to mock control. Arrow thickness correlates with the proposed metabolic flux relative to the other depicted metabolic pathways. For explanations, please see the discussion text. Amino acids are abbreviated according to three letter code, S6P, (sucrose-6-phosphate); Hex, (hexoses), H6P, (hexose-6-phosphate); G1P, (glucose-1-phosphate); UDPG, (UDP-glucose); F16BP, (fructose-1,6-bisphosphate); TP (triose phosphates); PEP, (phosphoenol pyruvate); 3-PGA, (3-phosphoglycerate); 2PG, (2-phosphoglycolate); Mal, (Malate); Icit, (isocitrate); αKG, (α-ketoglutarate); aro-aa, (aromatic amino acids); bc-aa, (branch-chained amico acids); cw-INV, (cell wall invertase); SPS, (sucrose phosphate synthase); SuSy, (sucose synthase); PFK, (Phosphofructokinase); PK, (pyruvate kinase); PDH, (pyruvate dehydrogenase); isocitrate DH, (isocitrate dehydrogenase); αKG DH, (α-ketoglutarate dehydrogenase); MDH, (malate dehydrogenase); PAL, (phenylalanine ammonia-lyase); AGPase – ADP-glucose pyrophosphorylase.

4.4 Maize alternative oxidase – a potential compatibility factor in the interaction with *C. graminicola*

As discussed above, respiratory metabolism (glycolysis, TCA cycle) was induced in maize leaves infected with *C. graminicola*. An enhanced transcription of the genes coding for the protein of the mitochondrial electron transport chain was also observed, including alternative oxidases. Transcripts of *alternative oxidase 3* (*AOX3*) accumulated already at early, pre-penetration, stages of the infection. Their amount was positively correlated with the

pathogenicity of the strain as shown during the experiment with wild type CgM2 and pathogenicity mutants of *C. graminicola*. Furthermore, inhibition of alternative oxidase on protein level by selective inhibitors of alternative respiration pathway; salicylhydroxamic acid (SHAM) or n-propyl gallate (nPG), led to restriction of growth of fungal mycelium. These results suggest that enhanced activity of the alternative oxidase promotes fungal proliferation *in planta*. The possible mechanism underlying this effect could be based on the altered reactive oxygen species (ROS) homeostasis. The elevated activity of the alternative oxidase results in the enhanced ROS quenching through alternative pathway of mitochondrial electron transport chain and subsequently decreased ROS concentration. Liao et al. (2012) showed that induction of alternative respiration in tomato plants upon tobacco mosaic virus inoculation leads to reduction of accumulation of hydrogen peroxide and to a lesser extent of superoxide anion. When leaves were pre-treated with SHAM (inhibitor of alternative respiration), ROS formation was greater compared to the leaves without pre-treatment. Application of potassium cyanide (inhibitor of cytochrome pathway of mitochondrial electron transport chain) to the leaves prior to infection resulted in decreased ROS formation due to enhanced activity of alternative pathway. Similarly, knock-down *Aox1a* tobacco plants induced strong superoxide burst when challenged with incompatible *P. syringae pv. phaseolicola* (Cvetkovska and Vanlerberghe, 2013) . In wild type plants no respiratory burst could be observed, most probable due to pathogen-induced AOX up-regulation. In addition Giraud et al. (2008) have observed enhanced accumulation of superoxide anion in Arabidopsis plants with knocked-out *Aox1a* gene under combined moderate light and drought stress conditions.

Thus, it can be assumed that induction of maize AOX expression results in enhanced quenching of ROS generated as a part of response to *C. graminicola.* Vargas et al. (2012) showed that ROS indeed accumulated in response to the infection with this fungus. In situ analysis revealed that hydrogen peroxide production occurred at the early stage i.e. 12h to 72h post inoculation. Hydrogen peroxide, which was the main ROS form, was detected beneath fungal appressoria and in the proximity of penetration peg.

Reactive oxygen species generated in mitochondria serve as signalling molecules through retrograde signalling pathway. A set of responses to various biotic stresses are induced or regulated by mitochondria-derived ROS as reviewed by Rhoads and Subbaiah (2007). It was shown that pathogen-derived elicitors could disturb mitochondrial functions leading to induction of defence via altered gene expression, as summarised in the next paragraph. The bacterial elicitor hairpin negatively impacted ATP synthesis in mitochondria and accelerated hypersensitive response in tobacco cell cultures. It also activated ROS-

dependent MAP-kinases and finally defence-associated genes in Arabidopsis. Transcript of *Aox1a* gene also accumulated in response to treatment with hairpin. Similarly, tobacco hypersensitive response to oomycete *Phytophtora cryptogea* was triggered by elicitor cryptogein which negatively impacted respiration and membrane depolarisation in mitochondria. While victorin, a host-selective toxin from *Cochliobolus victoriae* induced programmed cell death in oat via increased mitochondrial ROS production due to disruption of membrane potential. Thus, mitochondrial retrograde signalling contributes to regulation of expression of nuclear stress-associated genes. Likewise, a transcription of two maize defence-associated genes (*12-oxophytodienoate reductase 1* and *PR5*) was induced in plants treated with inhibitors of alternative oxidase (as shown in Fig. 68 in chapter 3.3.1.3). Accumulation of *AOX3* transcripts upon this treatment might suggest concomitant ROS accumulation, as maize *AOX* genes was shown to be responsive to increased formation of ROS. Karpova et al. (2002) observed that mutations of components of the mitochondrial electron transport chain in maize led to disturbances in ROS homeostasis and subsequently to the induction of *AOX* genes. The same effect was also observed upon treatment with inhibitors of the complexes of electron transport chain, like antimycin which inhibits complex III.

Taken together, the induction of maize AOX might attenuate ROS production and therefore ROS-mediated signalling and thereby dampen the induction of defence-associated genes. Dampened defence responses subsequently allow for more fungal growth *in planta*. It can be hypothesised that *C. graminicola* might alter the host defence by reprogramming host ROS-detoxifying mechanisms, making an alternative oxidase a compatibility factor in the interaction. Showing an effect of the absence of alternative oxidase activity on defence responses would be a pre-requisite to prove this hypothesis. Experiments with AOX inhibitors do not reflect the real situation upon pathogen colonisation as they influence electron flow through mitochondrial respiratory chain and ROS metabolism. Most convenient would be the usage of genotypes with down-regulated expression of *AOX* genes or *AOX* knock-out lines. Unfortunately, such lines are not available for maize. During the work for this thesis, efforts were made to suppress *AOX* gene expression via virus-induced gene silencing but plants with altered expression could not be obtained. Thus, a decision was made to elucidate a role of alternative oxidase in defence response in another well established *Colletotrichum* pathosystem i.e. in the *C. higginsianum*-Arabidopsis interaction.

4.5 Role of Arabidopsis AOX in the interaction with *C. higginsianum* could not be elucidated

Five genes encoding alternative oxidase were identified in Arabidopsis genome:, out of which *Aox1a* and *Aox1d* were expressed in leaves with *Aox1a* being most abundant transcript. Transcripts of these two genes were also induced in response to *C. higginsianum*, however, transcript accumulation was associated mostly with the necrotrophic stage of the infection and was not as strong as observed for the maize - *C. graminicola* interaction. Interestingly, respiration of mock wild type Col-0 plants was comparable to that of *Aox1a* anti-sense plants. Such an observation suggests a minor contribution of the alternative pathway to total respiration under normal conditions. However, the rate of alternative respiration was increased in *C. higginsianum*-infected Arabidopsis leaves, which confirms that alternative respiration is induced in Arabidopsis in response to biotic stress. Plants overexpressing *Aox1a* had higher respiration rates than wild type Col-0 plants, with a further increase in response to *C. higginsianum* infection at 3 dpi. In contrast, both mock and infected leaves of *Aox1d* knock-out plants exhibited similar respiration rates compared to wild type Col-0 plants. This suggests a limited contribution of the Aox1d isoform to alternative respiration.

However, plants with altered *Aox1a* levels did not show a significant change in susceptibility compared to wild type Col-0 plants, i.e. the expression level of *Aox1a* did not correlated with fungal proliferation *in planta*. It should be emphasised that rather AOX capacity than actual *in vivo* AOX activity was determined in *Aox1a* anti-sense and overexpressing lines. To this end, respiration rates were measured after treatment with KCN to block the cytochrome pathway. Under such conditions, whole electron flux is directed to alternative respiration. Thus, obtained rates reflect AOX capacity and not the activity. The latter one should be measured in physiological conditions, without additions of inhibitors, e.g. via oxygen isotope ($^{18}O/^{16}O$) partitioning. Alternative oxidase activity does not necessarily correlate with its capacity or with its transcripts / protein level. In *Nicotiana sylvestris* mitochondrial mutants, lacking functional complex I, transcription and translation of *Aox1a* gene and capacity of alternative respiration were constantly increased but without any measurable change in AOX activity compared to wild type plants (Vidal et al., 2007). On the other hand, treatment with bacterial elicitor hairpin led to increased activity of alternative oxidase in these mutants, with no influence on protein amounts. As discussed by Rasmusson et al. (2009), such a discrepancy can be explained by the fact that capacities of metabolic

enzymes are much higher than required under given conditions. This can be advantageous for counteracting short-term metabolic fluctuations e.g. under stress conditions. Such overcapacity of enzymes would allow for adjustment in case of transient changes in metabolite fluxes without influencing mean activity of the enzymes and serve as mechanism for rapid auto-regulation of metabolism. Once metabolic fluctuations sustain over a longer period of time, this would induce observable changes in mean enzyme activity.

Taken together, the conducted experiments do not allow for final conclusions, especially since it is possible that alternative oxidase activity in Arabidopsis line with constant induction of *Aox1a* gene was comparable to that of wild type Col-0 plants, although capacity of alternative respiration was increased. The measurement of ROS formation in wild type Col-0 and *Aox1a* overexpressing plants seems to confirm such scenario. Leaves overexpressing *Aox1a* were producing same amounts of ROS when treated with flg22 elicitor as wild type Col-0 leaves (see Fig. 76 in chapter 3.3.1.6.). If alternative oxidase activity is indeed not altered in *Aox1a* overexpressor, these could explain lack of observable change in *C. higginsianum* proliferation compared to wild type Co-0. However, no influence on proliferation of *C. higginsianum* could be observed in *Aox1a* anti-sense plants, although they accumulated significantly more ROS in leaves compared to wild type Col-0 leaves.

Furthermore, comparison of the analysis of *Aox1a* anti-sense and insertion mutant plants shows that reduction of *Aox1a* transcript in anti-sense line may not be sufficient. Umbach et al. (2005) observed minor changes in gene expression with just 14 potential stress-related genes being deregulated in *Aox1a* anti-sense lines. While ca. 3,000 genes in total, including genes involved in cell wall metabolism, flavonoid production or antioxidant defence, were altered in *Aox1a* insertion mutant (Giraud et al., 2008). Thus, analysis using *Aox1a* deletion mutants might be better suited to elucidate a role of host A*ox1a* for the interaction with *C. higginsianum*, unfortunately such lines were not available at the time when experiments were conducted.

In conclusion, it can be stated that experiments with *Aox1a*-affected Arabidopsis lines did not prove that alternative oxidase has an impact on the growth of *C. higginsianum in planta*. On the other hand, a lack of influence of *alternative oxidase* expression on the interaction can also not be excluded. Even if alternative oxidase would indeed not be a compatibility factor in this interaction, it is still probable that there is an influence of AOX activity on the interaction of maize with *C. graminicola*. As previously reported, the alternative oxidase can respond differently even to two different pathovars of a given pathogen in the same host plant. Cvetkovska and Vanlerberghe (2012) showed that transcripts

of *Aox1a* gene and AOX protein accumulated in the incompatible interaction of tobacco with *P. syringae* pv. *phaseolicola* but not in response to the other incompatible pathovar *maculicola*.

Finally, it is also possible that alternative oxidase does not serve as a compatibility factor specific for the interaction with *Colletotrichum* species but may instead be generally responsive in plant-pathogen interactions as the induction of AOX was observed in different kinds of interactions including fungal, bacterial and viral infections (reviewed by Vanlerberghe 2013).

4.6 Maize NAC transcription factors act in defence response network

Microarray analysis revealed that two genes coding for NAC transcription factors; *ZmNAC41* and *ZmNAC100*, were induced in maize leaves infected with *C. graminicola*. A more detailed analysis of the transcript accumulation by qRT-PCR showed that induction of *ZmNAC41* occured already at the pre-penetration stage. Thus, this protein could act as a component of the basal defence response. The involvement of NAC transcription factors in the early events of plant defence, i.e. following PAMP recognition, was reported for other species as well. The expression of barley *HvNAC6* in the epidermis was enhanced early after inoculation with *Blumeria graminis* f. sp. *hordei* (Jensen at al. 2007). Moreover, host resistance to powdery mildew correlated with the expression level of this gene. Silencing of *HvNAC6* impaired callose papilla formation, while complementation of *HvNAC6* in the anti-sense background enhanced resistance through increased formation of papilla. Likewise, an Arabidopsis orthologue of *HvNAC6, ATAF1* was also involved in the regulation of papilla formation in response to pathogens. A deletion of this gene was shown to attenuate non-host resistance to *Blumeria graminis* f. sp. *hordei* (Jensen at al. 2008). Taken together, both HvNAC 6 and ATAF1, seem to be involved in the control of basal defence. While the expression of barley *HvNAC6* and Arabidopsis *ATAF1* enhanced host resistance, the expression of maize *ZmNAC41* was positively correlated with the pathogenicity of the *C. graminicola* strain. The other NAC induced in the maize – *C. graminicola* interaction, *ZmNAC100*, accumulated solely in response to successful penetration events. These observations rather suggest the involvement of these two NAC family members during the induced defence response, which is under a tight control by the phytohormones jasmonic acid (JA), ethylene and salicylic acid (SA). Both *ZmNAC41* and *ZmNAC100* were induced by jasmonic acid (JA), while *ZmNAC100* was induced by treatment with salicylic acid analogue.

The transcription level of *ZmNAC100* upon treatment with jasmonate was two to five times lower compared to that observed in leaves infected with *C. graminicola*. In case of *ZmNAC41* the induction was more than 100 times weaker in jasmonate-treated leaves, although considerable concentrations of JA were applied. These results suggest that *ZmNAC41* and *ZmNAC100* are mainly induced by JA-independent processes. *NAC* genes from other species were reported to be responsive to jasmonate, e.g. *OsNAC5* and *OsNAC6* in rice (Takasaki et al. 2010) or *ANAC019* and *ANAC055* in Arabidopsis (Bu et al. 2008). The two Arabidopsis NACs transcription factors; ANAC019 and ANAC055, were furthermore shown to serve as transcriptional regulators of JA-responsive genes, like *VEGETATIVE STORAGE PROTEIN 1* and *LIPOXYGENASE2* and may thus probably act in a jasmonate feedback loop.

Moreover, transcripts of both maize *NAC* genes accumulated in senescing leaves, as revealed by qRT-PCR analysis. Senescence is a process to some extent overlapping with defence response through common signalling pathways. A number of transcription factors were reported to be associated with biotic stress and senescence, potentially regulating the interplay of both processes, like WKRY6 in Arabidopsis (Robatzek and Somssisch, 2002) or NAC transcription factors e.g. Arabidopsis NTL9 (Yoon et al., 2008; Block et al., 2014), grapevine VvNAC1 (Le Hénanff et al., 2013) or barley HvNAC013 (Kjaersgaard et al., 2011). A possibility that ZmNAC41 and ZmNAC100 might regulate both senescence and defence response in maize cannot be excluded.

Furthermore, promoter regions of the six pathogen inducible maize *NAC* genes were analysed towards the binding sequences of defence-associated transcription factors. In four of these maize *NACs*, recognition sites of ERF, TGA or Myc2 transcription factors, regulating ethylene, salicylic acid and jasmonate-dependent defence responses, respectively, were identified. The W-box, a WRKY-binding motif, was also present in four of them, while only promoters of *ZmNAC41* and *ZmNAC100* contained Whirly-response elements. Promoter regions of all six *NAC* genes comprised NAC-binding sites. Such composition of promoter elements could indicate that these NACs serve as regulatory components in the maize defence network. WRKY-binding motives and ERF recognition sites, both repeated 4 times, and three TGA motifs were identified in the promoter region of *OsNAC6*, a known transcriptional activator of rice biotic stress-associated genes (Nakashima et al., 2007). It is worth to note that orchestrating the defence network through different classes of transcription factors does occur not only at the level of *NAC* genes. NACs form homodimers and heterodimers with other NACs (Olsen et al., 2005) on the protein level and as such can regulate the expression of other defence-associated genes. Furthermore, it was recently shown that banana MaNAC5

physically interacted with MaWRKY1 and MaWRKY2 and this complex activated transcription of *PR* genes, contributing to resistance to *Colletotrichum musae* (Shan et al., 2015).

4.7 Most NAC transcription factors associated with plant defence are monophyletic

In this work, maize genome (cultivar B73) was screened for NAC transcription factors, which resulted in the identification of 116 maize *NAC* genes. Moreover, all genes were named based on their position in the genome (as described in chapter 3.3.2.5.). Subsequent phylogenetical analysis of derived protein sequences led to a systemic classification of maize NAC transcription factors. In this approach 12 clades including a group of distantly related NACs (group X) could be distinguished. A recent analysis of Fan et al. (2014) revealed 124 NAC proteins that clustered to 13 subfamilies in maize. These were more sequences than identified in the frame of this thesis and could be caused by inclusion of alternative splice variants as distinct NAC family members. Extensive comparison of more than 800 NAC sequences from nine species revealed 21 NAC subfamilies (Zhu et al., 2012). Maize representatives clustered to 15 subfamilies in the cross-species approach of Zhu et al., yielding a greater number of clades than presented here. However clade C identified in this work comprises two clearly distinct subclades, while clade G consists of three subclades. When considering these subclades as separate clades, this approach will finally yield 15 clades as well. These splits in clades C and G are probably more pronounced when a greater number and less related sequences are employed for the analysis, as by Zhu et al (2012).

NAC transcription factor families of higher plants are large, consisting of more than 100 members pro species. The evolutionary expansion of NACs in maize genome occurred through three main mechanisms; whole genome duplication and segmental as well as tandem gene duplication (Zhu et al., 2012). In maize, mainly gene duplication through segmental duplication events contributed to the expansion of NAC family (chapter 3.3.2.5, Fan et al., 2014). Through such evolutionary recent event two close paralogues described in this work, ZmNAC41 and ZmNAC100, have arisen.

Another phylogenetic analysis described in this work, performed with functionally characterised Arabidopsis and rice NACs showed that the majority of defence-associated representatives cluster to clade G. Four maize NACs induced in response to *C. graminicola* / *U. maydis* were also found in this clade. When comparing data presented here with the cross-species analysis of Zhu et al. (2012), clade G represents one of the evolutionary ancient group

of NAC proteins, where most of moss and lycophyte members can be found. The most ancient species, in which NACs have been identified, is *Physcomitrella patens*. This moss induces several defence mechanisms in response to pathogens, leading to SA-dependent and oxylipin (12-oxo-phytodienoic acid - OPDA) - dependent transcript accumulation (de León et al., 2012, 2015). The presence of jasmonic acid could not be identified in *P. patens*. However the moss responds to exogenously applied methyl jasmonate in the same way as to OPDA, suggesting that components of jasmonate signal perception and transduction are already present in this organism. Thus, it can be hypothesised that regulation of defence responses through SA and oxylipin signalling was one of the first acquired functions of NAC transcription factors during the evolution of plants.

4.8 CgUbc8 – a novel *C. graminicola* compatibility factor

Screening of the library of *C. graminicola* ATMT mutants for strains impaired in pathogenicity revealed an interesting candidate gene – *ubiquitin-conjugating enzyme 8* (*CgUbc8*). Both the *CgUbc8* ATMT mutant and subsequently generated *CgUbc8* knock-out strains showed reduced virulence *on planta* due to reduced penetration rate. Impaired pathogenicity could be confirmed by macroscopic observation of disease symptoms and chlorophyll fluorescence imaging on infected maize leaves. The latter analysis revealed that effective photosystem II quantum yield and electron transport rate were higher in maize leaves infected with mutant and knock-out strain than in CgM2 wild type-infected leaves. A cytological survey revealed that reduced penetration rate of *CgUbc8* ATMT mutant and *CgUbc8* knock-out strains might be caused by irregularities in appressoria or spore development. Indeed, appressoria of these strains exhibit lower melanisation rate as observed two days post inoculation (see Fig. 42 in chapter 3.1.7). Melanisation is a critical step in the differentiation of appressoria as it is important for development of high turgor pressure allowing mechanical penetration into the host tissue. Melanin incorporation into the walls of appressoria reduced cell wall pore size (Howard et al. 1991), allowing for transfer of water but not larger molecules such as glycerol (de Jong et al., 1997). Accumulation of glycerol and other osmotically active compounds in the appressorium enhances flux of water into the appressorium and subsequently increases turgor pressure. Failures in the melanisation of appressoria reduce turgor pressure and prevent penetration as reviewed by Deising et al. (2000). However, recently Ludwig et al. (2014) showed that in *C. graminicola* melanin was not essential for turgor generation inside the appressoria but it supported developing turgor

pressure through increasing appressorial wall rigidity. Analysis of *CgUbc8* mutants also revealed that incompletely melanised appressoria of these mutants exhibited similar turgor pressure as fully-melanised CgM2 wild type appressoria (Fig. 89).

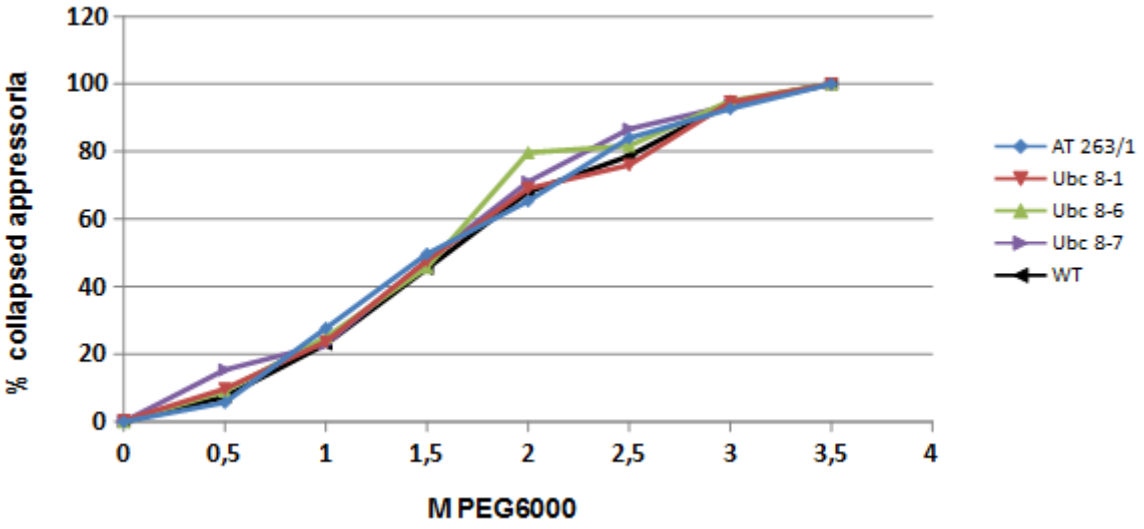

Fig. 89. Evaluation of turgor pressure exhibited by appressoria of *C. graminicola* wild type CgM2 (WT), insertion mutant strain with reduced expression of *CgUbc8* gene (AT263/1) and *CgUbc8* knock-out strains (Ubc8-1/Ubc8-6/Ubc8-7). Appressoria were incubated in solutions of polyethylene glycol of different concentrations (0-4 M) to estimate the ratio of induced cytorrhysis (cell collapse). Collapse of appressoria due to water loss depends on the balance of osmotically active compounds inside the appressoria and in the external solution. High external concentrations of PEG enhance water efflux from appresssoria and subsequently their collapse. No difference in the ratio of collapsed appressoria at all tested PEG concentrations indicate that there is no difference in the concentration of osmotically active compounds inside the appressoria and thus no difference in generated turgor pressure. Results courtesy of Steffen Münch (Martin-Luther-University Halle-Wittenberg).

Ubiquitin conjugating enzymes (Ubc) label target proteins with ubiquitin, which directs them for degradation in the proteasome. Thus, reduced virulence of *CgUbc8* mutant and knock-out strains might arise from impaired ubiquitination of CgUbc8 target proteins. Microarray analysis performed by Oh et al. (2012) showed that ubiquitination-associated transcripts were enriched in the total transcript pool during conidia germination of *M. oryzae*. The authors could also show that inhibition of ubiquitin-mediated protein degradation impairs conidia germination, appressoria formation and pathogenicity of *M. oryzae*. In *Saccharomyces cerevisiae*, Ubc8 targets one key enzyme of gluconeogenesis, fructose-1,6-bisphosphate (FBPase), to degradation and thus, acts as a negative regulator of this pathway. Lack of Ubc8 stabilises its target protein FBPase which subsequently would lead to constant activation of gluconeogenesis and accumulation of glucose (Schüle et al., 2000). In yeast, excessively produced glucose can be metabolised to glycogen. In *C. graminicola* lack of Ubc8 diminishes glycogen accumulation. Thus, lack of the encoded protein in *C. graminicola*

has got an opposite effect to that observed for its ortholog in *S. cerevisiae.* This could mean that CgUbc8 might stabilise FBPase, probably by targeting its negative regulator for degradation. Alternatively, it might target other enzymes involved in glucose/glycogen metabolism. Both et al. (2005) actually showed that FBPase was induced on the transcriptional level in ungerminated and germinating conidia of *Blumeria graminis* f. sp. *hordei* and dropped after the penetration event, indicating the importance of gluconeogenesis for pre-penetration stages. Although no consistent changes were observed in FBPase activity in conidia of *CgUbc8* mutant and knock-out strains, reduced penetration rate of strains lacking CgUbc8 protein might indeed arise from limited pool of storage compounds such as glycogen. Accumulation of glycogen and lipids and their mobilisation from conidia to appressoria is necessary for proper development of appressoria. *M. grisea MGA1* mutants, impaired in the mobilisation of storage compounds, were completely apathogenic as they were unable to form appressoria (Gupta and Chatoo, 2007). Glycogen and lipid droplets were abundant in both wild type and mutant conidia of *M. grisea*. However, these storage compounds were only mobilised in wild type conidia and subsequently accumulated in appressoria of the wild type to be further utilised during the melanisation and turgor generation. Glycogen and lipids pools were not mobilised in course of mutant conidia germination, leading to a delay in mutant germ tube development. The mutant strain also exhibited lower conidiation rate and, interestingly, reduced mycelium melanisation. Thus, based on the results obtained for *M. grisea*, it could be assumed that decreased glycogen pool in conidia of *C. graminicola* hampers appressorial development as less glycogen is provided for conidia germination and appressoria formation.

4.9 CgUbc8 acts as post-translational regulator of glucose metabolism

Apparently the *Ubc8* gene of *C. graminicola* might be involved directly or indirectly in the regulation of glycogen metabolism, as a lack of the encoded protein diminishes glycogen accumulation. Interestingly, wild type CgM2 strain grown on medium supplemented with glucose also accumulated significantly less glycogen, while the glycogen content in conidia of the insertion mutant strain with reduced expression of *CgUbc8* (AT263) and *CgUbc8* knock-out strain did not change upon presence of external glucose (Fig. 90). In both cases - with and without glucose supplementation - glycogen levels were similar to that of CgM2 wild type conidia on medium with glucose addition. This suggests that lack of CgUbc8 redirects metabolism in the same way as the presence of external glucose, indicating that

glucose sensing or metabolism is affected in insertion mutant strain with reduced expression of *CgUbc8* (AT263) and in *CgUbc8* knock-out strain. Thus, it could be assumed that CgUcb8 influences glucose utilisation via glycolysis and gluconeogenesis.

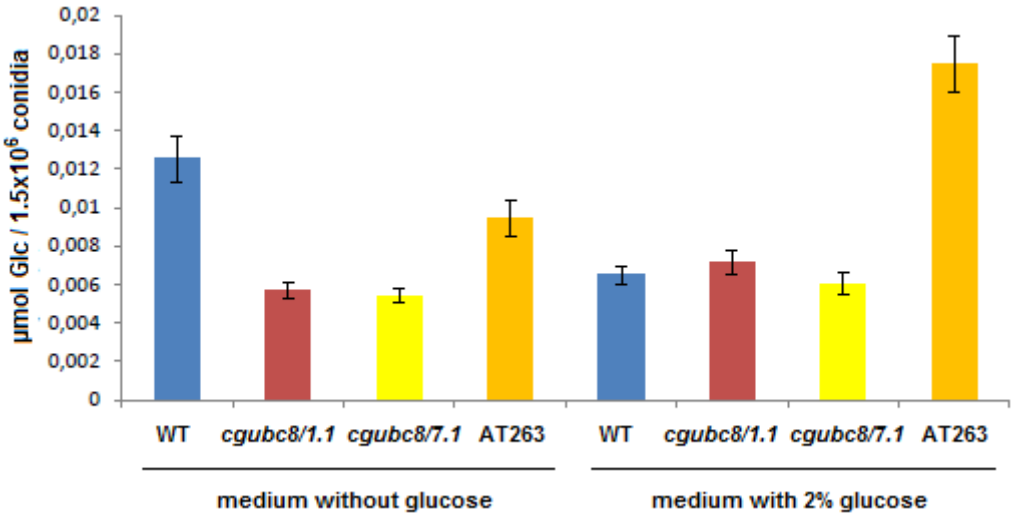

Fig. 90. Glycogen content in 1.5x10^6 conidia of *C. graminicola* wild type CgM2 (WT), two *CgUbc8* knock-out strains (*cgubc8/1.1* and *cgubc8/7.1*) and AT263 insertion mutant strain harvested from OMA medium without glucose (left side of the chart) and with 2% glucose (right side of the chart) eleven days after inoculation. Mean values are shown (n=4). Error bars represent standard error.

Evaluation of activities of gluconeogenetic and glycolytic enzymes revealed that glucose degradation was affected in insertion mutant AT263 and *CgUbc8* knock-out strains. The activity of phosphofructokinase, a key enzyme of glycolysis, was higher in mutant and knock-out conidia compared to wild type CgM2 when grown on medium supplemented with glucose. This could suggest that glucose utilisation via glycolysis is up-regulated when Ubc8 is absent in *C. graminicola*.

Moreover, a lower activity of malate dehydrogenase, a known target of carbon catabolite repression (CCR), in *C. graminicola* AT263 insertion mutant and *CgUbc8* knock-out conidia harvested from medium without additional glucose may suggest that CCR might be hampered. The activity of isocitrate lyase, another known CCR target enzyme, was lower in AT263 insertion mutant and one of two *CgUbc8* knock-out strains compared to wild type CgM2 when grown on medium without glucose supplementation. The other gluconeogenetic enzymes fructose-1,6-bisphosphatase and PEP-carboxykinase did not seem to be responsive to CCR in *C. graminicola*, as there were no difference in activity of these enzymes in CgM2 wild-type upon glucose supplementation.

Based on incomplete de-repression of malate dehydrogenase as CCR-target gene in *C. graminicola* together with enhanced glucose utilisation via glycolysis in mutant and knock-

out strain, a possible involvement of CgUbc8 in CCR regulation in this fungus may be hypothesised.

4.10 Putative role of CgUbc8 in control of CCR during development of pre-penetration infection structures of *C. graminicola*

As discussed above, CgUbc8 might possibly be involved in glucose sensing and regulation of CCR in *C. graminicola*. The question is, what might be the mechanism of such control and how it could influence pathogenicity of the fungus. CgUbc8 belongs to the family of ubiquitin-conjugating enzymes that are involved in post-translational regulation of other proteins by targeting them for degradation by the proteasome. Thus, CgUbc8 might hypothetically target regulator proteins controlling CCR. In *S. cerevisiae,* one of key regulators of CCR is a zinc finger protein Mig1 that recruits Ssn6/Tup1 repressor complex to promoters of CCR target genes (Treitel and Carlson, 1995). Mig1 is under control of repressor Snf1, which is inactivated via glucose-induced SUMOylation once CCR is on (Simpson-Lavy and Johnston, 2013). SUMOylation is mediated by E1-E3 ligases, analogous to ubiquitination, however modified proteins are not directed for degradation. In yeast there is only one E2 ligase involved in this process – Ubc9 (Johnson and Blobel, 1997). Srikumar et al. (2013) showed that Tup1 was also modified by attaching SUMO-conjugates.

In ascomycete fungi, CCR is under control of Cre proteins, homologues of yeast Mig-1. The involvement of CRE-1 in CCR of *Neurospora crassa* was shown by Sun and Glass (2011). There is also an evidence that RCM-1 and RCO-1, Ssn6 and Tup1 homologues respectively, may regulate expression of glucose-repressed genes in *N. crassa* (Lee and Ebbole, 1998). In *Aspergillus nidulans* CreA repressed CCR-target genes, however RcoA protein, a Tup1 homologue, had a minor effect on the repression of the targets (Hicks et al. 2001). Thus, these observations indicate that de-repression of CCR target genes via Mig1 / Cre proteins is conserved in ascomycete fungi but not the downstream regulation of this repression.

If lack of CgUbc8 would indeed inhibit full release from CCR, this might occur via stabilisation of repressor(s) of CCR-target genes. In this hypothetical scenario, CgUbc8, once present, would target this (these) repressor(s) for degradation (Fig. 91). But how could this process be relevant for the pathogenicity? Could be a control of glycogen accumulation a key component? Cupertino et al. (2015) showed that glycogen metabolism in *N. crassa* was under control of CRE-1, RCO-1 and RCM-1 with the first of them playing a central role. CRE-1

inhibited glycogen synthesis by repressing glycogen synthase, glycogen branching enzyme and glycoginin on the transcriptional level and by promoting glycogen degradation via transcriptional inhibition of glycogen phosphorylase. *Cre-1* knock-out strains accumulated more glycogen than wild type, while glycogen content was just slightly increased in *rco-1* and reduced in *rcm-1* knock-out strains. Surprisingly, glycogen synthase was more active in all three strains due to decreased phosphorylation. Thus, it can be concluded that glycogen metabolism is indeed under control of CCR in *N. crassa*, however the outcome i.e. glycogen accumulation differs depending on the CCR-component affected.

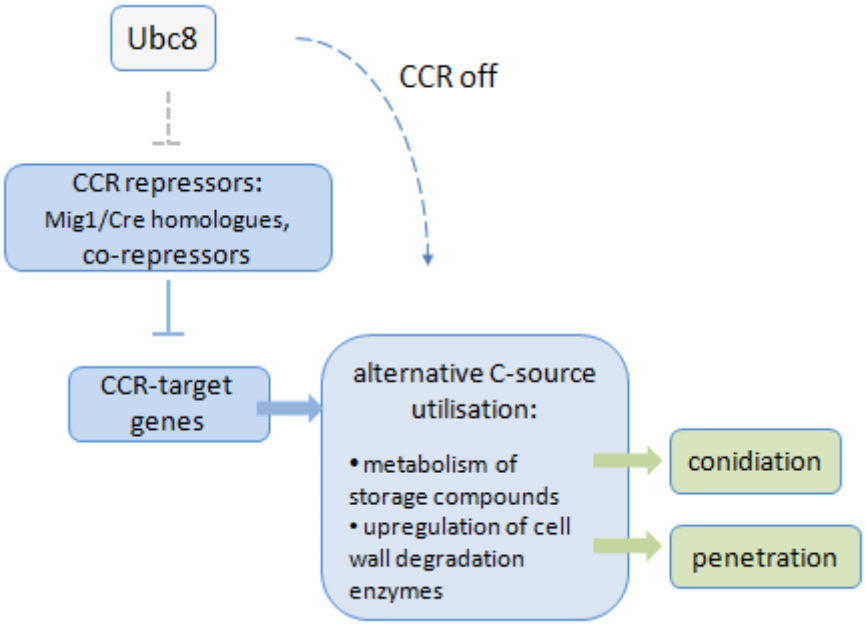

Fig. 91. Control of phytopathogenic fungi development via carbon catabolite repression (CCR). Arrows indicate up-regulation/induction, lines ended with horizontal bars – down-regulation/inhibition. Hypothetical role for Ubc8 in targeting CCR repressors for degradation was included, however there is no experimental evidence for such scenario. For explanation please see text in chapter 4.10.

Interestingly, Coral-Rammos et al. (2015) showed that *Fusarium oxysporum* mutants impaired in glycogen synthesis exhibited no reduction of virulence. The same was observed for *Magnaporthe oryzae* by Badaruddin et al. (2013). However, when catabolism of glycogen was affected, a reduced virulence was observed for mutants of both species. The authors argued that inhibition of glycogen metabolism into trehalose could be the main cause for such a phenotype. It was observed already by Neves (1991) that glucose from break-down of the glycogen pool can feed trehalose synthesis. Badaruddin et al. (2013) showed that mutants blocked in glycogen catabolism exhibit down-regulation of trehalose-phosphate synthase (Tps1) and lower levels of trehalose content in appressoria of *M. oryzae*. Tps1 was actually shown to affect virulence gene expression via glucose-6-phosphate sensing, which is a substrate for this enzyme. Under increasing concentrations of glucose-6-phosphate, Tps1

activated glucose-6-phosphate dehydrogenase, causing accumulation of NADPH. Due to increasing NADPH/NADP ratio, a group of NADP-dependent inhibitor proteins became inactivated which allows the expression of virulence-associated genes (Wilson et al. 2010). Loss of Tps1 led to apathogenicity due to formation of non-functional appressoria not able to penetrate the host tissue. The authors prove that this effect is not caused by simple loss of trehalose synthesis, as the mutation affecting catalytic activity of Tps1 did not affect the ability to cause disease. Apathogenicity could be clearly linked to the mutation preventing glucose-6-phosphate binding to Tps1 (Wilson et al., 2007). Fernandez et al. (2012) showed that Tps1 was also involved in mediating CCR and was triggering this repression via glucose-6-phosphate sensing in *M. oryzae*. *Tps1* knock-out strains exhibited down-regulation of genes coding for glucose import and metabolism and up-regulation of genes coding for utilisation of alternative carbon sources when grown on glucose. This observation suggests that the mechanism of glucose sensing is different in ascomycete phytopathogens compared to yeast, where CCR is induced by glucose and fructose phosphorylation via hexokinase and mediated by the Mig1 signalling cascade discussed above. Interestingly, as CCR was altered in *Tps1* knock-out strain, up-regulation of expression of cell-wall degrading enzymes (CWDEs) was observed. This indicates a dual role of Tps1 for virulence, i.e. promoting the expression of a subset of virulence genes associated with appressoria development, while inhibiting the expression of CWDEs as another subset of virulence genes. Thus, glucose sensing via Tps1 seems to allow for temporal and spatial regulation of pathogenicity-associated genes in *M. oryzae*.

As discussed in chapter 4.9, glucose sensing and metabolism was affected in *Ubc8* mutants and knock-out strains of *C. graminicola*. When we take into account that glycogen levels depend on both its synthesis and catabolism, it is possible that lower levels of glycogen in the mutants are caused not only by reduced synthesis but also by enhanced degradation. Down-regulation of glycogen catabolism might be a primary point of CgUbc8 action. In this hypothetical scenario, de-repression of CCR would be a secondary effect, caused by inhibition of glucose sensing (Fig. 92), hypothetically via trehalose-6-phosphatase, as shown for *M. oryzae* (discussed above).

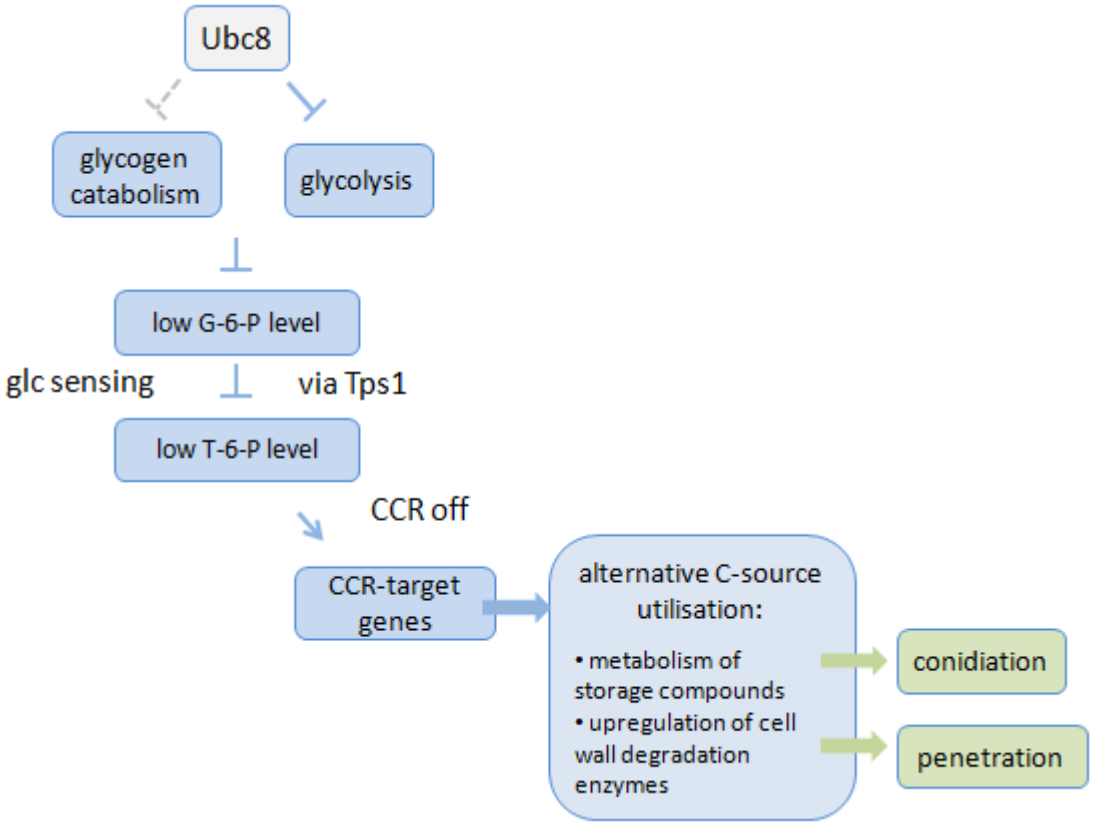

Fig. 92. Regulation of carbon catabolite repression (CCR) via glucose-6-phosphate (G-6-P) sensing in phytopathogenic fungi. A hypothetical role of *C. graminicola* Ubc8 in repression of glycogen catabolism is included (an alternative hypothetical role was presented in Fig. 90). Down-regulation of glycogen catabolism might be a primary target of CgUbc8 action, however there is no experimental evidence for this scenario. Arrows indicate up-regulation/induction, lines ended with horizontal bars denote down-regulation/inhibition. (T-6-P) trehalose-6-phosphate, Tps1 – trehalose-phosphate synthase. For explanation please see text in chapter 4.10.

Greenwald et al. (2010) showed that low glucose levels induced conidiation in *N. crassa*, while high levels had an opposite effect. Moreover, transcription factor RCO-1, involved in CCR on *N. crassa*, was first identified as repressor of conidiation-associated genes (Yamashiro 1996). *C. graminicola Ubc8* mutants and knock-out strains produced comparable amounts of conidia as the wild type CgM2 strain but conidiation was reduced on medium containing glucose in all strains (including wild type) compared to medium without glucose supplementation (Fig. 93).

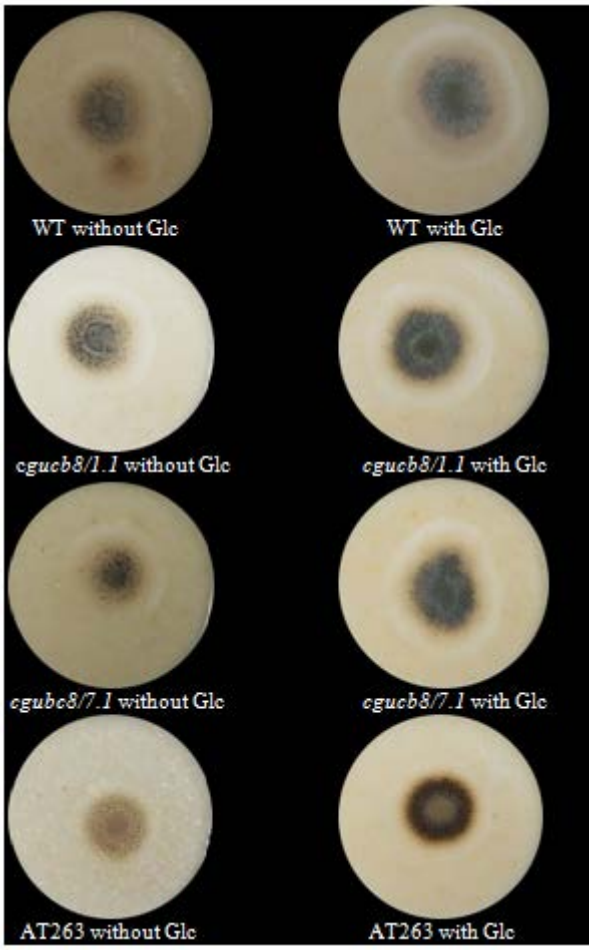

Fig. 93. Growth of *C. graminicola* wild type CgM2 (WT), two *CgUbc8* knock-out strains (*cgubc8/1.1* and *cgubc8/7.1*) and AT263 insertion mutant strain on OMA medium without glucose (left side) and with 2% glucose (right side). Representative plates, 6 days after plate inoculation, are shown.

This observation suggests that CgUbc8 might be not the only player in the repression of glucose sensing, as the loss of encoded protein had a weaker effect on conidiation compared to influence of external glucose supplementation. Moreover, CgUbc8 might support pathogenesis by regulating the expression of virulence-associated genes via carbon de-repression. In developing conidia, potential target genes might be involved in the synthesis of storage compounds (Wilson et al., 2010), while in germinating conidia and developing appressoria genes controlling the catabolism of storage compounds, e.g. glycogen mobilisation, might be targeted. There is evidence that during the appressoria penetration, genes coding for cell wall degrading enzymes (CWDEs) are regulated by CCR. Such control was observed in *M. oryzae* and in maize pathogen *Cocchliobolus carbonum*, where SNF1 homologue up-regulated expression of CWDEs genes by allowing for release from CCR. *SNF1* mutant strains of both species exhibited impaired development and pathogenicity (reviewed in Fernandez et al., 2014).

However, there is too less experimental evidence in support of the proposed hypothetical role of CgUbc8 in glucose sensing and regulation of CCR. No reduced conidiation was observed upon loss of CgUbc8, as it was observed for mycelium grown on glucose-supplemented medium. Furthermore, down-regulation of isocitrate lyase activity, which seems to be a CCR-target also in *C. graminicola*, was observed only in one of two *CgUbc8* knock-out strains, but also in ATMT mutant, compared to wild type CgM2 when grown on medium without glucose supplementation. However, a clear effect on the pathogenicity indicates that CgUbc8 is a compatibility factor in *C. graminicola* - maize interaction and it can be hypothesised that ubiquitination of CgUbc8-target proteins might play an important role for development of pre-penetration infection structures of this fungus.

REFERENCES

Abbasi AR, Saur A, Hennig P, Tschiersch H, Hajirezaei M, Hofius D, Sonnewald U, Voll LM (2009) Tocopherol deficiency in transgenic tobacco (*Nicotiana tabacum* L.) plants leads to accelerated senescence. Plant Cell and Environment **32:** 144-157

Ahmad S, Veyrat N, Gordon-Weeks R, Zhang Y, Martin J, Smart L, Glauser G, Erb M, Flors V, Frey M, Ton J (2011) Benzoxazinoid metabolites regulate innate immunity against aphids and fungi in maize. Plant Physiology **157**: 317-327

Alfano JR and Collmer A (1996) Bacterial Pathogens in Plants: Life up against the Wall. The Plant Cell **8**: 1683-1698

Almagro L, Gómez Ros LV, Belchi-Navarro S, Bru R, Ros Barceló A, Pedreño MA (2009) Class III peroxidases in plant defence reactions. Journal of Experimental Botany **60:** 377-390

Aparna G, Chatterjee A, Sonti RV, Sankaranarayanan R (2009) A cell wall-degrading esterase of Xanthomonas oryzae requires a unique substrate recognition module for pathogenesis on rice. The Plant Cell **21**: 1860-1873

Apel K, Hirt H (2004) Reactive oxygen species: metabolism, oxidative stress, and signal transduction. Annual Review of Plant Biology **55**: 373–399

Badaruddin M, Holcombe LJ, Wilson RA, Wang ZY, Kershaw MJ, Talbot NJ (2013) Glycogen metabolic genes are involved in trehalose-6-phosphate synthase-mediated regulation of pathogenicity by the rice blast fungus *Magnaporthe oryzae*. PLoS Pathogens **9:** e1003604

Bailey TL and Elkan C (1994) Fitting a mixture model by expectation maximization to discover motifs in biopolymers. Proceedings of the Second International Conference on Intelligent Systems for Molecular Biology, AAAI Press, Menlo Park, California, pp. 28-36

Balmer D, Planchamp C, Mauch-Mani B (2012) On the move: induced resistance in monocots. Journal of Experimental Botany doi: 10.1093/jxb/ers248

Beck M, Heard W, Mbengue M, Robatzek S (2012) The INs and OUTs of pattern recognition receptors at the cell surface. Current Opinion in Plant Biology **15**: 367–374

Beckerman JL, Ebbole DJ (1996) *MPG1*, a gene encoding a fungal hydrophobin of *Magnaporthe grisea*, is involved in surface recognition. Molecular Plant–Microbe Interactions **9**: 450-456

Benhamou N, Grenier J, Chrispeels MJ (1991) Accumulation of beta-fructosidase in the cell walls of tomato roots following infection by a fungal wilt pathogen. Plant Physiology **97**: 739–750

Berger S, Sinha AK, Roitsch T (2007) Plant physiology meets phytopathology: plant primary metabolism and plant-pathogen interactions. Journal of Experimental Botany **58**: 4019-4026

Berger S, Papadopoulos M, Schreiber U, Kaiser W, Roitsch T (2004) Complex regulation of gene expression, photosynthesis and sugar levels by pathogen infection in tomato. Physiologia Plantarum **122:** 419-428

Bergmeyer HU (1972) Methoden der enzymatischen Analyse, Ed 2. Verlag Chemie Weinheim, Weinheim

Bergstrom GC and Nicholson RL (1999) The biology of corn anthracnose. Plant Disease **83**: 596-608

Biemelt S and Sonnewald, U (2006) Plant–microbe interactions to probe regulation of plant carbon metabolism. Journal of plant physiology **163:** 307-318

Bilger W and Björkman O (1990) Role of the xanthophyll cycle in photoprotection elucidated by measurements of light-induced absorbance changes, fluorescence and photosynthesis in leaves of *Hedera canariensis*. Photosynthesis research **25:** 173-185

Block A, Toruño TY, Elowsky CG, Zhang C, Steinbrenner J, Beynon J, Alfano JR (2014) The Pseudomonas syringae type III effector HopD1 suppresses effector-triggered immunity, localizes to the endoplasmic reticulum, and targets the Arabidopsis transcription factor NTL9. New Phytologist **201**: 1358–1370

Blume B, Nürnberger T, Nass N, Scheel D (2000) Receptor-mediated increase in cytoplasmic free calcium required for activation of pathogen defense in parsley. Plant Cell **12**: 1425–1440

Bolton MD (2009) Primary metabolism and plant defence – fuel for the fire. Molecular Plant-Microbe Interactions **22**: 487-497

Bolton MD, Kolmer JA, Xu WW, Garvin DF (2008) *Lr34*-mediated leaf rust resistance in wheat: transcript profiling reveals a high energetic demand supported by transient recruitment of multiple metabolic pathways. Molecular Plant-Microbe Interactions **21**:1515-1527

Bonfig KB, Schreiber U, Gabler A, Roitsch T, Berger S (2006) Infection with virulent and avirulent *P. syringae* strains differentially affects photosynthesis and sink metabolism in Arabidopsis leaves. Planta **225**: 1–12

Both M, Csukai M, Stumpf MP, Spanu PD (2005) Gene expression profiles of Blumeria graminis indicate dynamic changes to primary metabolism during development of an obligate biotrophic pathogen. The Plant Cell **17:** 2107-2122

Bowyer P, Mueller E, Lucas J (2000) Use of an isocitrate lyase promoter – GFP fusion to monitor carbon metabolism of the plant pathogen *Tapesia yallundae* during infection of wheat. Molecular Plant Pathology **1**: 253–262

Bradley D, Kjellbom P, Lamb C (1992) Elicitor- and wound-induced oxidative cross-linking of a proline-rich plant cell wall protein: a novel, rapid defense response. Cell **70**: 21–30

Briggs SP and Johal GS (1994) Genetic patterns of plant host-parasite interactions. Trends in Genetics **10**: 12-16

Brutus A, Sicilia F, Macone A, Cervone F, De Lorenzo G (2010) A domain swap approach reveals a role of the plant wall-associated kinase 1 (WAK1) as a receptor of oligogalacturonides. Proceedings of the National Academy of Sciences USA **107**: 9452-9457

Bu Q, Jiang H, Li CB, Zhai Q, Zhang J, Wu X, Sun J, Xie Q, Li C (2008) Role of the *Arabidopsis thaliana* NAC transcription factors ANAC019 and ANAC055 in regulating jasmonic acid-signaled defense responses. Cell Research **18**:756–767

Chen C and Chen Z (2002) Potentiation of developmentally regulated plant defence response by AtWRKY18, a pathogen-induced *Arabidopsis* transcription factor. Plant Physiology **129**: 706-716

Chinchilla D, Bauer Z, Regenass M, Boller T, Felix G (2006) The *Arabidopsis* Receptor Kinase FLS2 Binds flg22 and Determines the Specificity of Flagellin Perception. The Plant Cell 18: 465-476

Chomczynski P and Sacchi N (1987) Single-step method of RNA isolation by acid guanidinium thiocyanate-phenol-chloroform extraction. Analytical Biochemistry **162**: 156-159

Chou HM, Bundock N, Rolfe SA, Scholes JD (2000) Infection of *Arabidopsis thaliana* leaves with *Albugo candida* (white blister rust) causes a reprogramming of host metabolism. Molecular Plant Pathology **1**: 99-113

Clarke YD, Liu Y, Klessig DF, Dong X (1998) Uncoupling PR gene expression from NPR1 and bacterial resistance - characterisation of the dominant Arabidopsis *cpr6-1* mutant. The Plant Cell **10**: 557-569

Cohen SA, Michaud DP (1993) Synthesis of a fluorescent derivatizing reagent, 6-aminoquinolyl-n-hydroxysuccinimidyl carbamate, and its application for the analysis of hydrolysate amino-acids via high-performance liquid-chromatography. Analytical Biochemistry **211:** 279-287

Corral-Ramos C and Roncero MIG (2015) Glycogen catabolism, but not its biosynthesis, affects virulence of *Fusarium oxysporum* on the plant host. Fungal Genetics and Biology **77**: 40-49

Covert SF, Kapoor P, Lee M, Briley A, Nairn CJ (2001) *Agrobacterium tumefaciens*-mediated transformation of *Fusarium circinatum*. Mycological Research **105**: 259–264

Cupertino FB, Virgilio S, Freitas FZ, de Souza Candido T, Bertolini MC (2015) Regulation of glycogen metabolism by the CRE-1, RCO-1 and RCM-1 proteins in

Neurospora crassa. The role of CRE-1 as the central transcriptional regulator. Fungal Genetics and Biology **77:** 82-94

Cvetkovska M and Vanlerberghe GC (2013) Alternative oxidase impacts the plant response to biotic stress by influencing the mitochondrial generation of reactive oxygen species. Plant, cell & environment **36:** 721-732

Cvetkovska M and Vanlerberghe GC (2012) Coordination of a mitochondrial superoxide burst during the hypersensitive response to bacterial pathogen in *Nicotiana tabacum*. Plant, cell & environment **35:** 1121-1136

Dangl JL and Jones JD (2001) Plant pathogens and integrated defence responses to infection. Nature **411**: 826-33

de Hoon MJL, Imoto S, Nolan J, Miyano S (2004) Open source clustering software. Bioinformatics **20:** 1453-1454

de Jong JC, McCormack BJ, Smirnoff N, Talbot NJ (1997) Glycerol generates turgor in rice blast. Nature **389:** 244–245

de León IP, Hamberg M, Castresana C (2015) Oxylipins in moss development and defense. Frontiers in Plant Science doi: 10.3389/fpls.2015.00483

de León IP, Schmelz EA, Gaggero C, Castro A, Álvarez A, Montesano M (2012) *Physcomitrella patens* activates reinforcement of the cell wall, programmed cell death and accumulation of evolutionary conserved defence signals, such as salicylic acid and 12-oxo-phytodienoic acid, but not jasmonic acid, upon *Botrytis cinerea* infection. Molecular Plant Pathology **13**: 960–974

Deising HB, Werner S, Wernitz M (2000) The role of fungal appressoria in plant infection. Microbes and Infection **2:** 1631−1641

Delessert C, Kazan K, Wilson IW, Straeten DVD, Manners J, Dennis ES, Dolferus R (2005) The transcription factor ATAF2 represses the expression of pathogenesis-related genes in Arabidopsis. The Plant Journal **43:** 745-757

Desikan R, Hancock JT, Bright J, Harrison J, Weir I, Hooley R, Neill SJ (2005) A role for ETR1 in hydrogen peroxide signaling in stomatal guard cells. Plant Physiology **137**: 831–834

Desikan R, Cheung MK, Bright J, Henson D, Hancock JT, Neill SJ (2004) ABA, hydrogen peroxide and nitric oxide signalling in stomatal guard cells. Journal of Experimental Botany **55**: 205–212

De Vit MJ, Waddle J, Johnston M (1997) Regulated nuclear translocation of the Mig1 glucose repressor. Molecular biology of the cell **8:** 1603-1618

DeZwaan TM, Carroll AM, Valent B, Sweigard JA (1999) *Magnaporthe grisea* pth11p is a novel plasma membrane protein that mediates appressorium differentiation in response to inductive substrate cues. The Plant Cell **11**: 2013-2030

Dietrich RA, Delaney TP, Uknes SJ, Ward ER, Ryals JA, Dangl JL (1994) Arabidopsis Mutant Simulating Disease Resistance Response. Cell **77**: 565-577

Divon HH and Fluhr R (2007) Nutrition acquisition strategies during fungal infection of plants. FEMS Microbiology Letters **266**: 65-74

Dixon RA (2001) Natural products and plant disease resistance. Nature **411**: 843-847

Donaldson RP, Karyotou K, Assadi M, Olcum T (2001) Peroxisomes and glyoxysomes in plants. Encyclopedia of Life Sciences. Internet publication of Nature/McMillan Press. www.naturereference.com/els

Draper J (1997) Salicylate, superoxide synthesis and cell suicide in plant defence. Trends in Plant Science **2**: 162–165

Drummond AJ, Ashton B, Buxton S, Cheung M, Cooper A, Duran C, Field M, Heled J, Kearse M, Markowitz S, Moir R, Stones-Havas S, Sturrock S, Thierer T, Wilson A (2011) Geneious v5.4, Available from *http://www.geneious.com/*

Dufresne M, Perfect S, Pellier AL, Bailey JA, Langin T (2000) A GAL4-like protein is involved in the switch between biotrophic and necrotrophic phases of the infection process of *Colletotrichum lindemuthianum* on common bean. The Plant Cell **12**: 1579–1589

Eichhorn H, Lessing F, Winterberg B, Schirawski J, Kamper J, Muller P, Kahmann R (2006) A ferroxidation/permeation iron uptake system is required for virulence in *Ustilago maydis*. Plant Cell **18:** 3332-3345

Epstein L, Lusnak K, Kaur S (1998) Transformation-mediated developmental mutants of *Glomerella graminicola*. Fungal Genetics and Biology **23**: 189–203

Eulgem T, Rushton PJ, Robatzek S, Somssich IE (2000) The WRKY superfamily of plant transcription factors. Trends in Plant Science **5**: 199-206

Fan K, Wang M, Miao Y, Ni M, Bibi N, Yuan S, Li F, Wang X (2014) Molecular Evolution and Expansion Analysis of the NAC Transcription Factor in *Zea mays*. PLOS ONE doi: 10.1371/journal.pone.0111837

Fang Y, You J, Xie K, Xie W, Xiong L (2008) Systematic sequence analysis and identification of tissue-specific or stress-responsive genes of NAC transcription factor family in rice. Molecular Genetics and Genomics **280**: 547–563

Fernandez J, Marroquin-Guzman M, Wilson RA (2014) Mechanisms of nutrient acquisition and utilisation during fungal infections of leaves. Annual review of phytopathology **52**: 55-174

Fernandez J, Wright JD, Hartline D, Quispe CF, Madayiputhiya N, Wilson RA (2012) Principles of carbon catabolite repression in the rice blast fungus: Tps1, Nmr1-3, and a MATE–Family Pump regulate glucose metabolism during Infection. PLoS Genet **8:** e1002673

Fotopoulos V, Gilbert MJ, Pittman JK, Marvier AC, Buchanan AJ, Sauer N, Hall JL, Williams LE (2003) The monosaccharide transporter gene, AtSTP4, and the cell-wall invertase, Atbetafruct1, are induced in Arabidopsis during infection with the fungal biotroph *Erysiphe cichoracearum*. Plant Physiology **132**: 821–829

Freeman J and Ward E (2004) *Gaeumannomyces graminis*, the take-all fungus and its relatives. Molecular Plant Pathology **5**: 235-252

Gancedo JM (1998) Yeast carbon catabolite repression. Microbiology and Molecular Biology Reviews **62:** 334-361

Genty B, Briantais, JM, Baker, NR (1989) The relationship between the quantum yield of photosynthetic electron transport and quenching of chlorophyll fluorescence. Biochimica et Biophysica Acta (BBA)-General Subjects **990:** 87-92

Gibon Y, Bläsing OE, Palacios-Rojas N, Pankovic D, Hendriks JH, Fisahn J, Höhne M, Günther M, Stitt M (2004) Adjustment of diurnal starch turnover to short days: depletion of sugar during the night leads to a temporary inhibition of carbohydrate utilisation, accumulation of sugars and post-translational activation of ADP-glucose pyrophosphorylase in the following light period. The Plant Journal **39:** 847-862

Giraud E., Ho LH, Clifton R, Carroll A, Estavillo G, Tan YF, Howell KA, Ivanova A, Pogson BJ, Millar AH, Whelan J (2008) The absence of ALTERNATIVE OXIDASE1a in Arabidopsis results in acute sensitivity to combined light and drought stress. Plant Physiology **147:** 595-610

Greenwald CJ, Kasuga T, Glass NL, Shaw BD, Ebbole DJ, Wilkinson HH (2010) Temporal and spatial regulation of gene expression during asexual development of *Neurospora crassa*. Genetics **186**: 1217-1230

Gunja-Smith Z, Patil NB, Smith EE (1977) Two pools of glycogen in Saccharomyces. Journal of Bacteriology **130**: 818-825

Gupta A and Chattoo BB (2007) A novel gene MGA1 is required for appressorium formation in *Magnaporthe grisea*. Fungal Genetics and Biology **44:** 1157-1169

He P, Chintamanani S, Chen Z, Zhu L, Kunkel BN, Alfano JR, Tang X, Zhou JM (2004) Activation of a COI1-dependent pathway in Arabidopsis by *Pseudomonas syringae* type III effectors and coronatine. The Plant Journal **37:** 589–602

He P, Warren RF, Zhao T, Shan L, Zhu L, Tang, Zhou JM (2001) Overexpression of *Pti5* in tomato potentiates pathogen-induced defense gene expression and enhances disease resistance to *Pseudomonas syringae* pv. tomato. Molecular Plant-Microbe Interactactions **14:** 1453–1457

Herbers K, Takahata Y, Melzer M, Mock HP, Hajirezaei M, Sonnewald U (2000) Regulation of carbohydrate partitioning during the interaction of potato virus Y with tobacco. Molecular Plant Pathology **1**: 51–59

Herbers K, Meuwly P, Frommer W B, Metraux JP and Sonnewald U (1996) Systemic acquired resistance mediated by the ectopic expression of invertase: possible hexose sensing in the secretory pathway. The Plant Cell **8:** 793-803

Hicks J, Lockington RA, Strauss J, Dieringer D, Kubicek CP, Kelly J, Keller N (2001) RcoA has pleiotropic effects on *Aspergillus nidulans* cellular development. Molecular microbiology **39:** 1482-1493

Hoi JWS, Herbert C, Bacha N, O'Connell R, Lafitte C, Borderies G, **Rossignol M, Rougé P, Dumas B** (2007) Regulation and role of a STE12-like transcription factor from the plant pathogen *Colletotrichum lindemuthianum.* Molecular Microbiology **64**: 68-82

Horbach R, Graf A, Weihmann F, Antelo L, Mathea S, Liermann JC, Opatz T, Thines E, Aguirre J, Deising HB (2009) Sfp-Type 4'-Phosphopantetheinyl Transferase Is Indispensable for Fungal Pathogenicity. The Plant Cell **21**: 3379-3396

Horst RJ, Engelsdorf T, Sonnewald U, Voll LM (2008) Infection of maize leaves with *Ustilago maydis* prevents establishment of C_4 photosynthesis. Journal of Plant Physiology **165:** 19-28

Howard RJ, Ferrari MA, Roach DH, Money NP (1991) Penetration of hard substances by a fungus employing enormous turgor pressures. Proceedings of the National Academy of Sciences of the USA **88:** 11281–11284

Huffaker A, Dafoe NJ, Schmelz EA (2011) ZmPep1, an ortholog of Arabidopsis elicitor peptide 1, regulates maize innate immunity and enhances disease resistance. Plant Physiology **155**: 1325-38

Hwang CH, Flaishman MA, Kolattukudy PE (1995) Cloning of a gene expressed during appressorium formation by *Colletotrichum gloeosporioides* and a marked decrease in virulence by disruption of this gene. The Plant Cell **7:** 183–193

Hwang CH and Kolattukudy PE (1995) Isolation and characterisation of genes expressed uniquely during appressorium formation by *Colletotrichum gloeosporioides* conidia induced by the host surface wax. Molecular and General Genetics **247:** 282–294

Idnurm A and Howlett BJ (2002) Isocitrate lyase is essential for pathogenicity of the fungus *Leptosphaeria maculans* to canola (*Brassica napus*). Eukaryotic Cell **1**: 719–724

Jakoby M, Weisshaar B, Dröge-Laser W, Vicente-Carbajosa J, Tiedemann J, Kroj T, Parcy F; bZIP Research Group (2002) bZIP transcription factors in Arabidopsis. Trends in Plant Science **7**: 106–111

Jensen MK, Hagedorn PH, de Torres-Zabala M, Grant MR, Rung JH, CollingeDB, Ryngkjaer MF (2008) Transcriptional regulation by an NAC (NAM-ATAF1,2-CUC2) transcription factor attenuates ABA signalling for efficient basal defence towards *Blumeria graminis* f. sp *hordei* in Arabidopsis. The Plant Journal **56**: 867–880

Jensen MK, Rung JH, Gregersen PL, Gjetting T, Fuglsang AT, Hansen M, Joehnk N, Lyngkjaer MF, Collinge DB (2007) The HvNAC6 transcription factor: a positive regulator of penetration resistance in barley and Arabidopsis. Plant Molecular Biology **65**: 137–150

Jobic C, Boisson AM, Gout E, Rascle C, Fèvre M, Cotton P, Bligny R (2007) Metabolic processes and carbon nutrient exchanges between host and pathogen sustain the disease development during sunflower infection by *Sclerotinia sclerotiorum*. Planta **226**: 251-265

Johnson ES and Blobel G (1997) Ubc9p is the conjugating enzyme for the ubiquitin-like protein Smt3p. Journal of Biological Chemistry **272:** 26799-26802

Jones JD and Dangl JL (2006) The plant immune system. Nature **444**: 323-329

Kangasjärvi S, Neukermans J, Li S, Aro EM, Noctor G (2012) Photosynthesis, photorespiration, and light signalling in defence responses. Journal of Experimental Botany doi: 10.1093/jxb/err402

Kariola T, Brader G, Li J, Palva ET (2005) Chlorophyllase 1, a damage control enzyme, affects the balance between defense pathways in plants. The Plant Cell **17**: 282–294

Karpova OV, Kuzmin EV, Elthon TE, Newton KJ (2002) Differential expression of alternative oxidase genes in maize mitochondrial mutants. The Plant Cell **14:** 3271-3284

Katagiri F (2004) A global view of defense gene expression regulation – a highly interconnected signaling network. Current Opinion in Plant Biology **7**: 506-511

Kjaersgaard T, Jensen MK, Christiansen MW, Gregersen P, Kragelund BB, Skriver K (2011) Senescence-associated Barley NAC (NAM, ATAF1,2, CUC) Transcription Factor Interacts with Radical-induced Cell Death 1 through a Disordered Regulatory Domain. The Journal of Biological Chemistry **286**: 35418–35429

Kocal N, Sonnewald U, Sonnewald S (2008) Cell Wall-Bound Invertase Limits Sucrose Export and Is Involved in Symptom Development and Inhibition of Photosynthesis during Compatible Interaction between Tomato and *Xanthomonas campestris* pv *vesicatoria*. Plant Physiology **148:** 1523-1536

Koeck M, Hardham AR, Dodds PN (2011) The role of effectors of biotrophic and hemibiotrophic fungi in infection. Cellular Microbiology **13**: 1849-1857

Korn M, Schmidpeter J, Dahl M, Müller S, Voll LM, Koch C (2015) A genetic screen for pathogenicity genes in the hemibiotrophic fungus *Colletotrichum higginsianum* identifies the plasma membrane proton pump Pma2 required for host penetration. PloS one **10:** e0125960

Kuzniak E and Sklodowska M (2005) Fungal pathogen-induced changes in the antioxidant systems of leaf peroxisomes from infected tomato plants. Planta **222**: 192–200

Lamb C and Dixon RA (1997) The oxidative burst in plant burst in plant disease resistance. Annual Review of Plant Physiology and Plant Molecular Biology **48**: 251-275

Law MY, Charles SA, Halliwell B (1983) Glutathione and ascorbic acid in spinach (*Spinacia oleracea*) chloroplasts - the effect of hydrogen peroxide and of paraquat. Biochemical Journal **210:** 899-903

Lee K and Ebbole DJ (1998) Tissue-Specific Repression of Starvation and Stress Responses of the *Neurospora crassa* con-10 Gene Is Mediated by RCO1. Fungal Genetics and Biology **23:** 269-278

Le Hénanff G, Profizi C, Courteaux B, Rabenoelina F, Gérard C, Clément C, Baillieul F, Cordelier S, Dhondt-Cordelier S (2013) Grapevine NAC1 transcription factor as a convergent node in developmental processes, abiotic stresses, and necrotrophic/biotrophic pathogen tolerance. Journal of Experimental Botany **64**: 4877-4893

Levine A, Tenhaken R, Dixon R, Lamb CJ (1994) H_2O_2 from the oxidative burst orchestrates the plant hypersensitive disease resistance response. Cell **79**: 583–593

Li J, Brader G, Palva ET (2004) TheWRKY70 transcription factor: a node of convergence for jasmonate-mediated and salicylate-mediated signals in plant defense. The Plant Cell **16**: 319–331

Liao YWK, Shi K, Fu LJ, Zhang S, Li X, Dong DK, Jiang YP, Zhou YH, Xia XJ, Liang WS, Yu JQ (2012) The reduction of reactive oxygen species formation by mitochondrial alternative respiration in tomato basal defense against TMV infection. Planta **235:** 225-238

Lingner U, Münch S, Deising HB, Sauer N (2011) Hexose transporters of a hemibiotrophic plant pathogen: functional variations and regulatory differences at different stages of infection. The Journal of Biological Chemistry **286**: 20913-22

Ludwig N, Löhrer M, Hempel M, Mathea S, Schliebner I, Menzel M, Kiesow A, Schaffrath U, Deising HB, Horbach R (2014) Melanin is not required for turgor generation but enhances cell-wall rigidity in appressoria of the corn pathogen *Colletotrichum graminicola* Molecular Plant-Microbe Interactions **27:** 315-327

Maleck K, Levine A, Eulgem T, Morgan A, Schmid J, Lawton KA, Dangl JL, Dietrich RA (2000) The transcriptome of *Arabidopsis thaliana* during systemic acquired resistance. Nature Genetics **26**: 403-410

Mendgen K and Hahn M (2002) Plant infection and the establishment of fungal biotrophy. Trends in Plant Science **7**: 352-356

Mittler R, Vanderauwera S, Gollery M, Van Breusegem F (2004) Reactive oxygen gene network of plants. Trends in Plant Science **9**: 490-498

Mittler R, Herr EH, Orvar BL, van CampW, Wilikens H, Inze D, Ellis BE (1999) Transgenic tobacco plants with reduced capability to detoxify reactive oxygen intermediates are hyperresponsive to pathogen infection. Proceedings of the National Academy of Sciences USA **96**: 14165–14170

Miya A, Albert P, Shinya T, Desaki Y, Ichimura K, Shirasu K, Narusaka Y, Kawakami N, Kaku H, Shibuya N (2007) CERK1, a LysM receptor kinase, is essential for chitin elicitor signaling in Arabidopsis. Proceedings of the National Academy of Sciences USA **104**: 19613–19618

Moore JW, Loake GJ, Spoel SH (2011) Transcription dynamics in plant immunity. The Plant Cell **23**: 2809-2820

Morel J, Fromentin J, Blein JP, Simon-Plas F, Elmayan T (2004) Rac regulation of NtrbohD, the oxidase responsible for the oxidative burst in elicited tobacco cell. The Plant Journal **37**: 282–293

Mullins ED, Chen X, Romaine P, Raina R, Geiser DM, Kang S (2001) Agrobacterium-mediated transformation of *Fusarium oxysporum*: an efficient tool for insertion mutagenesis and gene transfer. Phytopathology **91**: 173–80

Murray DC and Walters DR (1992) Increased photosynthesis and resistance to rust infection in upper, uninfected leaves of rusted broad bean (*Vicia faba* L.). New Phytologist **120**: 235-242

Münch S, Ludwig N, Floss DS, Sugui JA, Koszucka AM, Voll LM, Sonnewald U, Deising HB (2011) Identification of virulence genes in the corn pathogen *Colletotrichum graminicola* by *Agrobacterium tumefaciens*-mediated transformation. Molecular Plant Pathology **12**: 43-55

Münch S, Lingner U, Floss DS, Ludwig N, Sauer N, Deising HB (2007) The hemibiotrophic lifestyle of *Colletotrichum* species. Journal of Plant Physiology **165**: 41-51

Nakashima K, Tran LSP, Van Nguyen D, Fujita M, Maruyama K, Todaka D, Ito Y, Hayashi N, Shinozaki K, Yamaguchi-Shinozaki K (2007) Functional analysis of a NAC-type transcription factor OsNAC6 involved in abiotic and biotic stress-responsive gene expression in rice. The Plant Journal **51:** 617-630

Nasser W, de Tapia M, Kauffmann S, Montasser-Kouhsari S, Burkard G (1988) Identification and characterisation of maize pathogenesis-related proteins. Four maize PR proteins are chitinases. Plant Molecular Biology **11**: 529-538

Navarre DA, Wolpert TJ (1995) Inhibition of the glycine decarboxylase multienzyme complex by the host-selective toxin victorin. The Plant Cell **7:** 463-471

Neves MJ, Jorge JA, François JM, Terenzi HF (1991) Effects of heat shock on the level of trehalose and glycogen, and on the induction of thermotolerance in *Neurospora crassa*. FEBS letters **283:** 19-22

Nürnberger T and Lipka V (2005) Non-host resistance in plants: new insights into an old phenomenon. Molecular Plant Pathology **6**: 335-345

O'Conell RJ et al. (2012) Lifestyle transitions in plant pathogenic *Colletotrichum* fungi deciphered by genome and transcriptome analyses. Nature Genetics **44**: 1060-1065

Okinaka Y, Yang CH, Herman E, Kinney A, Keen NT (2002) The P34 syringolide elicitor receptor interacts with a soybean photorespiration enzyme, NADH-dependent hydroxypyruvate reductase. Molecular plant-microbe interactions **15:** 1213-1218

Oliver RP and Ipcho SV (2004) Arabidopsis pathology breathes new life into the necrotrophs-vs.-biotrophs classification of fungal pathogens. Molecular Plant Pathology **5**: 347-352

Olsen AN, Ernst HA, Leggio LL,Skriver K (2005) DNA-binding specificity and molecular functions of NAC transcription factors. Plant Science **169**: 785-797

Ono E, Wong HL, Kawasaki T, Hasegawa M, Kodama O, Shimamoto K (2001) Essential role of the small GTPase Rac in disease resistance of rice. Proceedings of the National Academy of Sciences USA **98**: 759–764

Ooka H, Satoh K, Doi K, Nagata T, Otomo Y, Murakami K, Matsubara K, Osato N, Kawai J, Carninci P, Hayashizaki Y, Suzuki K, Kojima K, Takahara Y, Yamamoto K, Kikuchi S (2003) Comprehensive Analysis of NAC Family Genes in Oryza sativa and Arabidopsis thaliana. DNA Research **10**: 239–247

Page RDM (2002) UNIT 6.2 Visualizing Phylogenetic Trees Using TreeView. Published Online: DOI: 10.1002/0471250953.bi0602s01

Parker D, Beckmann M, Zubair H, Enot DP, Caracuel-Rios Z, Overy DP, Snowdon S, Talbot NJ, Draper J (2009) Metabolomic analysis reveals a common pattern of metabolic re-programming during invasion of three host plant species by *Magnaporthe grisea.* The Plant Journal 59: 723-737

Peberdy JF (1979) Fungal protoplasts: isolation, reversion and fusion. Annual Review of Microbiology **33**: 21-39

Pego JV, Kortstee AJ, Huijser C, Smeekens SC (2000) Photosynthesis, sugars and the regulation of gene expression. Journal of Experimental Botany **51**: 407–416

Perfect SE and Green JR (2001) Infection structures of biotrophic and hemibiotrophic fungal plant pathogens. Molecular Plant Pathology **2**: 101-108

Perpetua NS, Kubo Y, Yasuda N, Takano Y, Furusawa I (1996) Cloning and characterisation of a melanin biosynthetic THR1 reductase gene essential for appressorial penetration of *Colletotrichum lagenarium*. Molecular Plant-Microbe Interactions **9**: 323-329

Petersen M, Brodersen P, Naested H, Andreasson E, Lindhart U, Johansen B, Nielsen HB, Lacy M, Austin MJ, Parker JE, Sharma SB, Klessig DF, Martienssen R, Mattsson O, Jensen AB, Mundy J (2000) *Arabidopsis* MAP Kinase 4 Negatively Regulates Systemic Acquired Resistance. Cell **103:** 1111-1120

Popov VN, Simonian RA, Skulachev VP, Starkov AA (1997) Inhibition of the alternative oxidase stimulates H2O2 production in plant mitochondria. FEBS Letters **415**: 87-90

Quirino BF, Noh YS, Himelblau E, Amasino, RM (2000) Molecular aspects of leaf senescence. Trends in Plant Science **5:** 278-282

Rasmusson AG, Fernie AR, Van Dongen JT (2009) Alternative oxidase: a defence against metabolic fluctuations? Physiologia plantarum **137**: 371-382

Reddan JR, Giblin FJ, Sevilla M, Padgaonkar V, Dziedzic DC, Leverenz VR, Misra IC, Chang JS, Pena JT (2003) Propyl gallate is a superoxide dismutase mimic and protects cultured lens epithelial cells from H_2O_2 insult. Experimental Eye Research **76**: 49-59

Rhoads DM and Subbaiah CC (2007) Mitochondrial retrograde regulation in plants. Mitochondrion **7:** 177-194

Rivas S and Thomas CM (2005) Molecular interactions between tomato and the leaf mold pathogen *Cladosporium fulvum*. Annual Review of Phytopathology **43:** 395–436

Robatzek S and Somssich IE (2002) Targets of AtWRKY6 regulation during plant senescence and pathogen defense. Genes & Development **16**: 1139-1149

Rochon A, Boyle P, Wignes T, Fobert PR (2006) The Coactivator function of Arabidopsis NPR1 requires the core of its BTB/POZ domain and the oxidation of C-terminal cysteines. The Plant Cell **18**: 3670–3685

Roitsch T, Balibrea ME, Hofmann M, Proels R, Sinha AK (2003) Extracellular invertase: key metabolic enzyme and PR protein. Journal of Experimental Botany **54**: 513–524

Rojas CM, Senthil-Kumar M, Wang K, Ryu CM, Kaundal A, Mysore KS (2012) Glycolate oxidase modulates reactive oxygen species–mediated signal transduction during nonhost resistance in *Nicotiana benthamiana* and *Arabidopsis*. The Plant Cell **24:** 336-352

Ronne H (1995) Glucose repression in fungi. Trends in Genetics **11**: 12-17

Römer P, Hahn S, Jordan T, Strauß T, Bonas U, Lahaye T (2007) Plant Pathogen Recognition Mediated by Promoter Activation of the Pepper *Bs3* Resistance Gene. Science **318:** 645-648

Sambrook J, Fritsch EF, Maniatis T (1989) Molecular Cloning: A Laboratory Manual, Ed 2. Cold Spring Harbor Laboratory Press, Cold Spring Harbor, NY

Sana TR, Fischer S, Wohlgemuth G, Katrekar A, Jung KH, Ronald PC, Fiehn O (2010) Metabolomic and transcriptomic analysis of the rice response to the bacterial blight pathogen *Xanthomonas oryzae* pv. *oryzae*. Metabolomics **6:** 451-465

Sandrock RW and Vanetten, HD (2001) The relevance of tomatinase activity in pathogens of tomato: disruption ofthe beta(2)-tomatinase gene in *Colletotrichum coccodes* and *Septoria lycopersici* and heterologous expression of the *Septoria lycopersici* beta(2)-tomatinase in *Nectria haematococca*, a pathogen of tomato fruit. Physiological and Molecular Plant Pathology **4**: 159 – 171

Scharte J, Schön H, Weis E (2005) Photosynthesis and carbohydrate metabolism in tobacco leaves during an incompatible interaction with *Phytophthora nicotianae*. Plant, Cell and Environment **28**: 1421–1435

Schnable PS et al. (2009) The B73 maize genome: complexity, diversity, and dynamics. Science **326:** 1112-1115

Scholes J and Rolfe SA (1996) Photosynthesis in localised regions of oat leaves infected with crown rust (*Puccinia coronata*): quantitative imaging of chlorophyll fluorescence. Planta **199**: 573–582

Scholes JD, Lee PJ, Horton P, Lewis DH (1994) Invertase: understanding changes in the photosynthetic and carbohydrate metabolism of barley leaves infected with powdery mildew. New Phytologist **126**: 213–222

Schüle T, Rose M, Entian KD, Thumm M, Wolf DH (2000) Ubc8 functions in catabolite degradation of fructose-1,6-bisphosphate in yeast. The EMBO Journal **19**: 2161-2167

Shan W, Chen JY, Kuang JF Lu WJ (2015) Banana fruit NAC transcription factor MaNAC5 cooperates with MaWRKYs to enhance the expression of pathogenesis-related genes against *Colletotrichum musae*. *Molecular plant pathology* DOI: 10.1111/mpp.12281

Shen H, Yin Y, Chen F, Xu Y, Dixon, RA (2009) A bioinformatic analysis of *NAC* genes for plant cell wall development in relation to lignocellulosic bioenergy production. BioEnergy Research **2:** 217

Siemens J, González M., Wolf S, Hofmann C, Greiner S, Du Y, Rausch T, Roitsch T, Ludwig-Müller J (2011) Extracellular invertase is involved in the regulation of clubroot disease in Arabidopsis thaliana. Molecular plant pathology **12:** 247-262

Simpson-Lavy KJ and Johnston M (2013) SUMOylation regulates the SNF1 protein kinase. Proceedings of the National Academy of Sciences **110:** 17432-17437

Singh KB, Foley RC, Oñate-Sánchez L (2002) Transcription factors in plant defense and stress responses. Current Opinion in Plant Biology 5: 430–436

Solomon PS, Lee RC, Wilson TJ, Oliver RP (2004) Pathogenicity of *Stagonospora nodorum* requires malatem synthase. Molecular Microbiology **53**: 1065–1073
Spanu PD (2012) The genomics of obligate (and nonobligate) biotrophs. Annual Review of Phytopathogoly 50: 91-109

Somssich I E and Hahlbrock K (1998) Pathogen defence in plants – a paradigm of biological complexity. Trends in Plant Science **3**: 86-90

Sørhagen K, Laxa M, Peterhänsel C, Reumann S (2013) The emerging role of photorespiration and non-photorespiratory peroxisomal metabolism in pathogen defence. Plant biology **15:** 723-736

Spanu PD (2012) The genomics of obligate (and nonobligate) biotrophs. Annual review of phytopathology **50:** 91-109

Srikumar T, Lewicki MC, Raught B (2013) A global S. cerevisiae small ubiquitin-related modifier (SUMO) system interactome. Molecular systems biology **9:** 668

Stephenson SA, Hatfield J, Rusu AG, Maclean DJ, Manners JM (2000) CgDN3: an essential pathogenicity gene of *Colletotrichum gloeosporioides* necessary to avert a hypersensitive-like response in the host *Stylosanthes guianensis*. Molecular Plant–Microbe Interactions **13**: 929-941

Sun J and Glass NL (2011) Identification of the CRE-1 cellulolytic regulon in *Neurospora crassa*. PLoS One **6:** e25654

Swarbrick PJ, Schulze-Lefert P, Scholes JD (2006) Metabolic consequences of susceptibility and resistance in barley leaves challenged with powdery mildew. Plant, Cell and Environment **29**: 1061–1076

Takasaki H, Maruyama K, Kidokoro S, Ito Y, Fujita Y, Shinozaki K, Yamaguchi-Shinozaki K, Nakashima K (2010) The abiotic stress-responsive NAC-type transcription factor OsNAC5 regulates stress-inducible genes and stress tolerance in rice. Molecular Genetics and Genomics **284**:173–183

ten Have A, Mulder W, Visser J, van Kan JA (1998) The endopolygalacturonase gene *Bcpg1* is required for full virulence of *Botrytis cinerea*. Molecular Plant–Microbe Interactions **11**: 1009-1016

Thevelein JM (1984) Regulation of trehalose mobilization in fungi. Microbiological Reviews **48**: 42–59

Thines E, Weber RW, Talbot NJ (2000) MAP kinase and protein kinase A-dependent mobilization of triacylglycerol and glycogen during appressorium turgor generation by *Magnaporthe grisea*. The Plant Cell **12**: 1703–1718

Thomma BP, Penninckx IA, Broekaert WF, Cammue BP (2001) The complexity of disease signalling in Arabidopsis. Current Opinion in Immunology **13**: 63-68

Thompson JD, Higgins DG, Gibson TJ (1994) CLUSTAL W: improving the sensitivity of progressive multiple sequence alignment through sequence weighting, position specific gap penalties and weight matrix choice. Nucleic Acids Research **22**:4673-80

Thon MR, Nuckles EM, Takach JE, Vaillancourt LJ (2002) *CPR1*: a gene encoding a putative signal peptidase that functions in pathogenecity of *Colletotrichum graminicola*. Molecular Plant–Microbe Interactions **15**: 120–128

Tonukari NJ, Scott-Craig JS, Waltonb JD (2000) The *Cochliobolus carbonum* SNF1 gene is required for cell wall–degrading enzyme expression and virulence on maize. The Plant Cell **12:** 237-247

Torres MA, Jones JD, Dangl JL (2006) Reactive oxygen species signaling in response to pathogens. Plant Physiology **141**: 373-378

Torres MA, Dangl JL, Jones JD (2002) Arabidopsis gp91phox homologues AtrbohD and AtrbohF are required for accumulation of reactive oxygen intermediates in the plant defense response. Proceedings of the National Academy of Sciences USA **99**: 517–522

Toyoda K, Collins NC, Takahashi A, Shirasu K (2002) Resistance and susceptibility of plants to fungal pathogens. Transgenic Research **11**: 567-582

Treitel MA and Carlson M (1995) Repression by SSN6-TUP1 is directed by MIG1, a repressor/activator protein. Proceedings of the National Academy of Sciences **92:** 3132-3136

Truman W, Zabala MT, Grant M (2006) Type III effectors orchestrate a complex interplay between transcriptional networks to modify basal defence responses during pathogenesis and resistance. The Plant Journal **46:** 14-33

Umbach AL, Fiorani F, Siedow JN (2005) Characterisation of transformed Arabidopsis with altered alternative oxidase levels and analysis of effects on reactive oxygen species in tissue. Plant Physiology **139**: 1806-1820

Vanlergerghe GC (2013) Alternative oxidase: a mitochondrial respiratory pathway to maintain metabolic and signaling homeostasis during abiotic and biotic stress in plants. International Journal of Molecular Sciences: **14:** 6805-6847

Vanlerberghe GC and Mclntosh L (1996) Signals regulating the expression of the nuclear gene encoding alternative oxidase of plant mitochondria **111**: 589-595

Vargas WA, Martín JMS, Rech GE, Rivera LP, Benito EP, Díaz-Mínguez JM, Thon MR, Sukno SA (2012) Plant defense mechanisms are activated during biotrophic and necrotrophic development of Colletotricum graminicola in maize. Plant Physiology **158:** 1342-1358

Vidal G, Ribas-Carbo M, Garmier M, Dubertret G, Rasmusson AG, Mathieu C, Foyer CH, De Paepe, R (2007) Lack of respiratory chain complex I impairs alternative oxidase engagement and modulates redox signaling during elicitor-induced cell death in tobacco. The Plant Cell **19:** 640-655

Voegele RT, Hahn M, Lohaus G, Link T, Heiser I, Mendgen K (2005) Possible roles for mannitol and mannitol dehydrogenase in the biotrophic plant pathogen *Uromyces fabae*. Plant Physiology **137**: 190–198

Voegele RT, Struck C, Hahn M, Mendgen K (2001) The role of haustoria in sugar supply during infection of broad bean by the rust fungus *Uromyces fabae*. Proceedings of the National Academy of Science **98**: 8133–8138

Vogel F (2009) Molekulare Analyse des Makromolekültransports in Pflanzen anhand eines viralen Transportproteins. Dissertation, Friedrich-Alexander-Universität Erlangen-Nürnberg

Voll LM, Zell MB, Engelsdorf T, Saur A, Wheeler MG, Drincovich MF, Weber AP, Maurino VG (2012) Loss of cytosolic NADP-malic enzyme 2 in *Arabidopsis thaliana* is associated with enhanced susceptibility to *Colletotrichum higginsianum*. New Phytologist **195**: 189-202

Voll LM, Horst RJ, Voitsik AM, Zajic D, Samans B, Pons-Kühnemann J, Doehlemann G, Münch S, Wahl R, Molitor A, Hofmann J, Schmiedl A, Waller F, Deising HB, Kahmann R, Kämper J, Kogel K-H, Sonnewald U (2011) Common motifs in the response of cereal primary metabolism to fungal pathogens are not based on similar transcriptional reprogramming. Frontiers in Plant Science **2011**, 2:39

Wahl R, Wippel K, Goos S, Kämper J, Sauer N (2010) A novel high-affinity sucrose transporter is required for virulence of the plant pathogen *Ustilago maydis*. Public Library of Science Biology **8**: e1000303. doi:10.1371/journal.pbio.1000303

Walton JD (1996) Host-selective toxins: agents of compatibility. The Plant Cell **8**: 1723-1733

Wang XE, Basnayake BVS, Zhang H, Li G, Li W, Virk N, Mengiste T, Song F (2009) The Arabidopsis ATAF1, a NAC transcription factor, is a negative regulator of defense responses against necrotrophic fungal and bacterial pathogens. Molecular Plant-Microbe Interactions **22:** 1227-1238

Wang ZY, Thornton CR, Kershaw MJ, Debao L, Talbot NJ (2003) The glyoxylate cycle is required for temporal regulation of virulence by the plant pathogenic fungus *Magnaporthe grisea*. Molecular Microbiology **47**: 1601–1612

Ward JL, Forcat S, Beckmann M, Bennett M, Miller SJ, Baker JM, Hawkins ND, Vermeer CP, Lu C, Lin W, Truman WM, Beale MH, Draper J, Mansfield JW, Grant M (2010) The metabolic transition during disease following infection of Arabidopsis thaliana by Pseudomonas syringae pv. tomato. The Plant Journal **63:** 443-457

Wei T, Ou B, Li J, Zhao Y, Guo D, Zhu Y, Chen Z, Gu H, Li C, Qin G, Qu LJ (2013) Transcriptional profiling of rice early response to Magnaporthe oryzae identified OsWRKYs as important regulators in rice blast resistance. PloS one **8:** e59720

Werner S, Sugui JA, Steinberg G, Deising HB (2007) A Chitin Synthase with a Myosin-Like Motor Domain Is Essential for Hyphal Growth, Appressorium Differentiation, and Pathogenicity of the Maize Anthracnose Fungus *Colletotrichum graminicola*. Molecular Plant–Microbe Interactions **20**: 1555-1567

Williams B, Kabbage M, Kim HJ, Britt R, Dickman MB (2011) Tipping the balance: *Sclerotinia sclerotiorum* secreted oxalic acid suppresses host defenses by manipulating the host redox environment. Public Library of Science Pathogens. **7:**e1002107

Wilson WA, Roach PJ, Montero M, Baroja-Fernández E, Muñoz FJ, Eydallin G, Viale AM, Pozueta-Romero J (2010) Regulation of glycogen metabolism in yeast and bacteria. FEMS microbiology reviews **34**: 952-985

Wilson RA, Jenkinson JM, Gibson RP, Littlechild JA, Wang ZY, Talbot NJ (2007) Tps1 regulates the pentose phosphate pathway, nitrogen metabolism and fungal virulence. The EMBO Journal **26:** 3673-3685

Wojtaszek P (1997) Oxidative burst : an early plant response to pathogen infection. Biochemical Journal **322**: 681-692

Yakoby N, Beno-Moualem D, Keen NT, Dinoor A, Pines O, Prusky D (2001) *Colletotrichum gloeosporioides pelB* is an important virulence factor in avocado fruit–fungus interaction. Molecular Plant–Microbe Interactions **14**: 988–995

Yamaguchi Y and Huffaker A (2011) Endogenous peptide elicitors in higher plants. Current Opinion in Plant Biology **14**: 351-357

Yamashiro CT, Ebbole DJ, Lee BU, Brown RE, Bourland C, Madi L, Yanofsky C (1996) Characterisation of rco-1 of Neurospora crassa, a pleiotropic gene affecting growth and

development that encodes a homolog of Tup1 of *Saccharomyces cerevisiae*. Molecular and cellular biology **16**: 6218-6228

Yi SY, Kim JH, Joung YH, Lee S, Kim WT, Yu SH, Choi D (2004) The pepper transcription factor CaPF1 confers pathogen and freezing tolerance in Arabidopsis. Plant Physiology **136**: 2862–2874

Yip JY and Vanlerberghe GC (2001) Mitochondrial alternative oxidase acts to dampen the generation of active oxygen species during a period of rapid respiration induced to support a high rate of nutrient uptake. Physiologia Plantarum **112**: 327-333

Yoon H-K, Kim S-G, Kim S-Y, Park C-M (2008) Regulation of Leaf Senescence by NTL9-mediated Osmotic Stress Signaling in Arabidopsis. Molecules and Cells **25**: 438-445

Yoshioka H, Numata N, Nakajima K, Katou S, Kawakita K, Rowland O, Jones JD, Doke N (2003) *Nicotiana benthamiana* gp91phox homologs NbrbohA and NbrbohB participate in H_2O_2 accumulation and resistance to *Phytophthora infestans*. Plant Cell **15**: 706–718

Zhang Y, Tessaro MJ, Lassner M, Li X (2003) Knockout analysis of Arabidopsis transcription factors TGA2, TGA5, and TGA6 reveals their redundant and essential roles in systemic acquired resistance. The Plant Cell 1**5:** 2647-2653

Zhang Y, Fan W, Kinkema M, Li X, Dong X (1999) Interaction of NPR1 with basic leucine zipper protein transcription factors that bind sequences required for salicylic acid induction of the *PR-1* gene. Proceedings of the National Academy of Sciences USA **96**: 6523–6528

Zhou JM, Trifa Y, Silva H, Pontier D, Lam E, Shah J, Klessig DF (2000) NPR1 differentially interacts with members of the TGA/OBF family of transcription factors that bind an element of the *PR-1* gene required for induction by salicylic acid. Molecular Plant-Microbe Interactions **13**: 191–202

Zhu T, Nevo E, Sun D, Peng J (2012) Phylogenetic analyses unravel the evolutionary history of NAC proteins in plants. Evolution 2012, **66:**1833–1866

APPENDIX

Supplemental Figure 1. Results of GenomeWalker™ PCR on genomic DNA isolated from (A) AT416, (B) AT36, (C) AT263 and (D) AT633. RB/LB – reactions performed with primers binding at the right/left border respectively. Lanes marked as "1" – primary PCR with GW_1F/GW_1R primer, lanes marked as "2" – nested or primary PCR with GW__2F/GW_2R primer, lanes marked as "3" – nested PCR with GW_3F/GW_3R primer. Names of the restriction enzymes represent enzymes used to digest genomic DNA, which was further used as a template for primary GenomeWalker™ PCR. Ladder – 1 kb DNA ladder (PeqLab).

A – AT416

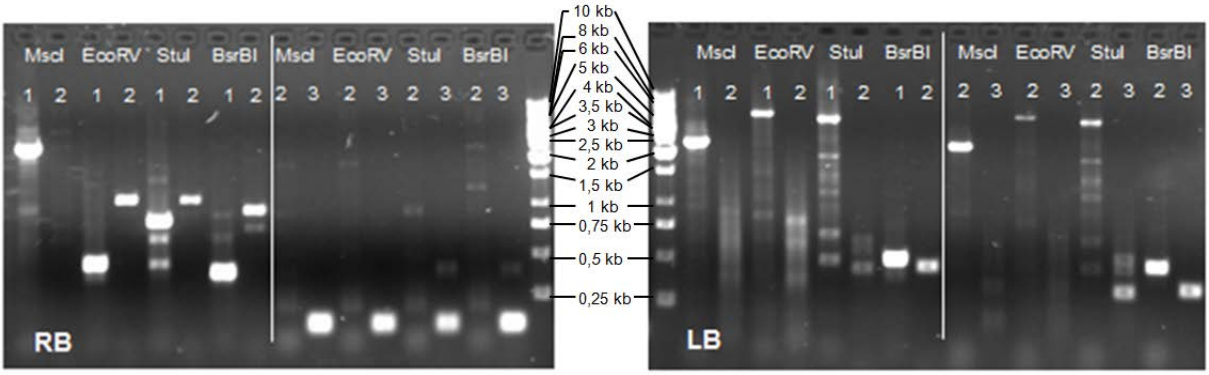

B – AT36

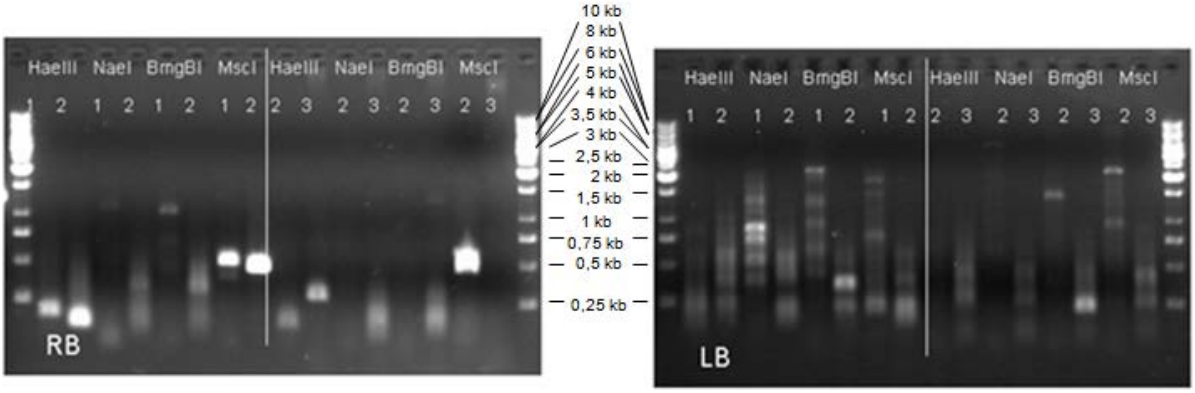

C – AT263

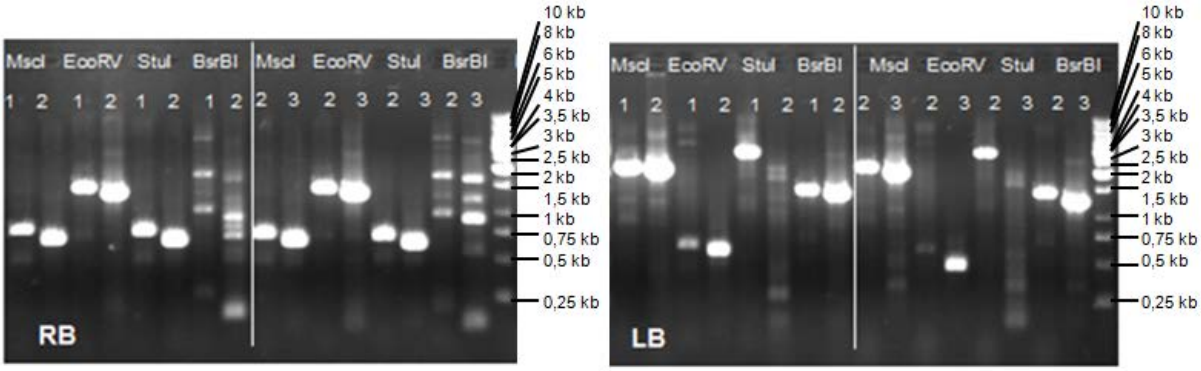

D – AT633

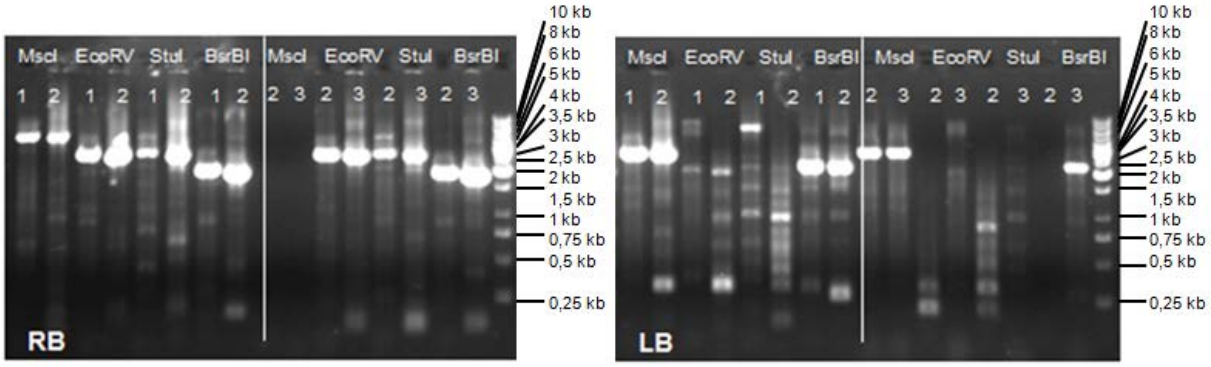

Supplemental Figure 2 Comparison of the protein sequence of hypothetical protein GLRG_05236.1 from *C. graminicola* (Query) with potential homologues protein CH063_01104.1 from *C. higginsianum* (Sbjct).

C. higginsianum IMI 349063: CH063_01104.1: hypothetical protein

Score = 392.504 (1007), Expect=0.0

Identities=201/349 (57%), Positives=242/349 (69%)

```
Query GQNLPDK----TGGEWKPWSSFSAKQQKLVQSKLNRRVRIDAANTGMVCRTHSGEPVKEL
      GQ LP+K    TGGEWKP SSFS KQQKLV  KL RRVRIDAANTGM CR HSGEPVKEL
Sbjct GQKLPEKFRCKTGGEWKPLSSFSNKQQKLVLDKLGRRVRIDAANTGMNCRFHSGEPVKEL

Query QCEGPCNRIRALDQFSKNNRSNGVNICKACQHWVNTQEPGYAPWGGPNTDLDPLEENDDF
      QCEGPC++I  LDQFSKNNR+NGVNICKACQHW+NTQEPGYAPW GP+TDLDP+E+  DF
Sbjct QCEGPCSQILVLDQFSKNNRTNGVNICKACQHWINTQEPGYAPWAGPHTDLDPIEQMGDF

Query ETRLPTEPSDIFDLYDHRPLAPITGTDGLTKLEDDEAGAPSLKFAGLNITHARQSIAPPH
      E R+P EPSDI + +D+RPLAPITGTDGLT L++DE G PSL  AGL+I HAR+ +  P
Sbjct EARMPAEPSDIVEFHDNRPLAPITGTDGLTALDNDETGLPSLGMAGLHIGHARRGLFAPR

Query LDTESVTSTQRASGSIISESASQPTPEDLGEASLWLSQAKIAXXXXXXXXXTSGRVTYNA
      LDT+S+++ Q          +SQ   E +G    W +Q+ +A         T GRV YNA
Sbjct LDTKSISTPQ-----TTESVSSQAMTESMGATEWWFTQSGLA------RDQTGGRVIYNA

Query WDSNGRQYQMSKTPTVQSGRSSVMSGMTPAXXXXXXXXXXXXXETALNSRPQSVTNIRPQ
      WDS G+++++ KTPTVQS +SS+M+ +  A                NSR  + T+IR Q
Sbjct WDSTGQKHELCKTPTVQSEQSSMMNSIAEAS----------------NSRSPNATDIRSQ

Query NSTNTSKPAT-GGTWDTKGRSSDRKHLTEKEHRELQRNIPQRQVNFPYG
       +     P T GGTW    R +DRK L+EKEHRELQRN+PQRQ   PYG
Sbjct KTAIAKTPTTGGGTW-AGNRQADRKQLSEKEHRELQRNMPQRQAIVPYG
```

Supplemental Figure 3. Result of PCR performed on genomic DNA of wild type strain of *C. graminicola* with primers designed for promoter (left flank – L) and terminator (right flank – R) regions of targeted genes: *ubiquitin-conjugating enzyme 8* (Ubc8), *ketopantoate hydroxymethyltransferase* (KPHMT) and two genes coding for hypothetical proteins affected in strain AT416: GLRG_05236.1 (GLRG) and CgORF416 (ORF). Clonat – product amplified with primers designed to *nourseothricin N-acetyl-transferase* gene from vector pPN2. Ladder – Gene Ruler^{TM} 1 kb DNA ladder.

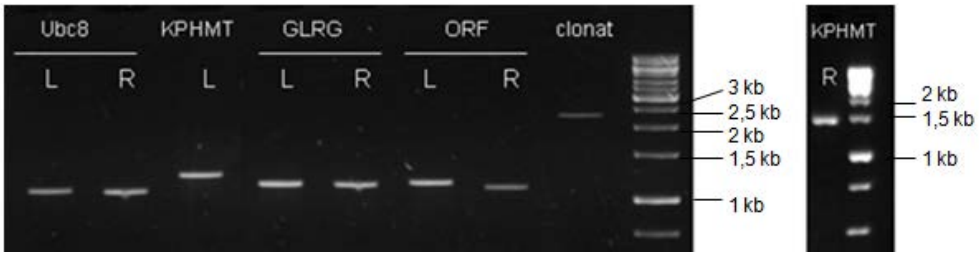

Supplemental Figure 4. Result of nested PCR performed on deletion cassettes constructed for targeted genes: *ubiquitin-conjugating enzyme 8* (1), *ketopantoate hydroxymethyltransferase* (2) and two genes coding for hypothetical proteins affected in strain AT416: *GLRG_05236* (3) and *CgORF416* (4). Ladder - Gene Ruler^{TM} 1 kb DNA ladder.

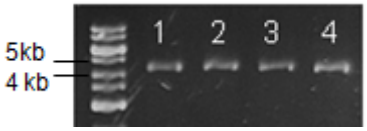

Supplemetanl Fig. 5. Genotyping of the putative knock-out strains with primers designed to the deletion cassette (left and right flank) and to the respective target gene. Numbers (1-6 in A, 1-8 in B and C, 1-4 in D) represent independent strains. Wt – positive control of primers on wild type *C. graminicola* CgM2 gDNA. Ladder - Gene Ruler^{TM} 1 kb DNA ladder.

A – *CgUbc8* KO

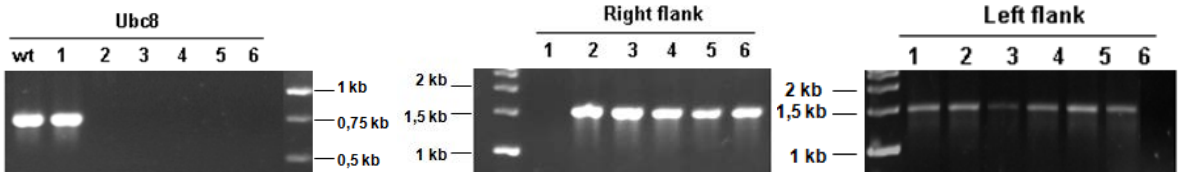

B – *CgORF416* KO

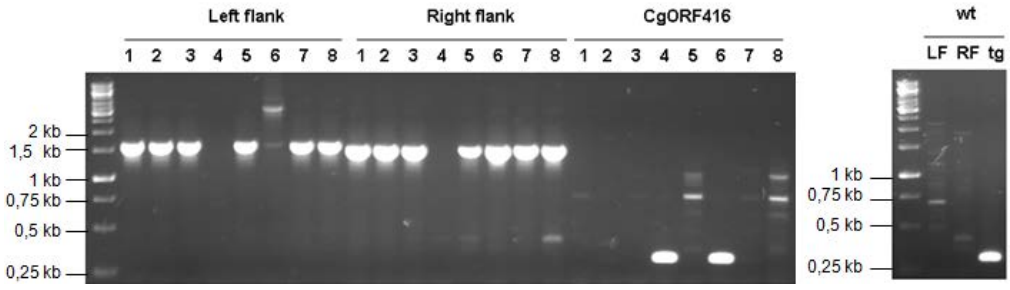

C – *CgKPHMT* KO

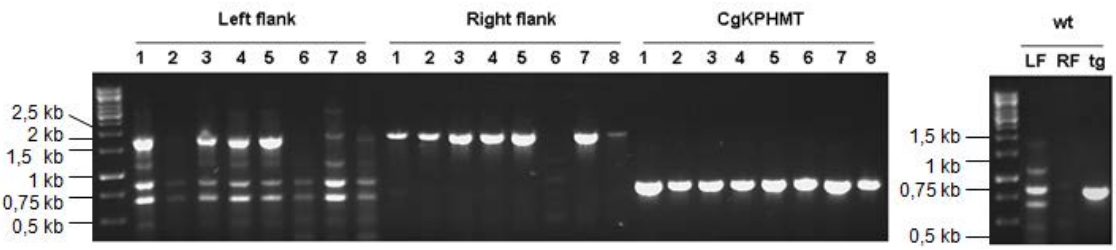

D – *CgGLRG_05236.1* KO

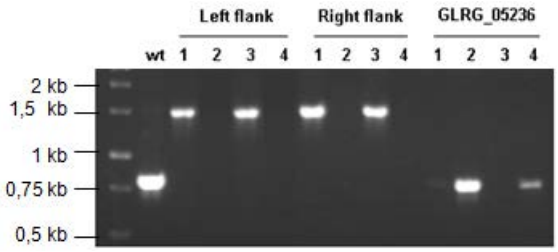

Supplemental Figure 6. Cluster analysis of metabolites extracted from mock-treated (C) and *C. graminicola* wild type CgM2-infected (INF) maize leaves, performed with Cluster 3.0 (similarity metric – Spearman Rank Correlation) and displayed with TreeView programme. Arabic numbers represent time points (hours post infection) when the analysed leaf material was collected, Roman numbers – replicates of the experiment.

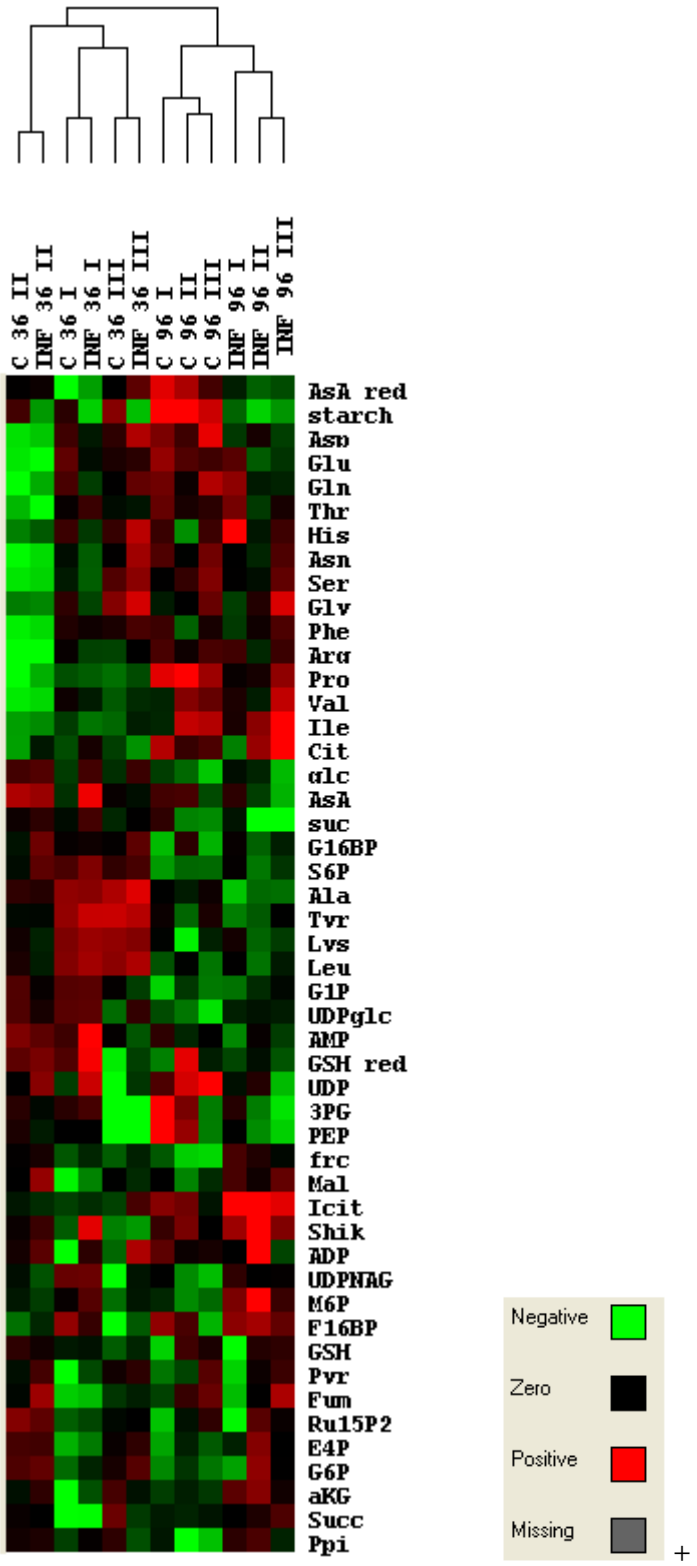

Supplemental Figure 7. Glutathione content (upper panel) and reduction status of glutathione (lower panel) in maize leaves infected with wild type *C. graminicola* CgM2 and mock-treated control plants at 36 hpi and 96 hpi. Mean values of all three repetitions of the CET are shown with the error bars representing the standard error (n=9-12).

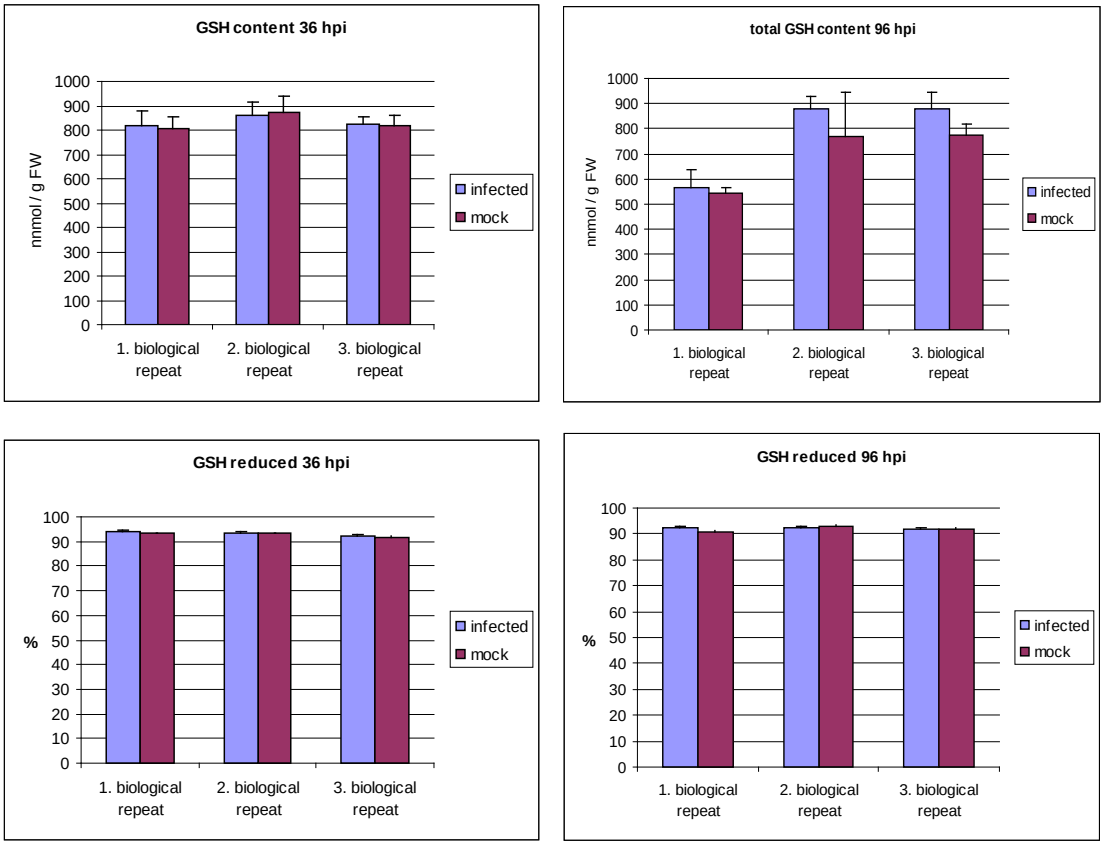

Supplemental Figure 8. Ascorbate content (upper panel) and reduction status of ascorbate (lower panel) in maize leaves infected with wild type *C. graminicola* CgM2 and mock-treated control plants at 36 hpi and 96 hpi. Mean values of all three repetitions of the CET are shown with the error bars representing the standard error (n=9-12).

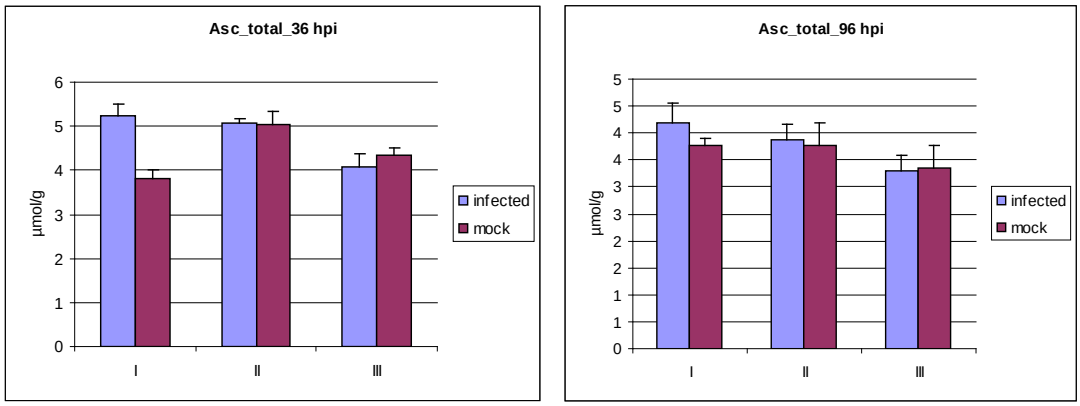

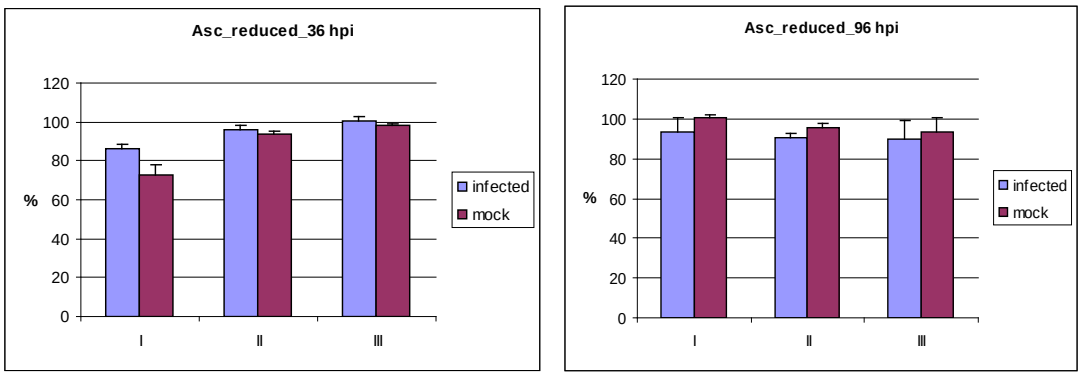

Supplemental Figure 9. Genotyping of Arabidopsis *Aox1d* knock-out line (representative result is shown). with primers designed to the wild type allele ("WT primers": GK-529D11_LP and GK-529D11_RP) and allele carrying T-DNA insertion ("T-DNA primers": GK-T-DNA and GK-529D11_RP) of *Aox1d* locus. Analysis was performed on genomic DNA (left) and cDNA (right) of Arabidopsis *Aox1d* knock-out mutant (AOX1d) and wild type Col-0 (WT) as control.

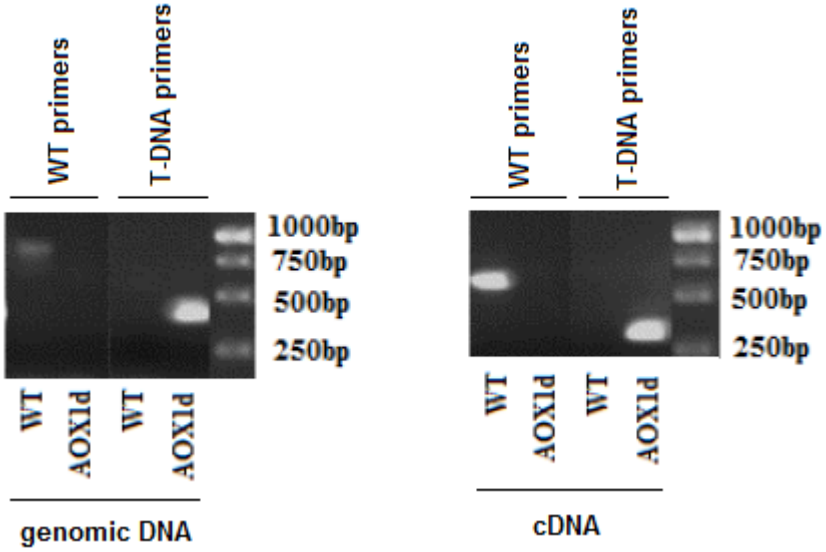

Supplemental Table 1. Chromosomal positions of the 116 identified *ZmNAC* genes in the maize genome.

ZmNAC number	Transcript Accession No. (www.maizesequence.org)	chromosome	chromosomal location (bp)	strand
ZmNAC1	GRMZM2G406204_T01	1	4,221,142-4,225,235	F
ZmNAC2	GRMZM2G025642_T01	1	5,608,665-5,615,614	R
ZmNAC3	GRMZM2G059428_T01	1	7,451,346-7,453,412	R
ZmNAC4	GRMZM2G077045_T02	1	25,171,943-25,180,175	F
ZmNAC5	GRMZM2G031001_T01	1	53,508,655-53,510,858	R
ZmNAC6	GRMZM2G011598_T01	1	53,720,811-53,723,055	R
ZmNAC7	GRMZM2G082709_T01	1	96,962,968-96,965,244	F
ZmNAC8	GRMZM2G475014_T01	1	178,262,968-178,264,453	R
ZmNAC9	GRMZM2G430522_T01	1	188,785,237-188,788,098	R
ZmNAC10	GRMZM2G054252_T02	1	195,185,126-195,188,536	F

ZmNAC11	GRMZM2G340305_T01	1	202,534,900-202,539,804	F
ZmNAC12	GRMZM2G152543_T01	1	212,357,010-212,358,734	R
ZmNAC13	GRMZM2G031120_T01	1	253,158,059-253,159,542	F
ZmNAC14	GRMZM2G163251_T01	1	283,250,286-283,252,184	F
ZmNAC15	GRMZM2G347043_T01	1	292,086,460-292,088,246	F
ZmNAC16	GRMZM2G156977_T01	2	9,413,823-9,416,383	R
ZmNAC17	GRMZM2G178998_T01	2	22,627,345-22,630,579	R
ZmNAC18	AC212859.3_FGT008	2	25,664,066-25,665,294	R
ZmNAC19	GRMZM2G176677_T01	2	26,430,610-26,438,582	F
ZmNAC20	GRMZM2G081930_T01	2	29,554,752-29,557,614	R
ZmNAC21	GRMZM2G450445_T02	2	37,553,208-37,559,085	F
ZmNAC22	GRMZM2G009892_T01	2	42,350,633-42,352,536	R
ZmNAC23	GRMZM2G099144_T01	2	47,463,966-47,465,401	F
ZmNAC24	GRMZM2G316840_T01	2	48,822,571-48,824,076	R
ZmNAC25	GRMZM2G018436_T01	2	150,029,400-150,030,906	R
ZmNAC26	GRMZM2G162739_T01	2	156,134,509-156,136,407	R
ZmNAC27	GRMZM2G008374_T01	2	190,853,955-190,855,836	R
ZmNAC28	GRMZM2G179049_T02	2	192,453,409-192,455,615	F
ZmNAC29	GRMZM2G309582_T01	2	234,214,819-234,216,187	F
ZmNAC30	GRMZM2G166721_T01	3	6,938,390-6,944,663	F
ZmNAC31	GRMZM2G062650_T01	3	31,804,625-31,806,595	R
ZmNAC32	GRMZM2G064541_T01	3	38,053,287-38,062,585	R
ZmNAC33	GRMZM2G099054_T01	3	56,889,788-56,890,479	F
ZmNAC34	GRMZM2G114850_T01	3	118,291,252-118,295,581	F
ZmNAC35	GRMZM2G139700_T01	3	133,824,688-133,826,888	F
ZmNAC36	AC203535.4_FGT002	3	157,575,853-157,577,265	R
ZmNAC37	GRMZM2G140174_T01	3	168,356,038-168,358,865	R
ZmNAC38	GRMZM2G014653_T02	3	169,147,924-169,150,379	R
ZmNAC39	GRMZM5G813651_T01	3	170,022,873-170,025,674	R
ZmNAC40	GRMZM5G832473_T01	3	176,510,723-176,512,231	F
ZmNAC41	GRMZM2G312201_T03	3	186,198,585-186,201,115	F
ZmNAC42	GRMZM2G122615_T01	3	209,087,673-209,088,984	F
ZmNAC43	GRMZM2G058518_T01	3	210,231,409-210,235,812	F
ZmNAC44	GRMZM2G069047_T01	4	37,865,207-37,867,670	R
ZmNAC45	GRMZM2G123246_T01	4	38,385,079-38,388,138	R
ZmNAC46	GRMZM2G100583_T01	4	46,934,197-46,936,936	F
ZmNAC47	GRMZM2G125777_T01	4	50,096,485-50,101,420	R
ZmNAC48	GRMZM2G048826_T01	4	66,656,098-66,657,207	R
ZmNAC49	AC198937.4_FGT005	4	90,882,483-90,883,873	F
ZmNAC50	GRMZM2G062009_T01	4	141,356,197-141,358,623	F
ZmNAC51	GRMZM2G354151_T01	4	147,940,834-147,944,741	R
ZmNAC52	GRMZM2G113950_T01	4	169,335,065-169,339,485	R
ZmNAC53	GRMZM2G140901_T01	4	171,283,804-171,286,057	F
ZmNAC54	GRMZM2G439903_T01	4	189,106,362-189,107,549	R
ZmNAC55	GRMZM2G336533_T01	5	2,890,745-2,892,534	R
ZmNAC56	GRMZM2G018553_T01	5	2,921,228-2,922,904	F
ZmNAC57	GRMZM2G112548_T01	5	5,316,262-5,317,730	R

ZmNAC58	GRMZM2G063522_T01	5	43,417,416-43,421,787	R
ZmNAC59	GRMZM2G389557_T01	5	62,577,490-62,579,931	R
ZmNAC60	GRMZM2G155816_T01	5	142,183,507-142,185,261	F
ZmNAC61	GRMZM2G094067_T01	5	172,920,167-172,921,326	R
ZmNAC62	GRMZM2G038073_T01	5	180,370,272-180,373,773	R
ZmNAC63	GRMZM2G315140_T01	5	188,733,586-188,737,966	R
ZmNAC64	GRMZM2G100593_T01	5	206,975,367-206,978,937	F
ZmNAC65	GRMZM2G052239_T01	6	715,291-716,504	F
ZmNAC66	GRMZM2G030325_T01	6	3,874,650-3,877,935	F
ZmNAC67	GRMZM2G092465_T01	6	4,310,921-4,313,522	F
ZmNAC68	GRMZM2G091490_T01	6	64,902,485-64,904,929	F
ZmNAC69	GRMZM2G074358_T01	6	81,605,322-81,606,777	F
ZmNAC70	GRMZM2G393433_T02	6	16,291,162-16,293,314	R
ZmNAC71	GRMZM2G041746_T02	6	106,251,283-106,253,155	R
ZmNAC72	GRMZM2G027309_T01	6	116,578,564-116,583,279	F
ZmNAC73	GRMZM2G086768_T01	6	116,657,254-116,667,015	F
ZmNAC74	GRMZM2G379608_T01	6	116,669,547-116,672,514	F
ZmNAC75	GRMZM2G078954_T01	6	116,673,745-116,677,264	F
ZmNAC76	GRMZM2G147867_T01	6	147,676,290-147,678,953	R
ZmNAC77	GRMZM2G456568_T01	6	147,921,021-147,925,808	R
ZmNAC78	GRMZM2G180328_T01	6	148,032,568-148,034,587	F
ZmNAC79	GRMZM2G465835_T01	6	149,397,669-149,398,803	R
ZmNAC80	GRMZM2G031200_T02	6	164,497,335-164,499,048	F
ZmNAC81	GRMZM2G479980_T01	7	4,588,708-4,589,876	F
ZmNAC82	GRMZM2G079632_T01	7	20,954,529-20,956,364	R
ZmNAC83	GRMZM2G159094_T01	7	111,666,002-111,668,186	F
ZmNAC84	GRMZM2G386163_T01	7	128,959,317-128,968,837	R
ZmNAC85	GRMZM2G004531_T01	7	134,099,371-134,102,423	R
ZmNAC86	GRMZM2G054277_T01	7	135,891,453-135,892,601	R
ZmNAC87	AC233865.1_FGT003	7	141,023,510-141,025,201	F
ZmNAC88	GRMZM2G179885_T02	7	152,569,734-152,571,931	R
ZmNAC89	GRMZM2G430849_T01	7	167,762,423-167,765,153	R
ZmNAC90	GRMZM2G181605_T01	7	167,987,646-167,989,471	F
ZmNAC91	GRMZM2G167492_T01	8	4,541,745-4,558,891	R
ZmNAC92	GRMZM2G109627_T01	8	6,989,712-6,992,428	F
ZmNAC93	GRMZM2G154182_T01	8	7,253,466-7,255,466	F
ZmNAC94	GRMZM2G112681_T01	8	20,827,673-20,834,211	F
ZmNAC95	GRMZM2G172264_T01	8	99,283,137-99,284,291	F
ZmNAC96	GRMZM2G134687_T01	8	102,146,169-102,149,099	R
ZmNAC97	GRMZM2G104400_T01	8	102,534,750-102,538,745	R
ZmNAC98	GRMZM2G163843_T01	8	150,569,499-150,570,962	R
ZmNAC99	GRMZM2G134073_T01	8	160,424,732-160,426,914	R
ZmNAC100	GRMZM2G068973_T01	8	170,862,648-170,864,431	F
ZmNAC101	GRMZM2G171395_T01	9	23,231,974-23,236,376	R
ZmNAC102	GRMZM2G440219_T01	9	28,053,913-28,055,660	F
ZmNAC103	GRMZM2G115721_T01	9	55,508,378-55,513,309	R
ZmNAC104	GRMZM2G104074_T01	9	62,014,374-62,016,303	F

ZmNAC105	GRMZM2G042494_T01	9	127,882,259-127,884,597	R
ZmNAC106	GRMZM2G159500_T01	9	128,441,746-128,443,938	F
ZmNAC107	GRMZM2G126936_T01	9	141,422,295-141,423,602	R
ZmNAC108	GRMZM5G894234_T01	9	146,252,099-146,255,810	F
ZmNAC109	GRMZM2G126817_T01	9	147,333,144-147,334,649	R
ZmNAC110	GRMZM2G174070_T01	9	149,633,474-149,637,919	R
ZmNAC111	GRMZM2G127379_T01	10	2,164,935-2,167,024	R
ZmNAC112	GRMZM2G083347_T01	10	14,502,416-14,504,294	F
ZmNAC113	GRMZM2G167018_T01	10	60,800,053-60,802,701	F
ZmNAC114	GRMZM2G003715_T01	10	78,128,657-78,132,883	F
ZmNAC115	GRMZM2G435824_T01	10	118,928,473-118,930,431	R
ZmNAC116	GRMZM2G043813_T01	10	130,249,115-130,251,885	F

Supplemental Table 2. A list of motifs detected within the 116 ZmNAC proteins. The protein sequences were screened with MEME (Multiple Em for Motif Elicitation, http://meme.nbcr.net/meme/cgi-bin/meme.cgi) at a cut off p-value of e-10. The motif location is given as follows: C-/N-term. – C-/N- terminus, NAC – NAC domain, sd. A-E – subdomain A-E.

Motif no.	Total no. of ZmNACs with given motif	p-value	motif location	motif sequence
1	87	1.1e-2111	NAC (sd. C)	WYFF[SC]P[RK]DRKYP[NT]G[ST]R[TP]NRATG[AS]G[YF]WKATGK
2	115	9.9e-1243	NAC (sd. A)	[LV]PPGFRFHPTDEEL[VI]
3	115	1.5e-1165	NAC (sd. D)	[LV]PPGFRFHPTDEEL[VI]
4	98	2.3e-1043	NAC (sd. B)	[IV]IA[ED]VDL[YN][KR]x[ED]PW[DE]LPE[KR]AK[IL]
5	108	3.8e-983	NAC (sd. D)	VAxxGRL[VI]G[ML][KR]KTLVFYRGRA
6	106	1.8e-662	NAC (sd. E)	xK[DE][ED]WV[LV]C[RK][VI][FY]KKxG
7	95	2.4e-412	NAC (sd. A)	[YHF]YL[RK]RK[VA]AGK[RP][LIF]P[VL][DE]
8	13	1.4e-385	NAC (sd. B,C)	HP[LF]IDEFIPT[IV][DE][EG][ED][ED]GICYTHP[EQ][KR]LPGV[KT][QK][DN]G[SL][VS][SR]HFFHR[PT][FS]KAY[TN]TGTR
9	4	4.5e-110	C-term.	MAAESNLPDFTTLPTDKHVGTVQEVVHNPEHNLYQLNRNCEI[SN]IEETVVL
10	4	6.2e-077	C-term.	DG[GC]SA[RK][TS][SG][DN]LFVDLSYDDIQGMYSGLDMLPP[AP]GED[LF]YSSLFASPRV[RK]GNQ
11	10	1.0e-062	NAC (sd. C)	[KIR][RQK][RTV][RHD][IC][ND][TV][DHQ][DGK][AG][ED][TV]RWHKTGKT[KR]
12	7	2.2e-045	C-term.	GP[QKR][NI]G[AE]QYGAPF[NV]EE[ED]W[ED][EDN][DA][DE]
13	10	2.0e-042	C-term.	[GS][IVT]TDW[RS][AVIM][LM]D[KR][FL][VL]AS[QH][LQ][NS]
14	6	1.2e-039	NAC (sd. C), C-term.	[ST]HS[WH][GS][ED]TRTPESEI[VD]D[ND][DP][FLP]P
15	4	1.1e-038	N-term.	W[IL][IM][DNT][SCG][QLR][GR][FIL]A[TEK]KI[KR][NSY][AT][SNT][GPQ][SG][AFLS][DNT][PHL][SHR][KIL][QGS][EK][LW][IFV][AG][NEK][PA][RS][KRT][EK]C[PT][KNY]C[SD][HCY][VI]ID[NI]S[DN]V[VAS][HLM][QV]W
16	33	3.4e-035	N-/C-term.	Q[QH]QQQQ
17	13	1.1e-034	NAC (sd. C)	[GA][GR][AR][SR]R[AT][TA][GP][SR]GYW[KR][PA][TS]GK[ED][KRE]PV
18	4	2.6e-025	C-term.	[DV][SAV][DN][PT][NS][AHN][NS][FS][DN][HL][SCY]E[DR]VD[GV][KN][HS]G[DL][FI][LV]S[DT][PAV][GN][AL][GP][KS][NT]F[FIL][HQ][HCY][VA]EP[GS][EK][KQ][NV]S[LFV][MHY]L[NS][GNP][NTV][IAP][ISV]
19	4	1.5e-015	C-term.	FKP[GR]DKNAQELTTSD
20	5	3.7e-014	C-term.	EWEKM[RQ][LQ][GQ]K[GET][AK][AVE][AKV][GK][AV][VAGM][KAE][EST][EK][EA]
21	4	2.3e-016	C-term.	[QT][LAG]PL[LS][LP][AF][AP][INS][SLM][DE]KWDWNP[LV][GL][EP][DS][AP][KT][AV][CR][DT][SY][FG]
22	4	7.1e-014	C-term.	S[VG]KT[TI]KDG[DY]NLQSQD
23	5	7.2e-014	C-term.	[CKS][TS][FS][DSF][QR][EP][VA][GA][IV][CGH][GR][DNQ][QS][HVF][HPQ][ASG][ANH][AQW][LA][AGN][RH][SF][ENA][NAPT][HKP][AHE][AI][AGE][ARL][GK][AQP]Q[PRL][HQL][GS][PQS][LVS][LA][APM]T[KIT]
24	4	2.8e-016	C-term.	I[DE]D[GN][FG]H[GL][HS][PT][AT][ST]ARS[ST][GP]S[KR][AG][AV][AV][TN][AM][PDE][KQ][KQ][DH][HN][KR][QT][QS]AS[PS][RS][SLM][AT]P[TMV][FP][DP]
25	4	3.4e-012	NAC (sd. A)	WHLMAKHGKSG
26	4	2.3e-009	C-term.	[ENV][PCS][TFH][DH][DN][ET][GN][LMT]EL[DS][CN][LT]DE[FLV][FR]LS[LQ][DI][DE][FY][DS][EQ][DV]S
27	4	1.3e-007	C-term.	[KL][EG][DG][DN][DY]W[FL][AT][DG][ILM]NLDDLQ[AIM][PS][GY][NDE]
28	7	1.1e-007	N-/C-term.	[NST][TL]A[KM]HCP[SH]CG[EH][HKR][AIL][DQ]
29	6	6.2e-007	NAC (sd. C)	[ED][RA][AEQ]WYF[FY][AV][PR][LR][DR][GR][KG]
30	14	3.1e-008	C-term.	[LF][ML][QKS]LP[PQ]LE[SV][PA]
31	7	1.6e-006	N-term.	RDAEAEL[ND]
32	6	4.5e-006	C-term.	F[FL][EY][DL][KS][DG]FED[ALM]A[ND]L[GD]FP[QL]G[WN][MG]
33	4	6.1e-006	N-term.	MSISVNGQ
34	10	7.0e-006	C-term.	[HV][HD]H[HQ]HH
35	6	1.0e-005	C-term.	[AV][ALN][AL][AN][AS][MN][GS][AG][ST][GMS][SA][ART][AIS][AP]IDELS[TR][LA][VI]GHV[HQ]
36	5	3.0e-003	C-term.	E[QL]V[PY]CFS
37	5	1.0e-004	C-term.	[YR][HSP]CK[PQV]E[LH]E[YL][HLV][HPS]
38	4	3.5e-003	C-term.	AMDM[SA]TSH
39	4	3.7e-003	C-term.	[RS][ISV][NS][FS][PG][FS][DNR][LG][GQ][AGV][DA][SGL][SAP][ED][DE][WA][RA][CM][ANST][IL][PD]W[DE]S[LF][LIP][CPST][PT]
40	4	4.4e-004	C-term.	[VD][LPS]E[PAQ][ND][FINP][GLQV][VGY]G[AS][PS]S[SP][AGP][RST][LFH][PAE][EDG][AL][GSY][ST][QD][LGT][NEV][CFV][LV][VDG][LV]P[DT][DG][QD][AQT][KAP][SD][SKM]T[IMY][GA][KGN][GAR][FLY][VA][AKRS][IMV][LD][DGH][SH][Q][PS]

Supplemental Figure 10. Domain architecture of maize NAC proteins. A multiple alignment of the consensus sequences of the whole length NAC proteins from each clade was compiled using ClustalW 2.0. Amino acid residues present in at least 50% of the subclade members are displayed in the consensus sequences.

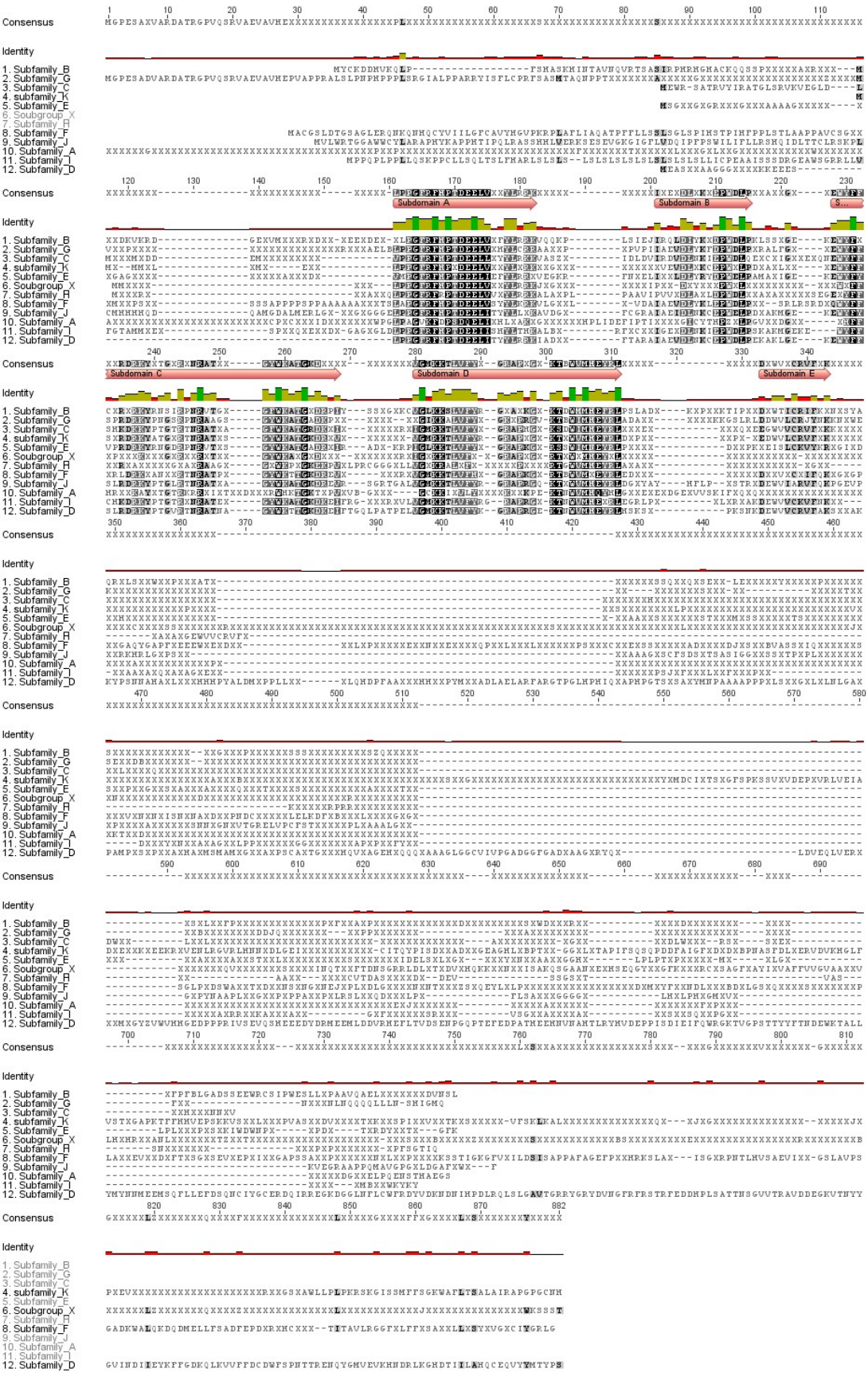

ACKNOWLEDGMENTS

I wish to express my sincere gratitude to Prof. Dr. Uwe Sonnewald for the project admission and enabling me to conduct this research in the division of biochemistry.

I would like to express my deep gratitude to PD Dr. Lars Voll for scientific supervision throughout my research, for his expertise and ideas and review of this thesis.

My sincere thanks to Prof. Dr. Christian Koch for serving as my examiner, for his “fungal” knowledge and valuable discussions. I extend my thanks to his team, especially Marlis, for their support in fungus-related problems.

I also thank Prof. Dr. Andreas Burkowski for co-review of this thesis and Prof. Dr. Benedikt Kost for serving as my examiner.

I would like to thank Prof. Dr. Holger Deising and Dr. Steffen Münch (both Martin-Luther-University of Halle-Wittenberg) for providing the *C. graminicola* insertion mutants and for performing the central experiment and microarray hybridisations together with Prof. Dr. Regine Kahmann, Prof. Dr. Jörg Kämper and Prof. Dr. Günther Döhlemann (all three at that time from the Max-Planck-Institute for terrestrial Microbiology, Marburg).

I would like to acknowledge the B.Sc. students Christopher McCollum and Claudia Kohout for their valuable contribution to this project.

I am thankful to the entire “Voll Lab” and all other colleagues at the “Lehrstuhl” for their support in everyday work. Special thanks to Jörg and his team from analytical lab.

My deepest thanks to Karina for her sincere way of life, for her warm support, especially in though moments, her constant believe in me and all the crazy things we have done together.

Special thanks to my family for everything, without you, I wouldn't be where I am.

W szczególności dziękuję mojej rodzinie, bez Was nie byłabym tu, gdzie jestem.

LIST OF PUBLICATIONS

Voitsik AM, Münch S, Deising HB, Voll LM (2013) Two recently duplicated maize NAC transcription factor paralogs are induced in response to *Colletotrichum graminicola* infection. BMC Plant Biology **13:** 85

Voll LM, Horst RJ, Voitsik AM, Zajic D, Samans B, Pons-Kühnemann, J, Doehlemann G, Münch S, Wahl R, Molitor A, Hofmann J, Schmiedl A, Waller F, Deising HB, Kahmann R, Kämper J, Kogel KH, Sonnewald U (2011) Common motifs in the response of cereal primary metabolism to fungal pathogens are not based on similar transcriptional reprogramming. Frontiers in Plant Physiology **2**: 39. doi: 10.3389/fpls.2011.00039

Münch S, Ludwig N, Floss DS, Sugui JA, Koszucka AM, Voll LM, Sonnewald U, Deising HB (2011) Identification of virulence genes in the corn pathogen Colletotrichum graminicola by Agrobacterium tumefaciens-mediated transformation. Molecular Plant Pathology **12:** 43-55

Batsukh T, Pieper L, Koszucka AM, von Velsen N, Hoyer-Fender S, Elbracht M, Bergmann JEH, Hoefsloot L H, Pauli S (2010) CHD8 interacts with CHD7, a protein which is mutated in CHARGE syndrome. Human Molecular Genetics **19:** 2858-2866

Koszucka AM and Dabrowska G (2006) Roślinne metalotioneiny (Plant metallothioneins). Postępy Biologii Komórki (Advances in Cell Biology) **33:** 285-302

CONFERENCE CONTRIBUTIONS

Analysis of host genes induced during the maize – *Colletotrichum graminicola* interaction: *ZmNAC41* and *ZmNAC100* are triggered in the early steps of the fungal infection; talk, **3rd Sophia Antipolis Workshop on Compatibility Mechanisms in Plant-Microbe Interactions**, Sophia Agrobiotech Institute, Sophia Antipolis, France, September 2011

Identification of virulence factors in the maize anthracnose fungus *Colletotrichum graminicola*; poster, **International Meeting: Communication in Plants and their Responses to the Environment**, Halle (Saale), May 2011

Identification of virulence factors in maize anthracnose fungus *Colletotrichum graminicola*; poster, **4th International Workshop Rauischholzhausen**, Rauischholzhausen, October 2010

Towards an elucidation of early events in the maize – *C. graminicola* interaction; talk, **4th Annual Meeting on Compatibility Mechanism FOR666**, Sophia Agrobiotech Institute, Sophia Antipolis, France, October 2009

Necrotrophic growth of the hemibiotrophic fungus *C. graminicola* induces respiratory metabolism in maize; poster, **Botanikertagung**, Leipzig, September 2009